KWAME NKRUMAH UNIVERSITY OF SCIENCE AND TECHNOLOGY

COLLEGE OF HEALTH SCIENCES

FACULTY OF PHARMACY AND PHARMACEUTICAL SCIENCES

DEPARTMENT OF PHARMACOGNOSY

PHYTOCHEMICAL CONSTITUENTS AND SOME BIOLOGICAL ACTIVITIES OF SELECTED MEDICINAL PLANTS FROM GHANA

BY

EVELYN AFUA MIREKU

SEPTEMBER 2016

PHYTOCHEMICAL CONSTITUENTS AND SOME BIOLOGICAL ACTIVITIES OF SELECTED MEDICINAL PLANTS FROM GHANA

A Thesis

Submitted in fulfilment of the requirement for the degree of

DOCTOR OF PHILOSOPHY

To the Department of Pharmacognosy

Faculty of Pharmacy and Pharmaceutical Sciences

College of Health Sciences

Kwame Nkrumah University of Science and Technology

By

EVELYN AFUA MIREKU

September 2016

DECLARATION

I declare that this thesis is my own work. I further declare that to the best of my knowledge, this thesis does not contain any material previously published by any person or any material which has been accepted for the award of any degree of a university, except where due acknowledgement has been made in the text.

…….. ……

Evelyn Afua Mireku

(PhD Candidate PG7865512) Date

..... ……

Professor Abraham Yeboah Mensah Date

(Supervisor)

…… ……..

Professor Merlin L. K. Mensah Date

(Supervisor)

..... ……...

(Head of Department) Date

ABSTRACT

In this study, three Ghanaian medicinal plants namely, *Anopyxis klaineana* (Pierre) Engl. (Rhizophoraceae), *Hexalobus monopetalus* (A. Rich.) Engl. & Diels (Annonaceae) and *Landolphia heudelotti* A. DC. (Apocynaceae), were investigated for some of their biological activities and phytochemical constituents. The methanol and ethyl acetate fractions of *A. klaineana* stem bark at 300 mg/kg inhibited peak inflammatory responses and total paw oedema by 62.40 ± 6.32 % and 49.10 ± 10.31 % respectively in the carrageenan induced paw oedema assay. The total phenolic content and antioxidant capacity of the crude methanol extract were determined to be 110.21 ± 10.15 mg/g (tannic acid equivalent) and 110.6 ± 11.15 mg/g (ascorbic acid equivalent) respectively. The extract also scavenged DPPH free radicals with IC_{50} of 2.71 ± 0.21 µg/mL. The ethyl acetate fraction showed antimicrobial activity against *Staphylococcus aureus* and *Streptococcus pyogens* with MIC of 312 µg/mL. The ethyl acetate fraction of *H. monopetalus* exhibited antimicrobial activity against *S. pyogens* and *Bacillus subtilis* with MIC of 312 µg/mL. The crude methanol extract was found to have a total phenolic content of 66.19 ± 21.15 mg/g (tannic acid equivalent) and scavenged DPPH free radicals with IC_{50} of 10.1 ± 1.26 µg/mL. The total antioxidant capacity was determined to be 77.1 ± 14.15 mg/g (ascorbic acid equivalent). The methanol fraction of *L. heudelotti* roots exhibited antimicrobial activity against *S. pyogens* and *B. subtilis* at 312 µg/mL. The total phenolic content and antioxidant capacity of the methanol extract were determined to be 98.14 ± 14.70 mg/g (tannic acid equivalent) and 108.8 ± 14.52 mg/g (ascorbic acid equivalent) respectively. The crude extract scavenged DPPH radicals with IC_{50} of 6.95 ± 0.81 µg/mL. Phytochemical investigation of *A. klaineana* stem bark led to the isolation and characterization of six limonoids, five tirucallane triterpenes and one protolimonoid.

Methyl angolensate and 3,23-dioxotirucalla-7,24-diene-21-oic acid exhibited significant competitive PGE_2 binding inhibition with IC_{50s} of 10.23 µM and 3.63 µM respectively. Most of the isolated compounds also demonstrated significant DPPH free radical scavenging property. From the stem bark of *H. monopetalus*, seven novel and two known prenylated indole alkaloids were isolated. These compounds are useful chemotaxonomic markers for the genus *Hexalobus* and closely related genera. From the roots of *L. heudelotti*, fourteen known compounds including neolignans, lignan, sesquilignans, an aromadendrane and a coumarin were isolated. The compounds showed DPPH radical scavenging and antimicrobial activity at concentration range between 12.5 and 100 µg/mL. The findings of this study have given some scientific justification to the uses of the selected medicinal plants in traditional medicine.

DEDICATION

I dedicate this thesis to my father, Dr. Emmanuel Kwasi Mireku and mother, Mrs. Philomina Mireku for their unfailing love, prayers and support throughout my PhD study.

ACKNOWLEDGEMENT

Praise be to God Almighty for his gifts of life and purpose.

I would like to express my deepest gratitude to my supervisors Prof. Abraham Yeboah Mensah (Department of Pharmacognosy, FPPS, KNUST) and Prof. Merlin L. K. Mensah (Department of Herbal Medicine, FPPS, KNUST) for their suggestions, critical reviews, fatherly advice and continuous support during my PhD research.

My sincere appreciation goes to my German host supervisor, Prof. Dr. Dr. h. c. Michael Spiteller for granting me the opportunity to further my PhD research at the Institute of Environmental Research (INFU), Faculty of Chemistry and Chemical Biology, University of Technology, Dortmund, Germany. I am grateful for his guidance and scientific discussions which ensured an efficient output of my 2-year research stay. I thank Dr. Souvik Kusari, Dr. Sebastian Zühlke and Dr. Ferdiannd Talontsi for their guidance and excellent comments.

I am also very grateful to Dr. Solomon Habtermariam (Pharmacognosy Research Laboratory, Faculty of Engineering Science, University of Greenwich, United Kingdom) for assisting in running of the NMR spectra for some of my compounds.

I thank the technical staff of the Departments of Pharmacognosy, Pharmacology and Pharmaceutics, Faculty of Pharmacy and Pharmaceutical Sciences, KNUST and the technical staff of INFU, TU- Dortmund, for the assistance offered me in all experiments carried out at their respective laboratories. I also thank Mr. Clifford Kofi Asare, for his assistance in the collection of the plants for this research.

I appreciate the encouragement and support of friends and colleagues throughout the period of this research.

I gratefully acknowledge the German Academic Exchange Program (DAAD) for the

_sandwich‘ doctoral scholarship.

I express my deep thanks to my family for their unconditional support, prayers and love.

God bless you.

TABLE OF CONTENT

LIST OF FIGURES

LIST OF TABLES

LIST OF EQUATIONS

ABBREVIATIONS

1D	One dimensional
2D	Two dimensional
^{13}C-NMR	Carbon-13 Nuclear Magnetic Resonance
^{1}H-NMR	Proton Nuclear Magnetic Resonance
AAE	Ascorbic acid equivalent
ANOVA	Analysis of variance
AST	Antimicrobial susceptibility test
ASTM	American Standard Test Method
ATCC	American Type Culture Collection
CAM	Complementary and alternative medicine
CFU	Colony forming unit
COSY	Correlation spectroscopy
COX	Cyclooxygenase
DMSO	Dimethyl sulfoxide
DSMZ	Deutche –Salmmung von Mikroorganismen und Zellkulteren
DPPH	2, 2-diphenyl-1-picrylhydrazyl
EtOAc	Ethyl acetate
GIT	Gastrointestinal
HESI	Heated electrospray ionization
HMBC	Hetero-nuclear Multiple Bond Correlation
HPLC	High performance liquid chromatography
HR-ESIMS	High Resolution electro spray ionization mass spectrometry
HRP	Horse radish peroxidase

HSQC	Hetero-nuclear Single Quantum Coherence
INF	Interferon
LC-MS	Liquid chromatography mass spectrometry
LOX	Lipoxygenase
MBC	Minimum bactericidal concentration
MDR	Multi drug resistant
MeOH	Methanol
MIC	Minimum inhibitory concentration
MTT	Dimethylthiazol-2-yl-diphenyltetrazolium
NCTC	National Collection of Type Cultures
NMR	Nuclear Magnetic Resonance
NOESY	Nuclear over-hauser enhancement spectroscopy
NSAIDS	Non-steroidal anti-inflammatory drugs
PGs	Prostaglandins
R_f	Retardation factor
ROS	Reactive oxygen species
Rpm	Revolutions per minute
TAE	Tannic acid equivalent
TLC	Thin layer chromatography
TNF	Tumour necrotic factor
UV	Ultraviolet
WHO	World Health Organisation

CHAPTER 1

INTRODUCTION

1.1 Background of study: Natural products in drug discovery

The history of drug discovery and development is firmly set in the study of natural therapies used to treat human ailments over centuries (Rishton, 2008). Since antiquity, mankind has depended on plants for their fundamental needs, in particular for medicines utilized in the treatment of various diseases (Cragg and Newman, 2013). Founded on observations and folklore, medicinal plant remedies were the first, and for a long time, the only medicines available to mankind. Leaves, barks and roots of higher plants were used as medicines and were initially in the form of crude preparations such as teas, tinctures, poultices and powders (McChesney *et al.*, 2007). These preparations were administered by traditional knowledge and practices passed down through oral history (Balunas and Kinghorn, 2005). In subsequent years, the practices and knowledge of the use of natural products were recorded in herbal pharmacopoeias. The oldest medical text came from ancient Mesopotamia in 2600 BC, in which approximately 1,000 plants and plant derived substances, such as the oils of cypress (*Cupressus sempevirens*), cedar (*Cedrus species*), frankincense (*Boswellia serrata*) and myrrh (*Commiphora species*) were recorded (Cragg and Newman, 2013).

Today, traditional medicines still play an important role in the health care of many people. It is reported that about half of the population of many industrialized countries rely on traditional/complementary and alternative medicine (TCAM) for their health needs and in less developed countries, the proportion is as high as 80 %

(Sato, 2012). In Ghana for example, medicinal plants and their products are highly patronized. Over 60 % of the country‘s population depends on plant parts for health delivery especially in poor communities (Agbovie *et al.*, 2002).

Despite the extensive use of plant medicines, for decades the identity of the chemicals that yielded their therapeutic effects remained unknown. In the eighteenth and nineteenth centuries, scientific analysis of medicinal plants led to the discovery of chemically diversified bioactive compounds that could be used directly as medicines or as templates for drug development (Fabricant and Farnsworth, 2001; Chin *et al.*, 2006). Beginning with the isolation of morphine [1] from the opium plant in 1806, further exploration of plant medicines led to the discovery of drugs used in modern medicine such as codeine [2], digitoxin [3], digoxin [4], vincristine [5], vinblastine [6], quinine [7], quinidine [8], aspirin [9] and more recently artemisinin [10] (Fig. 1.1) (Itokawa *et al.*, 2008). Moreover, between 1981 and 2002 about 75 % of drugs for infectious diseases and 60 % of anticancer compounds were either natural products or products derived from them (Newman *et al.*, 2003). Natural products, especially medicinal plants are therefore an important source of medicines useful for the treatment of a plethora of diseases.

Despite the recent interest in other drug discovery methods such as molecular modelling and combinatorial chemistry, natural product compounds still attract substantial attention from pharmaceutical and scientific communities (Cragg *et al.*, 1997). This is because compounds from natural sources have been shown to possess high chemical diversity and biochemical specificity and this gives room for novel mechanisms of action against several biological targets (Rout *et al.*, 2009). Recent innovative advances and the availability of quick and sensitive techniques have additionally made it conceivable to rapidly detect, isolate and structurally characterize biologically active agents from natural sources (Wolfender *et al.*, 2003).

This has accelerated intensive research in natural product drugs to promote discovery of alternatives for the treatment of old diseases as well as new ones such as zika virus, ebola, etc.

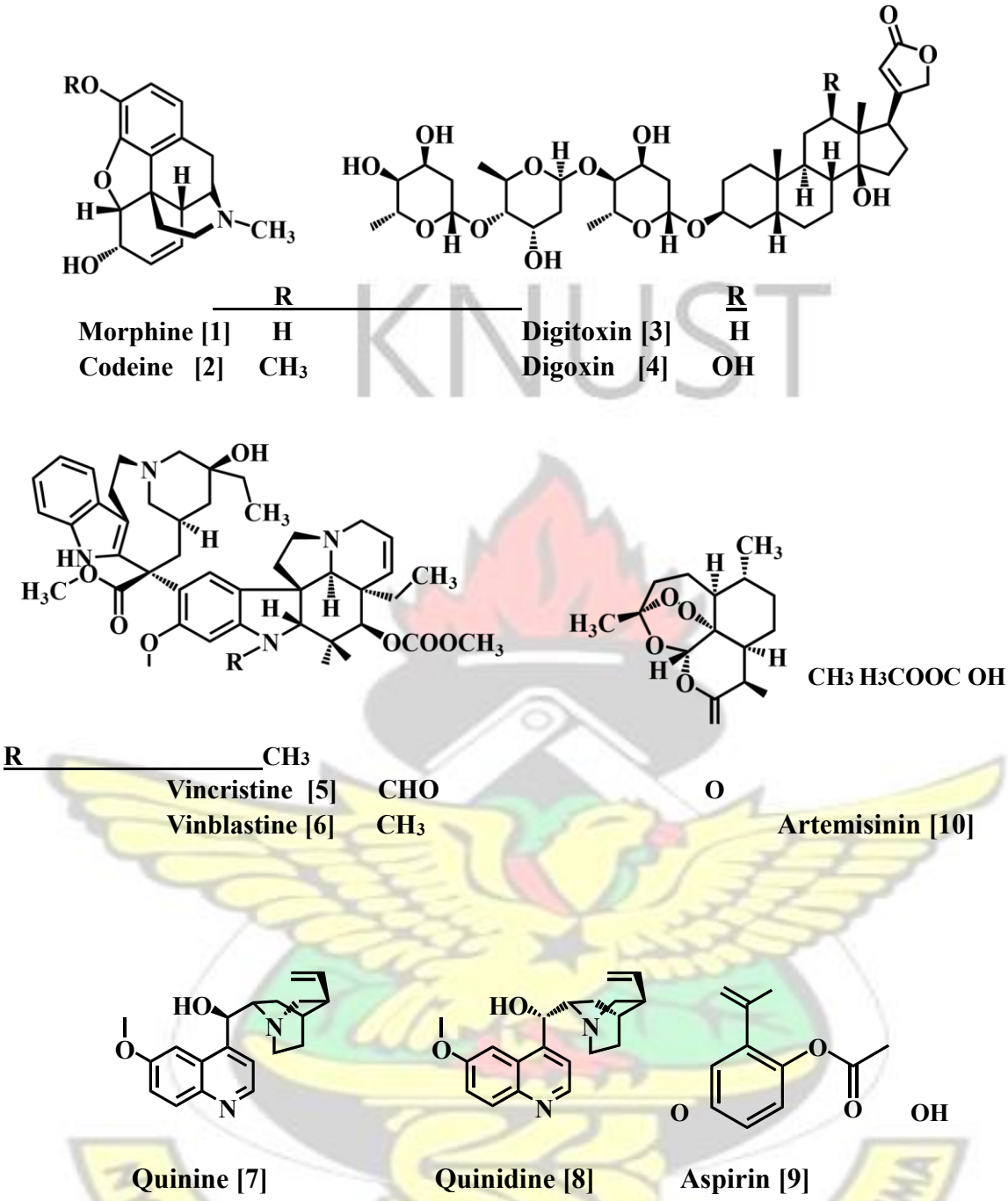

Fig. 1.1: Examples of useful drugs from plant sources

1.2 Problem statement

1.2.1 Infectious diseases and antimicrobial resistance

Infectious diseases are one of humanity‘s greatest problems. Worldwide, it is the primary cause of death accounting for about one-half of all deaths in tropical countries. The incidence of infectious diseases has increased especially in developing countries

and several pathogenic microbes have developed resistance to currently used antibiotics rendering these drugs less effective (Lowy, 2003). It is reported that the high death rate from chronic diseases in Africa is accompanied by a much more prominent burden of 69 % of deaths from infectious diseases (Stark *et al.*, 2013). Accordingly, it is not surprising that in 2006, Ghana recorded approximately 33 % of deaths from infectious and parasitic diseases (Tabi *et al.*, 2006).

The major obstacle to the treatment of infectious diseases is antimicrobial resistance. In the last few years, the recurrence and spectrum of antimicrobial- resistant infections have increased. This has rendered inadequate most of the presently used anti-infective agents (D'Costa *et al.*, 2011). Microorganisms have developed various barriers against antimicrobial agents by mechanisms such as the action of multidrug resistance pumps (MDRs), neutralizing enzymes like membrane translocases and βlactamases, alteration of target sites and metabolic pathways or by gene mutation. By these mechanisms, the microbial cells are protected against antimicrobials, resulting in failed therapy (Stermitz *et al.*, 2000).

In 2014, the World Health Organization (WHO) cautioned that considering the degree of antimicrobial resistance and the declining number of effective antimicrobials, the world will be heading for a post antibiotic era where common infections and minor injuries would be deadly if urgent action is not taken (WHO,

2014). This negative trend coupled with the adverse effects of some antibiotics (hypersensitivity reactions, haemolytic anaemia, nephrotoxicity, ototoxicity and hepatotoxicity) give an indication for the urgent need to identify novel and active molecules as leads for effective antimicrobial drug development (Ahovuo_Saloranta *et al.*, 2014).

1.2.2 Inflammatory diseases and challenges with anti-inflammatory therapy

Inflammatory conditions are a leading cause of disability and death. Although rheumatoid arthritis, asthma, colitis and hepatitis are the diseases commonly associated with inflammation, the pathogenesis of several other diseases such as cardiovascular and neurodegenerative diseases, liver fibrosis as well as some cancers have been linked to inflammation (Emery, 2006; Vaziri and Rodriguez-Iturbe, 2006; Khansari *et al.*, 2009). It is known that the excessive release of reactive oxygen molecules in certain conditions causes an imbalance in cellular functions and leads to tissue damage resulting in chronic inflammatory states (Hold, 2008).

Current medications available for the treatment of inflammatory conditions belong mainly to the class of Non-Steroidal Anti-Inflammatory Drugs (NSAIDs) such as ibuprofen, aspirin and diclofenac and steroidal anti-inflammatory drugs like dexamethasone and cortisone (Gotzsche, 2000). Though effective in most acute conditions, the anti-inflammatory therapy offered by NSAIDs has been hindered by adverse effects such as gastrointestinal ulceration, intestinal perforation, cardiovascular risks and exacerbation of allergic and asthma symptoms. The NSAIDs are also highly toxic to hepatic and glomeruli cells after prolonged use leading to liver and kidney dysfunctions respectively (Fürst and Zündorf, 2014). For these reasons, their use is limited in many cases. The search for new agents that can provide optimum anti-inflammatory effect with no accompanying adverse effects is thus crucial (Wu *et al.*, 2006).

1.3 Research Aim

To investigate three Ghanaian medicinal plants namely, *Anopyxis klaineana* (Pierre) Engl. (Rhizophoraceae), *Hexalobus monopetalus* (A. Rich.) Engl & Diels (Annonaceae) and *Landolphia heudelotti* A. DC. (Apocynaceae) for anti-

inflammatory, antimicrobial and antioxidant properties and correlate the bioactivities with the constituents present.

1.3.1 Specific Objectives

- To carry out one or more of the following bioassays- anti-inflammatory, antimicrobial and antioxidant activity, on the stem bark of *A. klaineana* and *H. monopetalus* and the roots of *L. heudelotti*.
- To isolate bioactive constituents from the plants using chromatographic methods and characterize the isolated compounds by spectroscopic methods.
- To test the isolated compounds for one or more of the following: antimicrobial, anti-inflammatory and anti-oxidant activities.

1.4 Justification

It is known that out of about 27 million plant species existing on planet earth, only about 10–15 % have been explored for pharmaceutical purposes. Thus many more useful natural lead compounds could be awaiting discovery (Harvey, 2000; Saklani and Kutty, 2008).

Several plants are used traditionally because of their anti-infective properties. The efficacy of plant extracts and phytochemical constituents as antimicrobial agents have been scientifically demonstrated by many researchers (Gibbons, 2004; González-Lamothe *et al.*, 2009). For instance, the oil from *Cinnamomum osmophloeum* has been shown to possess antibacterial activity against *Enterococcus faecalis*, *Escherichia coli*, *Staphylococcus aureus* (including methicillin resistant *S. aureus*) and *Vibrio parahaemolyticus*. Cinnamaldehyde was identified as the primary antibacterial component and this compound has been broadly utilized in antiseptic mouthwashes as a result of its inhibitory effects against oral microorganisms (Wallace, 2004). Some

plant-derived products have also demonstrated resistance modulating effects in bacterial strains possessing multidrug efflux mechanisms

(Gibbons, 2005). An example is 5′-methoxyhydnocarpin (5′-MHC), isolated as a minor component of chaulmoogra oil and also found in several *Berberis* species. Though 5′-MHC had no antimicrobial activity, the compound strongly potentiated the action of berberine against *S. aureus* by inhibiting a multidrug resistant pump of the human pathogen *Staphylococcus aureus* (Stermitz *et al.*, 2000).

Although the antibiotics produced by plant products have been generally weak compared to that of antibiotics from bacteria and fungi and there is currently no major antimicrobial drug developed from plants, there is still room for optimism (Gibbons, 2004). This is because drug discovery is not only a means to discover new bioactive pure compounds, but also to develop the most promising plant therapies into effective remedies alternative to conventional drugs in CAM therapy. Thus, based on the antimicrobial results of crude extracts, the most effective plant preparations could be properly processed and incorporated into primary health care systems (Stark *et al.*, 2013).

The discovery of the anti-inflammatory agent salicin and subsequently, aspirin from *Salix fragilis* is an empirical evidence to affirm the ability of plants to produce antiinflammatory compounds (Mahdi, 2010). Other plant products such as capsaicin (*Capsicum annum*), curcumin (*Curcuma longa*) and frankincense (*Boswellia serrata*) have been effectively utilized as adjuncts in the treatment of inflammatory conditions (Chi *et al.*, 2001; Kim *et al.*, 2004). Apart from being potent, these products have an added advantage of causing no significant adverse effects or toxicity to liver and kidney cells like other synthetic anti-inflammatory agents (Meschino, 2001). Medicinal plants are therefore recognized as sources of anti-inflammatory agents and

as practicable alternatives to conventional anti-inflammatory medicines. A number of plant secondary metabolites such as apigenin, quercetin, luteolin and silymarin have also been found to possess potent antioxidant properties (Eleni and Dimitra, 2003). Like other developing countries, Ghana continues to search for more effective and appropriate ways of providing for the health needs of its growing populace (Sato, 2012). The generally high cost of orthodox medications and additionally their unavailability to the rural areas has prompted a high interest for herbal medicines which have also been shown to be effective (Tabi *et al.*, 2006). In view of this, intensive efforts are being made to explore plants that might be of therapeutic significance to the Ghanaian community (Agbovie *et al.*, 2002).

1.5 Scope of Work

Several medicinal plant species in Ghana have been identified and their ethnomedicinal usage documented (Abbiw, 1990; Mshana *et al.*, 2000; Agbovie *et al.*, 2002). *Anopyxis klaineana* (Pierre) Engl. (Rhizophoraceae), *Hexalobus monopetalus* (A. Rich.) Engl. & Diels (Annonaceae) and *Landolphia heudelotti* A. DC. (Apocynaceae) are used traditionally for the treatment of a variety of ailments including skin, respiratory and sexually transmitted infections, pain, arthritis and for wound healing. This indicates the possible presence of constituents with antimicrobial, anti-inflammatory and antioxidant properties in these plants.

Currently, there is little or no scientific justification for their biological effects and the chemical constituents which could be responsible for the observed biological activity are yet unknown. This research was to investigate some biological properties of the plants and the constituents in them. A successful completion of this project would thus give scientific credence the ethno-medicinal use of the plants under investigation and

offer new compounds that may be potential drugs or lead structures for the synthesis of potent antibacterial, anti-inflammatory and antioxidant agents in future.

1.6 Limitation

The limitation of this study was the paucity of compounds obtained after chromatographic purification of crude extracts. This limited the performance of biological assays of some isolates.

CHAPTER 2

LITERATURE REVIEW

2.1 Inflammation

Inflammation is a complex defensive response of living tissues to injury, irritation or infection which is accompanied by typical symptoms of pain, swelling, redness and fever (Kim *et al.*, 2004). Although inflammation is a defensive mechanism, the complexity of events as well as the mediators released often result in the induction or aggravation of several disease conditions such as rheumatoid arthritis, chronic inflammatory bowel diseases, asthma, type 2 diabetes, cardiovascular diseases, neurodegenerative diseases and some cancers (Fürst and Zündorf, 2014).

The arachidonic acid pathway plays an important role in the pathophysiology of inflammation (Fig. 2.1). The release of arachidonic acid from membrane phospholipids (during injury or irritation) and its subsequent metabolism involves a cascade of enzymatic reactions and production of mediators which results in

inflammation. One of the major end products of arachidonic acid metabolism is prostaglandin E_2 (PGE_2), a prostanoid fatty acid derivative with a wide range of physiological functions including the regulation of inflammation and immunity (Frolov *et al.*, 2013). Its production is catalysed by three main enzymes namely phospholipase A_2 (facilitates the release of arachidonic acid from membrane bound phospholipids), cyclooxygenases, COX-1 and COX-2 (conversion of arachidonic acid to PGG_2 and PGH_2) and microsomal prostaglandin E synthetase (mPGES) (conversion of PGH_2 to PGE_2) (Ivanov and Romanovsky, 2004) (Fig. 2.1). COX and PGES exist in different isoforms that are activated by inflammatory stimuli to produce prostaglandins. Therefore compounds that can block one or more of the steps involved in the synthesis of PGE_2 such as COX-inhibitors (e.g. NSAIDs) and phospholipases inhibitors (e.g. corticosteroids) are potent anti-inflammatory agents (Jabbour *et al.*, 2002; Cipollone *et al.*, 2008; Hevesi *et al.*, 2009).

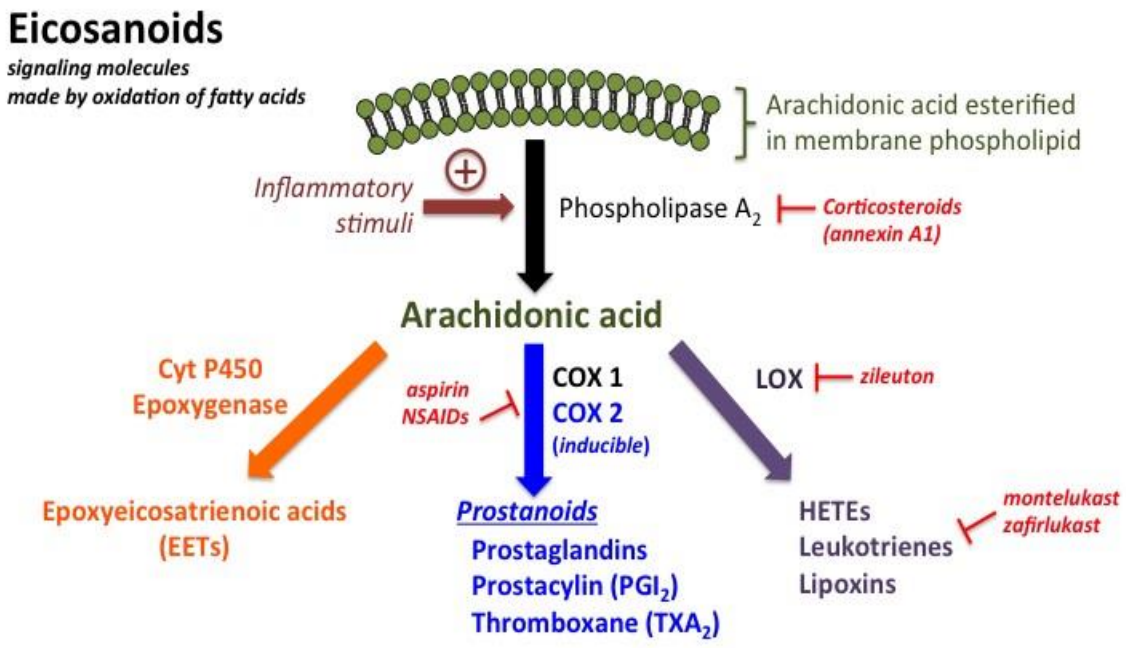

Fig. 2.1: Arachidonic acid metabolism pathway (http://tmedweb.tulane.edu/pharmwiki/doku.php/eicosanoids_draft)

The most commonly used drugs are those affecting the COX pathway called the nonsteroidal anti-inflammatory drugs (NSAIDs) which non-selectively block both COX1 & COX-2 and reduces the synthesis of prostanoids (prostaglandins). Prostaglandin however plays an important role in the body by protecting the stomach lining against injury by its acidic environment. This occurs as a result of the vasodilatory effects of prostaglandins which enhances mucosal blood flow and oxygen delivery to epithelial cells and promote the secretion of mucin and bicarbonates. The action of NSAIDs thus deprives the stomach of the cytoprotective effects of prostaglandins making the stomach more susceptible to GI side effects such as peptic ulceration (Seminerio *et al.*, 2014) (Fig. 2.2).

The structural differences between the active receptor sites for COX-1 and COX-2 enzymes permitted the development of drugs highly selective for inhibition of COX2 (e.g. celecoxib). These drugs are not highly expressed in the GIT and therefore act with fewer effects on the GIT. Nevertheless, the use of COX-2 selective inhibitors has been associated with an increased risk of cardiovascular diseases (Fig. 2.2) (Seminerio *et al.*, 2014).

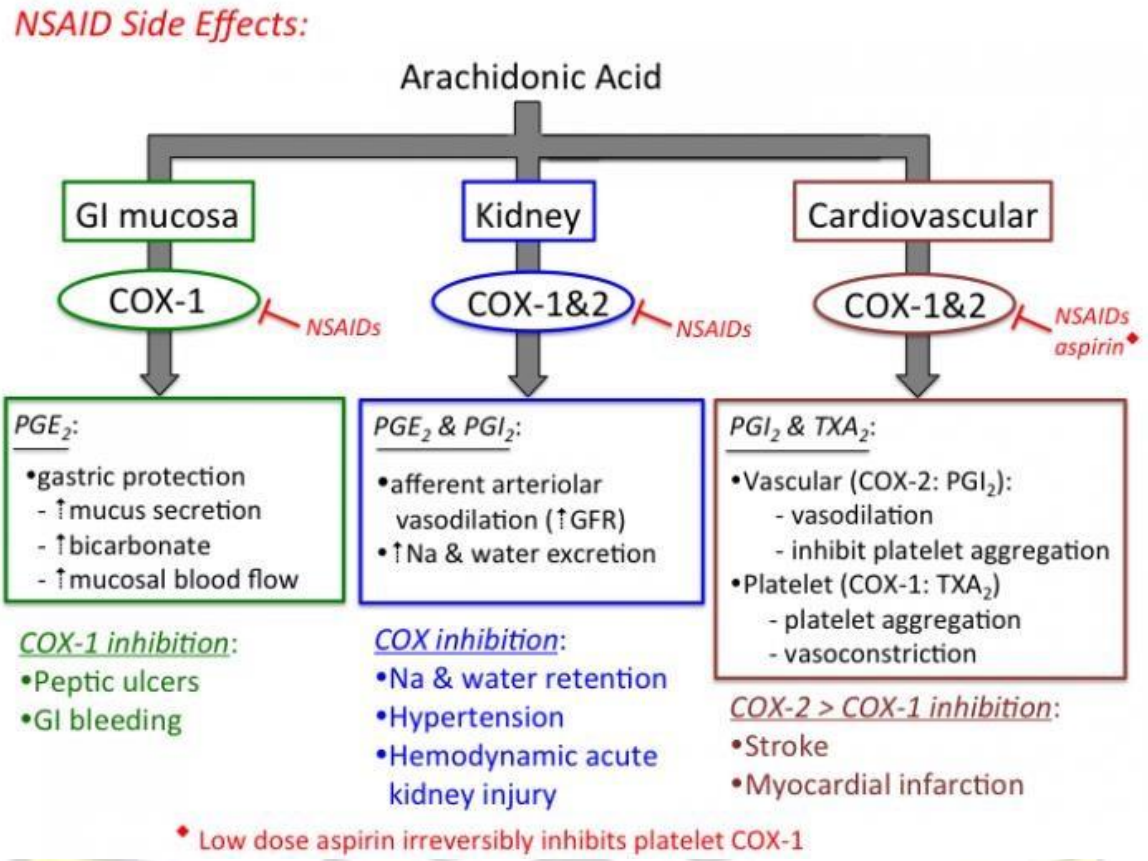

Fig. 2.2: Mechanisms of NSAIDs side effects

(http://tmedweb.tulane.edu/pharmwiki/doku.php/eicosanoids_draft)

2.1.1 Oxidative stress and inflammation

Small quantities of reactive oxygen species (ROS) such as superoxide ($O_2^{\cdot-}$), hydrogen peroxide (H_2O_2) and hydroxyl radical (OH^-), are generated under normal conditions as by-products of aerobic metabolism. These molecules play very important roles in the body as cell signalling molecules and as defence molecules against invading pathogens (Vaziri and Rodriguez-Iturbe, 2006; Seifried *et al.*, 2007). Under normal physiological conditions, ROS produced by the body are neutralized safely by the body‘s antioxidant defence system which includes neutralization by enzymes e.g. superoxide dismutase, catalase and glutathione peroxidase as well as by dietary antioxidants such as ascorbic acid, alpha- tocopherol and glutathione (Nimse and Pal, 2015). During pathological conditions however, an imbalance between the neutralization capacity of the body‘s

antioxidant defence system and the rate of ROS production may occur leading to a state referred to as oxidative stress. Numerous pathological conditions including chronic inflammatory diseases, cancers, cardiovascular diseases, diabetes mellitus and neurological disorder develop as a consequence of oxidative stress (Kinnula and Crapo, 2004; Singh and Jialal, 2006; Vaziri and Rodriguez-Iturbe, 2006; Waris and Ahsan, 2006).

Current studies have revealed that oxidative stress and inflammation are inseparably linked; one brings about the other to form a circuit (Gill *et al.*, 2010; Salzano *et al.*, 2014). Certain ROS function as messenger molecules to propagate inflammatory signals (Sen and Packer, 1996). A well-established example is the activation of the redox-sensitive signal transduction pathway of nuclear factor kappa B (NF-κB) cells by micro-molar concentrations of H_2O_2 (Schreck *et al.*, 1992; Hensley *et al.*, 2000). Since the production of ROS is an inherent property of activated immune cells, inflammation will always lead to oxidative stress in affected tissues and vice versa The role of antioxidants in the management of chronic inflammatory conditions is therefore very important (Wu *et al.*, 2006).

2.2 Anti-inflammatory agents from plant sources

Plant constituents including phenolic compounds, triterpenes and alkaloids have been shown experimentally to interfere with several inflammatory mediators and mechanisms (Kim *et al.*, 2004).

Plant phenolic compounds such as curcumin [11] (from *Curcuma longa*, Zingiberaceae), resveratrol [12] (from *Citrus paradisi*) and epigallocatechin gallate [13] (from *Camellia sinensis*), have demonstrated significant anti-inflammatory activity in various assay models (Fig. 2.3). Mechanisms of anti-inflammatory action

suggested for most phenolic compounds include *(i)* the inhibition of important proinflammatory signalling cascades such as cyclooxygenase (COX-) and lipoxygenase

(LOX) pathways and *(ii)* inhibition of nitric oxide production (iNOs) (Santos, 2003; Fürst and Zündorf, 2014). Flavonoids such as baicalein [14] and baicalin [15] (from *Scutellaria baicalensis,* Lamiaceae) have been shown to possess significant antiinflammatory activity (Lin and Shieh, 1996; Li *et al.*, 2000; Shen *et al.*, 2003). Other naturally occurring plant flavonoids such as luteolin [16], morin [17], chrysin [18], rutin [19], quercetin [20], wogonin [21] and apigenin [22] are also effective inhibitors of COX-2 activity (Kim *et al.*, 2004; Santos, 2004) (Fig. 2.3).

Pentacyclic triterpenes such as lupeol [23], ursolic acid [24] and oleanolic acid [25] are other examples of anti-inflammatory phytochemicals which have been shown to selectively inhibit COX-2 enzyme and prevent the release of PGE_2 in macrophages (Suh *et al.*, 1998; Ikeda *et al.*, 2008) (Fig. 2.3). Boswellic acid [26] and derivatives obtained from the gum resin of *Boswellia species* (Burseraceae) were also found to produce anti-inflammatory activity by the inhibition of lipooxygenase (LOX) enzyme in animal model experiments (Siemoneit *et al.*, 2011).

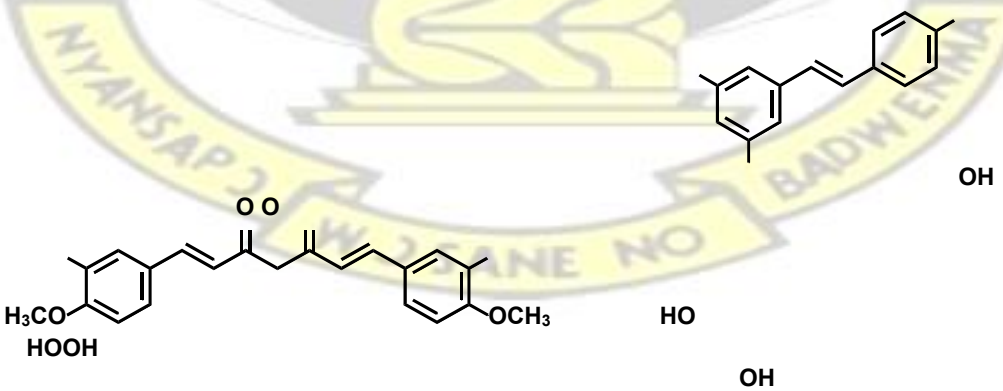

curcumin [11]

resveratrol [12]

	R1	R2	R3	R4
luteolin [16]	H	OH	OH	H
baicalin [14]	OH	H	H	H
chrysin [18]	H	H	H	H
wogonin[21]	H	H	H	OCH3
apigenin [22]	H	OH	H	H

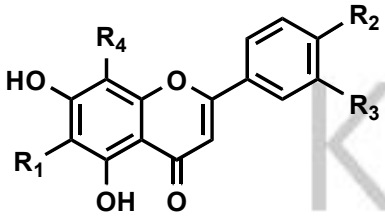

epigallocatechin gallate [13]

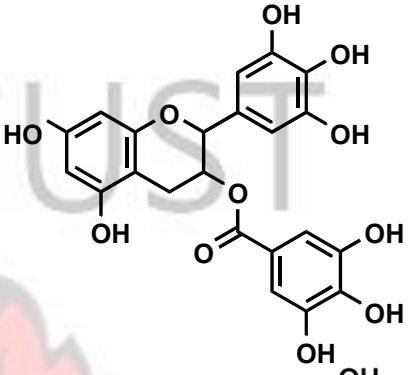

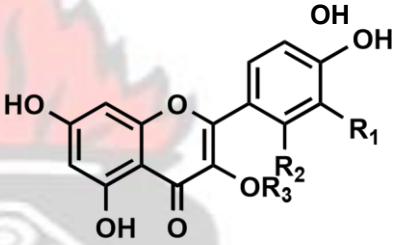

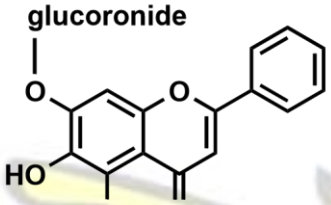

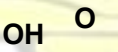

baicalein [15]

	R1	R2	R3
morin [17]	H	OH	H
rutin [19]	OH	H	Glu-Rha
quercetin [20]	OH	H	H

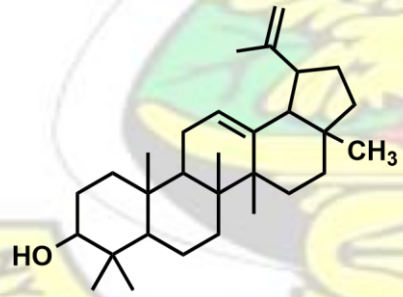

lupeol [23]

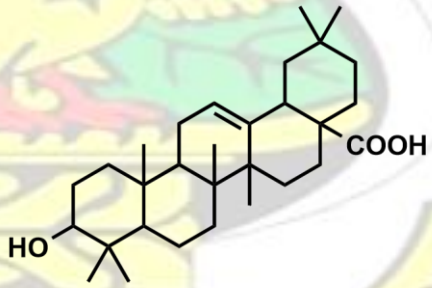

oleanolic acid[24]

Fig. 2.3: Anti-inflammatory and antioxidant agents from plant sources
(Refer to Section 2.2)

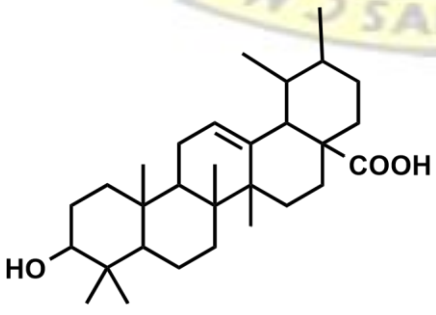

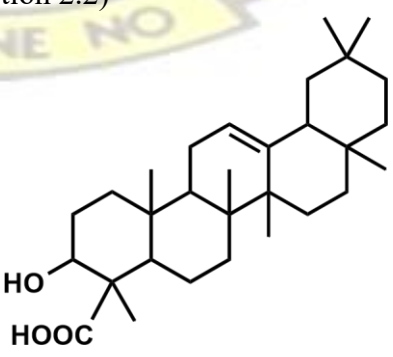

ursolic acid [25]

boswellic acid [26]

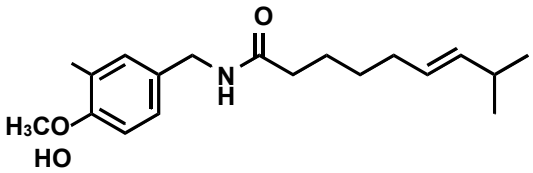

capsaicin [27]

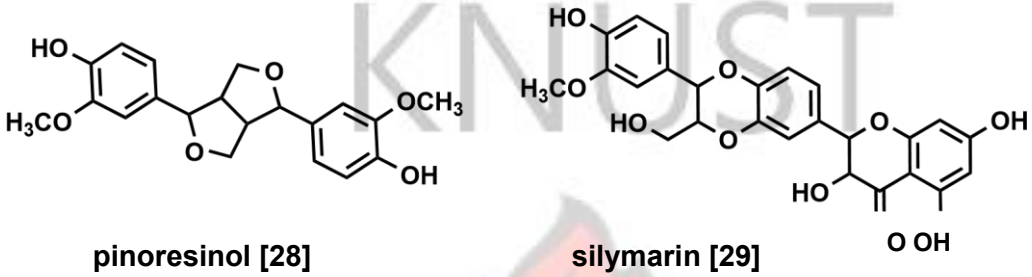

pinoresinol [28]

silymarin [29]

Fig. 2.3 *continued*: Anti-inflammatory and antioxidant agents from plant sources (Refer to Section 2.2)

Capsaicin [27], the well-known compound isolated from chilli peppers (*Capsicum species*; Solanaceae), is known to have both analgesic and anti-inflammatory activities (Santos, 2003). The anti-inflammatory effects of lignans, such as pinoresinol [28] (Fig. 2.3) have also been established (Cho *et al.*, 2001).

Currently, standardized extracts of some medicinal plants are in use for the management of various pathologies whose activities have been determined to be by the interference of prostanoid synthesis mainly by inhibition of LOX and COX enzymes. Examples of such plants include *Echinacea purpurea* (Asteraceae), *Hamamelis virginiana* L. (Hamamelidaceae), *Urticadioica* L. (Urticaceae), *Rheum palmatum* L. (Polygonaceae) and *Allium sativum* L. (Liliaceae) (Santos, 2003).

Apigenin, quercetin, luteolin and silymarin [29] (Fig. 2.3) are examples of plant constituents that have been found to exhibit potent antioxidant activities (Eleni and Dimitra, 2003; Mathew and Abraham, 2006). The mechanism of antioxidant action of phenolic compounds from plants have been proposed to be due to their redox

properties, which allow them to act as reducing agents, hydrogen donors and singlet oxygen quenchers. In addition, some have a metal chelation potential while others function as enzyme inhibitors (Rice-Evans *et al.*, 1997). The anti-inflammatory activity of most plant secondary metabolites have been linked to their antioxidant properties (Chi *et al.*, 2001; Eleni and Dimitra, 2003).

2.3 Anti-inflammatory screening methods

Based on the symptoms of inflammation, a number of *in vivo* and *in vitro* screening methods have been described to evaluate the anti-inflammatory activity of plant extracts and pure compounds. To measure the anti-inflammatory activity *in vivo*, the carrageenan induced paw oedema in rats or chicks, croton-oil or oxazolone induced ear oedema in mice, UV erythema in guinea pigs and pleurisy in mice are some applicable methods (Whiteley and Dalrymple, 2001). *In vitro* methods have mainly focused on the inhibition of various endogenous inflammatory mediators such as tumour necrosis factor alpha (TNF –α), interleukins (IL-4, IL-1) interferon-λ (IFN-λ), COX, LOX, PGE_2, nitric oxide and reactive oxygen species (Hariram Nile and Won Park, 2013). For the purposes of this study, the carrageenan induced paw oedema test and a modified prostaglandin E_2 (PGE_2) competitive inhibition assay were applied for *in vivo* and *in vitro* assays respectively and are hereby described.

2.3.1 Carrageenan–induced paw oedema assay

Paw swelling or footpad oedema has been shown to be a suitable method for evaluating inflammatory responses to antigenic challenges and irritants (Whiteley and Dalrymple, 2001). Carrageenan, a muco-polysaccharide extract from the red alga, *Chondrus crispus*, is a widely used irritant for the induction of inflammation in laboratory animals (Morris, 2003). The carrageenan induced paw oedema assay constitutes a

simple routine animal model (mouse, rat or chick) for the evaluation of swelling (oedema) at the site of inflammation (Necas and Bartosikova, 2013). The acute inflammation produced by carrageenan has been described as a biphasic event which results from the vasodilation of blood vessels leading to increased vascular permeability and cellular infiltration to the site of carrageenan injection (Posadas *et al.*, 2004). The initial phase of oedema (0 - 1 h) has been attributed to the release of histamine, serotonin and bradykinin and is not inhibited by non-steroidal antiinflammatory drugs. In contrast, the later phase of swelling (1 - 6 h) has been attributed to the release of prostaglandins (Roach and Sufka, 2003; Posadas *et al.*, 2004). Freshly prepared solution (1-2 %) of carrageenan in saline is injected into the paw of the animal. An inflammatory response, characterized by oedema formation (swelling at the site of injection) is measured for a period of time. The inflammatory response is quantified by increase in paw size (oedema) after carrageenan injection. Typically, test compounds are assessed for anti-inflammatory activity by examining their ability to reduce or prevent the development of paw swelling (Whiteley and Dalrymple, 2001; Roach and Sufka, 2003).

2.3.2 Modified prostaglandin E_2 (PGE_2) competitive inhibition assay

Monoclonal antibodies have been shown to possess catalytic groups, whose spatial arrangements resemble those observed in enzyme and receptor structures, implying that antibodies can mimic enzymes or receptors (Ducancel *et al.*, 1996). As demonstrated by the example of the bean α-amylase inhibitor (α-AL) which mimics the carbohydrate substrate of its enzyme target, antagonists or inhibitors often possess similar structural groups as the substrate (Transue *et al.*, 1998). Based on these principles, a forward sequential competitive binding technique in which molecules with anti-inflammatory structural groups in a sample (COX-inhibitory groups, PG analogues) compete with horseradish peroxidase (HRP)-labelled PGE_2 for a limited

number of binding sites on a mouse monoclonal antibody was employed (Hevesi *et al.*, 2009). This was to identify compounds with structural types that can competitively inhibit PGE_2 from binding to its receptors (the monoclonal antibody mimics the receptor). The anti-inflammatory structural groups in the sample are allowed to bind to the antibody in the first incubation, after which HRP-labelled PGE_2 binds to the remaining antibody sites. Following a wash to remove the unbound materials, a substrate solution is added to the wells to determine the bound enzyme activity by measuring the absorbance for each sample at 450 nm. There is an inverse relationship between optical density (OD) and the amount of PG analogues or anti-inflammatory structural groups in the analyte. As the concentration of antiinflammatory groups in the test sample increases, lesser HRP-PGE_2 binds to the antibody resulting in decreased optical density.

2.4 Antioxidant screening methods

A number of *in vitro* methods have been developed to ascertain the potential of natural products as antioxidant agents (Chanda and Dave, 2009; Nimse and Pal, 2015). These include the DPPH free radical scavenging assay, superoxide and hydroxyl scavenging assays, lipid peroxidation, phosphomolybdenum total antioxidant capacity and ferric reducing power assays. Due to the complexity of phytochemicals and their various reaction mechanisms, it is essential to use more than one assay method to assess the antioxidant capacity of plant extracts. The methods used as regards to this project are briefly discussed below:

2.4.1 2, 2-diphenyl-1-picrylhydrazyl (DPPH) free radical scavenging assay

DPPH is a free stable radical ion that reacts with compounds that can donate a hydrogen atom. The DPPH radical scavenging assay is based on the reduction of

methanol solution of DPPH by a hydrogen donating antioxidant to form the nonradical form DPPH-H (Fig. 2.4).

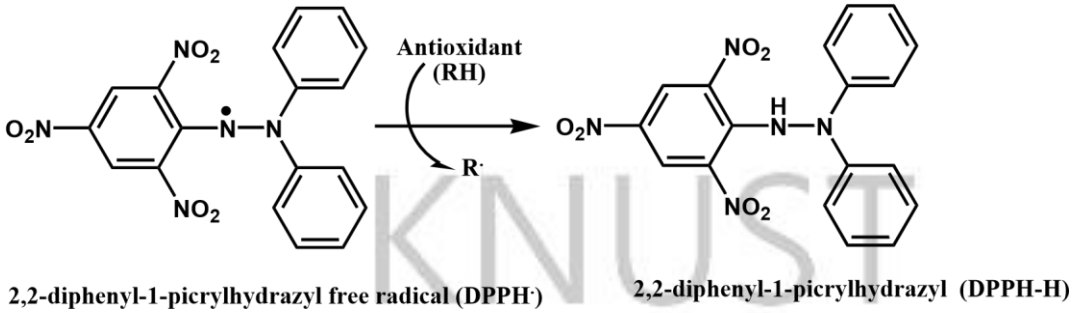

Fig. 2.4: Schematic presentation of DPPH scavenging by an antioxidant (Nimse and Pal, 2015)

A colour change form purple to yellow results due to this transformation and is measured by UV spectrometer at 517 nm (Nimse and Pal, 2015). There is a decrease in absorbance of DPPH at its absorption maxima of 517 nm, which is inversely proportional to concentration of free radical scavenger added to DPPH reagent solution. The result is expressed as the concentration required for decreasing the concentration of free radical by 50 % (IC_{50}).

2.4.2 Total phenolic content

Plant polyphenols, which include flavonoids, phenolic acids and tannins have ideal chemical structures which make them potent radical scavengers (Blokhina *et al.*, 2003). The total phenolic content is usually measured by a method using FolinCiocalteu reagent (McDonald *et al.*, 2001). The method is based on the reduction of the Folin-Ciocalteu‘s reagent by phenolic compounds to form a mixture of blue oxides with UV absorption maxima in the 760 nm region. Tannic acid is used as a standard and the total phenolic content is expressed in mg/g tannic acid equivalent (TAE).

2.4.3 Total Antioxidant capacity

This is a spectroscopic method for the quantitative determination of antioxidant capacity, through the formation of phosphor-molybdenum (Mo) complex. The assay is based on the reduction of Mo (VI) to Mo (V) by the sample analyte and subsequent formation of a green phosphate Mo (V) complex at acidic pH (Prieto *et al.*, 1999). Ascorbic acid is used as the standard reference and the result is expressed in mg/g ascorbic acid equivalent

2.5 Antimicrobial agents from plant sources

The apparent scarcity of disease and longevity of wild plants indicate that plant defence mechanisms in combating pathogenic infection may supersede that of the mammalian immune systems (Rios and Recio, 2005). Traditional healers have used plants to prevent or cure infectious diseases for many years and some of these remedies are still used in modern TCAM (Cowan, 1999; Martin and Ernst, 2003).

Though microorganisms have been the major source of antimicrobial compounds, plants products have been seriously considered as sources of antimicrobial agents. This is because plants have the ability to produce toxic agents (phyto-anticipins and phytoalexins) to protect themselves against invading pathogens (González-Lamothe *et al.*, 2009). Secondly, plant antibacterial products are synthesized following microbial attack to protect themselves against further attack by pathogenic microbes in their environment (Gibbons, 2004). It is also believed that due to the chemical diversity of plant secondary metabolites, their antimicrobial activities could be by mechanisms that are entirely different from the presently used antibiotics and may thus have clinical value in the treatment of resistant microbial strains. Such compounds may not have the problem of microbial resistance and with some

structural modification their activity could be diversified (Umeh *et al.*, 2005).

Some classes of antimicrobial phytochemical constituents include volatile and essential oils, polyphenols [36-38, 44], coumarins [39], quinones [40-41], flavonones [42-43], flavonoids, tannins, alkaloids [45-47], and terpenes [48] (Fig. 2.5) (Cowan, 1999; Rios and Recio, 2005; Das *et al.*, 2010).

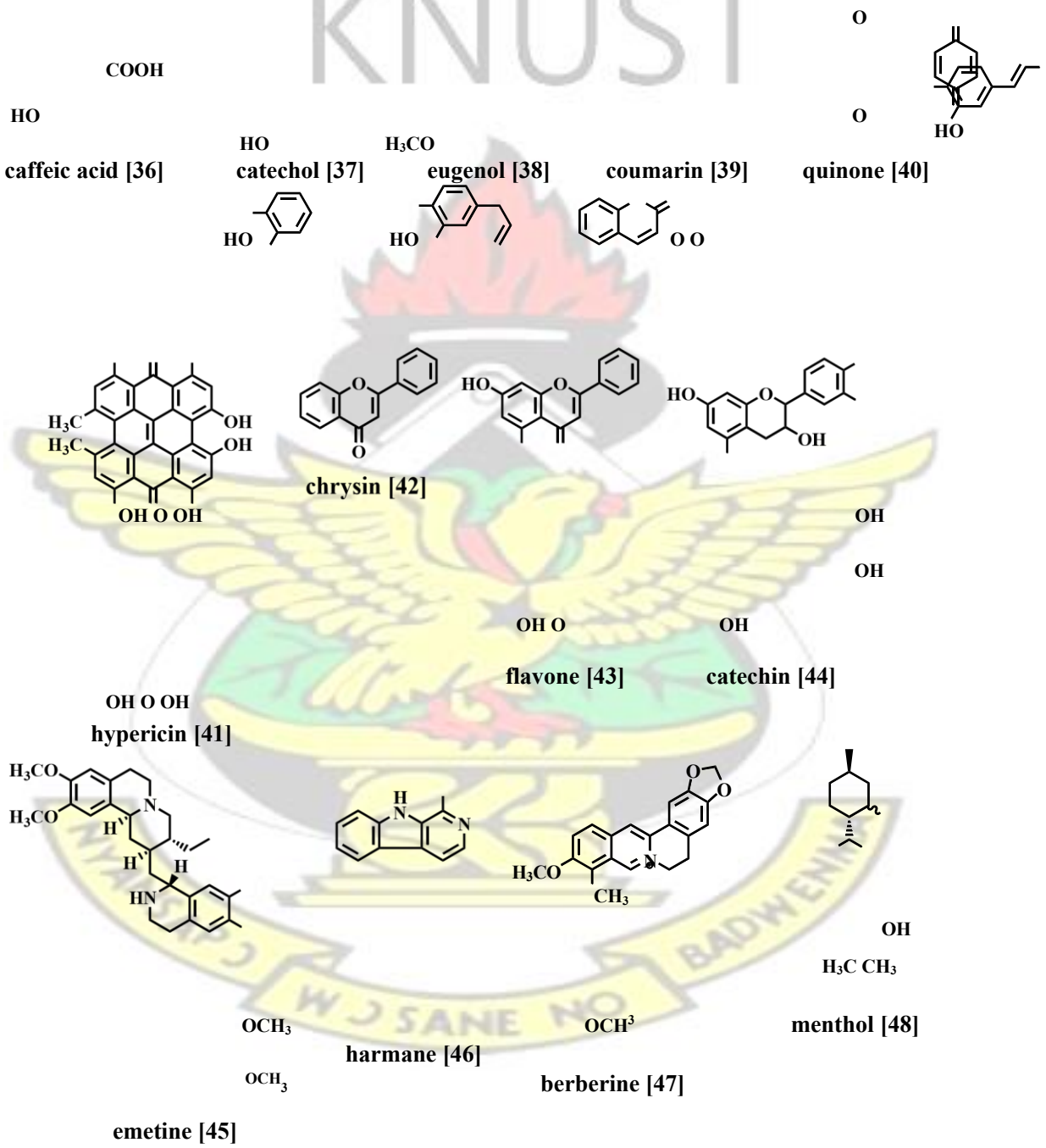

Fig. 2.5: Antimicrobial constituents from plant sources

(Refer to Section 2.5)

2.6 Antimicrobial screening methods

The antimicrobial susceptibility test (AST) is the first step towards new anti-infective drug development (Ncube *et al.*, 2008). It is used in ethno-pharmacology research to screen potential antimicrobials from natural product extracts for efficacy against microbial species and to determine their minimum inhibitory concentrations (MIC). AST is divided into diffusion and dilution methods (Das *et al.*, 2010).

2.6.1 Agar diffusion method

The basic principle underlying the diffusion methods is the transfer of the active principle from a reservoir into a pre-inoculated solidified medium. The two main assay methods based on this principle are the disc diffusion and agar well diffusion methods (Salie *et al.*, 1996; Norrel and Messley, 1997). The difference between the two methods is the reservoir from which the test samples diffuse into the growth medium. While the former employs a sterile impregnated paper disc as its reservoir, the latter requires a punched hole in the growth medium as a reservoir.

The TLC bio-autography is a variation of the agar diffusion method which is employed to detect the active components of crude extracts after separation of components on a TLC plate (Silva *et al.*, 2005). In this method, the analyte, in this case, the extract, is adsorbed onto a thin layer chromatography plate by developing with appropriate solvent systems. A standardized inoculum of organism in growth medium is then sprayed or poured over the developed plate and incubated. Microbial indicators (usually tetrazolium salts) are used as growth detectors (Silva *et al.*, 2005). Antimicrobial activity of extracts is detected as clear (white) zones on the TLC plate against a purple background.

The main advantage of the diffusion methods is the ability to test different extracts (or different concentrations of test samples) against a single organism on one plate. The diffusion methods are however not suitable for non-polar compounds which are unable to sufficiently diffuse into the aqueous growth media. All diffusion methods are also qualitative and suitable in preliminary screening and identification of leads but not for quantification of bioactivity (Hammer *et al.*, 1999; Nostro *et al.*, 2000; Langfield *et al.*, 2004). They do not distinguish between bactericidal and bacteriostatic effects and MICs are usually not determined by this method (Parekh *et al.*, 2006). The disadvantage of the TLC bio-autography method is the disruption of synergism among active constituents in an extract, thereby reducing its activity (Schmourlo *et al.*, 2005).

2.6.2 Dilution methods

Dilution methods are useful for quantitative determination of the bioactivity of large numbers of test samples against a range of organisms. Either solid or liquid media may be used for the dilution assays (Vanden-Berghe and Vlientinck, 1991; Eloff, 1998). Different concentrations of the test samples are added to a pre-inoculated volume of liquid media and incubated for a period of time. To determine the antimicrobial activity, measurements of turbidity or redox indicators such as tetrazolium salts e.g. 3-(4,5-Dimethylthiazol-2-yl)-2,5-diphenyltetrazolium bromide (MTT) or resazurin dye are employed (Umeh *et al.*, 2005). The advantages of dilution methods over the diffusion methods are the increased sensitivity for both polar and non-polar extracts, the possibility to distinguish between bacteriostatic and bactericidal effects and the quantitative determination of the minimum inhibitory concentration (MIC) (Langfield *et al.*, 2004).

2.7 Current approaches for the isolation of natural products

Drug discovery from medicinal plants has evolved to include numerous fields of inquiry and various methods of analysis. Screening of natural products for new lead compounds or for scientific validation of their ethno-pharmacological uses involves the isolation of active secondary metabolites from biologically complex mixture of constituents (Vuorela *et al.*, 2004; Singh and Barrett, 2006). The characteristic diversity of plant metabolites, though attractive, is accompanied by significant technical difficulties for the separation, detection and rapid characterization of biologically active chemical structures present in the screened mixtures. It is thus essential to have efficient systems available for the rapid screening of plant extracts selected for investigation.

Over the years, rapid chromatographic techniques which do not lead to material loss, decomposition or artefact formation have been used to overcome known complex separation problems (Hostettmann and Marston, 2002). The use of high performance liquid chromatography (HPLC) coupled with various spectroscopic techniques such as high resolution mass spectrometry (LC/HRMS), UV diode array (LC/UV) or nuclear magnetic resonance (LC/NMR) has resulted in efficient separation and rapid characterization of natural products (Wolfender *et al.*, 2003; Vuorela *et al.*, 2004). The introduction of High-Throughput Screening (HTS) for the chemical analysis and characterization of libraries of natural products as well as automated online biological activity testing has also accelerated the drug discovery process in pharmaceutical industries (Eldridge *et al.*, 2002).

Bioassay-guided fractionation which is an approach requiring that each chromatographic separation is followed by a separate *in vitro* or *in vivo* bioactivity testing of crude extracts, fractions, sub-fractions and pure isolates enables the

researcher to eliminate inactive fractions from further processing and focus on the highly active fractions (Singh and Barrett, 2006; Stark *et al.*, 2013). Once the novelty or biological activity of an individual constituent is established, the plant extract may be processed in the same manner to isolate other derivatives (Hostettmann, 1998; Gurib-Fakim, 2006). However, it must be noted that the biological activity of crude extracts may also be as a result of synergistic effects of a number of chemical constituents. Therefore inactivity of individual pure compounds does not imply inactivity of the total extract (Schmourlo *et al.*, 2005)

2.8 Selection of plants for phytochemical and biological study

The selection of plants for investigation was based on the principle that the indigenous use of medicinal plants in traditional medicine can offer indications to their biological activities (Oubre *et al.*, 1997; Iwu and Wootton, 2002).

2.8.1 Anopyxis klaineana (Pierre) Engl. (Rhizophoraceae)

Anopyxis klaineana (Pierre) Engl. is a medium-sized tree (up to 50 m tall and 120 cm wide) distributed in the evergreen forests of most tropical countries including Ghana (Oteng-Amoako, 2011). It is the only species of the genus *Anopyxis* which was earlier considered to be an un-described genus of the family Meliaceae due to striking similarities of its inflorescence to plants of the family Meliaceae, especially its flower style that is commonly referred to as an *Entandrophragma style* (Steentoft, 1988). The plant was eventually determined to belong to the family Rhizophoraceae, near the genus *Macarisia* due to more closer similarities in inflorescence, habitat and the general anatomical features of the leaf and stem (Sprague and Boodle, 1909). It is commonly known as the white oak and traded in Ghana as ―kokoti(e)‖ (*Akan*) (Burkill, 1997).

2.8.1.1 Geographical distribution and ecology

Anopyxis klaineana is widespread, occurring in Sierra Leone, Central African Republic, DR Congo, Cote d'Ivoire, Angola and Ghana. The plant grows in wet evergreen and semi-deciduous forests, and its abundance increases with rainfall (Burkill, 1997).

2.8.1.2 Morphological description

The outer stem bark surface is longitudinally fissured, greyish-brown, with a pale orange-pink inner bark. It has leathery, glabrous leaves which are simple and entire and occur in whorls of two to four. The leaf blade is oblong to elliptical in shape and obovate to obtuse at base. Flowers are bisexual, regular, usually greenish white. It has short-hairy stamens which are fused into a tube and a superior ovary. The fruit is an ovoid to obovoid capsule, dehiscing with 5 woody valves, with up to ten seeds. Seeds are slightly curved, flattened and brownish in colour (Oteng-Amoako, 2011).

(a)  (b) 

(c) 

Fig. 2.6: Leaf (a), outer stem bark (b) and inner stem bark (c) of *A. klaineana*

2.8.1.3 Ethno-medicinal uses

The stem bark macerate of *A. klaineana* is used in traditional medicine to treat gonorrhoea and as an enema to treat gastrointestinal infections. The pounded bark is also applied topically against arthritis, bronchitis, skin infections and wounds. A decoction of the bark is administered to treat lower abdominal pain (Burkill, 1997; Oteng-Amoako, 2011). In Ghana, the leaves are also used to treat malaria (Asase *et al.*, 2012).

2.8.1.4 Reported biological activity or bioactive compounds

There are no previous scientific reports on the biological activities or phytochemistry of *Anopyxis klaineana*.

2.8.2 Hexalobus monopetalus (A. Rich.) Engl. & Diels (Annonaceae)

The genus *Hexalobus* consists of five species of large trees or shrubs distributed across tropical Africa. *Hexalobus monopetalus* (A. Rich) Engl. & Diels (also known as *Hexalobus senegalensis* A. DC.) is one of the five species with the second widest distribution for the African Annonaceae (Botermans *et al.*, 2011). The plant is locally known in Ghana as *etwa prada* or *endwa* (Akan).

2.8.2.1 Geographical distribution and ecology

H. monopetalus is located in most parts of West and South Africa. The specie is often found growing on sandy soil in dry ecosystems such as savannah and woodlands (Botermans *et al.*, 2011).

2.8.2.2 Morphological description

H. monopetalus is a deciduous shrub or small tree of about 10 to 15 m tall with erect or spreading habitat and low branches. The reddish brown bark may be rough or smooth, fissured or flaking with a fibrous fracture. The leaf blade is elliptic with obtuse apex. The base is rounded. The upper surface of the leaf is often faintly glossy and glabrous while the lower surface is densely covered with light-brown hairs. The flowers are found in whorls of 1-3. The plant produces red fruits in clusters of 4-5.

The whitish fruit pulp bears dull, brown slightly flattened ellipsoid to ovoid seeds about 2-11 in number (Burkill, 1985; Botermans *et al.*, 2011).

(a)  (b) 

Fig. 2.7: Leaf (a), stem bark (b) of *H. monopetalus*

2.8.2.3 Ethno-medicinal uses

The roots of *H. monopetalus* are macerated and applied topically on cuts and wounds to heal (Arnold and Gulumian, 1984). A decoction of root bark is used against inflammatory disorders such as arthritis, rheumatism, articular pains, cramps and joint

stiffness (Akah and Nwambie, 1994). The leaves, stems and root bark decoctions are also used to treat sexually transmitted diseases such as syphilis, gonorrhoea, chlamydia and trichomoniasis (Kayode and Kayode, 2008). The stem bark maceration is applied topically to treat various skin infections (Bouquet and Debray, 1974). The stem bark decoction is used to treat gastric ulcers, colic and dyspepsia (Kerharo and Adam, 1964).

2.8.2.4 Phytochemistry of the genus *Hexalobus*

Two species in the genus *Hexalobus* have been investigated for their phytochemical constituents. These are *Hexalobus crispiflorus* and *Hexalobus monopetalus*. From these two species, alkaloids belonging to two classes- prenylated indole alkaloids (Figs. 2.8-2.10) and nor-aporphinoid alkaloids (Fig. 2.11) have been previously identified.

The prenylated indole alkaloids were identified as the major constituents of the stem bark, leaves and fruits of *H. crispiflorus* and *H. monopetalus* (Achenbach, 1986; Achenbach *et al.*, 1995; Malebo *et al.*, 2014). The summary of compounds identified from the genus *Hexalobus* is presented in Figs. 2.8-2.10 and Tables 2.1-2.3. Geranial, neral, linalool (E)-anethole and caryophyllene oxide were also identified in the leaf oil (Leclercq *et al.*, 1997).

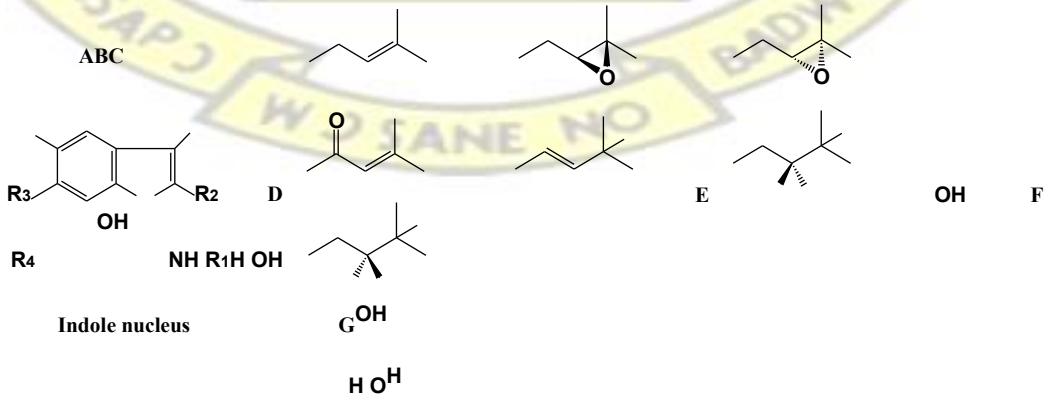

Fig. 2.8: Prenylated indole alkaloids from the genus *Hexalobus*

Table 2.1: Diprenylated alkaloids isolated from the genus *Hexalobus*

Name of compound	**R_1**	**R_2**	**R_3**	**R_4**
3,5-Hexalobine A	H	A	A	H
3,6-Hexalobine A	H	A	H	A
3,5-Hexalobine B	H	C	A	H
3,6- Hexalobine B	H	B	H	A
3,5-Hexalobine C	H	C	B	H
3,6-Hexalobine C	H	B	H	B
3,5-Hexalobine D	H	C	D	H
3,5-Hexalobine E	H	C	E	H
2,3-Hexalobine E	E	B/C	H	H

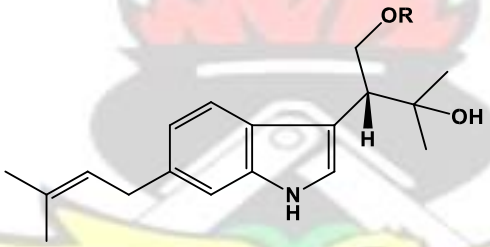

Fig. 2.9: Prenylated indole alkaloids from the genus *Hexalobus*

Table 2.2: Diprenylated alkaloids isolated from the genus *Hexalobus*

Name of compound	**R**
(2'R)- 3- (3'-Hydroxy-3'-methyl-l' -palmitoyloxybut-2'-yl) -6-(3"-methyl2"-butenyl)indole	Palmitoyl
(2'R) -3- (3'-Hydroxy-3'-methyl-l '-oleoyloxybut-2'-yl) -6- (3"-methyl-2"butenyl) indole	Oleoyl
(2'R)- 3-(1' ,3'-Dihydroxy-3'-rnethylbut-2-yl-) 6 -(3"-methyl-2"butenyl)indole	H

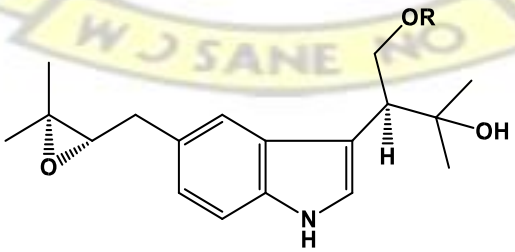

Fig. 2.10: Prenylated indole alkaloids from the genus *Hexalobus*

Table 2.3: Diprenylated alkaloids isolated from the genus *Hexalobus*

Name of compound	**R**
(2'S,2"S)-5-(2",3"-Epoxy-3 -methylbutyl -) 3'-methyl-l'-palmitoyloxybut2'-yl)indole	Palmitoyl
(2'S,2"S)- 5-(2",3"-Epoxy-3"-methyl butyl-)3- (3'-hydroxy-3' -methyl-1 'oleoyloxybut-2'-yl) indole	Oleoyl
(2'S,2"S)- 5- (2",3"-Epoxy-3"-methyl butyl-)3 - (3'-hydroxy-l'- (Z,Z)-linoleoyloxy-3'-methylbut-2'-yl)indole	Linoleoyl
5-(2‘‘,3-epoxy-3-methylbutyl)-3-(3‘-hydroxy-3‘-methyl-1‘-aceotxy-but2‘-yl)indole	-C-OCH_3

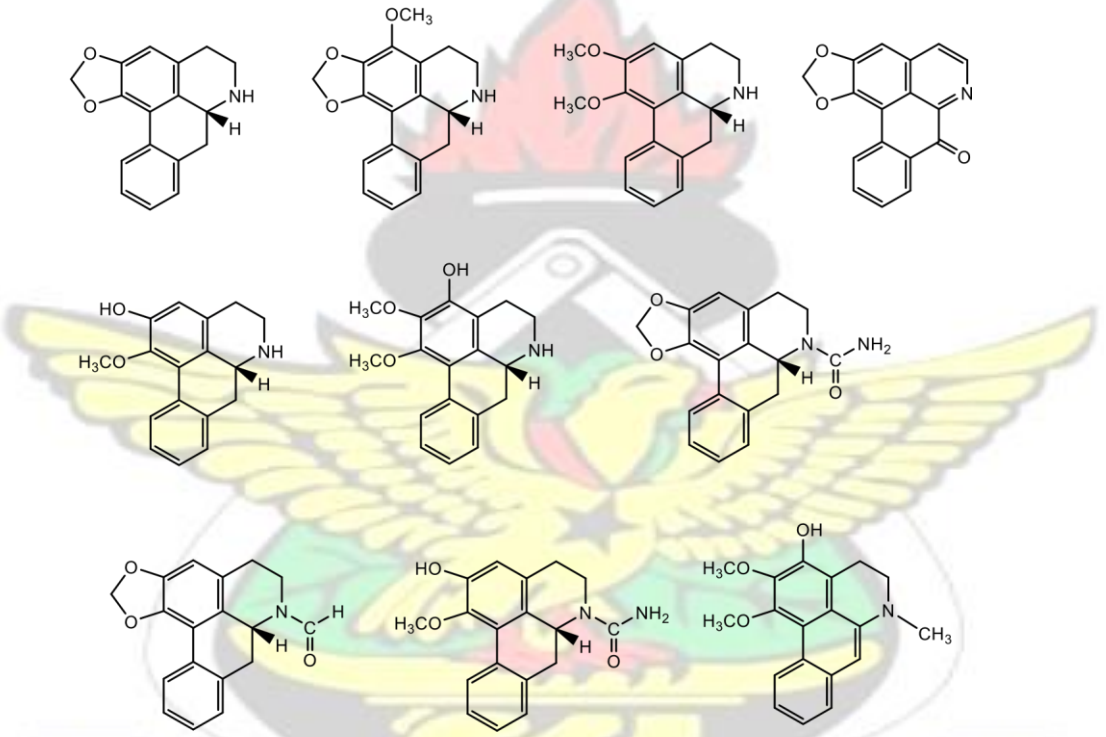

Fig. 2.11: Nor-aporphine alkaloids from *Hexalobus crispiflorus* (Achenbach et al., 1986)

2.8.2.5 Biological activity

The crude ethanol extract of the root bark of *H. monopetalus* exhibited cytotoxicity in the brine shrimp lethality assay with IC_{50} values ranging between 0.56 and 66.7 µg/mL. The root extract also showed anti-plasmodial activity against multidrug resistant and chloroquine sensitive *Plasmodium falciparum* strains. Further, the extract exhibited

trypanocidal activity against *Trypanosoma brucei rhodesiense* with MIC of 11 µg/mL (Malebo *et al.*, 2014).

Diprenylated indole alkaloids (hexalobines) isolated from *H. crispiflorus* and *H. monopetalus* showed antifungal activity against the plant pathogenic fungi *Botrytis cinerea*, *Rhizoctonia solani* and *Saprolegnia asteropho* at 150 µg/mL as well as *Candida albicans* at 100 µg/mL (Achenbach *et al.*, 1995; Malebo *et al.*, 2014).

2.8.3 Landolphia heudelotti A. DC. (Apocynaceae)

The genus *Landolphia* consists of sixty-three species of lianes climbing up to 12 m or more with milky latex in the young bark and unripe fruit. *Landolphia heudelotti* is a bushy or climbing shrub that can produce stems up to 15 m long. The specie was at one time the main commercially useful rubber producing plant in Senegal, Guinea and Mali. It is widely distributed in West Africa commonly found in Senegal and Ghana. It grows mainly in the savannah but also in open forests and on laterite and sandy soils (Persoon, 1992). In Ghana, the plant is locally called _*samyeduru*‘ or _*ahomoahoma*‘ (Akan).

(a)  (b) 

Fig. 2.12: Roots (a-b) of *Landolphia heudelotti*

2.8.3.1 Medicinal Uses

The root and stems of *L. heudelotti* are well known in most sub-Saharan African countries for their useful medicinal properties. A decoction of the stems or roots is

used for the treatment of enteritis, gastric ulcers and stomach cramps. The ground stem bark paste is taken as a vermifuge. The sticky latex from the young stem is instilled in the eyes to treat cataract and conjunctivitis. The root maceration is used to treat leprosy. The root decoction is used for the treatment of arthritis, rheumatism and articular pains. Decoctions of leaf and bark are taken orally for treatment of diarrhoea, dysentery and cholera. The root decoction is used as an aphrodisiac and as a general tonic (Arbonnier, 2000).

2.8.3.2 Biological activity of *Landolphia* species

The aqueous leaf and root extracts of *L. dulcis* exhibited antimicrobial activity against *S. dysenteriae*, *P. aeruginosa*, *E. coli*, *S. typhi*, *B. cereus*, *S. aureus* and *K. pneumonia* (Okeke *et al.*, 2001). In another study, the ethanol leaf and root extracts of *L. owariensis* exhibited antimicrobial activity against *Staphylococcus aureus*, *Proteus sp.* and *Escherichia coli* (Nwaogu *et al.*, 2010).

The leaf extract of *L. owariensis* significantly inhibited carrageenan induced paw oedema in rats by 40-60 % at 100 mg/mL. Further, the extract exhibited antinociceptive activity in both tail immersion and acetic acid writhing tests (Owoyele *et al.*, 2001). The methanol root extract also exhibited significant antioxidant activity in the DPPH, superoxide and hydroxyl scavenging assays as well as in the inhibition of lipid peroxidation (Awah *et al.*, 2012).

Significant anti-trypanosomal activity was exhibited by the leaf, stem and root bark extracts of *L. uniflora* (Atawodi and Alafiatayo, 2007). The ethanolic root extract of *L. dulcis* exhibited aphrodisiac activity by causing an increase in serum testosterone levels as well as prolonged ejaculation latencies in male rats (Ilodigwe *et al.*, 2013).

2.8.3.3 Phytochemistry

There is currently no report on the phytochemical constituents of *L. heudelotti* but a few reports exist on the phytochemical constituents of other *Landolphia species*. The seed pulp of *L. owariensis* yielded flavonoids and ascorbic acid as the major constituents (Okonkwo and Osadebe, 2013). (E)-chlorogenic acid, (E)-chlorogenic acid methyl ester, protocatechuic acid and 3β–sitosterol were isolated from the seed pulp of *L. owariensis* (Okonkwo *et al.*, 2016). In another study, Stærk et al., (2004) isolated aromadendrane type sesquiterpenes from the ethanolic root extracts of *L. dulcis* (Stærk *et al.*, 2004).

Table 2.4: Phytochemical compounds from the genus *Landolphia*

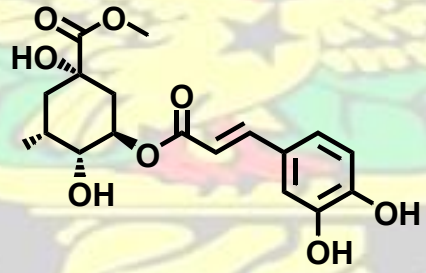

Name of compound	Structure of compound	Reference
(E)-chlorogenic acid	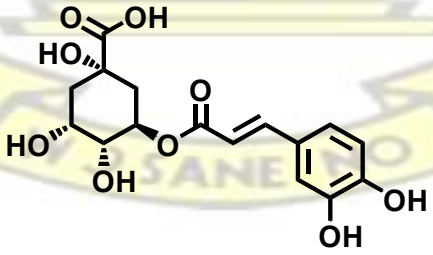	Okonkwo *et al.*, (2016)

(E)-chlorogenic acid Okonkwo *et al.*, methyl ester (2016)

HO

Protocatechuic acid	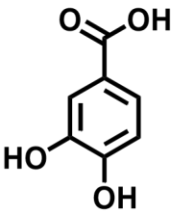	Okonkwo *et al.*, (2016)
β-sitosterol	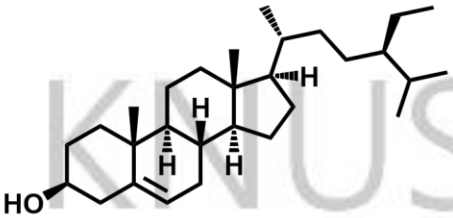	Stærk *et al*., (2004)
2-Hydroxy-1(10)-aromadendren-14-oic acid 2,14-lactone	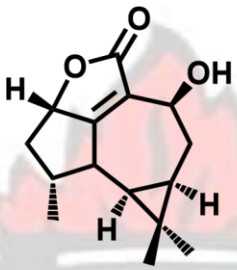	Stærk *et al*., (2004)

(Refer to Section 2.8.3.3)

CHAPTER 3

MATERIALS AND METHODS

3.1 Materials

3.1.1 Growth Media

Nutrient agar (Carl Roth Co. GmbH), nutrient broth (Sigma-Aldrich Chemie, GmbH), potato dextrose broth (Carl Roth Co. GmbH) and Sabouraud dextrose agar (Sigma-Aldrich Chemie, GmbH) were employed as growth media for the antimicrobial assays. The media were prepared according to the manufacturer‘s instructions.

3.1.2 Microorganisms

The microorganisms used for the preliminary antimicrobial assay were:

Gram positive bacteria: *Staphylococcus aureus* (ATCC25923), *Staphylococcus aureus* (DSM 799), *Bacillus subtilis* (NCTC10073), *Bacillus subtilis* (DSM 1088), *Streptococcus pyogens* (clinical strain) and *Streptococcus pyogens* (DSM 11728)

Gram negative bacteria: *Escherichia coli* (NCTC9002), *Escherichia coli* (DSM 682), *Escherichia coli* (DSM 1116), *Pseudomonas aeruginosa* (ATCC27853), *Pseudomonas aeruginosa* (DSM1128), *Pseudomonas aeruginosa* (DSM 22644), *Salmonella typhi* (NCTC 6017), *Acinetobacter spp*. (DSM 586)

Fungi: *Candida albicans* (clinical strain), *Rhizoctonia solani*, *Pythium ultimum*, *Mucor miehei*

The typed cultures for preliminary antimicrobial assay were obtained from the Department of Pharmaceutics, FPPS, KNUST and clinical strains from Komfo Anokye Teaching Hospital (KATH), Kumasi, Ghana. The standard pathogenic control strains for the final antimicrobial assays on isolated compounds were obtained from Leibniz-Institut DSMZ, Braunschweig, Germany.

3.1.3 Animals

One day old cockerels (*Gallus gallus*: strain Shaver 579, Akate Farms, Kumasi, Ghana)

3.1.4 Chemicals

All chemicals used were purchased from Sigma-Aldrich Co Ltd. Irvine, UK. All organic solvents used [petroleum ether (Pet-ether), ethyl acetate (EtOAc), methanol (MeOH) and chloroform ($CHCl_3$)] for the experiments were of analytical grade and obtained from BDH, Laboratory Supplies (Merck Ltd, Lutterworth, UK).

3.2 Methods

3.2.1 Collection of plant samples

The medicinal plants were collected from different locations in the Eastern region of Ghana. The plants were identified and authenticated respectively by Mr Clifford Asare and Dr George Henry Sam of the Herbal Medicine Department, Faculty of Pharmacy and Pharmaceutical Sciences (FPPS), KNUST. Voucher specimens were deposited at the Department's herbarium. The detailed information regarding the names, sample codes and sampling sites of the plants is given in Table 3.1 below.

Table 3.1: Collection details of plants under investigation

Name	Site	Date	Voucher number
Anopyxis klaineana	Kwahu Asakraka N 06° 37′; 43′ W 000° 41; 21.00′	Nov., 2013	KNUST/AK1/2013/S005
Hexalobus monopetalus	Kotoso-Afram Plains N 06°42 ′ 17.26 ′ N 0° 39 ′ 1.13 ′ W	June, 2014	KNUST/HM/2014/H014
Landolphia heudelotti	Kwahu-Bepong N 06° 38; 042′ W 000° 41; 719′	Dec., 2014	KNUST/HM/2016/12

3.2.2 Processing and preparation of plant material

The fresh plant materials were cleaned by washing under running tap water to remove foreign materials. They were then cut into smaller pieces, air-dried at room temperature and coarsely powdered with a mechanical grinder. The dried powdered samples were kept in air tight glass containers and stored in the dark at room temperature until required for use.

3.2.3 Preparation of crude extracts for biological activity

To prepare the total crude extract for bioassay, 100 g each of powdered plant material was extracted by cold maceration with 500 mL methanol (MeOH) for 48 h. The extract obtained after filtration was evaporated to dryness using a rotary evaporator (R-114,

Buchi, Switzerland) under reduced pressure at 40 °C. The crude MeOH extract was re-dissolved in 200 mL of methanol (MeOH) and water (1:1) and fractionated into non-polar, semi- polar and polar fractions by solvent-solvent partitioning in a separating funnel beginning with the non-polar solvent, petroleum ether (200 mL × 3) then with ethyl acetate (EtOAc) (200 mL × 3). Thus three fractions, petroleum ether, EtOAc and MeOH were obtained.

3.2.4 Preparation of extracts for phytochemical screening

The air-dried and powdered stem barks of *A. klaineana* (1.2 kg), *H. monopetalus* (1.5 kg) and *L. heudelotti* (1.2 kg) were individually cold macerated with a mixture of MeOH-$CHCl_3$ (4:1) (2.0 L each) for 48 h at room temperature. The extracts of *A. klaineana* and *H. monopetalus* were further partitioned into polar and non-polar fractions by solvent-solvent partitioning as described in **section 3.3** (Table 3.2).

Table 3.2: Details of crude extracts obtained from plants

Plant material	**Total extract (weight, % yield)**	**MeOH**	**EtOAc**
***A. klaineana* (1.2 kg)**	Reddish brown powder (111.5 g, 9.29 %)	68.4 g	35 g
***H. monopetalus* (1.5 kg)**	Brown gum (88.5 g, 5.86 %)	57.5 g	19.5 g
***L. heudelotti* (1.2 kg)**	Brown oil (19.2 g, 1.60 %)	-	-

3.2.5 Biological assays

3.2.5.1 Antimicrobial assay

Preparation of working culture

The working culture was prepared by inoculating the test organism in nutrient broth (incubated at 37 ˚C for 24 h) for bacteria and in Sabouraud dextrose broth (incubated at 25 °C for 48 h) for fungi. The standardized suspensions of microorganisms were prepared from overnight broth cultures. For the agar dilution assay method, the working suspension was prepared by serial dilutions of cultures in sterile normal saline

to achieve a suspension of equal turbidity with 0.5 Mc Farland standards. This dilution contained approximately 10^5 CFU/mL.

Assay Protocols Agar disc diffusion assay

The disk diffusion assay, according to a previously described method was used (Li *et al.*, 2014). All agar plates were prepared in 90 mm (diameter) sterile petri dishes (TPP, Trasadingen, Switzerland) with 22 mL of sterile molten agar, to give a final depth of 4 mm (nutrient agar for bacteria and potato dextrose agar for fungi). The overnight broth inoculum suspension culture (200 µL) was spread on the solid media plates using the standard spread-plate technique. For fungi, the mycelia were first thoroughly macerated with sterile water to yield a homogeneous inoculum. The test compounds (refer to Sections 4.3, 4.7, 4.11 for details on isolated compounds), were dissolved in HPLC-grade MeOH at concentrations of 0.1, 0.5, 1, 5 and 10 µg/ml or 12.5, 25, 50 and 100 µg/ml. Sterile paper disks (Schleicher & Schuell GmbH, Dassel, Germany; 6.0 mm in diameter) were impregnated with 40 µL of the samples, airdried under the laminar airflow hood and placed on inoculated plates. The plates were then kept at 4 °C for 2 hours and incubated at 37 °C for 24 h for bacteria or at 28 °C for 48 h for fungi. Negative and positive controls were included in the assay. The viability of test organism was verified by a seeded petri dish excluding a test sample. The negative control included a disk treated with 40 µL of HPLC grade MeOH or sterile double-distilled H_2O. Streptomycin (Sigma-Aldrich Chemie GmbH, Steinheim, Germany), gentamicin (Sigma-Aldrich Chemie GmbH, Steinheim, Germany) and propiconazole (Dr Ehrenstorfer GmbH, Augsburg, Germany) were used as reference standards in parallel to reveal the comparative antimicrobial efficacy of compounds against the tested organisms. Each test was performed in triplicate.

Agar dilution method

In the determination of the antimicrobial susceptibility and minimum inhibitory concentration (MIC) of crude fractions, the solid agar dilution method was used (Vanden-Berghe and Vlientinck, 1991). Plant extracts were dissolved in 2 %$^{v}/_{v}$ DMSO and prepared to concentrations between 5 mg/mL and 0.312 mg/mL. An equal volume of (liquid) double strength nutrient agar was mixed with each concentration of test extract to give concentrations between 2.5 mg/mL and 0.156 mg/mL. Wells of a sterile micro titre plate were filled with 300 µL of these solutions at 50 °C to prevent solidification while filling. After solidification at room temperature, all wells were inoculated with 5 µL of serially diluted (1:100) overnight standardized suspensions of cultures of test organisms. The inoculated wells were then incubated at 37 °C for 24 h for bacteria and 28 °C for 48 h for fungus. The presence or absence of growth was determined by visual examination of growth by microscopic examination and confirmed with methyl thiazolyl tetrazolium chloride (2 % MTT) dye as indicator. Wells with growth showed dark blue or purple colouration while wells without growth maintained the yellow colour of the MTT dye. Ciprofloxacin and ketoconazole were used as positive controls and 2 % DMSO as negative control. All experiments were carried out in triplicate.

3.2.5.2 Anti-inflammatory assay

One day old cockerels (*Gallus gallus*: strain Shaver 579, Akate Farms, Kumasi, Ghana) were housed in stainless steel cages (34 × 57 × 40 cm^3) in groups of 10 to 12 chicks per cage. The chicks were fed on chick mash (GAFCO, Tema, Ghana) and water. Chicks were kept at a temperature of 29 °C with overhead incandescent illumination on a 12 h light-dark cycle. Seven (7)-day old chicks were used for the experiment. All procedures and techniques used in this study were in accordance with

the Guidelines for the care and use of laboratory animals (Institute of laboratory animal resources) (Clark *et al.*, 1996) and approved by the College of Health Sciences Ethics Committee.

Carrageenan-induced foot oedema in the chicks

The carrageenan-induced foot oedema model of inflammation in chick was used to evaluate the anti-inflammatory properties of crude fractions (Roach and Sufka, 2003; Mensah and Amoh-Barimah, 2009). Chicks were randomly selected and put into groups of five. Initial foot volumes were measured by water displacement as described by Fereidoni *et al.*, (2000). Oedema was induced by the sub-plantar injection of freshly prepared carrageenan (100 µL of a 2 % suspension in normal saline) into the right footpads of the chicks. Chicks were then randomly selected and placed into four groups- negative control group (vehicle: normal saline), treatment group (test sample: 30, 100 and 300 mg/kg for crude fractions given orally (p.o.) (refer to Section 3.3); 3, 10 and 30 mg/kg for compound **AK1** (refer to Section 4.3.1) (p.o.) and positive control group (diclofenac: 10, 30 and 100 mg/kg, given intra peritoneal (i.p.)). The test extracts were administered 1 hour and standard drugs 30 minutes before the injection of carrageenan. The oedema component of inflammation was quantified by measuring the difference in foot volume before carrageenan injection and at hourly intervals for 5 hours (Fereidoni *et al.*, 2000) .

Data analysis

The values of foot pad volumes were individually normalized as percentage difference from the initial foot volumes at 0 h and averaged for each treatment group. Time course curves were plotted and subjected to two-way (treatment versus time) repeated measures analysis of variance (ANOVA) with Bonferroni's *post hoc* test.

The total foot volume for each treatment was then calculated as the area under curve (AUC) and used to determine the percentage inhibition of oedema for each treatment group using the formula:

Equation 3.1: Percentage inhibition of oedema

$$\%\ Inhibition\ of\ oedema = \frac{AUC\ (control) - AUC\ (test\ sample)}{AUC(control)} X\ 100\ \%$$

Differences in AUCs were analysed by one-way ANOVA followed by Student-Newman Kuels' *post hoc* test. The dose responsible for 50 % of the maximal effect (ED_{50}) was determined using an iterative computer least squares method, with the following non-linear regression equation:

Equation 3.2: Non-linear regression equation for the determination of ED_{50}

$$Y = \frac{a+(b-a)}{(1+10)(logED50-X)}$$

Where X is the logarithm of dose and Y is the response. Y starts at _a' (the bottom) and goes to _b' (the top) with a sigmoid shape.

The fitted midpoints (ED_{50}) of the curves were compared statistically using the *F* test. Graph pad prism for Windows version 5 (Graph pad software, San Diego, CA, USA) was used for all statistical analysis and ED_{50} determinations. $p<0.05$ was considered statistically significant

Prostaglandin E_2 (PGE_2) competitive inhibition assay

The PGE_2 forward sequential competitive enzyme immunoassay was performed according to manufacturer's instructions (R&D Systems Europe, Ltd., Abingdon, United Kingdom). The compounds were tested at 40, 20, 10 and 5 µM. Test samples were reconstituted in dimethyl sulfoxide (DMSO) by serial dilution. Different

concentrations of standard PGE_2 was included in the assay and used to develop a standard curve.

Wells of a 96-well polystyrene microplate coated with a goat anti-mouse polyclonal antibody were filled with 150 µL of each test sample. 50 µL of the primary antibody solution was added to each well, securely covered with a plate sealer and incubated for 1 hour at room temperature on a horizontal orbital micro plate shaker (0.12" orbit). After the incubation period, 50 µL of horseradish peroxidase-labelled PGE_2 conjugate was added to each well and incubated for 2 hours at room temperature. Subsequently, the wells were thoroughly washed with a wash buffer solution to remove any unbound material. A substrate solution (200 µL) was then added to each well to generate an optimal colour after 30 minutes. The reaction was terminated by addition of 100 µL of a stop solution. The bound enzyme activity was then determined by measuring the absorbance at 450 nm. The intensity of colour development is inversely proportional to the amount of possible anti-inflammatory structural groups in the test sample. A standard calibration curve was developed from the mean absorbance for the standard PGE_2. The concentration of anti-inflammatory structural groups (PG analogues)in the test samples corresponding to the various absorbances were intrapolated from the standard curve. The IC_{50} was calculated by linear regression of plots, where the x-axis represented the concentration of test sample and the y-axis, the average per cent of bound enzyme activity.

3.2.5.3 Anti-oxidant assay

TLC-DPPH free radical scavenging test (Qualitative)

An aliquot (3 µL) of the test extract or fraction in solution (1 mg/mL) was deposited as spots or bands on the TLC plates. The spotted TLC plates were dried and developed

in a pre-saturated solvent chamber with cylcohexane and EtOAc (3:2). The TLC plates were developed in duplicate and one set was used as the reference chromatogram. The developed TLC plates were air-dried and sprayed with a solution of DPPH (2.54 mM in MeOH) for derivatization. Bands of compounds with DPPH scavenging activity were observed as white or yellow bands on a purple background.

Quantitative DPPH free radical scavenging assay

For the quantitative antioxidant test, concentrations of 6-100 µg/mL (for crude extracts) and 10-50 µg/mL (for pure compounds) were used. The reaction mixture consisted of a solution of DPPH in methanol (20 mg/L) and test extract in the ratio 3:1. The mixture was incubated for 30 minutes in dark, after which the absorbance for each concentration was measured at 517 nm (Cecil CE 7200 spectrophotometer, Cecil instrument limited, Milton Technical Centre, England). In this assay, ascorbic acid and trolox (6-hydroxy-2,5,7,8-tetramethylchroman-2-carboxylic acid) were used as positive controls and the negative control used was MeOH. Each test was carried out in triplicate. The percentage DPPH scavenging (I %) was calculated using the formula:

Equation 3.3: Percentage DPPH free radical scavenging

$$I\ \% = \frac{Abs[control] - Abs[sample]}{Abs[control]} X\ 100$$

Where; *Abs [control]* = the absorbance of negative control; *Abs [sample]* = absorbance of extract or positive control. The concentration required to cause a 50% decrease in the initial DPPH concentration (IC_{50}) was calculated by linear regression of plots, where the x-axis represented the concentration of test sample and the y-axis, the average per cent of scavenging capacity.

Total Phenol Content

The amount of total phenols in the crude extracts was determined by Folin-Ciocalteu reagent method (McDonald *et al.*, 2001). The solution mixture contained 500 µL of extract (3, 30, 100, 300 µg/mL) and 100 µL of Folin-Ciocalteu reagent (0.5 N). The mixture was incubated at room temperature for 15 minutes after which 2.5 mL of saturated sodium carbonate solution was added and further incubated for 120 minutes at room temperature. Absorbance was then measured at 760 nm (Cecil CE 7200 spectrophotometer, Cecil instrument limited, England). A standard curve was prepared by using tannic acid (3 – 300 μgmL^{-1}) and the total phenolic content of extract was intrapolated from this curve. The total phenolic content was expressed in terms of tannic acid equivalent (TAE) as mg/g of dried extract.

Total antioxidant capacity assay

Test tubes containing l mL each of the test extracts (3, 30, 100, 300 µg/mL) and 3 mL of the reagent solution (0.6 M sulphuric acid, 28 mM disodium phosphate and 4 mM ammonium molybdate) were incubated at 95 °C for 90 minutes. After the mixture had cooled to room temperature, the absorbance of the solution was measured at 695 nm. A standard curve was prepared using ascorbic acid (3-300 µg/mL) and the antioxidant capacity of extract was intrapolated from this curve. The total antioxidant capacity was expressed as ascorbic acid equivalent (AAE) in mg/g of dried extract. A negative control test using distilled MeOH was conducted.

3.2.6 Phytochemical Screening

3.2.6.1 Preliminary phytochemical screening

The dried powdered plant material was subjected to general phytochemical screening following standard methods (Evans, 2002).

3. 2.6.2 Chromatographic purification of crude extracts

The chromatographic methods used for the purification of extracts included column chromatography (CC) using silica gel or sephadex LH-20 as stationary phase and reversed phase high performance liquid chromatography (RP-HPLC).

Thin layer chromatography

Thin layer chromatography (TLC) was performed using pre-coated fluorescent aluminium backed silica gel plates 60 F_{254} (0.25 mm thickness). Samples were dissolved in the suitable solvent, spotted on the TLC plate and developed in presaturated chromatanks containing appropriate solvent systems consisting of hexane: EtOAc or EtOAc: MeOH in different ratios. The developed plates were dried and analysed by viewing under UV lamp and further by spraying with H_2SO_4-EtOH (1:9, $^{v}/_{v}$) followed by heating.

Column chromatography

Column chromatography (CC) was performed using silica gel or sephadex LH-20 as stationary phase. For chromatography using silica gel, the dry packing method was employed as follows: the glass column (90 × 6 cm; 75 × 3 cm) was filled with dry silica (Silica gel 60; 70−230 mesh; AppliChem, GmbH, Darmstadt, Germany) carefully to prevent the formation of cracks or air spaces in the packed column. The sample to be purified was dissolved in ethyl acetate (or methanol) and adsorbed unto silica, dried and packed onto the silica in the column. Separation of constituents was carried out by gradient elution with cyclohexane and ethyl acetate, then with EtOAc and methanol with increasing the polarity starting with cyclohexane.

For the LH-20 sephadex (25−100 μm; Amersham Biosciences), the sephadex beads were soaked (saturated) overnight with MeOH. The slurry was then packed into the

column (75 × 3 cm) and the solvent was allowed to slowly drain off. The extract was dissolved in MeOH evenly deposited on the surface of sephadex and eluted with MeOH.

High Performance Liquid chromatography (HPLC)

High performance liquid chromatography was performed using a Phenomenex® Gemini C18 column (10×250 mm, 10 µm particle size) using a chromeleon software system. The set up consisted of a Gynkotek pump equipped with a Dionex DG-1210 degasser, a Dionex UVD 340S detector and a Dionex Gina 50 auto-sampler. During the separation of one mixture, the percentage of MeOH-H_2O solvent system used as well as the flow rate for travelling the RP column was modified for different samples. For some separations, 0.1 % formic acid (HCOOH) was used as buffer.

3. 2.6.3 Isolation of constituents from *Anopyxis klaineana*

Both MeOH and EtOAc fractions of *A. klaineana* stem bark exhibited significant anti-inflammatory activity (section 4.1.1). However, the EtOAc fraction further showed more potent antimicrobial activity than the MeOH fraction (section 4.1.3) hence the EtOAc fraction was selected for further fractionation. A schematic presentation of the isolation procedure is elaborated by Fig. 3.1.

Thirty-five grams (35 g)of the EtOAc fraction was subjected to column chromatography over silica gel 60 (70-230 mesh) by gradient elution with cyclohexane and EtOAc to obtain 52 fractions (500 mL each) which were bulked based on TLC profiling into 7 fractions, AK/A to AK/G. Fraction AK/C [cyclohexane-EtOAc, 4:1, 0.6 g] yielded a white precipitate which was re-dissolved and subjected to purification by semi-preparative HPLC [MeOH-H_2O + 0.1% HCOOH, 98:2, 2 $mLmin^{-1}$] to yield compound **AK6** (12 mg, retention time 14.5 min). Fraction AK/D yielded compound **AK1** (5 g) as colourless prismatic crystals.

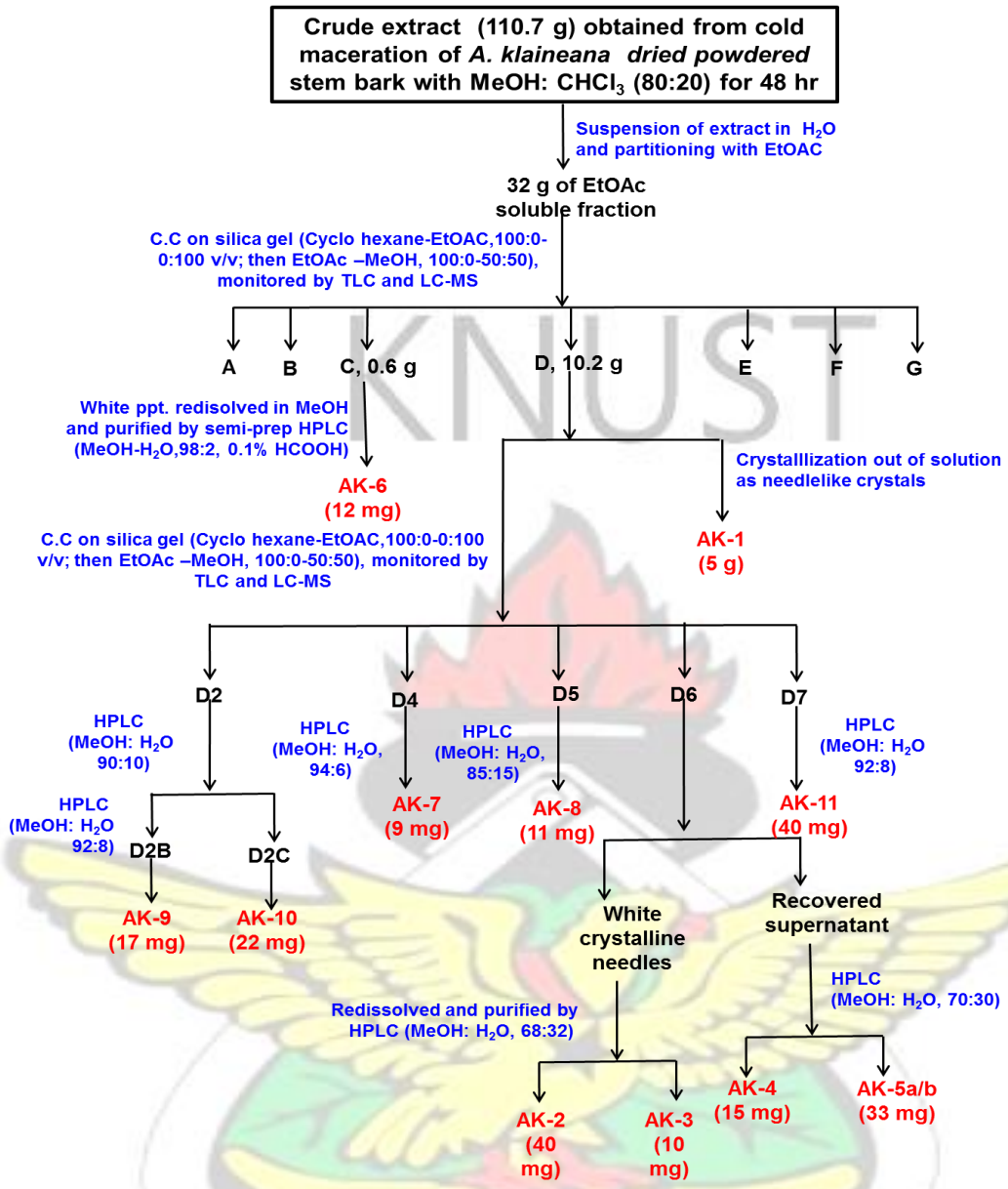

Fig. 3.1: Isolation scheme for *A. klaineana* stem bark extract

Analysis of the LC-HRMS of all fractions obtained revealed that the majority of constituents (known and unknown) were accumulated in fraction AK/D [cyclohexane-EtOAc, 3:2-1:1, 10 g]. Thus, fraction AK/D was further subjected to silica gel column chromatography eluting with increasing polarities of mixtures of cyclohexane-EtOAc to obtain 45 sub-fractions of 100 mL each, which were bulked into 10 sub-fractions (AK/D1- AK/D10). Semi-preparative HPLC of sub-fraction AK/D2 by isocratic elution with MeOH-H_2O + 0.1% HCOOH [98:2, 2 $mLmin^{-1}$] yielded compounds **AK9**

(17 mg, retention time: 22 min)and **AK10** (22 mg, retention time: 10 min). Sub-fraction AK/D4 was purified by semi-preparative HPLC [MeOH-H_2O + 0.1% HCOOH, 94:6, 2 $mLmin^{-1}$] to yield compound **AK7** (9 mg, retention time: 19.5 min). Sub-fraction AK/D5 yielded compound **AK8** (11 mg, retention time: 25.5 min) by purification on semi-preparative HPLC [MeOH-H_2O + 0.1% HCOOH, 85:15, 2 $mLmin^{-1}$]. Sub-fraction AK/D6 yielded colourless crystals which were identified based on its HR-MS profile to be a mixture of two compounds. The crystals were re-dissolved in MeOH and purified on semi-preparative HPLC by isocratic elution with a mixture of MeOH-H_2O + 0.1% HCOOH[68:32, 2 $mLmin^{-1}$] to yield compounds **AK2** (4 mg, retention time: 21.5 min) and **AK3** (10 mg, retention time: 19.5 min). The supernatant from fraction AK/D6 was further purified by semi-preparative HPLC [MeOH-H_2O + 0.1% HCOOH, 70:30, 2 $mLmin^{-1}$] to yield compounds **AK5a/b** (33 mg, retention time: 10 min) and compound **AK4** (15 mg, retention time: 13.5 min). Purification of sub-fraction AK/D7 by semipreparative HPLC [MeOH-H_2O + 0.1% HCOOH, 92:8, 2 $mLmin^{-1}$] yielded

compound **AK11** (4 mg, retention time: 18 min).

3. 2.6.4 Isolation of constituents from *Hexalobus monopetalus*

Among the three fractions of *H. monopetalus* stem bark, the EtOAc fraction exhibited the most significant antimicrobial activity (section 4.5.1) and was thus subjected to further phytochemical investigation. A schematic presentation of the isolation procedure described is elaborated by Fig. 3.2.

Repeated chromatography of the EtOAc fraction (15 g) over silica gel (50 g) by gradient elution with cyclohexane and EtOAc yielded 110 fractions (500 mL each) which were bulked based on TLC and HR-MS profiling into 10 main fractions

HM/A to HM/J. Purification of fraction HM/B (0.4 g) [cyclohexane-EtOAc (9.5:0.5)] by silica gel column chromatography afforded 45 fractions (200 mL) bulked into 9 sub-fractions (HM/B1 HM/B9) based on TLC and HRMS profiling. Further purification of fraction HM/B2 (0.025 g) by preparative HPLC [MeOH-H_2O; 70:30, 2 $mLmin^{-1}$] yielded compounds **HM6** (9 mg, retention time: 22 min) and **HM7** (10 mg, retention time: 24 min). Fraction HM/C (0.15 g) [cyclohexane-EtOAc (9:1)] was purified by LH sephadex (100% MeOH) to obtain 25 fractions (35 mL each) which were bulked into 8 sub-fractions HM/C1 HM/C8 based on HRMS analysis. Sub-fraction HM/C5 (0.028 g) was further purified by semi-preparative HPLC [MeOH-H_2O; 4:1, 2 $mLmin^{-1}$] to yield compounds **HM1** (7 mg, retention time: 20 min), **HM2** (4 mg, retention time: 15 min) and **HM3** (5 mg, retention time: 17 min). Fraction HM/E (0.18 g) yielded compounds **HM4** (10 mg, retention time: 15 min), **HM8** (5 mg, retention time: 11 min), **HM9** (10 mg, retention time: 12 min) and compound **HM5** (2 mg, retention time: 9 min) after purification by silica gel column chromatography and further by preparative HPLC [MeOH-H_2O; 70:30, 2 $mLmin^{-1}$].

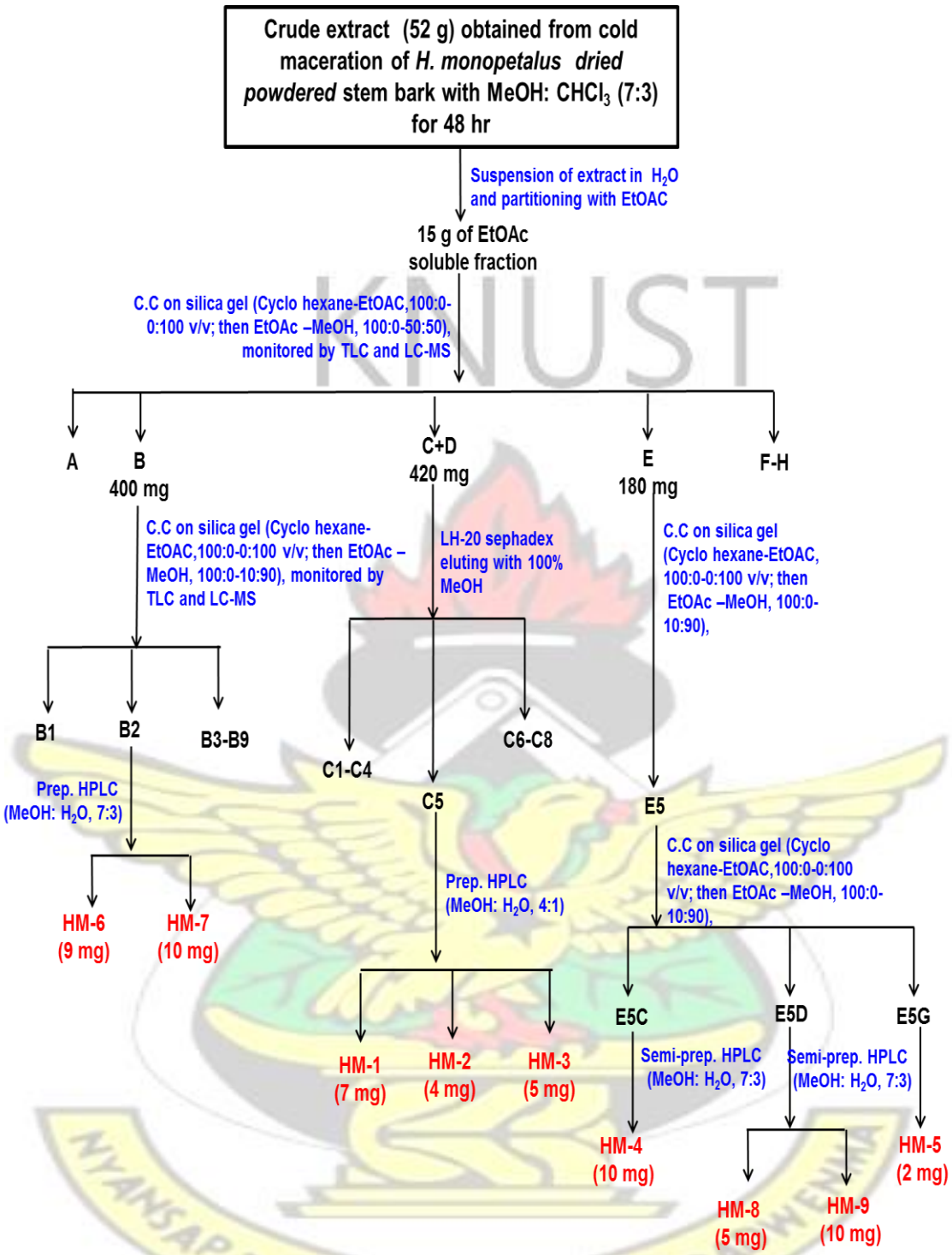

Fig. 3.2: Isolation scheme for *H. monopetalus* stem bark extract

3. 2.6.5 Isolation of constituents from *Landolphia heudelotti*

The MeOH fraction of *L. heudelotti* showed the most significant antimicrobial activity among the three tested fractions. However, due to the low yield of crude extract obtained (1.6 %) after cold maceration with MeOH-$CHCl_3$ (4:1), the total extract was

used directly for chromatographic separation without fractionation. Moreover, from earlier fractionation results, the inactive non-polar fraction was only about 0.12 % of the total extract and could be easily removed as the first fraction during silica gel column chromatography. A schematic presentation of the isolation procedure described is elaborated by Fig. 3.3.

L. heudelotti root MeOH extract (19.2 g) was subjected to column chromatography over silica gel (60 g) eluting with increasing polarities of cyclohexane-EtOAc then with EtOAc-MeOH. Based on TLC monitoring, 73 fractions (500 mL each) were bulked to obtain eight sub-fractions, LH/A to LH/H. Fractions LH/A to LH/C [100% cyclohexane-9:1 cyclohexane-EtOAc] were identified by LC-MS profiling to contain mainly fatty acids and were not further investigated. Moreover, preliminary TLC DPPH assays (Appendix C, Fig. C-43) indicated fractions D-F as the fractions with most antioxidant constituents. Thus, fraction LH/D [cyclohexane-EtOAc, 4:1-7:3, 1.6 g] was further purified over LH-20 sephadex eluting with 100% MeOH to obtain 18 fractions (30 mL each) which were bulked together into 6 sub-fractions, LH/D1-LH/D6. Sub-fraction LH/D2 was subjected to purification by the HPLC proceeding with an isocratic elution with MeOH-H_2O [80:20, flow rate: 2.5 $mLmin^{-1}$] to yield compound **LH-14** (3 mg).

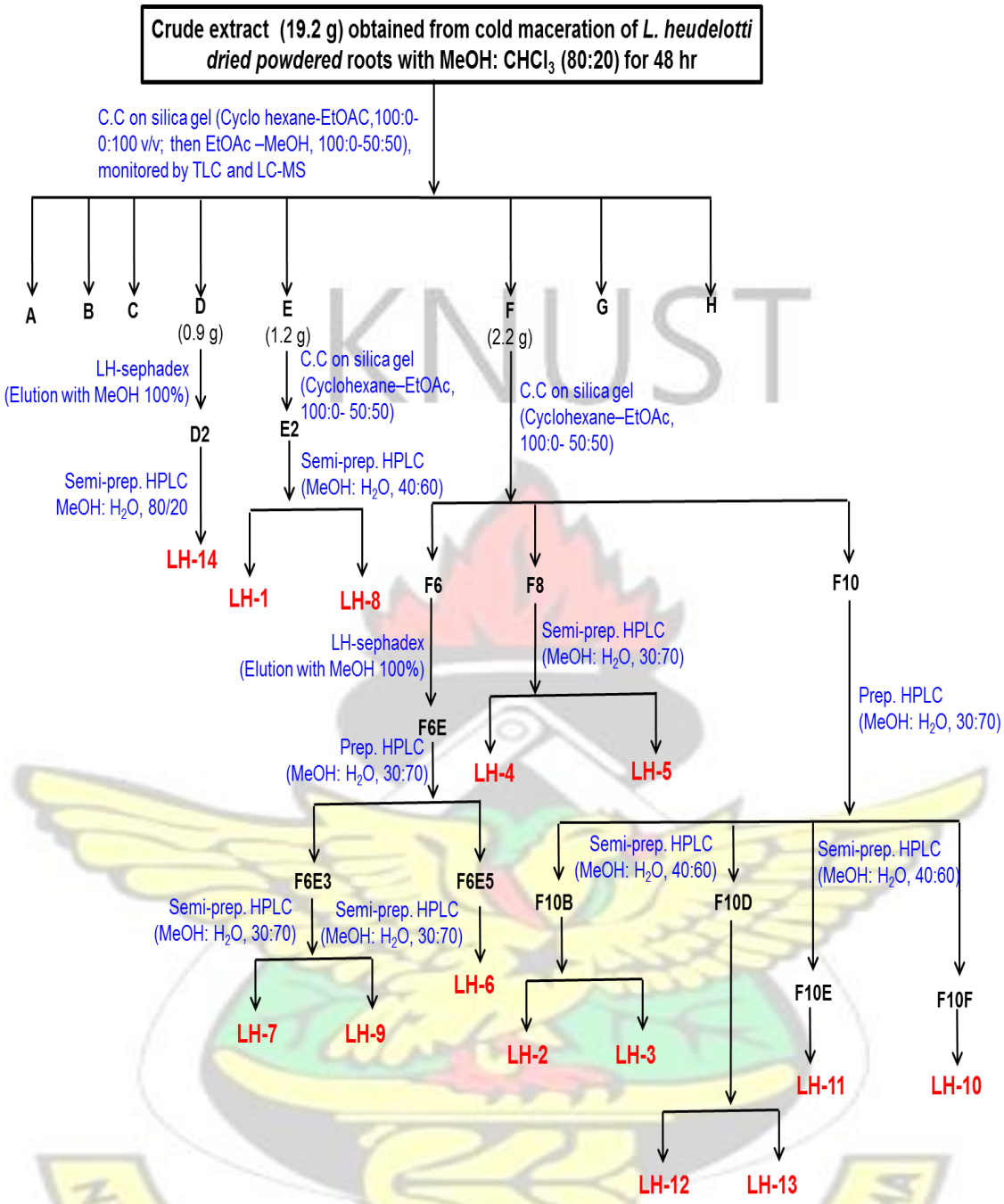

Fig. 3.3: Isolation scheme for *L. heudelotti* root extract

Fraction LH/E [cyclohexane-EtOAc, 3:2-1:1, 1.3 g] was subjected to a second silica gel CC eluting by gradient elution with cyclohexane and EtOAc to obtain 56 fractions (250 mL each) which were bulked based on TLC profiling to obtain 6 fractions (LH/E1-LH/E6). Sub-fraction LH/E2 was purified by semi-preparative

HPLC eluting with an isocratic system consisting of MeOH-H_2O [40:60, flow rate: 2 $mLmin^{-1}$] to yield compounds **LH-1** (11.8 mg) and **LH-8** (8.6 mg). Fraction LH/F [cyclohexane-EtOAc, 3:7-1:9, 1.8 g] was subjected to silica gel CC eluting with cyclohexane/EtOAc with increasing polarities to obtain 76 sub-fractions (250 mL each), bulked into 10 fractions, LH/F1-LH/F10. Sub-fraction LH/F6 was subjected to LH-20 sephadex CC eluting with 100% MeOH to obtain 24 fractions. Fraction LH/F6E was subjected to preparative [MeOH-H_2O; 40:60, flow rate: 6 $mLmin^{-1}$] and further to semi-preparative HPLC [MeOH-H_2O; 3:7, flow rate 2.5 $mLmin^{-1}$] to yield compounds **LH-6** (9 mg), **LH-7** (2 mg) and **LH-9** (3 mg). Sub-fraction LH/F8 was directly purified by semi-preparative HPLC with a solvent system consisting of MeOH-H_2O [30:70, flow rate: 2.5 $mLmin^{-1}$] to give compounds **LH-4** (2 mg) and

LH-5 (3 mg). Sub-fraction LH/F10 was subjected to preparative [MeOH-H_2O; 30:70, flow rate: 6 $mLmin^{-1}$] and semi preparative HPLC [MeOH-H_2O; 40:60, flow rate: 2.5 $mLmin^{-1}$] to yield compounds **LH-2** (1.7), **LH-3** (2.1 mg), **LH-10** (6 mg), **LH-11** (7 mg), **LH-12** (8 mg), **LH-13** (11 mg).

3.2.7 Structural elucidation

3. 2.7.1 Liquid chromatography- mass spectrometry (LC-MS)

LC-HRMS was employed to check the purity and provide the exact mass and molecular formula of the isolated compounds. Mass fragmentation ($MS^{2/3}$) experiments were performed by collision-induced dissociation (CID) to evaluate the structural features of compounds based on the fragment information. The HPLCHRMS experiments were carried out on a LTQ Orbitrap spectrometer (Thermo Fisher, USA) equipped with a HESI-II source. The spectrometer was equipped with an Agilent 1200 (Santa Clara, USA) HPLC system consisting of a pump, PDA detector,

column oven (30 °C) and an auto-sampler. The spectrometer was operated with nominal mass resolving power of 60 000 at *m/z* 400 with a scan rate of 1 Hz to afford high-accuracy mass measurements within 2 ppm deviation. The HPLC separations were performed using a Luna C18 (2) column (50 x 3 mm, 3 µm particle size) (Phenomenex, Torrance, USA) with H_2O (+ 0.1 % HCOOH) (A) / MeOH (+ 0.1 % HCOOH) (B), gradient flow rate 350 µL/min. Samples were analysed by using a gradient programme as follows: linear gradient from 5 % to 100 % B over 14 min, 100 % B isocratic for 4 min, after which the system returned to its initial condition (95 % A, 5 % B) within 0.5 min and was equilibrated for 4.5 min. The following parameters were used for experiments in positive mode: nitrogen sheath gas flow (arbitrary units) 55, nitrogen auxiliary gas flow (arbitrary units) 8, spray voltage 5 kV, vaporizer temperature 400 °C, capillary temperature 300 °C, capillary voltage 20 V and tube lens 100 V. In negative mode, the spectrometer was operated by the following parameters: nitrogen sheath gas (arbitrary units) 50, nitrogen auxiliary gas (arbitrary units) 5, spray voltage 4.5 kV, capillary temperature 300 °C, capillary voltage -35 V and tube lens -110 V. MS/MS experiments were achieved by collisioninduced dissociation (CID, 35 eV) in the Orbitrap mass analyser. Argon was used as a collision gas. The LC-HRMS data was analysed through the software Thermo Xcalibur 2.2 SP1.48 (Thermo Fisher Scientific Inc., USA).

3. 2.7.2 Nuclear Magnetic Resonance (NMR)

One dimensional (1D) NMR spectroscopic techniques including ^{1}H and ^{13}C NMR, together with two dimensional (2D) NMR spectroscopic techniques such as correlation spectroscopy (COSY), hetero-nuclear single quantum correlation (HSQC), hetero-nuclear multiple bond correlation (HMBC) and nuclear over-hauser enhancement spectroscopy (NOESY) were used for the structural elucidation of compounds. 1D

NMR, COSY, HSQC and HMBC afforded the detailed information which was applied to assign the planar structure of the compounds. For compounds with chiral centres, NOESY correlation was used in comparison with reported literature to assign the relative configuration of the molecule. The solvents used for NMR analysis were deuterated chloroform ($CDCl_3$) and methanol-d_4 (CD_3OD)

(Deutero GmbH, Kastellaun, Germany). The pure compound was dissolved in the NMR solvent and transferred into an NMR tube (5 × 203 mm) for measurements (Deutero GmbH, Kastellaun, Germany). NMR spectra were recorded at 25 ºC on a Bruker Avance DRX-500 (500 MHz), Varian Unity Inova (500 MHz), Varian Unity Inova spectrometer (600 MHz) or AVANCE III HDX-700 (Bruker BioSpin GBMH; 700 MHz). Chemical shifts (δ) were quoted in parts per million (ppm) from internal standard tetramethylsilane (TMS).

3. 2.7.3 Optical rotation

Optical rotations were recorded on a Perkin Elmer polarimeter. The value was calculated according to the equation:

Equation 3.4: Optical rotation

$$[\alpha] = \frac{\alpha \times 100}{c \times d}$$

Where α refers to the optical rotation, d is the optical path length = 1 dm, and the concentration, c is in g/100 mL. MeOH or $CHCl_3$ was used as solvent and measurements were taken at 20 °C.

3. 2.7.4 Circular dichroism (CD)

CD measurements were performed using a Jasco J-715 spectro polarimeter (Tokyo, Japan). MeOH was employed as solvent at room temperature to dissolve the compound (0.1 mg/mL) in a 0.1 cm quartz cuvette. The spectra ranged from 200-400 nm and were

obtained using a scan speed of 100 nm/min, response time of 1 s, resolution of 1 nm and an accumulation of 5 scans.

3. 2.7.5 Other methods

Infrared (IR) spectra were recorded using a PerkinElmer (model 1600) FT-IR spectrometer. Ultraviolet-visible (UV-Vis) spectra were obtained from the photodiode array (PDA) detector in LC-HRMS and from a VWR UV-6300 PC double beam spectrophotometer.

3. 2.7.6 Mosher's method for determination of absolute configuration

The Mosher's technique is an empirically derived method for deducing the absolute configuration of a stereogenic carbon in secondary alcohols like compound **HM1** (**section 4.5.1**). This method involves the coupling of the hydroxyl group of the molecule under investigation with a chiral, enantiomerically pure carboxylic acid to form the corresponding ester whose ^{1}H NMR spectra is analysed to determine the configuration. Mosher's chloride (α-methoxy-α-trifluoromethyl-phenylacetyl chloride; MTPA-Cl) or Mosher's acid (α-methoxy-α-trifluoromethyl-phenylacetic acid; MTPA-OH) is usually used as the derivatizing agent (Hoye *et al.*, 2007).

The principle underlying the Mosher ester analysis is that, the diastereomeric MTPA esters formed after derivatization with MTPA-OH or MTPA-Cl have different physical and spectroscopic properties and therefore display different arrays of chemical shifts in their ^{1}H NMR spectra. The MTPA ester adopts a conformation in which the carbinol proton (H), the carbonyl bond (C=O), and the trifluoromethyl group (CF_3) are located in the same plane, called the "MTPA plane". In this case, the aryl group (the phenyl substituent) of the MTPA ester, imposes an anisotropic magnetic shielding effect on protons residing in the same plane with it. This shielding results in an up-field chemical

shift in the ^{1}H NMR of all spatially proximal proton (s) in the same plane as the phenyl ring while the de-shielded protons (in the opposite plane of the phenyl or in the same plane with OMe) experience a downfield chemical shift (Fig. 3.4).

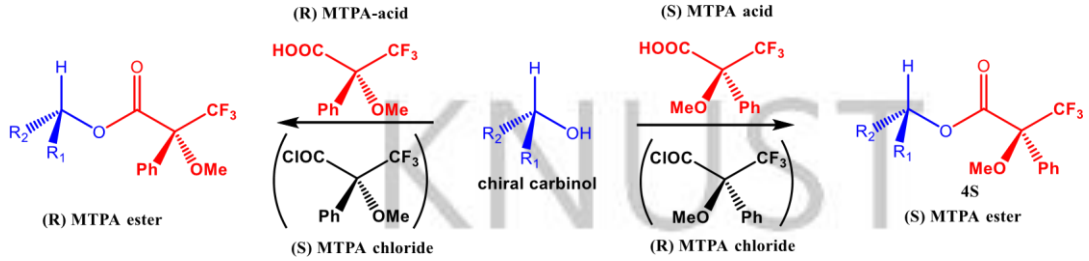

Fig. 3.4: Synthesis of R and S- Mosher esters from a carbinol

(Hoye *et al.*, 2007)

From the above illustration (Fig. 3.4), for the case of the (R) MTPA ester, protons residing in the R_1 plane would be relatively more shielded and thus experience an upfield chemical shift, while protons in the R_2 plane would experience a downfield chemical shift. The vice versa is true for the (S) MTPA ester. The consequence of the above is that the difference between R_1 proton chemical shifts of the (S) and (R) esters [δ_{R1} (*S-MTPA ester*) - δ_{R1} (*R-MTPA ester*)] will give a positive $\Delta\delta$ value while [δ_{R2} (*S-MTPA ester*) - δ_{R2} (*R-MTPA ester*)] will give a negative $\Delta\delta$ value. Finally, applying the Cahn Ingold Prelog conversion nomenclature, the configuration can be determined (Hoye *et al.*, 2007).

Preparation of (R)- and (S)- MTPA esters of compound HM1

Two portions of compound **HM1** (1 mg each, 3.7 µmol) in 10 µL of pyridine was treated separately with (*R*) and (*S*)-MTPA chloride (1.38 µL, 7.4 µmol) and 4dimethylaminopyridine (DMAP) (0.90 mg, 7.3 µmol) stirring at room temperature. The two reactions were conducted simultaneously and the progress was monitored by TLC. After complete consumption of **HM1**, the solvent was evaporated and the

reaction product was dissolved in $CDCl_3$ and transferred into NMR tubes. The ^1H NMR as well as ^1H-^1H COSY was measured to correctly assign signals for interpretation of results.

CHAPTER 4

RESULTS AND DISCUSSION

4.1 Biological activities of the stem bark of *Anopyxis klaineana*

4.1.1 Antimicrobial activity of the crude fractions of A. klaineana

The MeOH and EtOAc fractions of *A. klaineana* stem bark exhibited broad spectrum antimicrobial activity. The highest activity was exhibited by the EtOAc fraction against *S. aureus* and *S. pyogens* at 312 µg/mL. The petroleum ether fraction showed no activity (Table 4.1).

Table 4.1: Antimicrobial assay of fractions of *A. klaineana*

	Minimum inhibitory concentration (MIC), µg/mL				
	AKP	**AKE**	**AKM**	Ciprofloxacin	Ketoconazole
S. aureus	-	312	-	0.25	-
B. subtilis	-	625	625	0.10	-
S. pyogens	-	312	1250	0.10	-
E. coli	-	625	1250	0.10	-
P. aeruginosa	-	-	1250	0.10	-
S. typhi	-	625	-	0.25	-
C. albicans	-	-	625	-	5

AKP- petroleum ether fraction, AKE- EtOAc fraction, AKM-MeOH fraction

4.1.2 Antimicrobial activity of compounds from A. klaineana

The isolated compounds, **AK1** to **AK11** exhibited no antimicrobial activity at concentrations of 0.1, 0.5, 1, 5 and 10 µg/mL against *S. aureus*, *S. pyogens*, *B. subtilis*, *E. coli* and *P. aeruginosa*.

4.1.3 Anti-inflammatory activity

The carrageenan induced paw oedema assay was performed using three solvent fractions of *A. klaineana* stem bark specifically; the MeOH (AKM), EtOAc (AKE) and petroleum ether (AKP) fractions (refer to Section 3.4).

All test fractions and the positive control exhibited a dose dependent inhibition of carrageenan induced oedema formation. The highest effect was given by AKM and AKE. Chicks treated with 300, 100 and 30 mg/kg of AKM showed significant ($p < 0.001$) reduction in the peak inflammatory response to the *sub-plantar* injection of carrageenan. As demonstrated by the time course curve of AKM (300 mg/kg), (Fig. 4.1a), ≈ 40 % increase in paw volume was recorded between the 2nd and 3rd hours of observation whereas the untreated group showed ≈ 70 % increase in paw volume within one hour after the *sub-plantar* injection of carrageenan.

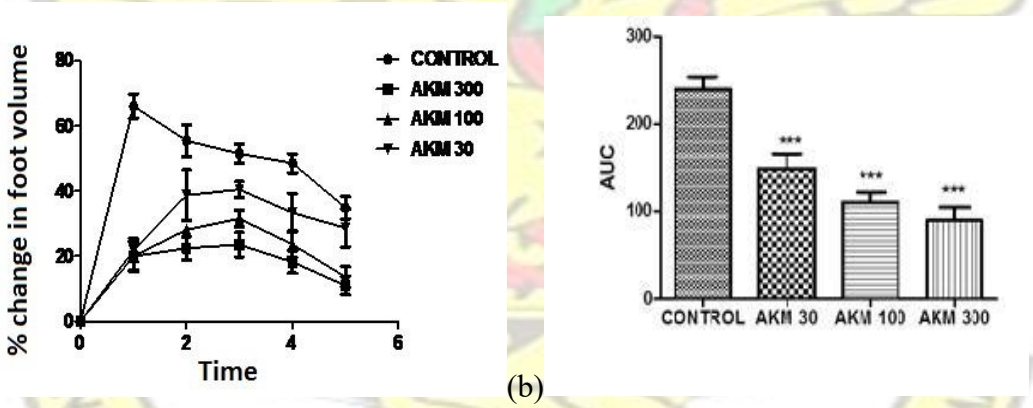

(a) (b)

Fig. 4.1a: Time course curve of inflammation in the presence of **AKM**
Fig. 4.1b: Total oedema response, calculated as AUCs; values recorded as the mean ± SEM (n=5); *** $p < 0.001$, ** $p < 0.01$, * $p < 0.05$ compared to the negative control group; **AKM**- *A. klaineana* stem bark MeOH fraction

In chicks that received AKE (300 mg/kg), the peak oedema response was recorded during the 2nd and 3rd hours as 50% increase of paw volume (Fig. 4.2a). The petroleum ether fraction showed the least anti-inflammatory effect (Fig. 4.3a,b).

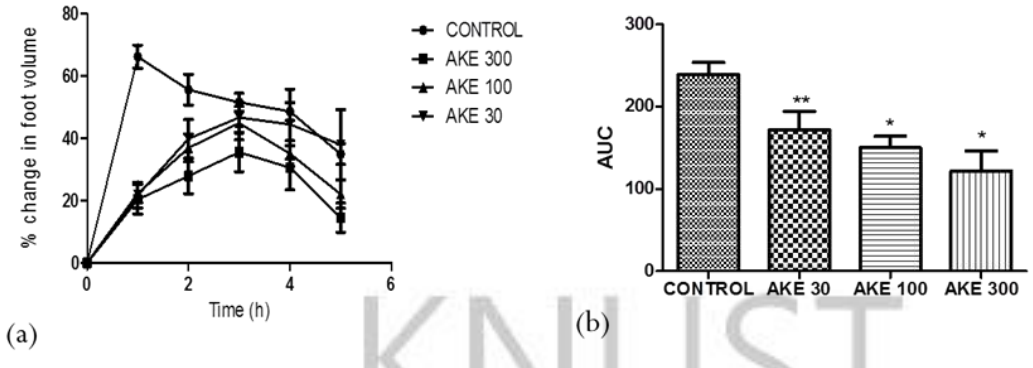

Fig. 4.2a: Time course curve of inflammation in the presence **AKE**
Fig. 4.2b: Total oedema response, calculated as AUCs; values recorded as the mean ± SEM (n=5); *** $p < 0.001$, ** $p < 0.01$, * $p < 0.05$ compared to the negative control group; **AKE**- *A. klaineana* stem bark EtOAc fraction

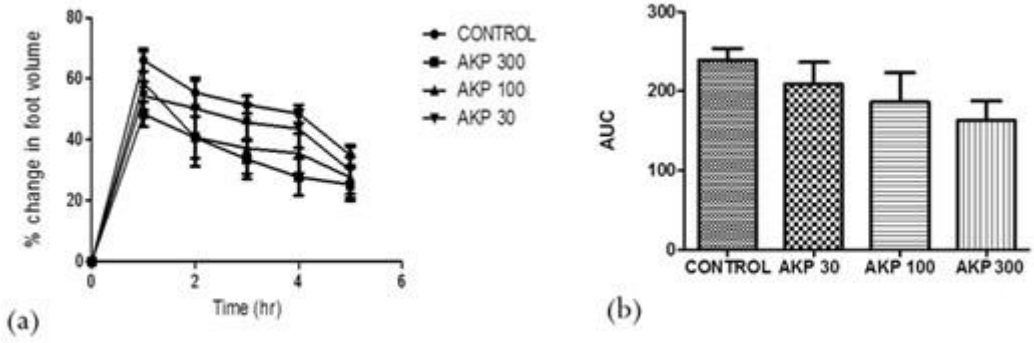

Fig. 4.3a: Time course curve of inflammation in the presence of **AKP**
Fig. 4.3b: Total oedema response, calculated as AUCs; values recorded as the mean ± SEM (n=5); *** $p< 0.001$, ** $p< 0.01$, * $p< 0.05$ compared to the negative control group; **AKP**- *A. klaineana* stem bark pet-ether fraction

The NSAID, diclofenac, however exhibited a better anti-inflammatory activity at all doses (10, 30, 100 mg/kg) than the crude fractions of *A. klaineana* (Fig. 4.4a,b).

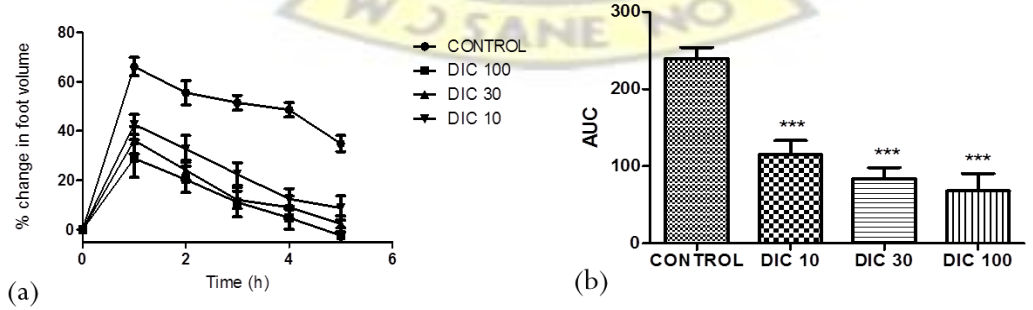

Fig. 4.4a: Time course curve of inflammation in the presence of diclofenac
Fig. 4.4b: Total oedema response, calculated as AUCs; values recorded as the mean ± SEM (n = 5); *** $p < 0.001$, ** $p < 0.01$, * $p < 0.05$ compared to the negative control group; (DIC-diclofenac)

The area under the curve (AUC) for each treatment was used to estimate the total oedema response for each group and to calculate the percentage inhibition of oedema. The results are stated in Table 4.2. The most significant anti-inflammatory effect among the tested fractions was exhibited by **AKM** (300 mg/kg) with a 62.40 % inhibition of total paw oedema ($p < 0.001$). In the presence of the **AKE** (300 mg/kg), the total paw oedema was inhibited by 49.1 % ($p < 0.01$).

Table 4.2: Percentage inhibition of carrageenan induced oedema

	AKM 300	**AKM 100**	**AKM 30**	**AKE 300**	**AKE 100**	**AKE 30**	**AKP 300**	**AKP 100**	**AKP 30**
% I.O	62.40 ± 6.32	53.88 ± 4.90	37.76 ± 7.17	49.10 ± 10.31	37.21 ±5.94	28.21 ±9.38	31.70 ±5.19	22.20 ±4.21	12.60 ± 3..21
	DICLO 100	**DICLO 30**	**DICLO 10**						
% I.O	71.50 ± 9.38	65.00 ± 6.11	51.80 ± 7.61						

% I.O- % inhibition of oedema; AKP- petroleum ether fraction, AKE- EtOAc fraction, AKM- MeOH fraction

4.1.4 In vivo anti-inflammatory effects of methyl angolensate (AK1)

(Refer to Section 4.2 for details on the isolated compounds from *A. klaineana*)

Methyl angolensate (**AK1**), the major constituent of the stem bark of *A. klaineana*, was obtained in large quantity and evaluated for anti-inflammatory activity by the carrageenan induced paw oedema assay. As observed in the time course curve (Fig. 4.5a), the peak oedema response was recorded an hour after the *sub-plantar* injection of carrageenan and declined from the 2nd to the 5th hour (Fig. 4.5a). The highest dose

of **AK1** (30 mg/kg) inhibited the total inflammation by 45.51 ± 6.26 % (Fig. 4.5b) while that given by diclofenac at the same dose showed 65 ± 6.14 % inhibition of oedema with reference to the negative control group. The anti-inflammatory activity of **AK1** was further compared with the positive controls through ED_{50} analysis. **AK1** had an ED_{50} value of 4.05 ± 0.003 which was less potent than diclofenac and dexamethasone which had an ED_{50s} of 2.49 ± 0.023 and 1.95 ± 0.003 respectively (Fig. 4.5c).

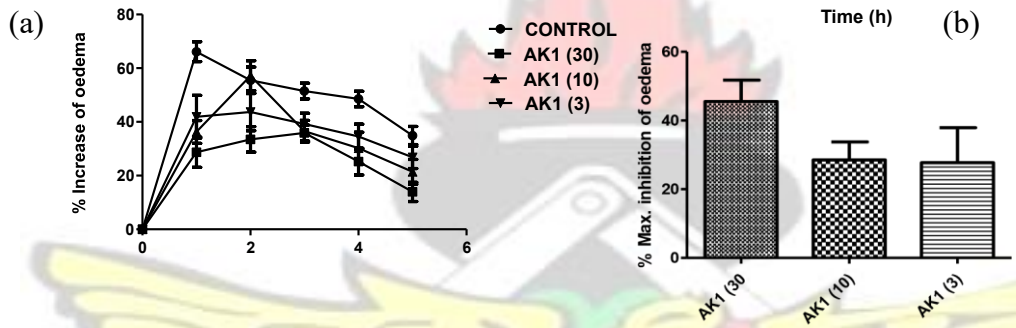

Fig. 4.5: (a) Time course of inflammation progression in the presence of **AK1** (b) Maximum percentage inhibition of oedema, calculated from AUC's; values are recorded as the mean ± S.E.M (n=5)

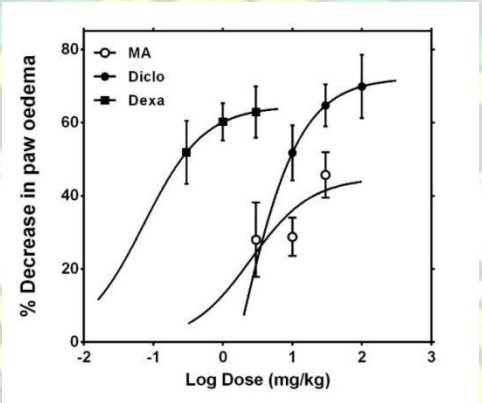

Fig. 4.5: (c) Dose response curves for methyl angolensate (MA) Dexamethasone (Dexa) and Diclofenac (Diclo)

4.1.5 Prostaglandin E_2 (PGE_2) competitive inhibition assay

(Refer to Section 4.2 for details on the isolated compounds from *A. klaineana*)

The potential of compounds **AK1**, **AK2**, **AK3**, **AK5a/5b**, **AK6**, **AK7**, **AK8** and **AK11** to compete with the inflammatory mediator PGE_2 for a number of binding sites on a mouse monoclonal antibody was investigated by an *in vitro* modified PGE_2 competitive inhibition assay. Compounds **AK4**, **AK9** and **AK10** could not be investigated due to the paucity of sample obtained. The results of the assay are stated in Table 4.3. The tirucallane triterpene acid, **AK6**, demonstrated the highest competitive inhibition of PGE_2 binding (IC_{50} = 3.63 μM). This was followed by methyl angolensate (**AK1**) with an IC_{50} of 10.23 μM.

Table 4.3: PGE_2 inhibition assay

Compound	**AK1**	**AK2**	**AK3**	**AK5a/5b**	**Cortisone**
IC_{50} (μM)	10.23	31.01	21.43	26.02	2.59
Compound	**AK6**	**AK7**	**AK8**	**AK11**	
IC_{50} (μM)	3.63	193.52	41.22	56.72	

4.1.6 Antioxidant activity of the crude MeOH extract of A. klaineana

DPPH free radical scavenging activity

The crude methanol extract of *A. klaineana* stem bark exhibited a dose dependent DPPH radical scavenging activity with an IC_{50} of 2.7 ± 0.21 µg/mL comparable to the activity of the standard reference drug, ascorbic acid (IC_{50} = 2.4 ± 0.01 µg/mL) (Fig. 4.6a-b).

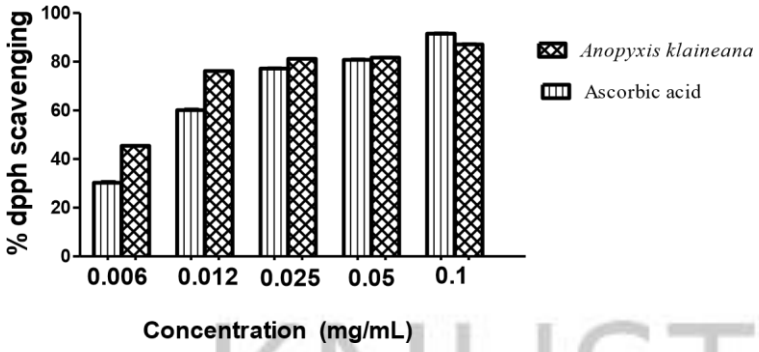

Fig. 4.6a: Percentage DPPH scavenging effect of different concentrations of *A. klaineana* crude MeOH extract

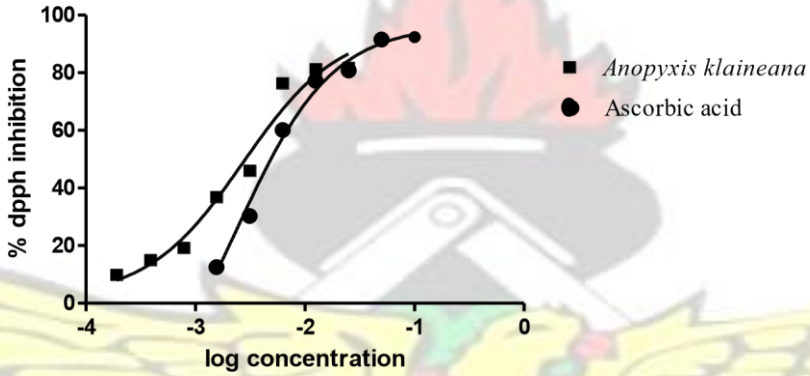

Fig. 4.6b: Log concentration versus percentage DPPH inhibition of *A. klaineana* crude extract

Total antioxidant capacity

The total antioxidant capacity of the extract was determined to be 110.6 ± 11.15 mg/g (ascorbic acid equivalent) implying that for every 1 g of dried extract, 110.6 mg of substance has antioxidant capacity equivalent to that of ascorbic acid.

(Standard curve of ascorbic acid: $y = 6.907x + 0.04604$, $r^2 = 0.9832$).

Total phenolic content

The crude MeOH extract of *A. klaineana* stem bark was found to have a total phenolic content of 110.21 ± 10.1 mg/g of dried extract (expressed as tannic acid equivalent, standard curve of tannic acid: $y = 23.92x + 0.01604$, $r^2 = 0.9996$).

4.1.7 Antioxidant activity of compounds from A. klaineana

The isolated compounds demonstrated significant DPPH free radical scavenging activity (Table 4.4). The tirucallane triterpenes showed a better scavenging activity than the limonoids.

Table 4.4: Free radical scavenging effects of compounds from *A. klaineana*

Compound	**AK1**	**AK2**	**AK3**	**AK5a/b**	**AK6**	AK7
IC_{50}(*μ*g/ml)	19.5	15.3	49.1	8.3	9.8	4.2

Compound	**AK8**	**AK9**	**AK10**	**AK11**	**Trolox**
IC_{50} (*μ*g/ml)	5.1	3.9	7.3	4.3	1.1

4.2 Structural elucidation of isolated compounds from *A. klaineana*

Chromatographic separation of the EtOAc fraction of *A. klaineana* led to the isolation of twelve compounds including six limonoids [**AK1-5a/5b**], five tirucallane triterpenes [**AK6-10**] and a protolimonoid [**AK11**] (Figs. 4.7a-b). Three (3) novel compounds (**AK6**, **AK7** and **AK8**) were isolated. The characterization of compounds was done by HR-ESIMS, IR and nuclear magnetic resonance (NMR) analysis, and by comparison of all data obtained with published literature on related compounds. [All HR-ESIMS and NMR spectra for the compounds from *A. klaineana* can be found in **Appendix A**].

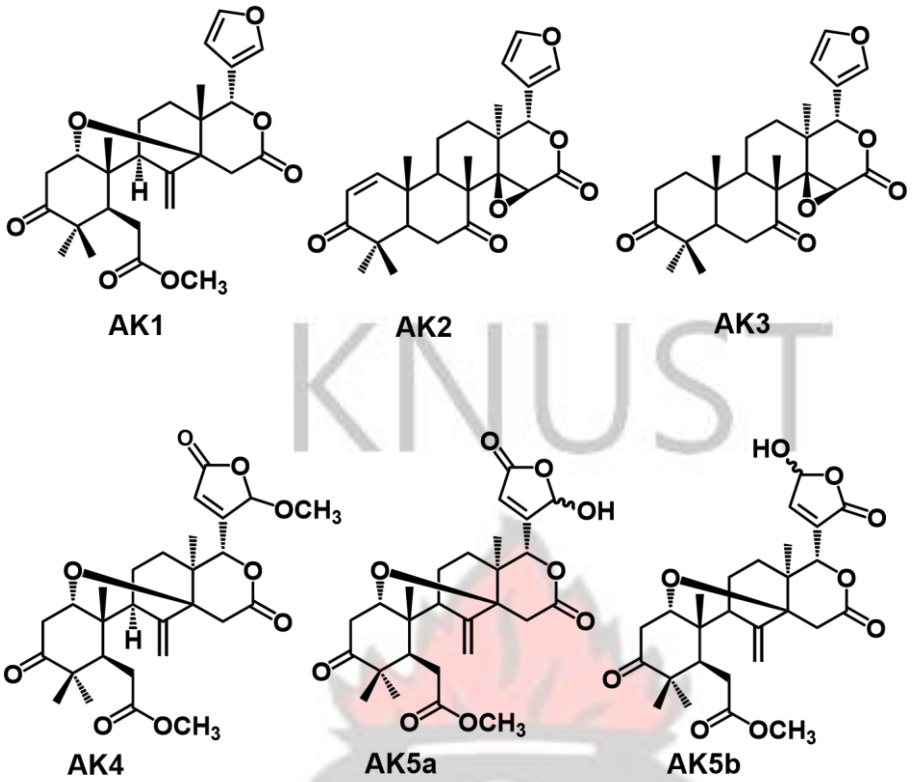

Fig. 4.7a: Limonoids isolated from *A. klaineana*

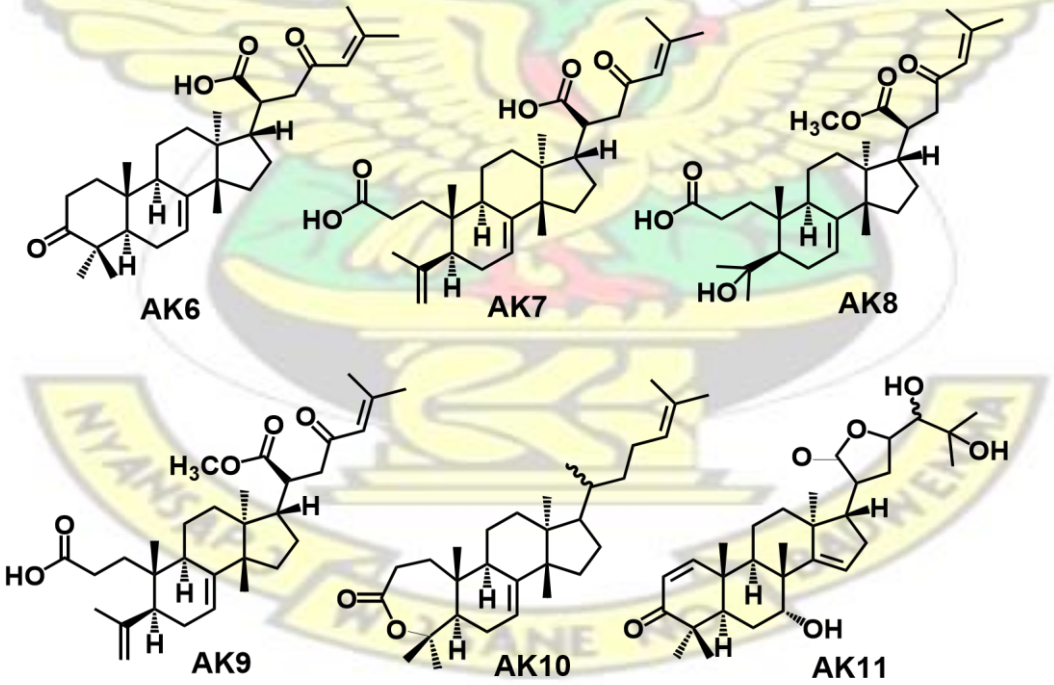

Fig. 4.7b: Tirucallane triterpenes from *A. klaineana*

Structural elucidation of compounds

4.2.1: Methyl angolensate (AK1)

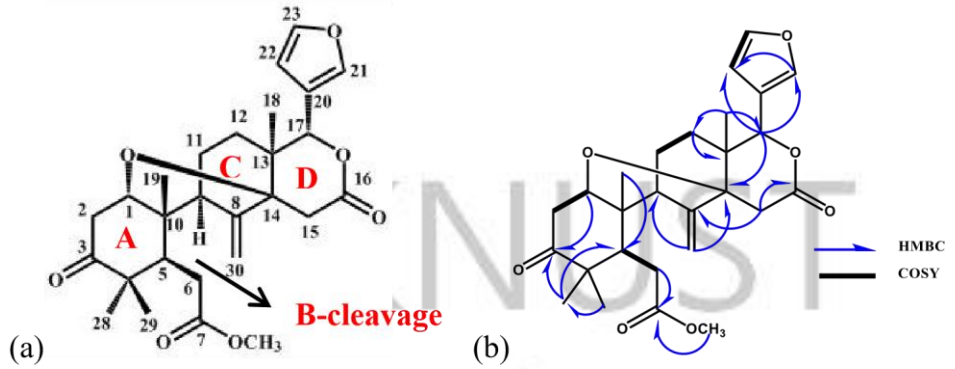

(a) (b)

Fig. 4.8 (a): **AK1**; (b): HMBC & COSY correlations for **AK1**

AK1 was obtained as colourless needle-like crystals. The UV spectrum gave a maximum absorption at 210 nm. The HR-ESIMS analysis showed a quassimolecular ion peak at *m/z* 471.23122 $[M + H]^+$ and suggested the molecular formula $C_{27}H_{34}O_7$ with eleven degrees of unsaturation.

From the ^1H NMR data, four singlet methyl signals [δ 0.83, δ 0.94, δ 1.04 and δ 1.18], one methoxyl [δ 3.70, s] and a characteristic signal for an exomethylene [δ 4.89/5.14, s, 1H each, CH_2-30] were observed. Further, three low field protons for a mono-substituted furan ring at δ 7.42 (brt, J = 1.0, CH-21), δ 6.37 (brs, CH-22) and δ 7.37 (t, J = 2.0, CH-23)], an oxymethine [δ 3.51, (dd, J = 6.0, 4.0, CH-1) and a low field proton signal at δ 5.65 (brs, CH-17)] were observed (Table 4.5).

The ^{13}C NMR data gave signals for twenty-seven carbons. Signals for four methyls [δ 13.9, δ 21.8, δ 26.0, δ 21.6], a methoxyl [δ 52.2] and an exomethylene group at C8/C30 [δ 145.9/111.7] were observed. Chemical shifts for the mono-substituted furan ring were identified at δ 121.0 (C-20), 140.9 (C-21), δ 110.1 (C-22) and δ

142.9 (C-23). Further, two oxymethines at δ 77.4 (C-1) and δ 79.7 (C-17) as well as four quaternary carbons, a ketone [δ 212.9] and two ester carbons [δ 174.0 and 170.2] were assigned (Table 4.5).

Table 4.5: ^{1}H (500 MHz) and ^{13}C (125 MHz) NMR data of AK1

Position	δ C	δ H *(mult, J, Hz)*	Position	δ C	δ H *(mult, J, Hz)*
1	77.4 (CH)	3.51, dd (6.0, 4.0)	**15**	33.9 (CH_2)	2.91, d (6.0), 2.58, m
2	39.6 (CH_2)	2.48, dd (14.0, 4.0) 2.88, brs	**16**	170.2 (C)	-
3	212.9 (C)	-	**17**	79.7 (CH)	5.65, brs
4	48.2 (C)	-	**18**	13.9 (CH_3)	0.83, s
5	43.1 (CH)	2.87, d (4.5)	**19**	21.8 (CH_3)	0.94, s
6	32.8 (CH_2)	2.26, d (16.5) 2.63, d (15.0)	**20**	121.0 (C)	-
7	174.0 (C)	-	**21**	140.9 (CH)	7.42, br t (1.0)
8	145.9 (C)	-	**22**	110.1 (CH)	6.37, brs
9	50.1 (CH)	2.17, m	**23**	142.9 (CH)	7.37, t (2.0)
10	44.2 (C)	-	**28**	26.0 (CH_3)	1.04, s
11	23.9 (CH_2)	2.23, m; 1.56, m	**29**	21.6 (CH_3)	1.18, s
12	29.5 (CH_2)	1.11, dd (5.0 13.5) 1.89, td (5.0, 14.0, 19.0)	**30**	111.7(CH_2)	4.89, s 5.14, s
13	41.6 (C)	-	**OMe-7**	52.2	3.70, s
14	80.4 (C)	-			

Chemical shifts (ppm) are referenced to solvent ($CDCl_3$) peak (δ H 7.26)

Ring A was characterized based on ^{1}H-^{1}H COSY correlations between the oxymethine at δ 3.74 (H-1) and the methylene at δ 2.48/2.88 (H-2) and HMBC cross peaks from H-1 and CH_3-28/29 to the ketone at δ 212.9 (C-3). The methyl ester chain at C-5 was confirmed by HMBC correlations from the methoxyl (δ 3.70) and methine proton at δ 2.87 (H-5) to the carbon at δ 174.0 (C-7). The ring B (C-7/C-8) cleavage was confirmed by the absence of HMBC correlations from H-6 to C-8 and C-9 and the presence of a C8/C30 exomethylene group. HMBC correlations from the exomethylene protons (4.89/5.14) to C-8, C-9 and C-14 were observed. The oxygen bridge between C-1 and C-14 was confirmed by the HMBC correlation from H-1 (δ

3.51) to C-14. The lactone ring (ring D) was characterized based on HMBC correlations from the oxymethine proton at δ 5.65 (H-17) and the methylene at δ 2.91/2.58 (CH_2-15) to the ester carbonyl at 170.2 (C-16). The C-17 furan ring was assigned based on ^{1}H-^{1}H COSY correlations between the olefinic protons at δ 6.37 (CH-22) and δ 7.37 (CH-23) as well as HMBC correlations from H-22 to C-21 (δ 140.9) and C-17 (δ 79.7). HMBC correlations were also observed from the oxymethine proton at δ 5.65 (H-17) to δ 140.9 (C-21) and δ 110.1 (C-22) confirming the attachment of the furan side chain to C-17. The NMR and mass spectral data of **AK1** were in agreement with the spectral data published for methyl angolensate (Fig. 4.8a) (Abdelgaleil and Nakatani, 2003; da Silva *et al.*, 2009; Lin *et al.*, 2009). The structure of **AK1** was confirmed by HR-MS^2 fragmentation which showed mass fragments at *m/z* 453 ($C_{27}H_{33}O_6$) for the loss of a molecule of water, *m/z* 439 ($C_{26}H_{31}O_6$) for the loss of a methoxyl group, *m/z* 421 ($C_{26}H_{29}O_5$) for the combined loss of a molecule of water and a methoxy, *m/z* 411 ($C_{25}H_{31}O_5$) for the loss of the methyl ester group and *m/z* 393 ($C_{25}H_{29}O_4$) for the combined loss of the methyl ester and a molecule of water (Fig. 4.9).

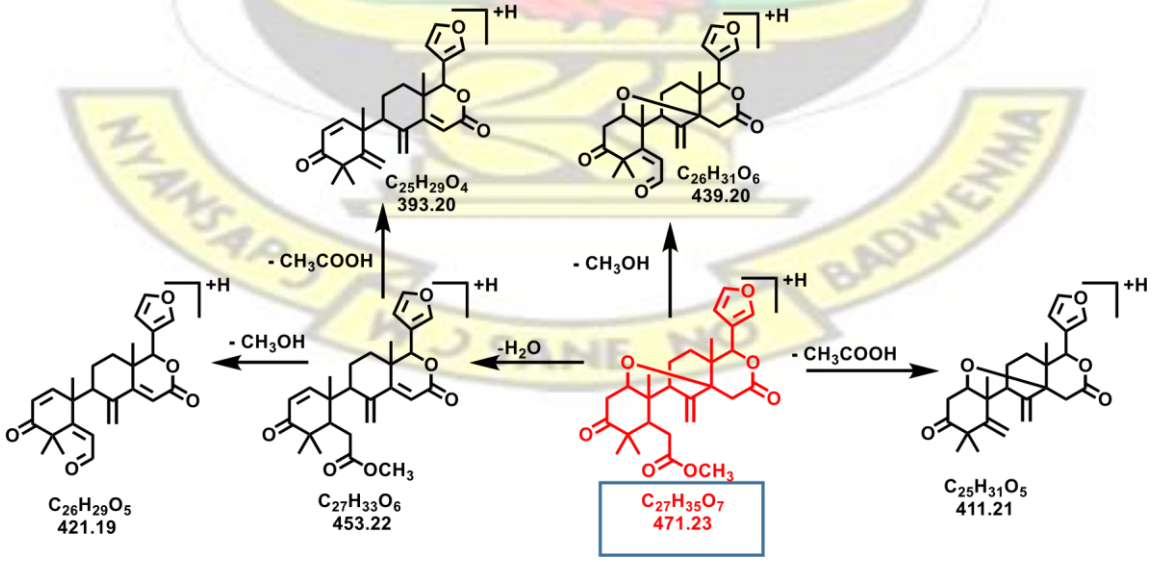

Fig. 4.9: HR-MS^2 fragmentation pattern of compound **AK1** (*m/z* 471)

4.2.2: 7-deacetoxy-7-oxo gedunin (AK2)

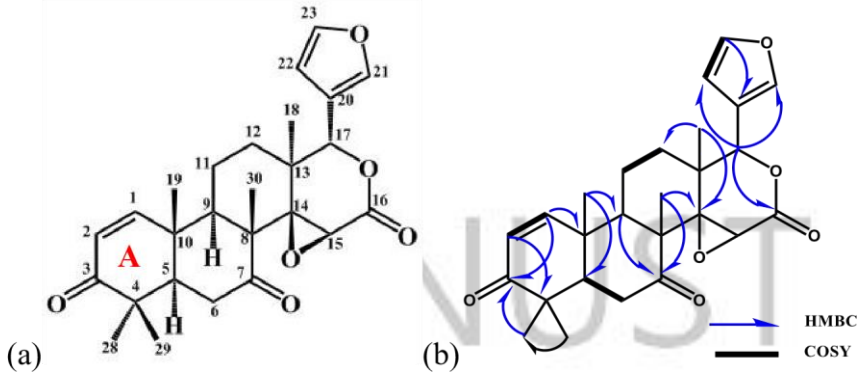

Fig. 4.10 (a):**AK2**; (b): HMBC & COSY correlations of **AK2**

AK2 was obtained as colourless crystal. Its molecular formula was determined to be $C_{26}H_{30}O_6$ with twelve degrees of unsaturation as deduced from its pseudo-molecular ion peak at *m/z* 439.2120 $[M + H]^+$.

From the ^{1}HNMR data (Table 4.6), five methyl singlets at δ 1.16, 1.35, 1.13, 1.22 and 1.20, two olefinic protons at δ 7.08 (d, *J* = 10.0, H-1) and δ 5.91 (d, *J* = 10.0, H2), an oxymethine at 3.87, (brs, H-15) and a low field proton at δ 5.47 (brs, H-17) were observed. The ^{13}C NMR gave signals for twenty-six carbons. Characteristic chemical shifts for two ketones [δ 203.4 (C-3) and δ 208.3(C-7)], two olefinic carbons [δ 156.0 (C-1), δ 126.6 (C-2)] and two oxymethines [53.8 (C-14), 78.2 (C17)] were observed. Signals for a mono-substituted furan ring were assigned as described for **AK1** (C20-C23).

Theα, β unsaturated hexenone ring (Ring A) was assigned based on ^{1}H-^{1}H COSY correlations between the olefinic methine protons at 7.08 (H-1) and 5.91 (H-2) as well as HMBC correlations from H1/H2 and the germinal methyl protons (H_3-28/29) to the ketone at δ 203.4 (C-3). The C-7 ketone group was established based on HMBC correlations from the methyl protons at δ 1.20 (s, CH_3-30) and the methine at δ 2.19 (H-5) to the carbonyl at δ 208.3 (C-7). The lactone ring (ring D) was assigned as

described for **AK1**. The presence of the C-14/15 epoxide ring was also confirmed by HMBC correlations from the methyl protons, CH_3-30 and CH_3-18 to δ 65.8 (C-14) as well as from the oxymethine proton at δ 3.87 (H-15) to C-14 (Fig. 4.10b).The C-17 furan side chain was characterized as described for **AK1**. All mass spectral and NMR data for **AK2** matched those for 7-deacetoxy-7-oxo gedunin (Fig. 4.10a) previously isolated from *Carapa guianensis* (da Silva *et al.*, 2009), *Entandrophragma angolense* (Nsiama *et al.*, 2011) and *Ekebergia capensis* (Murata *et al.*, 2008).

Table 4.6: ^{1}H (500 MHz) and ^{13}C (125 MHz) NMR data of AK2

Position	**δ C**	**δ H *(mult, J, Hz)***	**Position**	**δ C**	**δ H *(mult, J, Hz)***
1	156.0 (CH)	7.08, d (10.0)	**14**	65.8 (C)	-
2	126.6 (CH)	5.91, d (10.0)	**15**	53.8 (CH)	3.87, brs
3	203.4 (C)	-	**16**	167.0 (C)	-
4	45.4 (C)	-	**17**	78.2 (CH)	5.47, brs
5	47.8 (CH)	2.19, o	**18**	21.1 (CH_3)	1.16, s
6	36.9 (CH_2)	2.40, m; 2.92, m	**19**	20.0 (CH_3)	1.35, s
7	208.3 (C)	-	**20**	120.4 (C)	-
8	53.8 (C)	-	**21**	141.2 (CH)	7.39, brt (1.0)
9	54.8 (CH)	2.19, o	**22**	110.0 (CH)	6.36, brs
10	39.8 (C)	-	**23**	143.3 (CH)	7.39, t (2.0)
11	17.4 (CH_2)	2.02, m; 1.78, m	**28**	17.6 (CH_3)	1.22, s
12	32.4 (CH_2)	1.85, m; 1.48, m	**29**	20.8 (CH_3)	1.13, s
13	37.9 (C)	-	**30**	27.2 (CH_3)	1.20, s

Chemical shifts (ppm) are referenced to solvent ($CDCl_3$) peak (δ H 7.26)

4.2.3: 1, 2-dihydro-7-deacetoxy-7-oxo gedunin (AK3)

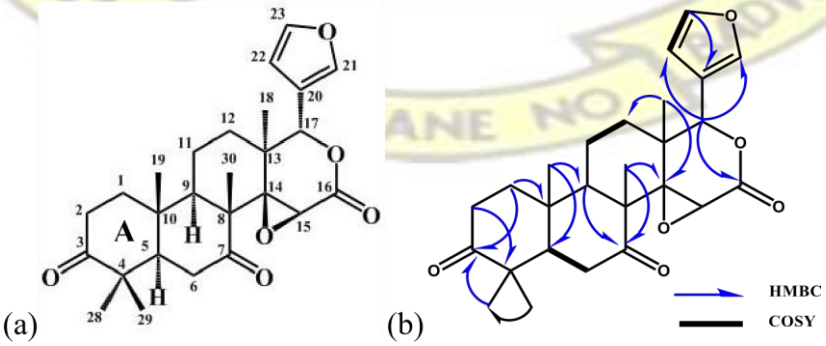

Fig. 4.11 (a): **AK3**; (b): HMBC & COSY correlations of **AK3**

AK3 was obtained as colourless crystals with the molecular formula $C_{26}H_{32}O_6$ with eleven degrees of unsaturation as deduced from its positive molecular ion peak at *m/z* 441.2278 $[M+H]^+$. The ^1H and ^{13}C NMR data of **AK3** (Table 4.7) showed similar chemical shifts and pattern of signals as those of **AK2** (described in Section 4.3.2). This indicated that **AK2** and **AK3** shared the same basic skeleton with the key difference being the absence of unsaturation at C-1/C-2 of ring A in **AK3**. From 2D NMR experiments, strong COSY between the methylene protons at δ 1.47, m ($CH_2$1) and δ 2.02, m (CH_2-2) and HMBC correlations from the germinal methyls at 1.09/1.10 (CH_3-28/29) and the methylene protons (CH_2-1/2) to the ketone at δ 214.7 (C-3) confirmed the structure of ring A (Fig. 4.11b). A comparison of the spectral data of **AK3** to reported data for similar compounds in literature led to its characterization as 1, 2-dihydro-7-deacetoxy-7-oxo gedunin (Fig. 4.11a), a gedunin derivative previously isolated from *Ekebergia capensis* (Murata *et al.*, 2008).

Table 4.7: ^1H (500 MHz) and ^{13}C (125 MHz) NMR data of AK3

Position	**δ C**	**δ H *(mult, J, Hz)***	**Position**	**δ C**	**δ H *(mult, J, Hz)***
1	38.5 (CH_2)	1.47, m; 2.02, m	**14**	65.4 (C)	-
2	32.5 (CH_2)	1.45, m; 1.82, m	**15**	53.5 (CH)	3.77, s
3	214.7 (C)	-	**16**	166.9 (C)	-
4	47.5 (C)	-	**17**	78.1 (CH)	5.45, brs
5	55.9 (CH)	2.20, m	**18**	21.0 (CH_3)	1.13, s
6	37.1 (CH_2)	2.36, dd (14.0, 4.0) 2.87, t (14.0)	**19**	16.8 (CH_3)	1.17, s
7	209.0 (C)	-	**20**	120.3 (C)	-
8	53.0 (C)	-	**21**	141.0 (CH)	7.40, o
9	51.8 (CH)	2.02, o	**22**	109.8 (CH)	6.36, brs
10	38.5 (C)	-	**23**	143.1 (CH)	7.39, o
11	17.4 (CH_2)	1.99, o; 1.75, m	**28**	26.4 (CH_3)	1.09, s
12	33.2 (CH_2)	1.22, m; 2.58, m	**29**	20.3 (CH_3)	1.10, s
13	37.5 (C)	-	**30**	16.5 (CH_3)	1.18, s

Chemical shifts (ppm) are referenced to solvent ($CDCl_3$) peak (δH 7.26)

4.2.4: Deacetoxy domesticulide D- 21 methyl ether (AK4)

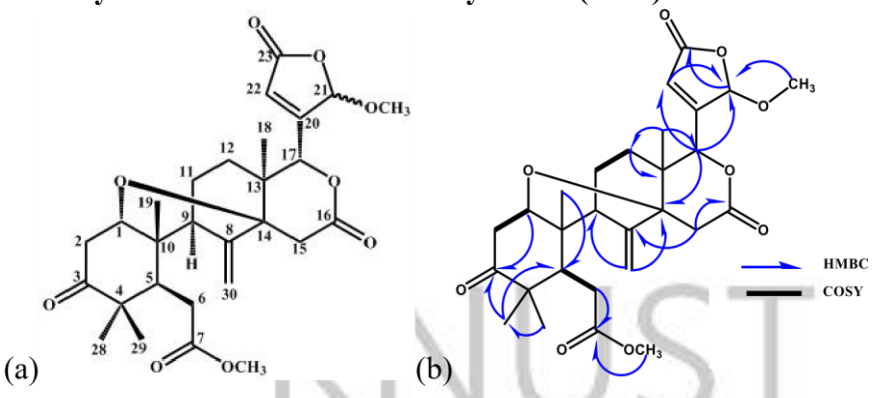

Fig. 4.12 (a): **AK4**; (b): HMBC & COSY correlations of **AK4**

AK4 was obtained as a white amorphous powder. Its HR-ESIMS spectrum showed a quassi-molecular ion peak at *m/z* 517.24438 $[M+H]^+$ in accordance with the molecular formula $C_{28}H_{36}O_9$.

From the ^1H NMR data (Table 4.8), characteristic signals for four methyls [δ 0.91, δ 0.87, δ 1.10, δ 1.19, s], two methoxyls [δ 3.7, s and δ 3.59, s], an exomethylene [δ 4.91 (d, *J* = 2.5), δ 5.16 (d, *J* = 3.5), CH_2-30], an oxymethine [δ 3.49, m, CH-1)] and two low field oxymethine proton signals at δ 5.63 [s, CH-17) and δ 5.78 (brs, H-21)] were observed. The ^{13}C NMR data gave signals for all twenty-eight carbons. Signals for four methyls [δ 13.7, δ 21.8, δ 27.1, δ 21.4], two methoxyls [δ 52.2 and δ 57.4] and an exomethylene group at C8/C30 [δ 145.7/112.0] were observed. Further, two oxymethines at δ 77.14 (C-1) and δ 77.4 (C-17), a ketone [δ 212.6 (C-3)] and three ester carbons [δ 173.4 (C-7), 169.2 (C-16) and 168.3 (C-23)] were assigned.

Careful analysis of 1D NMR data revealed that **AK4** possessed the same planar skeleton of **AK1** with a ring B, C-7/C-8 cleavage as earlier described for **AK1**. The oxygen bridge between C-1 and C-14, the exomethylene at C-8 and the methyl ester at C-5 were confirmed by HMBC correlations as described for **AK1**. The key difference between **AK1** and **AK4** was modification of the C-17 furan side chain by

substitution at C-21 and C-23 to obtain a γ-hydroxybutenolide (21-methyl ether) nucleus in **AK4**. This was confirmed by the presence of two broad singlets at δ 5.78 (C-21) and 7.18 (C-22) and ^{13}C resonances at δ 135.1 (C-20), 102.4 (C-21), 147.6 (C-22), 168.3 (C-23). HMBC correlation was observed from the methoxyl protons at δ 3.59 to the carbon at δ 102.4 (C-21) implying the attachment of a methoxy at position 21 (δ 102.4). Cross peaks were also observed from the H-17 (δ 5.63) to the carbons at δ 102.4 (C-21) and δ 147.6 (C-22). Further, the olefinic proton signal at 7.18 (H-22) and the oxymethine proton at δ 5.78 (H-21) had HMBC correlations with the ester carbonyl at δ 168.3 (C-23). All NMR and mass spectral data of **AK4** matched those reported for deacetoxy domesticulide D-21-methyl ether (Fig. 4.12a) previously isolated from *E. angolense* (Nsiama *et al.*, 2011). The structure of **AK4** was confirmed by HR-MS^2 fragmentation (*m/z* 517.59) which showed major fragments at *m/z* 499 for the loss of a molecule of water, *m/z* 485 for the loss of a methoxyl, *m/z* 467 for the combined loss of water and methoxyl and *m/z* 457 for the loss of the methyl ester group (Fig. 4.13).

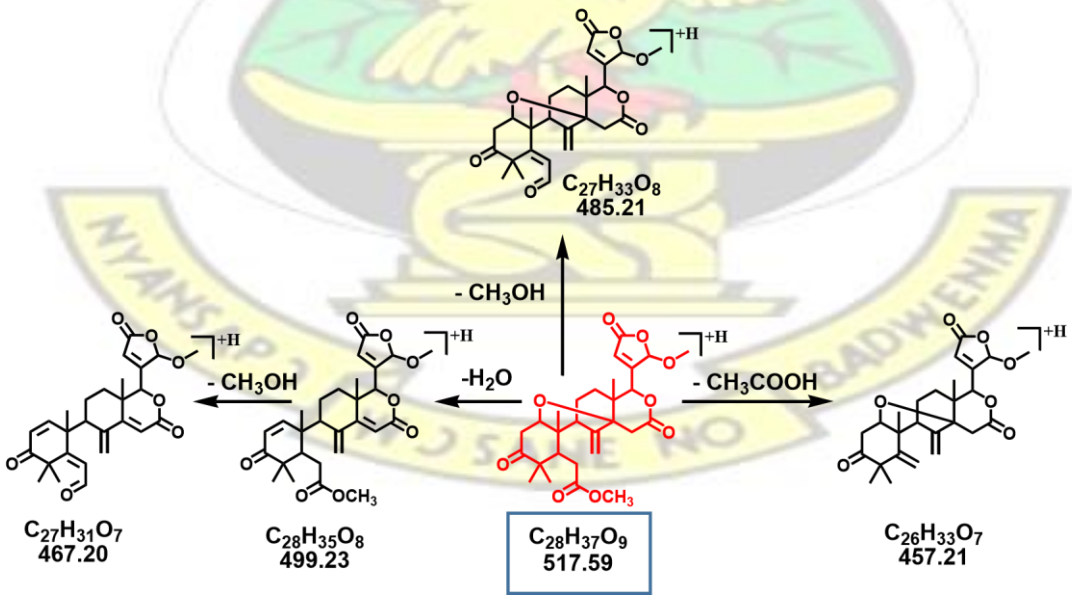

Fig. 4.13: HR-MS^2 fragmentation pattern of compound **AK4** (*m/z* 517)

Table 4.8: ^1H (500 MHz) and ^{13}C (125 MHz) NMR data of AK4

Position	δ C	δ H *(mult, J, Hz)*	Position	δ C	δ H *(mult, J, Hz)*
1	77.1 (CH)	3.49, m	**15**	33.9 (CH_2)	2.92, d (18.0); 2.56, m
2	39.9 (CH_2)	2.62, m 2.80, dd (14.5, 7.0)	**16**	169.2 (C)	-
3	212.6 (C)	-	**17**	77.4 (CH)	5.63, s
4	48.1 (C)	-	**18**	13.7 (CH_3)	0.91, s
5	43.2 (CH)	2.94, d (10.5)	**19**	21.8 (CH_3)	0.87, s
6	33.2 (CH_2)	2.60, m; 2.28, o	**20**	135.1 (C)	-
7	173.4 (C)	-	**21**	102.4 (CH)	5.78, brs
8	145.7 (C)	-	**22**	147.6 (CH)	7.18, brs
9	49.7 (CH)	2.19, d (5.0)	**23**	168.3 (C)	-
10	44.4 (C)	-	**28**	27.1 (CH_3)	1.10, o
11	23.7 (CH_2)	2.24, o; 1.62, m	**29**	21.4 (CH_3)	1.19, s
12	29.1 (CH_2)	1.09, o; 2.28, o	**30**	112.0 (CH_2)	4.91, d (2.5); 5.16, d (3.5)
13	41.9 (C)	-	**OMe-7**	52.2	3.71, s
14	79.5 (C)	-	**OMe-21**	57.4	3.59, s

Chemical shifts (ppm) are referenced to solvent ($CDCl_3$) peak (δH 7.26)

4.2.5: Deacetoxy domesticulide D (AK5a/b)

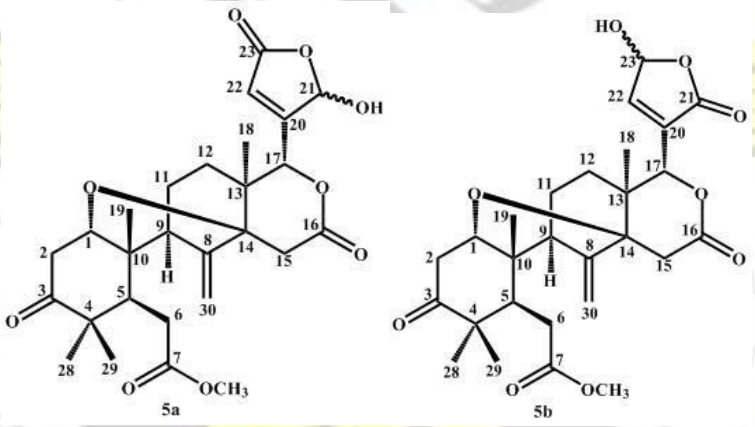

Fig. 4.14: Structures of AK5a/b

AK5a/b was obtained as a white amorphous powder. The HR-ESIMS gave a quassimolecular ion peak at *m/z* 503.22812 $[M + H]^+$ and suggested the molecular formula

$C_{27}H_{34}O_9$.

The chemical shifts and pattern of signals in the ^1H and ^{13}C NMR data (Tables 4.94.10) of **AK5a/b** were similar to those of **AK4**. Careful analysis of the NMR data indicated that the difference between **AK4** and **AK5a** was demethylation of the C-21 methoxyl

in **AK4** to obtain a hydroxyl group in **AK5a** (Fig. 4.14). The appearance of pairs of proton and carbon signals in ^{1}H and ^{13}C NMR spectrum suggested that **AK5** was a mixture of isomers. It was further revealed by HSQC analysis that the position 17 was assigned by two different carbon and proton signals [δ_C 78.2, δ_H 5.60 (AK5a) and δ_C 79.8, δ_H 5.62 (AK5b)] with the HMBC correlations from each proton to a different set ^{13}C NMR chemical shifts. Thus, the H-17 signal at δ 5.60 had key HMBC correlations with the oxymethine carbon at δ 97.3 (C-21) and the olefinic at δ 150.1 (C-22) whiles H-17 signal at δ 5.62 had HMBC correlations with the olefinic carbon at δ 121.4 (C-22) and the ester carbonyl carbon at δ 169.8 (C-21). This critical observation led to the conclusion that the difference between the two isomers was that in **AK5a** the hydroxyl group was located at C-21 and the carbonyl ester carbon at C-23 whiles the reverse was true for **AK5b**. All other chemical shifts were assigned based on HSQC, HMBC and COSY correlations as earlier described for

AK4. **AK5a/b** was thus determined to be a mixture of 6-deacetoxy domesticulide D (**AK5a**) and 6-deacetoxy domesticulide C (**AK5b**) based on comparison of spectral data to those published in literature. The compounds were previously isolated from *Xylocarpus moluccensis* (Wu *et al.*, 2010) and *Entandrophragma angolensis* (Nsiama *et al.*, 2011).

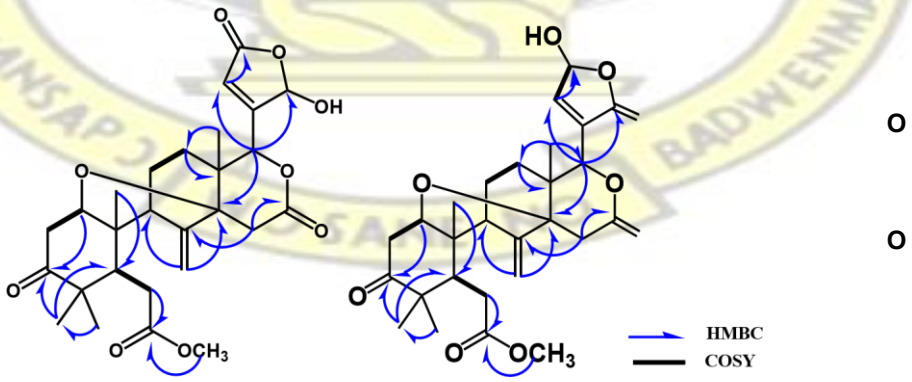

Fig. 4.15: HMBC, COSY correlations of compounds AK5a/b

Table 4.9: ^{1}H (500 MHz) and ^{13}C (125 MHz) NMR data of AK5a

Position	δ C	δ H *(mult, J, Hz)*^{o}	Position	δ C	δ H *(mult, J, Hz)*^{o}
1	77.2 (CH)	3.51	**15**	33.9 (CH_2)	2.56, 2.93
2	39.7 (CH_2)	2.52, 2.86	**16**	170.0 (C)	-
3	213.0 (C)	-	**17**	78.2 (CH)	5.60
4	48.1 (C)	-	**18**	13.6 (CH_3)	0.95
5	43.1 (CH)	2.89	**19**	21.8 (CH_3)	0.92
6	33.1 (CH_2)	2.28, 2.58	**20**	133.6(C)	-
7	174.0 (C)	-	**21**	97.3 (CH)	-
8	145.4 (C)	-	**22**	150.1 (CH)	7.32
9	49.7 (CH)	2.21	**23**	169.5 (C)	6.17
10	44.2 (C)	-	**28**	21.5 (CH_3)	1.18
11	23.7 (CH_2)	1.59, 2.21	**29**	26.4 (CH_3)	1.07
12	28.9 (CH_2)	1.09, 2.16	**30**	112.1 (CH_2)	5.18, 4.92
13	42.0 (C)	-	**OMe-7**	52.3	3.71
14	79.8 (C)	-			

Chemical shifts (ppm) are referenced to solvent ($CDCl_3$) peak (δ H 7.26), o-overlapping signals

Table 4.10: ^{1}H (500 MHz) and ^{13}C (125 MHz) NMR data of AK5b

Position	δ C	δ H *(mult, J in Hz)*^{o}	Position	δ C	δ H *(mult, J, Hz)*^{o}
1	77.2 (CH)	3.52	**15**	33.9 (CH_2)	2.56, 2.93
2	39.5 (CH_2)	2.48, 2.91	**16**	170.0 (C)	-
3	212.8 (C)	-	**17**	79.8 (CH)	5.62
4	48.2 (C)	-	**18**	14.4 (CH_3)	0.95
5	43.1 (CH)	2.85	**19**	21.8 (CH_3)	0.90
6	32.8 (CH_2)	2.26, 2.63	**20**	164.2 (C)	-
7	174.0 (C)	-	**21**	169.8 (C)	-
8	145.0 (C)	-	**22**	121.4 (CH)	6.22
9	49.7 (CH)	2.21	**23**	98.6 (CH)	6.18
10	44.1 (C)	-	**28**	21.6 (CH_3)	0.95
11	24.0 (CH_2)	1.62, 2.27	**29**	25.9 (CH_3)	1.00
12	33.1 (CH_2)	1.34, 2.04	**30**	112.6 (CH_2)	4.91, 5.20
13	42.0 (C)	-	**OMe-7**	52.4	3.72
14	79.8 (C)	-			

Chemical shifts (ppm) are referenced to solvent ($CDCl_3$) peak (δ H 7.26), o-overlapping signals

4.2.6: 3,23-dioxotirucalla-7,24-diene-21-oic acid (AK6, new compound)

AK6 was isolated as white amorphous powder. Its molecular formula was established as $C_{30}H_{44}O_4$ from its pseudo-molecular ion peak at *m/z* of 469.33176 $[M + H]^+$

($C_{30}H_{45}O_4$) and its sodium adduct, *m/z* of 491.31 ($C_{30}H_{44}O_4Na$) in the HRESIMS spectrum. The IR spectrum of **AK6** showed a characteristic absorption band at 1701 cm^{-1} due to carbonyl groups.

The ^{13}C NMR data (Table 4.11) gave signals for all 30 carbons. Characteristic signals for seven tertiary methyls, two olefinic groups [δ 118.5/145.6 (C-7/8) and δ 123.3/156.9, (C-24/25)], two ketones [δ 216.8 (C-3) and δ 199.1 (C-23)], and an acid carbon [δ 179.11 (C-21)] were observed. From the ^1H NMR spectrum, signals for seven methyl singlets [δ 0.97, 0.98, 1.89, 2.14, 1.05, 1.11 and 1.00] and two olefinic protons [δ 5.31 (brs, CH-7) and δ 6.05 (brs, C-24)] were clearly identified. These ^1H and ^{13}C NMR data were consistent with those reported for tirucallane triterpenes (Mohamad *et al.*, 1999; Orisadipe *et al.*, 2005).

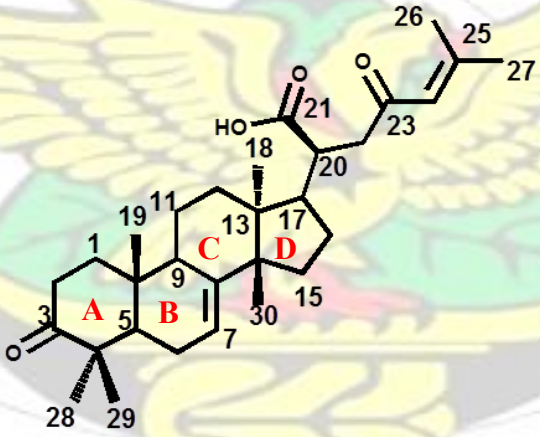

Fig. 4.16: Structure of **AK6**

A careful analysis of all ^1H and ^{13}C NMR chemical shifts (Table 4.11) and comparison to the published NMR data for tirucallane derivatives revealed that **AK6** possessed a similar tirucallane structure as 3,23-dioxotirucalla-7,24-diene-21-al previously isolated from *Entandrophragma angolense* (Orisadipe *et al.*, 2005). The key difference however was a C-21 acid group (δ 179.1) in **AK6** as opposed to the C-21 aldehyde (204.7) in 3, 23-dioxotirucalla-7, 24-dien-21-al.

The position of the acid group was confirmed at C-20 based on HMBC correlations from H-22 (δ 2.65/2.86) and H-20 (δ 2.80) to δ 178.8 (C-21) (Fig. 4.17a). The C-3 keto functional group was identified by HMBC correlations from the germinal methyl protons at δ 1.05/1.11 (CH_3-28/29) to δ 216.8 (C-3). ^{1}H-^{1}H COSY correlations between δ 2.08 (H_2-6) and δ 5.31 (H-7) as well as HMBC correlations from δ 1.00 (CH_3-30) to the olefinic carbon at δ 145.6 (C-8) confirmed the olefinic group at C-7/C-8. The methyl protons at δ 1.89/2.14 (CH_3-26/27) had HMBC correlations with the olefinic carbons at δ 123.3 (C-24) and 156.9 (C-25), confirming the olefinic group at C-24/25 and establishing a terminal isopropylidene group (Fig. 4.17a). HMBC cross peaks from δ 6.05 (H-24) and δ 2.65/2.86 (H-22) to δ 199.1 (C-23) established the ketone at C-23. All-together, this data confirmed the 3,23-dioxo7,24-diene tirucalla skeleton. **AK6** was thus characterized as 3,23-dioxotirucalla-7, 24-diene-21-oic acid (Fig. 4.16). Based on the common relative configurations of tirucallane triterpenes (Akihisa *et al.*, 1996), and by NOESY correlations (Fig. 4.17b), H-17, CH_3-19, CH_3-29 and CH_3-30 were designated as β-oriented, whereas H-5, H-9, H-20, CH_3-28 and CH_3-18 were designated as α-oriented (Mireku *et al.*, 2015).

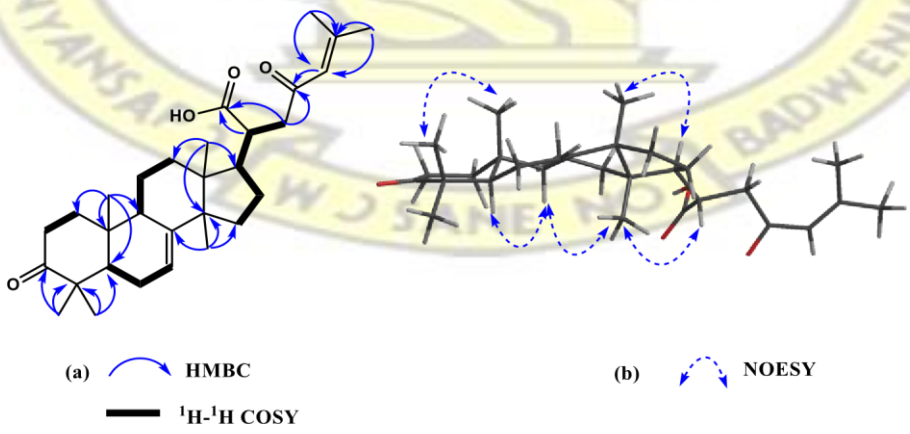

Fig. 4.17: HMBC, COSY (a) and NOESY (b) correlations for compound **AK6**

The structure of **AK6** was confirmed by HR-MS^2 fragmentation which showed fragment ions for the losses of a molecule of H_2O [*m/z* 451], $2H_2O$ [*m/z* 433] and a combined loss of H_2O and CO [*m/z* 423]. Further, fragment ions at *m/z* 413 $[M+HC_4H_8]^+$, 369 $[M+H-C_4H_8-CO_2]^+$ and 353 $[M+H-H_2O-C_6H_{10}O]^+$ were observed (Fig.

4.18).

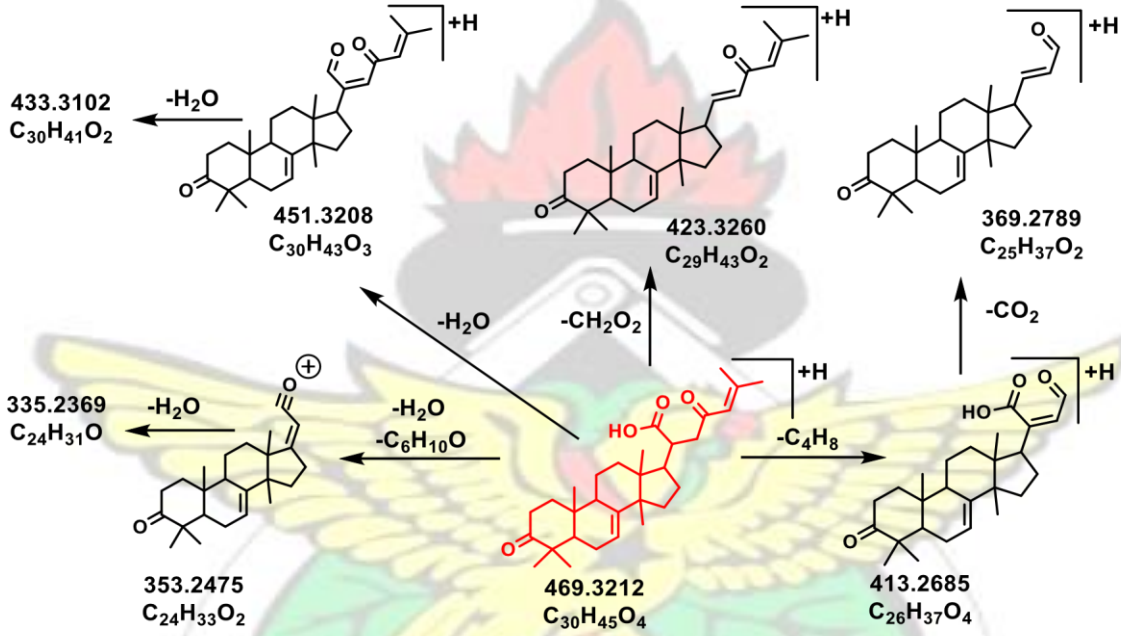

Fig. 4.18: HR-MS^2 fragmentation pattern of **AK6** (*m/z* 469)

Table 4.11: ^1H (500 MHz) and ^{13}C (125 MHz) NMR data of AK6

Position	δ C	δ H (J in Hz)
1	38.7 (CH_2)	1.45, m; 1.94, m
2	35.2 (CH_2)	2.23, m; 2.73, dd (14.5, 5.5)
3	216.8 (C)	-
4	48.0 (C)	-
5	52.5 (CH)	1.73, dd (17.0, 8.5)
6	24.6 (CH_2)	2.08, m
7	118.5 (CH)	5.31, brs
8	145.6 (C)	-
9	48.4 (CH)	2.26, m

10	35.0 (C)	-
11	18.1 (CH_2)	1.54, m
12	30.1 (CH_2)	1.72, o, 1.63, m
13	43.6 (C)	-
14	51.1 (C)	-
15	33.6 (CH_2)	1.34, m, 1.53, m
16	27.7 (CH_2)	1.95, o; 1.31, m
17	49.5 (CH)	2.02, m
18	21.6 (CH_3)	0.97, s
19	12.9 (CH_3)	0.98, s
20	42.4 (CH)	2.80, dd (10.5, 2.0)
21	179.1 (C)	-
22	46.6 (CH_2)	2.65, dd (17.0, 2.0); 2.86, dd (17.0, 10.0)
23	199.1 (C)	-
24	123.3 (CH)	6.05, (br. s)
25	156.9 (C)	-
26	21.1 (CH_3)	1.89, s
27	28.0 (CH_3)	2.14, s
28	21.8 (CH_3)	1.05, s
29	24.8 (CH_3)	1.11, s
30	27.6 (CH_3)	1.00, s

Chemical shifts (ppm) are referenced to solvent ($CDCl_3$); o- overlapping signals

Physicochemical properties of AK6: White amorphous powder; $[\alpha]\ ^{20}_{D}$:−38.9 ° (*c* 0.07 in $CHCl_3$); UV λ_{max}: 234 nm; IR V_{max} (KBr) cm^{-1}: 2927, 1701, 1627.

4.2.7: 3,4-secotirucalla-23-oxo-4(28)7,24-trien-3,21-dioic acid (AK7, new compound)

AK7 was obtained as white amorphous powder and its molecular formula was determined to be $C_{30}H_{44}O_5$ based on its quassi-molecular ion peak at *m/z* 485.32642 ($C_{30}H_{45}O_5$; $[M + H]^+$) requiring nine degrees of unsaturation. A characteristic band at 1704 cm^{-1} for carbonyls was identified in the IR spectrum.

The ^{13}C and ^{1}H NMR data (Table 4.12) gave signals for six methyls, six methines, including two olefinic groups [δ_C 118.3, δ_H 5.22, brs (CH-7); 146.0 (C-8) and δ_C 123.1, δ_H 6.03 brs (CH-24)], 156.9 (C-25)], nine methylenes, including an exomethylene [δ_C

114.2, δ_H 4.80, brs, (CH_2-28)], three quaternary carbons, two acid carbons, [δ_C 181.1 (C-3) and δ_C 182.4, (C-21)], and one ketone [δ_C 198.6 (C-23)].

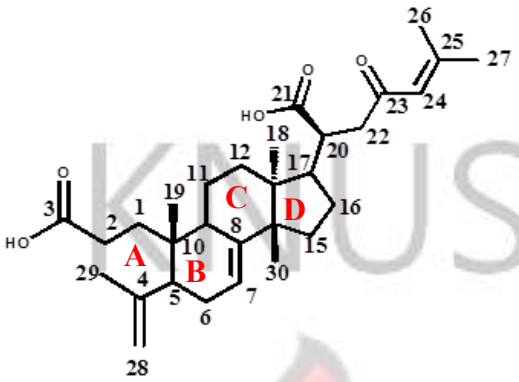

Fig. 4.19: Structure of **AK7**

Three intact rings (rings B/C/D of compound **AK6**) were identified by 1D and 2D NMR as described for **AK6**. From the 2D NMR analysis, key ^{1}H-^{1}H COSY and HMBC correlations (Fig. 4.20a) such as COSY correlation between δ 1.59 m, (H_2-1) and δ 2.37 m, (H_2-2) and the HMBC correlations from δ 2.37/2.51 m (H_2-2) to δ 181.1 (C-3) and δ 36.6 (C-10); from the methyl protons at δ 0.83 s (H_3-19) to δ 31.0 (C-1), δ 50.3 (C-5), δ 41.1 (C-9) and δ 36.6 (C-10); from the exomethylene, δ 4.80 brs (H_2-28) to δ 50.3 (C-5) and δ 22.1 (C-29) and from δ 1.76 s (H_3-29) to δ 147.6 (C-4), δ 50.3 (C-5) and δ 114.2 (C-28) established a 3,4-seco ring-A system bearing an acid group at position 3 similar to the ring A structure of Aphanamgrandin J, a tirucallane triterpene isolated from *Aphanamixis grandifolia* (Zeng *et al.*, 2012). The absence of HMBC correlations from the 4.80 (H_2-28) and 1.76 (H_3-29) to 181.1 (C3) confirmed the C-3/C-4 cleavage (Fig. 4.20a). The same C-17 side chain was identified for this compound as described for **AK6**.The structure of **AK7** was therefore characterized as 3,4-secotirucalla-23-oxo-4(28)7,24-trien-3,21-dioic acid

(Fig. 4.19) (Mireku *et al.*, 2015). Characteristic NOESY correlations (Fig. 4.20b) of **AK7** confirmed the configurations at H-17, CH_3-19, C-21 and CH_3-30 as β-oriented and H-5, H-9, H-20 and CH_3-18 as α-oriented (Orisadipe *et al.*, 2005).

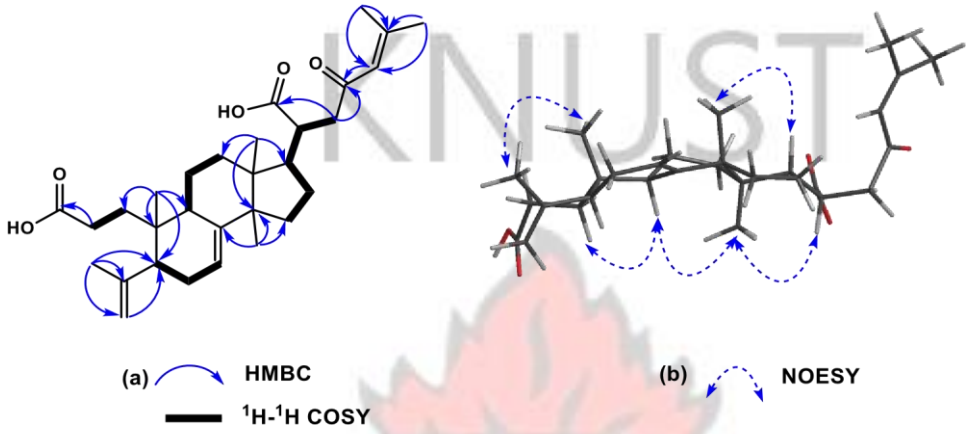

Fig. 4.20: HMBC, COSY (a) and NOESY (b) correlations for compound **AK 7**

The structure was further confirmed by HR-MS^2 fragmentation in the negative ESI mode which showed peaks at 439 $[M –H- CO_2]^+$, 421 $[M-H-CO_2-H_2O]^+$ and 383 $[MH-CO_2-C_4H_8]^+$.

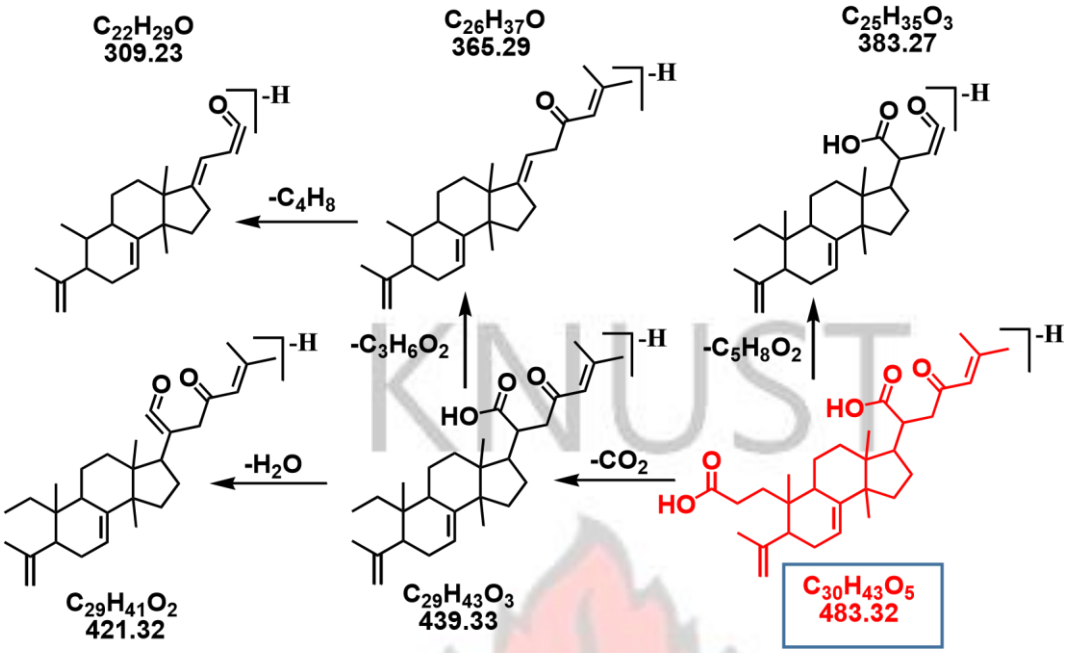

Fig. 4.21: HR-MS$^{2/3}$ fragmentation pattern of compound **AK7** (*m/z* 483)

Table 4.12: ^{1}H (500 MHz) and ^{13}C (125 MHz) NMR data of AK7

Position	δ C	δ H *(J in Hz)*
1	31.0 (CH_2)	1.59, m
2	28.0 (CH_2)	2.51, m; 2.37, m
3	181.1 (C)	-
4	147.6 (C)	-
5	50.3 (CH)	2.41, dd (12.0, 6.6)
6	30.3 (CH_2)	2.04, m; 2.21, m
7	118.3 (CH)	5.22, br. s
8	145.8 (C)	-
9	41.1 (CH)	2.48, m
10	36.6 (C)	-
11	18.3 (CH_2)	1.53, *o*; 1.33, m
12	29.8 (CH_2)	1.72, m; 1.57, m
13	43.7 (C)	-
14	51.7 (C)	-
15	33.7 (CH_2)	1.49, m; 1.56, m
16	28.0 (CH_2)	1.97, *o*; 1.00, m
17	50.0 (CH)	1.97, m
18	21.2 (CH_3)	0.98, s
19	16.1 (CH_3)	0.83, s
20	43.5 (CH)	2.72, m
21	182.4 (C)	-
22	46.8 (CH_2)	2.62, dd (16.6, 10.6); 2.79, dd (17.0, 8.5)
23	198.4 (C)	-

24	123.1 (CH)	6.03, brs

Table 4.12 *continued*: ^{1}H (500 MHz) and ^{13}C (125 MHz) NMR data of AK7

Position	**δ C**	**δ H *(J in Hz)***
25	156.7 (C)	-
26	21.1 (CH_3)	1.88, s
27	27.3 (CH_3)	2.13, s
28	114.2 (CH_2)	4.80, brs
29	22.1 (CH_3)	1.76, s
30	27.3 (CH_3)	0.98, s

Chemical shifts (ppm) are referenced to solvent ($CDCl_3$), o- overlapping signals

Physicochemical properties of AK7: White amorphous powder; $[\alpha]^{20}_{D}$: −6.6 ° (*c* 0.15 in $CHCl_3$); UV λ_{max}: 220 nm; IR V_{max} (KBr) cm^{-1}: 2954, 1704, 1621

4.2.8: 3, 4-secotirrucalla-4-hydroxy-23-oxo-7,24-diene-3,21-dioic acid 21-methyl ester (new compound, AK8)

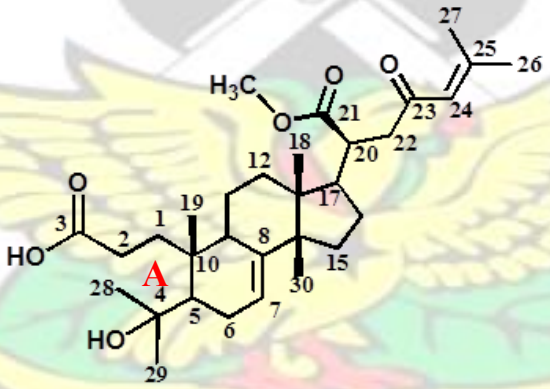

Fig. 4.22: Structure of **AK8**

AK8 was obtained as white amorphous powder and its HR-ESIMS gave a quassimolecular ion peak at *m/z* 517.35291 $[M+H]^{+}$ corresponding to a molecular formula $C_{31}H_{48}O_6$ with eight ring and double bond equivalents.

The ^{1}H and ^{13}C NMR spectral data (Table 4.13) gave signals for all thirty-one carbons and where assigned as seven methyls, eight methylenes, six methines, one methoxyl at δ_C 51.8, δ_H 3.70, three quaternary carbons, a ketone at δ 199.0, two acid or ester carbons at δ 177.1 and 176.6 and an oxygen bearing carbon at δ 76.9. Analysis of

HSQC, COSY and HMBC NMR data revealed that **AK8** had a similar 3, 4 ring-A seco tirucallane skeleton as that described for **AK7**. However, key HMBC correlations from the methyl protons, δ_H 1.25/1.33 (H_3-28/29) to δ_C 76.9 (C-4) as well as that observed from δ 1.91, (d, *J*=5, H-5) to δ_C 76.6 (C-4) confirmed the presence of a hydroxyl bearing carbon at position 4 (Fig.4.23a). The side chain for compound **AK8** showed identical spectral frequencies as described for compounds **AK6** and **AK7**. However, a methyl ester group at C-21 (instead of an acid in AK6, AK7) was identified based on strong HMBC correlation from the methoxyl protons (δ 3.70) to the carbonyl at δ 176.6 (C-21) (Fig. 4.23a). All other proton and carbon resonances of compound **AK8** were assigned from cross peaks in HMBC, COSY and NOESY spectra as shown in Fig. 4.23a-b. **AK8** was assigned 3, 4-secotirrucalla-4hydroxy-23-oxo-7,24-diene-3,21-dioic acid 21- methyl ester (Fig. 4.22) (Mireku *et al.*, 2015).

From the HR-MS^2 fragmentation in negative mode, fragment ions at *m/z* 483 [M H CH_3OH] , 471 [M H CO $_2$] and 457 [M H C_3H_6O] confirmed the presence of methoxyl, acid and the iso-propanol groups in the structure of **AK8** (Fig. 4.24).

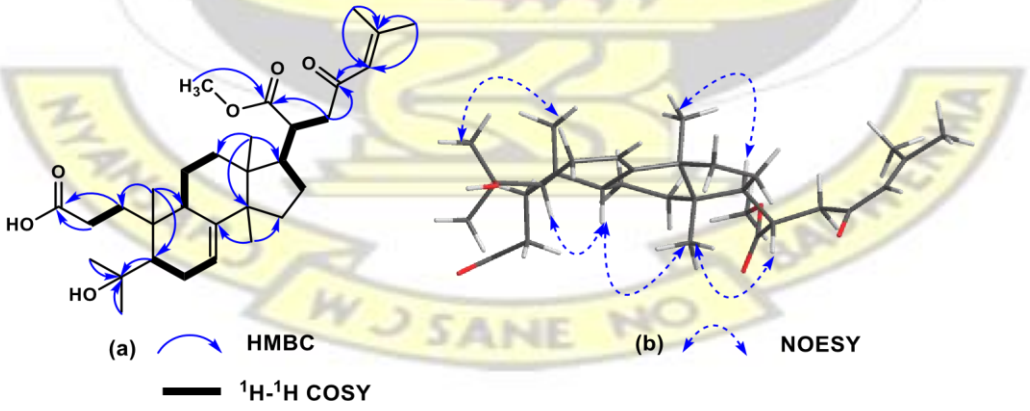

Fig. 4.23: HMBC, COSY (a) and NOESY (b) correlations for compound AK8

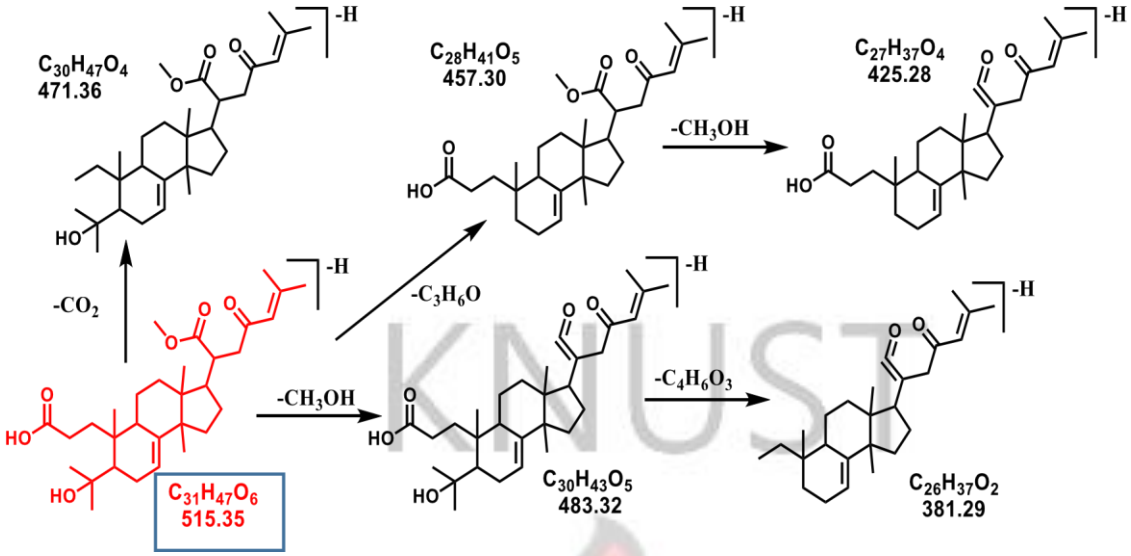

Fig. 4.24: HR-MS^2 fragmentation pattern of compound **AK8** (*m/z* 515)

Table 4.13: ^{1}H (500 MHz) and ^{13}C (125 MHz) NMR data of AK8

Position	**δ C**	**δ H *(J in Hz)***
1	32.9 (CH_2)	1.68, m; 2.23, *o*
2	29.3 (CH_2)	2.78, m; 2.22, *o*
3	177.1 (C)	-
4	76.9 (C)	-
5	49.5 (CH)	1.91, d (5.0)
6	28.3 (CH_2)	1.82, m; 2.21, m
7	118.3 (CH)	5.20, brs
8	146.0 (C)	-
9	41.9 (CH)	2.36, m
10	38.5 (C)	-
11	17.4 (CH_2)	1.49, m
12	30.0 (CH_2)	1.62, m; 1.37, m
13	43.3 (C)	-
14	51.2 (C)	-
15	33.9 (CH_2)	1.50, m
16	27.6 (CH_2)	1.96, m; 1.30, m
17	49.9 (CH)	1.96, m
18	21.8 (CH_3)	0.94, s
19	17.1 (CH_3)	0.86, s
20	42.5 (CH)	2.80, m
21	176.6 (C)	-

Table 4.13 *continued*: ^{1}H (500 MHz) and ^{13}C (125 MHz) NMR data of AK8

Position	δ C	δ H *(J in Hz)*
22	47.1 (CH_2)	2.61, dd (17.0, 2.5); 2.85, dd, (16.5, 10.5)
23	199.0 (C)	-
24	123.5	6.02, brs
25	156.1 (C)	-
26	21.0 (CH_3)	1.87, s
27	27.9 (CH_3)	2.11, s
28	34.1 (CH_3)	1.25, s
29	26.1 (CH_3)	1.33, s
30	27.6 (CH_3)	0.97, s
OMe-21	51.8	3.70, s

Chemical shifts (ppm) are referenced to solvent ($CDCl_3$); o- overlapping signals

Physicochemical properties of AK8: White amorphous powder; $[\alpha]^{20}_D$: −5 ° (*c* 0.06 in $CHCl_3$); UV λ_{max} 224 nm; IR V_{max} (KBr) cm^{-1}: 2953, 1730, 1439, 1379.

4.2.9:3, 4-Secotirucalla-23-oxo-4(28) 7, 24-trien-3, 21-dioic acid (21-methyl ester (AK9)

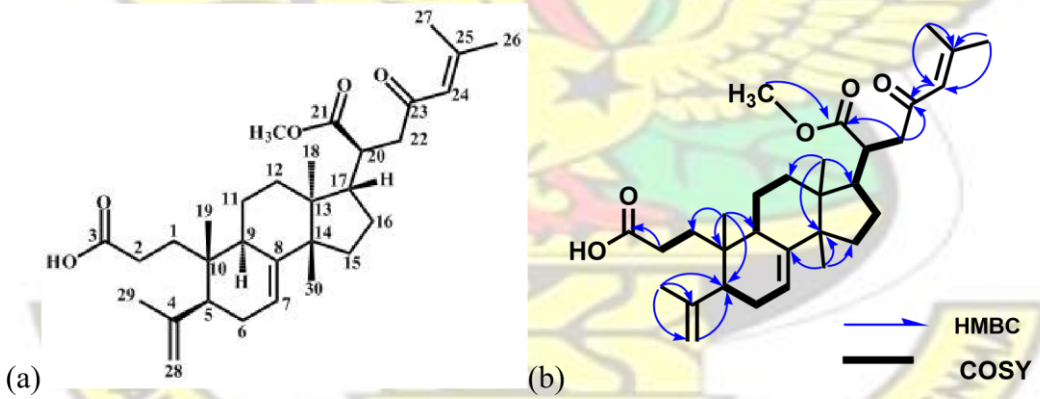

Fig. 4.25 (a): **AK9**; (b): HMBC & COSY correlations of **AK9**

The HR-ESIMS of **AK9** showed a pseudo-molecular ion peak at *m/z* 499.34232 $[M + H]^+$ and a sodium adduct ion at *m/z* 521.32 $[M + Na]^+$suggesting the molecular formula $C_{31}H_{46}O_5$. The ^1H and ^{13}C NMR data (Table 4.14) of **AK9** gave similar chemical shifts as **AK7**. However, signals for methoxyl group (δ_H 3.69, δ_C 51.8) was observed. Analysis of the 2D NMR data indicated that compound **AK9** had the same tirucallane

skeleton as described for compound **AK7** with the only difference being the methylation of the C-21 acid group to obtain a methyl ester (δ_C 176.5). HMBC correlation from the methoxyl (δ 3.69) to the carbonyl (δ 176.5) was observed (Fig.4.25b). The NMR and mass spectral data of **AK9** matched those reported for 3,4-secotirucalla-23-oxo-4(28),7,24-trien-3,21-dioic acid (21-methyl ester) (Fig. 4.25a) previously isolated from *Entandrophragma angolensis* (Orisadipe *et al.*, 2005).

Table 4.14: ^{1}H (500 MHz) and ^{13}C (125 MHz) NMR data of AK9

Position	**δ C**	**δ H *(J in Hz)***	**Position**	**δ C**	**δ H *(J in Hz)***
1	31.8 (CH_2)	1.50, m; 1.70, m	**16**	27.7 (CH_2)	1.26, m; 1.95, o
2	28.0 (CH_2)	2.25, m; 2.40, o	**17**	50.0 (CH)	1.95, o
3	178.7 (C)	-	**18**	21.9 (CH_3)	0.98, s
4	147.4 (C)	-	**19**	16.1 (CH_3)	0.83, s
5	49.7 (CH)	2.41, o	**20**	42.6 (CH)	2.77, m
6	30.4 (CH_2)	2.00, m; 2.15, m	**21**	176.5 (C)	-
7	118.5 (CH)	5.24, brs	**22**	47.1 (CH_2)	2.61, dd (17.0, 2.0); 2.84, dd (17.0,10.0)
8	146.0 (C)	-	**23**	199.0 (C)	-
9	40.9 (CH)	2.45, m	**24**	123.5 (CH)	6.03, brs
10	36.9 (C)	-	**25**	156.0 (C)	-
11	18.2 (CH_2)	1.40-1.56, m	**26**	27.9 (CH_3)	1.87, s
12	30.1 (CH_2)	1.35, m; 1.60, m	**27**	21.9 (CH_3)	2.11, s
13	43.4 (C)	-	**28**	114.2 (CH_2)	4.80-4.84, d (2.4)
14	51.5 (C)	-	**29**	22.5 (CH_3)	1.78, s
15	33.7 (CH_2)	1.45-1.66, m	**30**	27.4 (CH_3)	0.97, s
			OMe-21	51.8	3.69, s

4.2.10: Entandrolide (AK10)

AK10 was isolated as white amorphous powder. From its quassi-molecular peak at *m/z* 441.3730 $[M + H]^+$ and its sodium adduct ion at 463.36 $[M + Na]^+$, the molecular formula $C_{30}H_{48}O_2$ requiring seven ring and double bond equivalents was deduced.

The ^{1}H and ^{13}C NMR data (Table 4.15) for **AK10** gave signals indicating the presence of eight methyls, nine methylenes, six methines four quaternary carbons, an ester

carbon at δ 179.2 and two olefinic groups. The ^{1}H, ^{13}C and 2D NMR data of **AK10** were consistent with the presence of three intact rings whose structures were identified to match rings B/C/D of compound **AK6**. The ring A lactone was assigned based on ^{1}H-^{1}H COSY correlation between H_2-1 and H_2-2 and HMBC correlation from H_2-2 to the carbonyl at 179.2 (C-3). The terminal isopropylidene group of the C-17 side chain was assigned as described for **AK6**. The secondary methyl protons at C-21 (δ 0.81, brs) showed COSY correlation with the methine proton at δ 1.39 (C-20) as well as HMBC correlations with δ 53.0 (C-17) and δ 36.4 (C-22). All 1D and 2D NMR data of compound **AK10** matched with those reported for entandrolide (Fig. 4.26a), a tirucallane triterpene previously isolated from the seeds of *Entandrophragma angolense* (Orisadipe *et al.*, 2005).

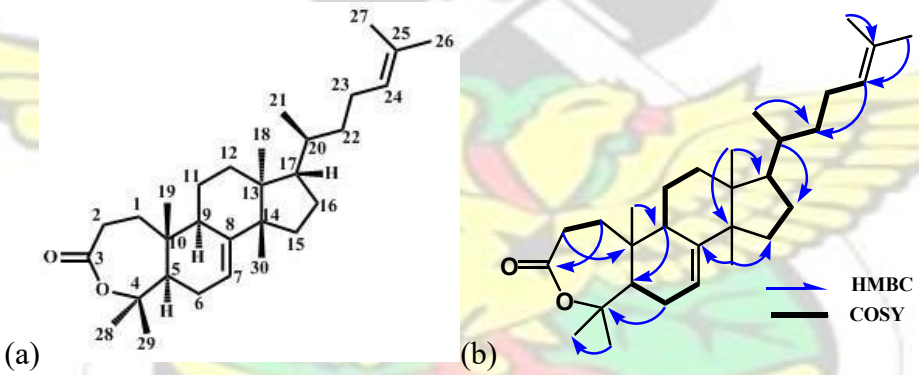

Fig. 4.26 (a): **AK10**; (b): HMBC & COSY correlations of **AK10**

Table 4.15: ^{1}H (500 MHz) and ^{13}C (125 MHz) NMR data of AK10

Position	δ C	δ H *(J in Hz)*	Position	δ C	δ H *(J in Hz)*
1	32.8 (CH_2)	1.66, m; 2.24, m	**16**	28.5 (CH_2)	1.28, m; 1.95, m
2	29.2 (CH_2)	2.24, m; 2.78, m	**17**	53.0 (CH)	1.49, m
3	179.2 (C)	-	**18**	22.2 (CH_3)	0.98, s
4	76.4 (C)	-	**19**	17.2 (CH_3)	0.89, s
5	49.6 (CH)	1.91, m	**20**	36.2 (CH)	1.39, m
6	28.3 (CH_2)	2.21, m; 1.83, m	**21**	18.5 (CH_3)	0.81, s
7	117.8 (CH)	5.20, brs	**22**	36.4 (CH_2)	1.05, m; 1.45, m
8	146.5 (C)	-	**23**	25.2 (CH_2)	1.89, m; 2.04, m
9	42.1 (CH)	2.40, brs	**24**	125.4 (CH)	5.10, t (7.0)

10	38.4 (C)	-	**25**	131.1 (C)	-
11	17.8 (CH_2)	1.53, m	**26**	17.8 (CH_3)	1.61, s
12	33.8 (CH_2)	1.65, m; 1.83, m	**27**	25.9 (CH_3)	1.68, s
13	43.5 (C)	-	**28**	26.0 (CH_3)	1.32, s
14	51.4 (C)	-	**29**	34.0 (CH_3)	1.23, s
15	34.4 (CH_2)	1.47, m	**30**	27.5 (CH_3)	0.87, s

Chemical shifts (ppm) are referenced to solvent ($CDCl_3$) peak (δ H 7.26)

4.2.11: Prototiamin B (AK11)

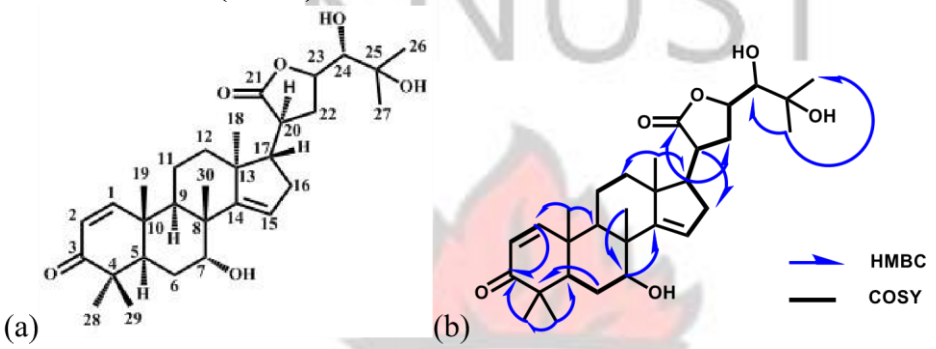

Fig. 4.27 (a): **AK11**; (b): HMBC & COSY correlations of **AK11** Compound

AK11 was obtained as a white amorphous powder. Its high resolution mass spectra exhibited a protonated ion peak at *m/z* 501.3214 $[M + H]^+$ and indicated the molecular formula, $C_{30}H_{44}O_6$. The IR spectrum displayed absorption bands that were typical of hydroxyl (3441 cm^{-1}) and carbonyl (1763 cm^{-1} and 1663 cm^{-1} (α, β- unsaturated carbonyl)) groups.

The ^1H and ^{13}C NMR data indicated signals for seven methyls, five methylenes, ten methines including three oxymethines [δ_C 71.9, δ_H 4.00 (t, *J* = 2.5, CH-7); δ_C 77.7, δ_H 4.63, (ddd, *J* = 8.5, 5.5, 2.0, CH-23) and δ_C 76.2, δ_H 3.29, (brs, CH-24)] and three olefinic methines [δ_C 158.4, δ_H 7.13 (d, *J* = 8.5, CH-1), δ_C 125.7, δ_H 5.82 (d, *J* = 8.5 CH-2) and δ_C 119.8, δ_H 5.53 (d, *J* = 2.5, CH-15)], five quaternary carbons, signals for a ketone at δ 205.2 (C-3), an ester carbon at δ 177.7 (C-21), an sp^2 carbon at δ 161.0 (C-14) and a hydroxy bearing tertiary carbon at δ 72.7 (C-25).

Ring A was assigned as an α, β-unsaturated cyclohexenone nucleus based on ^{1}H-^{1}H COSY correlation between δ 7.12 (H-1) and δ 5.82 (H-2), HMBC correlations from 1.17 (CH_3-19) to δ 158.4 (C-1), δ 44.8 (C-5) and δ 37.0 (C-9); from the olefinic at δ 7.13 (H-1) to 205.3 (C-3), 44.8 (C-5) and 37.0 (C-9) and from the germinal methyls at δ 1.17/1.09 (H_3-28/29) to δ 205.3 (C-3). The double bond between C-14 and C-15 was confirmed by HMBC cross peaks from δ 1.15 (H_3-30) and δ 1.06 (H_3-18) to δ 160.0 (C-14) and from δ 2.32 (H-17) to δ 160.0 (C-14) and δ 119.8 (C-15). The positions of the three hydroxyl groups were located at C-7, C-24 and C-25 by HMBC and COSY correlations as shown in Fig. 4.27. The presence of this γ-lactone ring was confirmed by HMBC correlations from H-17, H-22 and H-23 to the ester carbonyl at δ_C 177.6 (C-21) as described in literature (Han *et al.*, 2013; Happi *et al.*, 2015). All-together, these data corresponded to those reported in literature for Prototiamin B, a protolimonoid previously isolated from *Entandrophragma congöense* (Happi *et al.*, 2015).

Table 4.16: ^{1}H (500 MHz) and ^{13}C (125 MHz) NMR data of AK11

Position	δ C	δ H *(J in Hz)*	Position	δ C	δ H *(J in Hz)*
1	158.4 (CH)	7.13, d (8.5)	**16**	32.8 (CH_2)	2.31, m; 2.19, dd (6.5, 3.0)
2	125.7 (CH)	5.82, d (8.5)	**17**	54.4 (CH)	2.32, m
3	205.3 (C)	-	**18**	20.5 (CH_3)	1.06, s
4	44.4 (C)	-	**19**	19.1 (CH_3)	1.17, s
5	44.8 (CH)	2.40, t (4.5, 2.5)	**20**	39.8 (CH)	2.75-2.79, m
6	24.5 (CH_2)	1.86, t (5.0, 2.5) 1.91, dd (10.5,2.0)	**21**	177.7 (C)	-
7	71.9 (CH)	4.00, t (2.5)	**22**	30.0 (CH_2)	2.39-2.43, m; 2.25, m
8	45.1 (C)	-	**23**	77.7 (CH)	4.63, ddd (8.5, 5.5,2.0)
9	37.0 (CH)	2.21, d (6.0)	**24**	76.2 (CH)	3.29, brs
10	40.3 (C)	-	**25**	72.7 (C)	-
11	16.5 (CH_2)	1.74, m; 1.99, m	**26**	26.8 (CH_3)	1.36, s
12	32.3 (CH_2)	2.23, m; 1.53, m	**27**	26.9 (CH_3)	1.30, s
13	47.0 (C)	-	**28**	27.3 (CH_3)	1.17, s
14	161.0 (C)	-	**29**	21.7 (CH_3)	1.09, s
15	119.8 (CH)	5.53, d (2.5)	**30**	27.9 (CH_3)	1.15, s

Chemical shifts (ppm) are referenced to solvent ($CDCl_3$) peak (δ H 7.26)

4.3 Discussion

The crude fractions of the stem bark of *Anopyxis klaineana* demonstrated considerable anti-inflammatory, antimicrobial and antioxidant activities.

The MeOH fraction (AKM) exhibited the most significant ($p < 0.001$) antiinflammatory activity by reducing carrageenan induced paw oedema by 62.4, 53.8 and 37.7 % at 300, 100 and 30 mg/kg respectively. At 300 mg/kg, the EtOAc fraction (AKE) also inhibited paw oedema by 49.1 % ($p < 0.01$). These fractions inhibited oedema from the 1st hour and gradually throughout the experiment indicating that their anti-inflammatory effect may be by the inhibition of mediators involved in both the early and later phases of inflammation (Abotsi *et al.*, 2012).

Considerable antimicrobial activity was observed for the MeOH and EtOAc fractions. The highest activity was exhibited by the EtOAc fraction against *S. aureus* and *S. pyogens* at 312 µg/mL. The susceptibility of both Gram positive and Gram negative organisms to the active fractions support the folkloric use of the plant for the treatment of sexually transmitted, gastrointestinal, upper respiratory tract and skin infections.

The crude MeOH extract also demonstrated significant DPPH free radical scavenging activity (IC_{50} = 2.7 µg/mL) and gave a high total antioxidant capacity which could be attributed to the presence of high amounts of phenolic compounds (110.21 mg/g TAE) in the stem bark. The antioxidant activity of the crude extract may contribute to the overall anti-inflammatory effect of the crude fractions of *A. klaineana* stem bark, since inflammatory states deteriorate with the excessive production of ROS. The presence of antioxidants therefore attenuates the inflammatory process and promote tissue repair.

In the isolation and characterization of constituents, limonoids and tirucallane triterpenes were identified as the main constituents of the stem bark of *A. klaineana*. Twelve compounds including six limonoids, five tirucallane triterpenes and one protolimonoid were isolated and characterized.

The limonoids are a class of biologically significant triterpenes derived from tirucallane or euphane triterpenes (Roy and Saraf, 2006). These are highly oxygenated, modified terpenoids with a prototypical structure either containing or derived from a precursor with a 4, 4, 8-trimethyl-17-furanylsteroid skeleton. In most cases, limonoids contain a furan ring attached to the D-ring, at C-17, as well as oxygen containing functional groups at C-3, C-4, C-7, C-16 and C-17 (Roy and Saraf, 2006). Some bioactivities reported for limonoids and tirucallane triterpenes include anticancer, anti-plasmodial, antimicrobial, insecticidal, anti-feedant and antiinflammatory properties (Tan and Luo, 2011).

The potential of limonoids as an important class of anti-inflammatory compounds has been investigated by several authors (Yang *et al.*, 2011; Yuan *et al.*, 2013; Sarigaputi *et al.*, 2014; Xia *et al.*, 2014). In a study by Penido et al. (2006), methyl angolensate (**AK1**), 6a-acetoxygedunin, 7-deacetoxy-7-oxogedunin (**AK2**), andirobin, gedunin and 6α-acetoxyepoxyazadiradione (as a combined formulation) inhibited zymosan-induced increase in knee joint diameter and the extravasation of protein into synovial cavity within 6 hours of treatment. The high levels of TNFαand IL-1β that were detected in knee synovial extracts of untreated mice were significantly reduced in the mice treated with the limonoids. Deacetylgedunin and 7deacetoxy-7-oxogedunin (**AK2**) also exhibited potent inhibition of nitric oxide production from activated macrophages indicating their potential anti-inflammatory property (Ravangpai *et al.*, 2011). Altogether, these results indicated that limonoids belonging to the gedunin and

andirobin class, possess anti-inflammatory properties (Penido *et al.*, 2006). Thus, the current results for methyl angolensate (**AK1**) and similar analogues (**AK5a/b**) and the gedunin derivatives (**AK2** and **AK3**) are in agreement with previous studies on the anti-inflammatory potential of limonoids.

Inhibitors of PGE_2 are also considered as promising therapeutics for intervention in inflammatory and pain disorders. In previous studies,several tirucallane triterpenes (tirucallic acids) showed remarkable anti-inflammatory activity through the inhibition of PGE_2 and its biosynthetic enzyme, microsomal PGE_2 synthase 1 (mPGES-1) (Siemoneit *et al.*, 2011; Guo *et al.*, 2012; Hu *et al.*, 2014; Verhoff *et al.*, 2014). In the current study, a rapid screening to identify compounds with structural types that can competitively inhibit binding of PGE_2 to a specific antibody was performed to give an indication of the anti-inflammatory potential of the test compounds. From the results, 3,23-dioxo tirucalla-7,24-diene-21-oic acid (**AK6**) exhibited the most remarkable competitive inhibition of PGE_2 binding (IC_{50} = 3.63 μM) while the other tirucallane triterpenes showed weak activity. Methyl angolensate also demonstrated remarkable activity in this assay (IC_{50} = 10.23 μM). Considering the structure-activity-relationship (SAR) among the new tirucallane triterpenes, it could be inferred that the presence of an intact ring A with a C-3 keto moiety is beneficial for the competitive antagonism of PGE_2 on the mouse monoclonal antibody (Fig. 4.28). As previously established by Verhoff *et al.* (2014), a C-3 oxygenated functionality in tirucallic acids is important for anti-inflammatory activity while ring A opening and the formation of C-3 acid groups lead to reduced or diminished anti-inflammatory effects (Verhoff *et al.*, 2014). In other studies, the presence of tertiary hydroxyl and α, β-unsaturated ketone groups have been shown to enhance the anti-inflammatory effects of tirucallane triterpenes (Guo *et al.*, 2012).

Therefore, the presence of a free tertiary hydroxyl group at position 4 of compound **AK8** may have influenced the better anti-inflammatory activity observed over compound **AK7.**

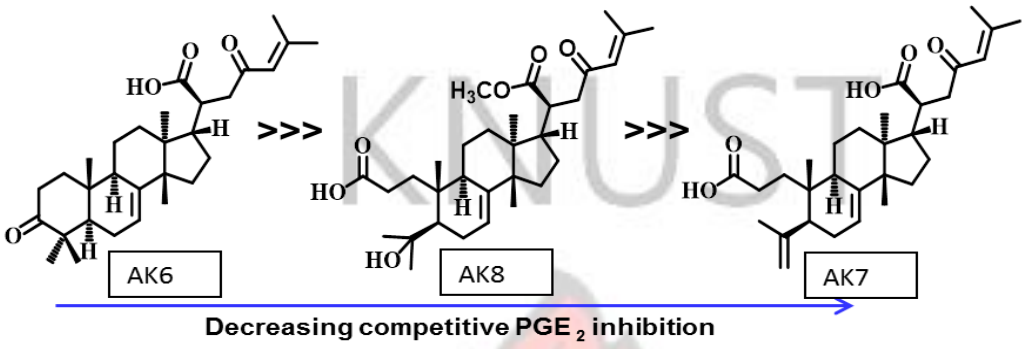

Fig. 4.28: Competitive PGE_2 inhibition by tirucallic acids **AK6-AK8**

As established by Nick et al., (1995), a keto functionality at C-3 of tirucallane triterpenes, as seen for compound **AK6**, is a pre-requisite for the selective cleavage of the C3-C4 bond through a Bayer-Villiger oxidation reaction to form the ring A 3,4 seco compounds (**2-4**) (Nick *et al.*, 1995). Thus, compound **AK6** is the possible biogenetic precursor for the other tirucallane triterpenes through oxidative reactions at the C-3 keto group (Fig. 4.29). In the biogenetic pathway, a reactive intermediate lactone ring A (same as ring A of **AK10**), undergoes the final cleavage to form the 3, 4 seco compounds. This hypothetical biogenetic relationship is described for similar ring A-3,4 seco compounds by Zeng *et al*. (2012). The C-21-oxidized groups are frequently encountered in tirucallane triterpenes and have been shown to enhance biological activity in most of these compounds (Liu and Abreu, 2006).

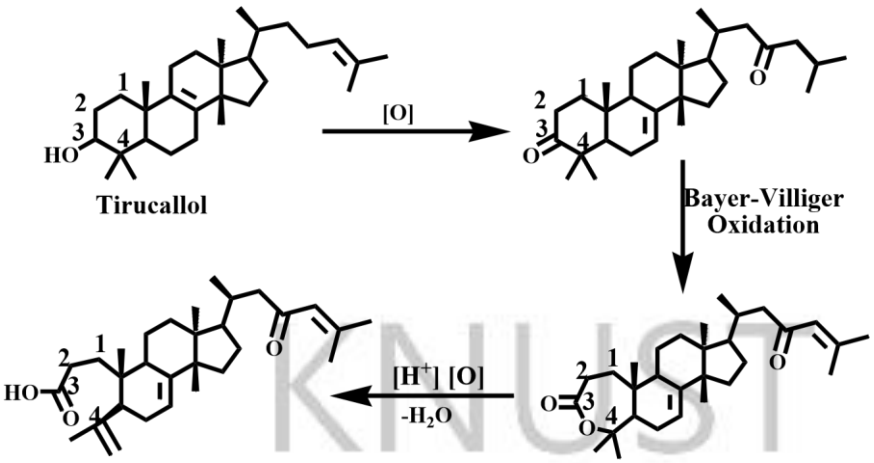

Fig. 4.29: Proposed biogenetic relationship between tirucallane triterpenes

The limonoids and tirucallane triterpenes also demonstrated remarkable antioxidant activity as shown in the DPPH free radical scavenging effect. The tirucallane triterpenes however exhibited a better scavenging effect similar to the positive control trolox, than the limonoids.

In summary, the biological activity screening of crude extracts of the stem bark of *A. klaineana* clearly demonstrated considerable anti-inflammatory, antimicrobial and anti-oxidant effects of the plant, justifying its traditional medicinal uses. Though the crude fractions exhibited some antimicrobial activity, the isolated compounds showed no anti-bacterial effects at the concentrations tested. It is hereby appreciated that the biological activity of some crude extracts may be as a result of the combined effects of a number of chemical constituents (or potentiation of one constituent by another). Therefore separation or isolation of individual constituents may lead to a loss of activity. The antioxidant effect of both crude extract and isolated compounds may contribute to the overall therapeutic effect of the crude extract in traditional medicine. This was the first report of the phytochemical constituents and biological activity of the stem bark of *A. klaineana* (Mireku *et al.*, 2014; Mireku *et al.*, 2015).

4.4 Biological activities of the stem bark of *Hexalobus monopetalus*

4.4.1 Antimicrobial activity of H. monopetalus fractions

The petroleum ether, EtOAc and MeOH fractions of *H. monopetalus* were investigated for antimicrobial activity by the agar dilution assay. The highest activity was exhibited by the EtOAc fraction with MIC range of 312-625 µg/mL towards all test organisms. The results are stated in Table 4.17.

Table 4.17: Antimicrobial activity of *H. monopetalus* fractions

	Minimum inhibitory concentration (MIC), µg/mL				
	HMP	HME	HMM	Ciprofloxacin	Ketoconazole
S. aureus	1250	625	-	0.25	-
B. subtilis	1250	312	1250	0.10	-
S. pyogens	625	312	-	0.10	-
E. coli	1250	625	1250	0.10	-
P. aeruginosa	-	625	-	0.10	-
S. typhi	-	625	1250	0.25	-
C. albicans	625	625	1250	-	5

HMP-petroleum ether fraction; HME- EtOAc fraction; HMM- MeOH fraction

4.4.2 Antimicrobial activity of compounds isolated from H. monopetalus

(Refer to Section 4.5 for details on the isolated compounds from *H. monopetalus*)

HM1−HM9 were tested for antimicrobial activities against the bacteria, *Staphylococcus aureus*, *Escherichia coli*, and fungi, *Mucor miechei*, *Rhizoctonia solani* and *Pythium ultimum* at 0.1, 0.5, 1, 5 and 10.0 µg/mL but showed no inhibitory effects towards the organisms.

4.4.3 Anti-oxidant activity of the crude MeOH extract H. monopetalus

The crude MeOH extract of *H. monopetalus* showed a concentration dependent DPPH free radical scavenging activity (Fig. 4.30a). The IC_{50} was determined as 10.10 ± 1.26 µg/mL, about four-fold lesser than the standard, ascorbic acid which had an IC_{50} of 2.4 µg/mL (Fig. 4.30b). The total phenolic content of the extract was determined as

66.19±21.15 mg/g of dried extract expressed as tannic acid equivalent (standard curve of tannic acid, y = 6.907x + 0.04604, r^2 = 0.9832). The total antioxidant capacity was determined to be 77.1±14.15 mg/g of dried extract expressed as ascorbic acid equivalent (standard curve of ascorbic acid, y = 23.92x + 0.01604, r^2 = 0.9996). Thus for every 1 g of dried *H. monopetalus* stem bark extract, 77.1 mg have an antioxidant capacity equivalent to that given by ascorbic acid.

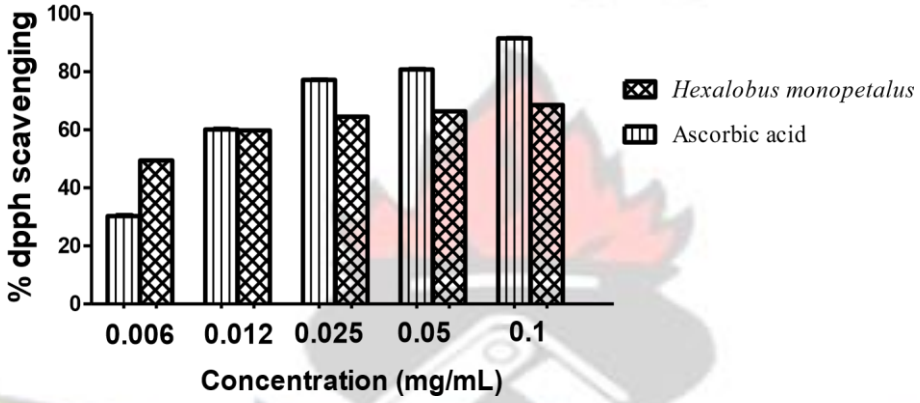

Fig. 4.30a: Percentage DPPH scavenging of various concentrations of *H. monopetalus* crude MeOH extract

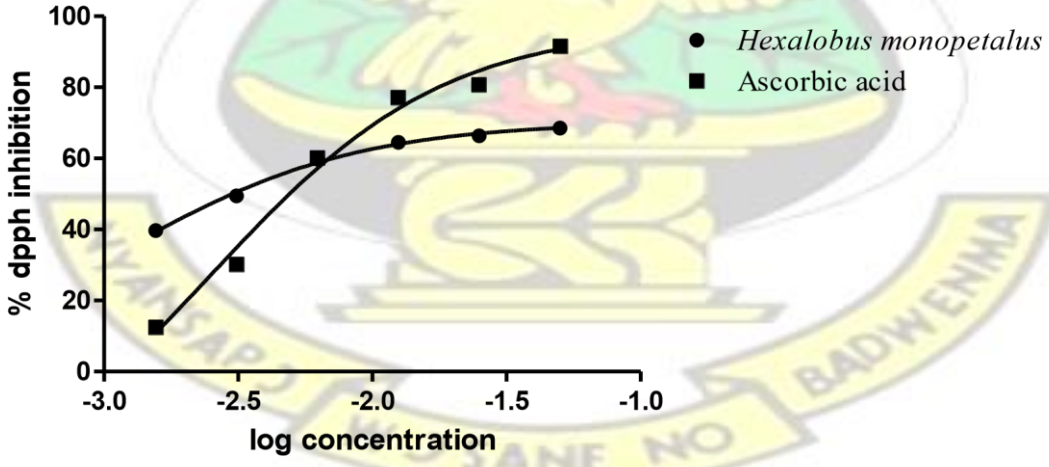

Fig. 4.30b: Log concentration versus percentage DPPH scavenging effect of *H. monopetalus* crude MeOH extract

4.5 Structural elucidation of compounds from *H. monopetalus*

Repeated chromatography of the EtOAc fraction of the stem bark of *H. monopetalus* resulted in the isolation of nine prenylated indole alkaloids (**HM1-HM9**) (Fig. 4.31). Severn novel compounds (**HM1-HM7)** were isolated. Their structures were elucidated based on NMR analysis and their fragmentation patterns as well as by comparison with reported data for similar compounds in literature. [All HR-ESIMS and NMR (1D and 2D) spectra for described compounds from *H. monopetalus* can be found in **Appendix B**].

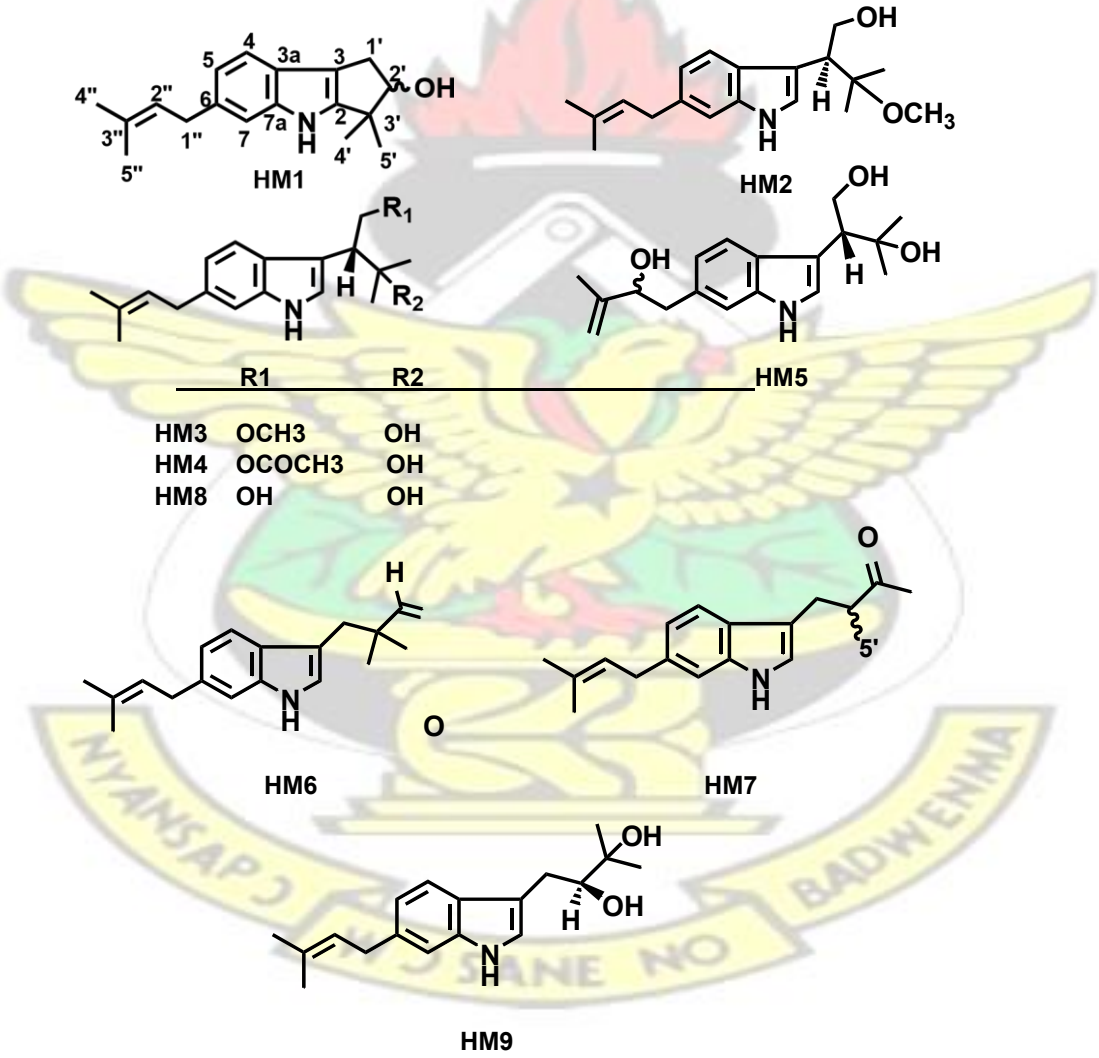

Fig. 4.31: Prenylated indole alkaloids from the stem bark of *H. monopetalus*

Structural elucidation of compounds

4.5.1: 6-(3″-methyl-2″-butenyl)-2′-hydroxy-3′, 3′-dimethylcyclopenta[*b*]indole

(HM1, new compound)

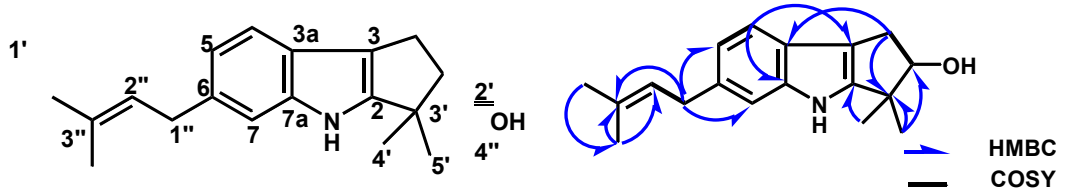

(a) 5" (b)

Fig. 4.32 (a): **HM1**; (b): HMBC & COSY correlations of **HM1**

Compound **HM1** was isolated as white powder with the molecular formula $C_{18}H_{23}ON$ as derived from its quassi-molecular ion peak (*m/z* 270.18524 $[M + H]^+$, calculated for $C_{18}H_{24}ON$, 270.18524) in the HR-ESIMS analysis.

The ^{13}C NMR data (Table 4.18) showed signals for all 18 carbons. The ^{1}H NMR data (table 4.18) gave signals for four methyls, [δ 1.22, 1.35, 1.76 (2 CH_3)], one oxymethine [δ 4.43 (t, J = 6.5)], an olefinic (δ 5.37, tm) and two methylene protons [δ 3.43, d, J = 7 (2H); 3.24 (dd, J = 14.0, 6.5) and δ 2.65 (dd, J = 14.0, 6.0) 1 H each].

In the low field region, a broad singlet at δ 7.73 typical for the indoyl N-H proton and resonances due to two *ortho*-coupled aromatic protons at δ 7.34, (d, J = 8, H-4) and δ 6.94, (dd, J = 8.0, 1.0, H-5) were observed. The broad singlet at δ 7.13 (H-7) indicated substitution at C-6 and was further confirmed by the absence of an H-6 proton signal (Achenbach *et al.*, 1995). Detailed analysis of 2D NMR revealed the C6 substituent as 3-methyl-2-butenyl as determined by ^{1}H ^{1}H COSY correlation between δ 3.43 (H_2-1″) and δ 5.38 (H-2″) and HMBC correlations from the geminal methyl protons at δ 1.76 (CH_3-4″/ CH_3-5″) to the olefinic carbons at δ 124.3 (C-2″) and δ 132.0 (C-3″) as well as from the methylene protons at δ 3.43 (H_2-1″) to C-7, C-6, C-5, C-2″ and C-3″ (Fig. 4.32b).

Table 4.18: ^{1}H (500 MHz) and ^{13}C (125 MHz) NMR data of HM1

Position	δ C	δ H (mult, *J in Hz)*

N	-	7.73, brs
2	147.6 (C)	-
3	111.6 (C)	-
3a	123.0 (C)	-
4	118.6 (CH)	7.34-7.36, d (8.0)
5	120.9 (CH)	6.94-6.95, dd (8.0, 1.0)
6	134.9 (C)	-
7	111.1 (CH)	7.13, brs
7a	140.2 (C)	-
1′	33.3 (CH_2)	3.23-3.27, dd (14.0, 6.5); 2.64-2.66, dd (14.0, 6.0)
2′	85.3 (CH)	4.43, t, (6.5)
3′	43.1 (C)	-
4′	25.6 CH_3	1.35 , s
5′	20.6 (CH_3)	1.22, s
1″	34.7 (CH_2)	3.43-3.44, d (7.0)
2″	124.3 (CH)	5.38, tm
3″	132.0 (C)	-
4″	26.0 (CH_3)	1.76, s
5″	18.0 (CH_3)	1.76, s

Chemical shifts (ppm) are referenced to solvent ($CDCl_3$) peak (δ H 7.26)

Further analysis of 2D NMR indicated the indole C-2/3 substituent as a cyclopenta [*b*] indole ring similar to that reported for Bruceolline D (Koike and Ohmoto, 1994; Lopchuk *et al.*, 2013). The difference was a position 2′ hydroxyl group in **HM1** as opposed to a 2′ ketone in Bruceolline D. This was confirmed by HMBC cross peaks from the oxymethine proton at δ 4.43 (H-2′) to δ 147.6 (C-2), δ 111.6 (C-3), δ 25.6 (C-4′) and 20.6 (C-5′). The methyl protons [δ 1.35 (H-4′)/ 1.22 (H-5′)] also showed HMBC correlations to the oxymethine [δ 85.3 (C-2′)], the quaternary carbon [δ 43.1 (C-3′)] and to δ 147.6 (C-2) implying a five membered ring with the methyls ($CH_3$4′/5′) attached at C-3′ and the hydroxyl at C-2′ (Fig. 4.32b). The configuration of the C-2′ stereocenter was determined by application of the Mosher's method (Hoye *et al.*, 2007). Accordingly, in the ^{1}H NMR spectrum of the (*S*) MTPA ester, CH_3-4′ and CH_3-5′ were shielded (up-field shift) whereas H_2-1′ appeared deshielded (downfield shift). The reverse was observed for (*R*) MTPA ester. Thus a positive $\Delta\delta^{SR}$ (δs δ_R) was obtained for H_2-1′ and a negative $\Delta\delta^{SR}$ (δs δ_R) for CH_3-4′ and CH_3-5′ (Table

4.18). The configuration at C-2′ was thus concluded to be *R*. **HM1** was characterized as 6-(3-methyl-2-butenyl)-2-hydroxy-3′,3′-dimethylcyclopenta[*b*] indole (Fig. 4.32a).

Table 4.19: Chemical shift difference between (*S*)- and (*R*)- MTPA esters of HM1

	Chemical shift (δH) in δ values (ppm) from TMS ($CDCl_3$, 500 MHz)			
	H-1′α	**H-1′β**	**CH_3-4′**	**CH_3-5′**
HM1	3.241	2.652	1.343	1.226
(*S*)-MTPA ester	3.207	2.624	1.336	1.209
(*R*)-MTPA ester	3.202	2.617	1.339	1.213
$\Delta\delta^{SR}(\delta S \quad \delta_R)$	+0.005	+0.007	-0.003	-0.004

The HR-MS^n fragmentation of compound HM**1** gave a base peak at *m/z* 198.12 [M H 72] $^+$ for the loss of one molecule of water and four carbons from the prenyl side chain. Again, fragment ions at *m/z* 202.12 [M H 68] $^+$, 184.11 [M H 68 18] $^+$ and 130.06 [M H 68 18 54] $^+$ could be attributed to the successive and combined losses of the prenyl chain, water and four carbons from the C-3 prenyl group respectively (Fig. 4.33).

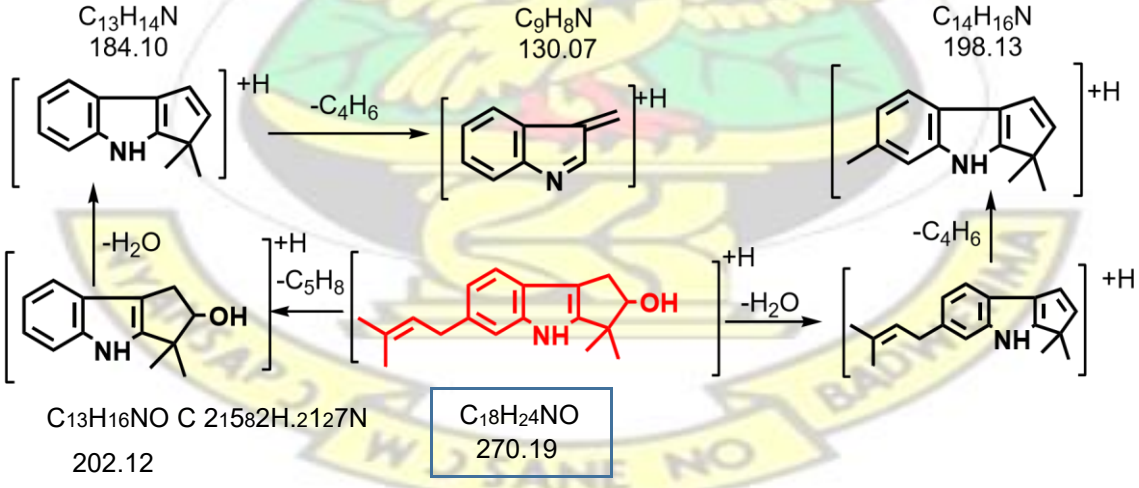

Fig. 4.33: Proposed fragmentation pattern of compound **HM1**

Physicochemical properties of HM1: White amorphous solid; $[\alpha]^{20}_{D} = +18°$ (*c* 0.10, MeOH); CD: $\Delta\varepsilon_{230}$ + 1.63 (*c* = 3.71 x 10^{-4} $molL^{-1}$; in MeOH); UV λ_{max} nm: 231 (in MeOH); IR ν_{max} cm^{-1}: 3401 (>N−H, O−H), 2964.

4.5.2: 3-(1′-hydroxy-3′-methoxy-3′-methyl-but-2′-yl)-6-(3″-methyl-2″-butenyl) indole (HM2, new compound)

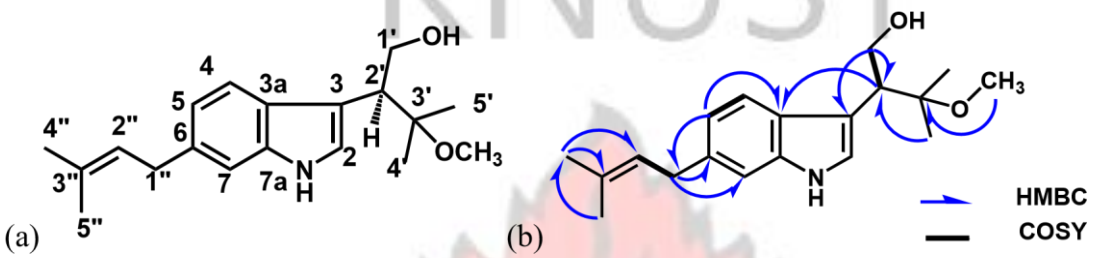

Fig. 4.34 (a): **HM2**; (b): HMBC & COSY correlations of **HM2**

HM2 was isolated as colourless oil. Its molecular formula was assigned as $C_{19}H_{27}O_2N$ as indicated by its sodium adduct in the HR-ESIMS analysis (*m/z* 324.19353 $[M + Na]^+$, calculated for $C_{19}H_{27}O_2NNa$, 324.19340). The ^1H NMR spectrum (Table 4.20) exhibited five low field protons at δ 8.03 (brs), 7.02 (d, *J* = 2.5), 7.56 (d, *J* = 8.5), 6.99 (dd, *J* = 8.5, 1.0) and 7.18 (brs) which were attributed to the protons of a di-substituted indole ring with the broad singlet at δ 8.03 (1H) typical for the indoyl N-H proton. The methine proton signal at δ 7.02 (H-2,1H) appeared as a doublet as a result of the coupling effect with the indoyl N-H and thus indicated substitution at C-3 as also confirmed by the absence of an H-3 resonance in the ^1H and HSQC NMR analysis. Proton resonances at δ 7.56 (d, *J* = 8.5), 6.99 (dd, *J*= 8.5, 1.0) and 7.18 (brs) were attributed to the indole positions 4, 5 and 7 respectively as inferred from the multiplicities of their signals as well as the chemical shifts of their carbon atoms, indicating an ABX system arrangement of protons of the benzene ring and further suggesting that position C-6 was substituted (Malebo *et al.*, 2014). The ^1H NMR spectrum further gave signals for four methyls (δ 1.77, 1.78,

1.28, 1.20, s, 3H each), a methoxyl (δ 3.34, s, 3H), a methine (δ 3.90, dd, *J* = 5.0, 8.0), an olefinic (δ 5.39, tm) and an oxymethylene proton at δ 3.90, (dd, *J* = 11.0, 5.0, 1H) / δ 4.18 (dd, *J* = 11.0, 8.5, 1H) and a methylene at δ 3.46 (d, *J* = 7.5, 2H). The ^{13}C NMR spectrum (Table 4.20) gave signals for all 19 carbon atoms and confirmed the presence of a 3,6-di-substituted indole nucleus based on the downfield shifts for C-3 and C-6 as earlier explained for compound **HM1** (Achenbach, 1986).

Table 4.20: ^{1}H (500 MHz) and ^{13}C (125 MHz) NMR data of HM2

Position	**δ C**	**δ H (mult, *J in Hz*)**
N	-	8.03, brs
2	121.9 (CH)	7.02-7.03, d (2.5)
3	114.4 (C)	-
3a	126.4 [a] (C)	-
4	119.4 (CH)	7.56-7.58, d (8.5)
5	120.9 (CH)	6.99-7.01, dd (8.5, 1.0)
6	136.2 (C)	-
7	110.4 (CH)	7.18, brs
7a	136.4 [a] (C)	-
1′	64.8 (CH_2)	3.90, dd (11.0, 5.0), 4.18, dd (11.0, 8.5)
2′	47.0 (CH)	3.90, dd, (5.0, 8.0)
3′	80.5 (C)	-
4′	20.8 (CH_3)	1.28, s
5′	24.6 (CH_3)	1.20, s
1″	34.7 (CH_2)	3.46-3.47, d (7.5)
2″	124.0 (CH)	5.41, tm
3″	132.2 [a] (C)	-
4″	26.0 (CH_3)	1.77, s
5″	18.0, (CH_3)	1.78, s
OCH_3	49.4 (C-3′)	3.34, s

Chemical shifts (ppm) are referenced to solvent ($CDCl_3$) peak (δ H 7.26), [a] assigned from HSQC spectrum

All data obtained, corroborated with literature survey, indicated that **HM2** is an analogue of 3-(1′,3′-dihydroxy-3′-methyl-but-2′-yl)-6-(3″-methyl-2″-butenyl) indole previously isolated from *Hexalobus crispiflorus*(Achenbach *et al.*, 1995). The difference between these two compounds was methylation of the 3′-hydroxyl group in the latter to obtain a methoxyl in compound **HM2**. This was confirmed by strong

HMBC correlation from the methoxyl protons (δ 3.34) to the tertiary carbon at δ 80.5 (C-3′) (Fig. 4.34b). The C-6 substituent was identified as 3-methyl-2-butenyl based on 2D NMR analysis as described for compound **HM1**. **HM2** was thus characterized as 3-(1-hydroxy-3-methoxy-3-methyl-but-2-yl)-6-(3-methyl-2-butenyl) indole (Fig. 4.34a). The structure was confirmed by $HRMS^2$ fragmentation which showed a base peak at *m/z* 270.18533 [M H 32] $^+$ for the loss of a methoxyl; *m/z* 202.12242 [M H 32 68] $^+$ for the combined losses of methoxy and prenyl groups and at *m/z* 198.12 [M H 32 18 54] $^+$ for the combined losses of methoxy, water and four carbons of the C-6 prenyl chain (Fig. 4.35).

Physicochemical properties of HM2: Colourless oil; [α] 23 ° (*c* 0.10, $MeOH_2$); CD: Δ ε_{230} – 3.65 (*c* = 3.32 x 10^{-4} $molL^{-1}$; in MeOH); UV: λ_{max} nm: 226 (in MeOH); IR: ν_{max} cm^{-1}: 3409 (> N-H, O-H), 2969, 1569.

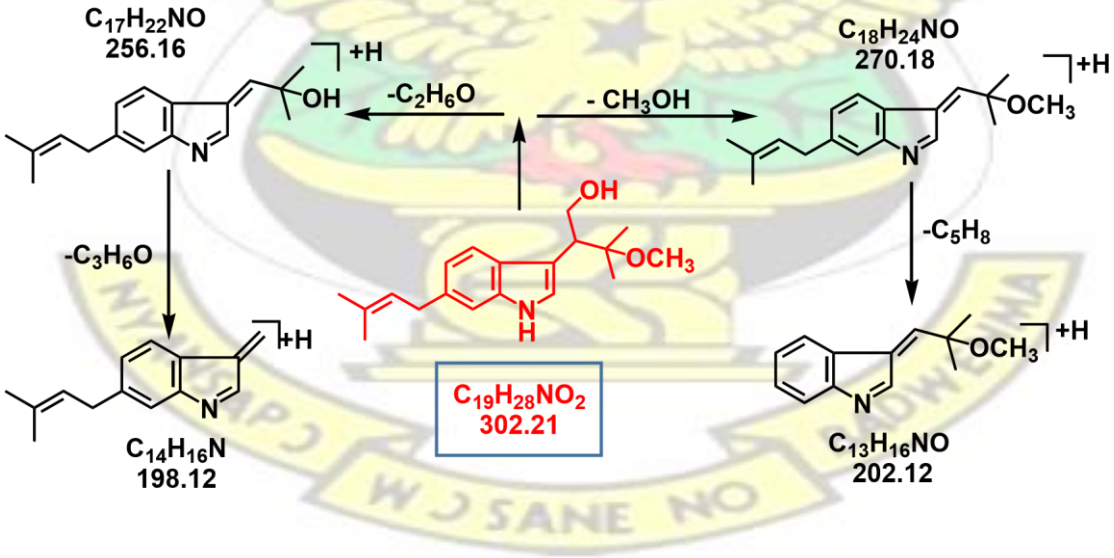

Fig. 4.35: Proposed fragmentation pattern of compound **HM2**

4.5.3: 3-(1′- methoxy -3′- hydroxy -3′-methyl-but-2′-yl)-6-(3″-methyl-2″butenyl) indole (HM3, new compound)

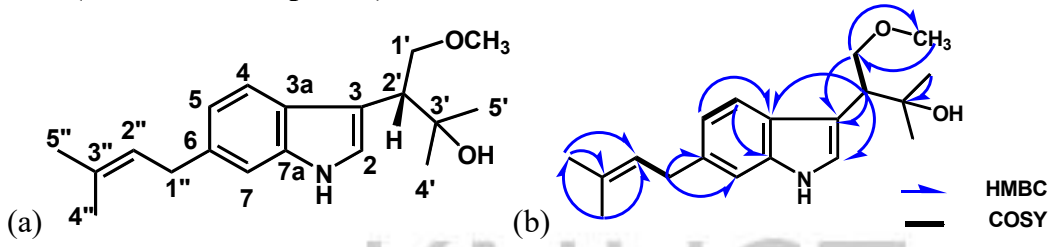

Fig. 4.36 (a): **HM3**; (b): HMBC & COSY correlations of **HM3** The HR-ESIMS of compound HM**3**, a colourless oil, gave the same molecular formula as compound HM**2** (*m/z* 324.1935 [M + Na] $^{+}$, calculated for $C_{19}H_{27}O_2NNa$, 324.19340). The ^{1}H and ^{13}C NMR data of **HM3** (Table 4.21) showed the same pattern of signals and similar chemical shifts as found in HM**2** and were consistent with the presence of a 3,6-di-substituted indole nucleus with the same C-6 prenyl side chain as described for compound **2**.

Table 4.21: ^{1}H (500 MHz) and ^{13}C (125 MHz) NMR data of HM3

Position	**δ C**	**δ H (mult, *J in Hz*)**
N	-	8.02, brs
2	121.7 (CH)	7.03-7.04, d (2.5)
3	114.6 (C)	-
3a	126.2 (C)	-
4	119.3 (CH)	7.54-7.55, d (8.5)
5	120.8 (CH)	6.97-6.99, dd (8.5, 1.0)
6	136.2 (C)	-
7	110.4 (CH)	7.16, brs
7a	136.2 (C)	-
1′	75.3,(CH_2)	3.77-3.78, dd (9.5, 5.0); 3.91, dd (9.5, 8.5)
2′	46.0 (CH)	3.33-3.39, dd (8, 3.5)
3′	74.0 (C)	-
4′	26.4 (CH_3)	1.27, s
5′	29.4 (CH_3)	1.20, s
1″	34.7 (CH_2)	3.44-3.45, d (7.5)
2″	124.1 (CH)	5.39, tm
3″	132.2 (C)	-
4″	26.0 (CH_3)	1.75, s
5″	18.1 (CH_3)	1.76, s
OCH_3	59.2 (C-1′)	3.39, s

Chemical shifts (ppm) are referenced to solvent ($CDCl_3$) peak (δ H 7.26),

Major differences were however detected in ^{1}H and ^{13}C chemical shifts for the C-3 substituent. From the HMBC analysis, the methoxyl protons at δ 3.39 only showed correlation with the oxymethylene carbon at δ 75.3 (C-1′) indicating that the methoxyl group was attached to the methylene (CH_2-1′) (Fig. 4.36b). In turn, HMBC correlations were also observed from the protons of the methylene (H_2-1′) to the methoxy (δ 59.2), the methine (δ 46.0, C-2′) and the hydroxylated tertiary carbon at δ 74.0 (C-3′). HMBC correlations from the germinal methyl protons (CH_3-4′/5′) to δ 74.0 (C-3′) and δ 46.0 (C-2′) were observed and this indicated the attachment of the methyls to the carbon bearing the hydroxyl group (C-3′) (Fig. 4.36b). Compound HM**3** was thus characterized as 3-(3′-hydroxy-1′-methoxy-3′-methyl-but-2-yl)-6-(3″methyl-2″-butenyl)indole. In the HRMS^2 fragmentation of HM**3**, the loss of water and the combined loss of a methyl and prenyl chain led to a fragment ion peaks at *m/z* 284.20 and 216 respectively (Fig. 4.37).

Physicochemical properties of HM3: Colourless oil; [α] –22 ° (*c* 0.10, MeOH); CD: Δ ε_{230} – 4.56 (*c* = 3.32 x 10^{-4} $molL^{-1}$; in MeOH); UV: λ_{max} nm: 224 (in MeOH); IR: ν_{max} cm^{-1}: 3405 (> N-H, O-H), 3071, 1587.

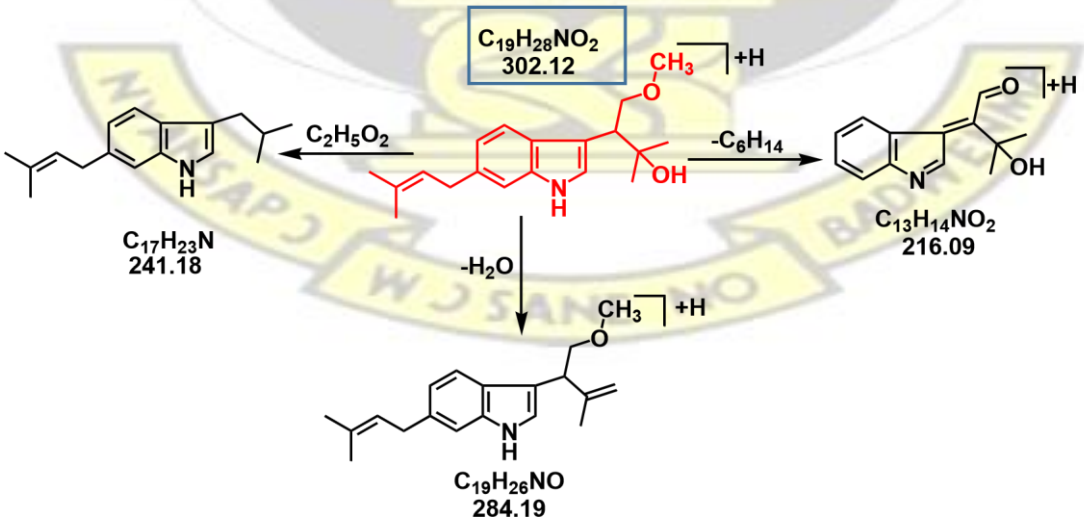

Fig. 4.37: Proposed fragmentation pattern of compound **HM3**

4.5.4: 3-(3′-hydroxy-3′-methyl-1′-acetoxy-but-2′-yl)-6-(3″-methyl-2″-butenyl) indole (HM4, new compound)

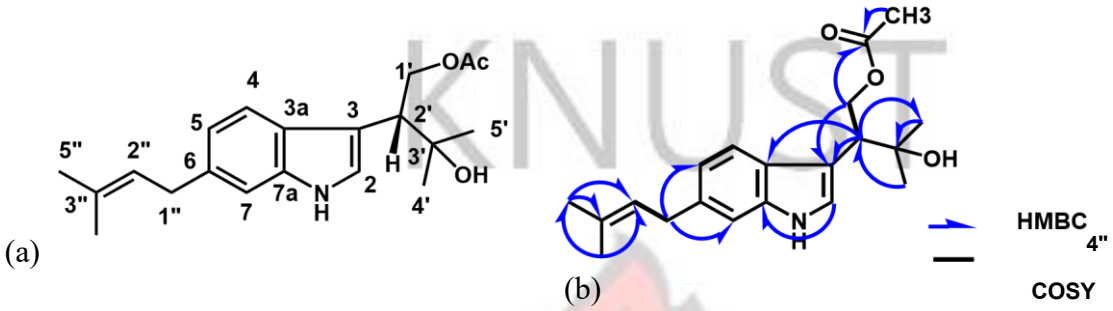

Fig. 4.38 (a): **HM4**; (b): HMBC & COSY correlations of **HM4**

The HR-ESIMS of **HM4** displayed a sodium adduct ion peak at *m/z* 352.18841 [M + Na] $^{+}$ and suggested the molecular formula $C_{20}H_{27}O_3N$. From 1H, NMR data, five low field protons [δ 8.11 (N-H); 7.04 (brs, H-2); 7.55 (d, *J* = 8.5, H-4); 6.98 (brd, *J* = 8.5, H-5); 7.18 (brs, H-7)] were attributed to protons of the di-substituted indole skeleton as described for **HM2** and **HM3**. Other important ^{1}H and ^{13}C signals as deduced from HSQC experiments included five methyls, an oxymethylene (δ_C 65.6; δ_H 4.59 (dd, *J* = 11.5, 6.0); δ_H 4.49 (dd, *J* = 11.0, 8.0) 1H each CH_2-1′), an olefinic methine (δ_C 124.0, δ_H 5.40, CH-2″) an ester carbon at δ 171.3, an oxygen bearing saturated carbon at δ 72.8 (C-3′) and an olefinic at δ 132.3 (C-3″). The difference between **HM4** and **HM3** was the replacement of the methoxyl (-OCH_3) at C-1′ (in **HM3**) with an acetoxy (CH_3COO-) (in **HM4**). This was confirmed by the strong

HMBC correlation from the methyl protons at δ 1.94 to the carbonyl at δ 171.3 (Fig. 4.38b). The downfield shift of the methylene protons (CH_2-1′) indicated its attachment to a more de-shielding functional group which was identified in this case as the acetoxy group. HMBC cross peaks were observed from the methylene protons

(H_2-1′) to the ester carbon at δ 171.3. All other proton and carbon resonances (Table 4.22) for the substituted indole ring appeared at the anticipated chemical shifts as described for **HM-3**. **HM4** was thus assigned as 3-(3′-hydroxy-1′-acetoxy-3′-methyl but-2′-yl)-6-(3″-methyl-2″-butenyl) indole (Fig. 4.38a).

Table 4.22: ^{1}H (500 MHz) and ^{13}C (125 MHz) NMR data of HM4

Position	**δ C**	**δ H (mult, *J in Hz*)**
N	-	8.11, brs
2	122.0 (CH)	7.04, brs
3	113.7 (C)	-
3a	126.6 (C)	-
4	119.6 (CH)	7.54-7.56, d (8.5)
5	121.0 (CH)	6.98-6.99, brd (8.5)
6	136.3 (C)	-
7	110.5 (CH)	7.18, brs
7a	136.6 (C)	-
1′	65.6 (CH_2)	4.59-4.60, dd (11.5, 6.0); 4.49-4.53, dd (11.0, 8.0)
2′	46.6 (CH)	3.39-3.40, dd (14.0, 6.5)
3′	72.8 (C)	-
4′	28.4 (CH_3)	1.29, s
5′	28.2 (CH_3)	1.27, s
1″	34.7 (CH_2)	3.44-3.46, d (7.0)
2″	124.0 (CH)	5.40, tm
3″	132.3 (C)	
4″	26.0 (CH_3)	1.76, s
5″	18.0 (CH_3)	1.76, s
COO<u>CH₃</u>	21.3	1.94, s
<u>C</u>OOCH₃	171.3	-

Chemical shifts (ppm) are referenced to solvent ($CDCl_3$) peak (δ H 7.26),

The HR-MS^2 fragmentation of *m/z* 352.18 showed major fragments indicating the elimination of water (*m/z* 312.20), combined losses of water and acetoxy (*m/z* 252.17) as well as the combined losses of water, acetoxy and four carbons of the prenyl chain (*m/z* 198.13) (Fig. 4.39).

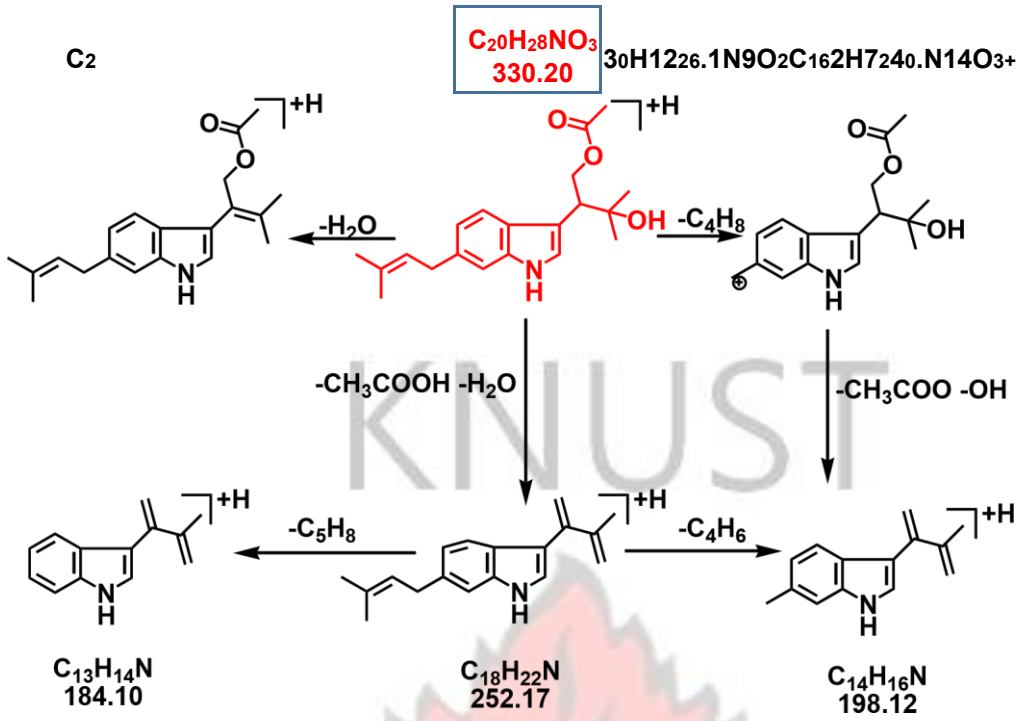

Fig. 4.39: Proposed fragmentation pattern of compound **HM4**

Physicochemical properties of HM4: Pale yellow oil; [α] – 24 ° (*c* 0.10; MeOH); CD Δ ε_{230} – 7.98 (*c* = 3.03 x 10^{-4} $molL^{-1}$; in MeOH); UV: λ_{max} nm: 230 (in MeOH); IR: ν_{max} cm^{-1}: 3408 (> N-H, O-H), 1723 (> C=O).

4.5.5: 3-(1′, 3′-dihydroxy-3′-methylbut-2′-yl)-6-(2″-hydroxy-3″-methyl-3″butenyl) indole (HM5, new compound)

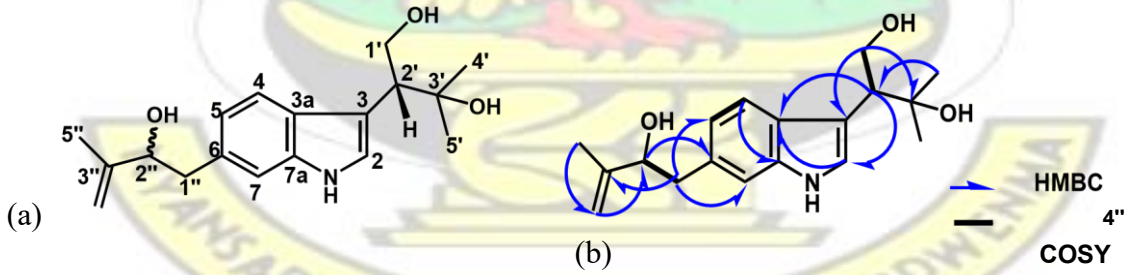

Fig. 4.40 (a): **HM5**; (b): HMBC & COSY correlations of **HM5**

Compound **HM5** was isolated as colourless oil. Its sodium adduct ion at *m/z* 326.1726 $[M + Na]^+$ was used to assign its molecular formula as $C_{18}H_{25}O_3N$. The ^1H and ^{13}C NMR data (Table 4.23) indicated a 3, 6- di-substituted indole nucleus as described for previous compounds in this text. Signals for three methyls, an oxymethylene [δ_C 64.5,

δ_H 4.10, (d, J = 6.0)], an oxymethine [δ_C 76.9, δ_H 4.31, (dd, J = 9.0, 4.0), CH-2″] and a hydroxyl bearing tertiary carbon [δ 74.5, C-3′] were identified. A characteristic signal for an exomethylene group was also observed at δ_C 111.1, δ_H 4.88/5.01 (brs, CH_2-4″). Analysis of 2D NMR data indicated that **HM5** had a similar indole C-3 substituent as described for **HM3** except for demethylation of the C-1′ methoxyl group to obtain a 1,3-dihydroxy-3-methylbut-2-yl group. At the C-6 substituent, ^{1}H ^{1}H COSY correlation was observed between methylene protons (δ 2.83, dd, J = 14.0, 9.0; 3.03, dd, J = 13.0, 4.0, H_2-1″) and the oxymethine proton (δ 4.31, H-2″). Further HMBC correlations were also observed from the exomethylene protons at δ 4.88/5.01 (H_2-4″) to the methyl (δ 18.5, CH_3-5″), the olefinic carbon (δ 147.1, C-3″) and the oxymethine (δ 76.9, C-2″). Similarly, the oxymethine proton (δ 4.31, H-2″) showed HMBC correlations to the methyl carbon at δ 18.5 (CH_3-5″), the exomethylene at δ 111.1 (C-4″) and to 132.7 (C-6) (Fig. 4.40b). The C-6 side chain was identified as 2-hydroxy-3-methyl-3-butenyl. **HM5** was thus assigned as 3-(1,3dihydroxy-3-methylbut-2-yl)-6-(2-hydroxy-3-methyl-3-butenyl) indole (Fig. 4.40a).

Table 4.23: ^{1}H (500 MHz) and ^{13}C (125 MHz) NMR data of HM5

Position	**δ C**	**δ H (mult, *J in Hz*)**
N	-	8.12, brs
2	122.4 (CH)	7.19-7.20, brd (3.0)
3	114.0 (C)	-
3a	127.1 (C)	-
4	119.7 (CH)	7.57-7.58, d (8.0)
5	121.6 (CH)	7.02-7.04, dd (8.0, 1.5)
6	132.7 (C)	-
7	112.0 (CH)	7.27, brs
7a	136.4 (C)	-
1′	64.5 (CH_2)	4.10 -4.11, d (6.0)
2′	48.2 (CH)	3.26-3.28, m
3′	74.5 (C)	-
4′	29.4 (CH_3)	1.33, s

5′	27.6 (CH_3)	1.27, s
1″	42.7 (CH_2)	2.81-2.85, dd (14.0 9.0); 3.03-3.06, dd (13.0, 4.0)
2″	76.9 (CH)	4.31-4.33, dd (9.0, 4.0)

Table 4.23 *continued*: ^{1}H (500 MHz) and ^{13}C (125 MHz) NMR data of HM5

Position	**δ C**	**δ H (mult, *J in Hz)***
3″	147.1 (C)	-
4″	111.3 (CH_2)	4.88, brs; 5.01, brs
5″	18.5 (CH_3)	1.85, s

Chemical shifts (ppm) are referenced to solvent ($CDCl_3$) peak (δ H 7.26)

From the $HRMS^2$ experiments, the successive losses of two molecules of water were observed at *m/z* 286.17 [M H 18] $^{+}$ and 268.16 [M H 36] $^{+}$ respectively. The loss of a mass unit 72 (C_4H_8O) to form a peak at *m/z* 232.13 [M H 72] $^{+}$ confirmed the structure of the indole C-6 prenyl chain (Fig. 4.41).

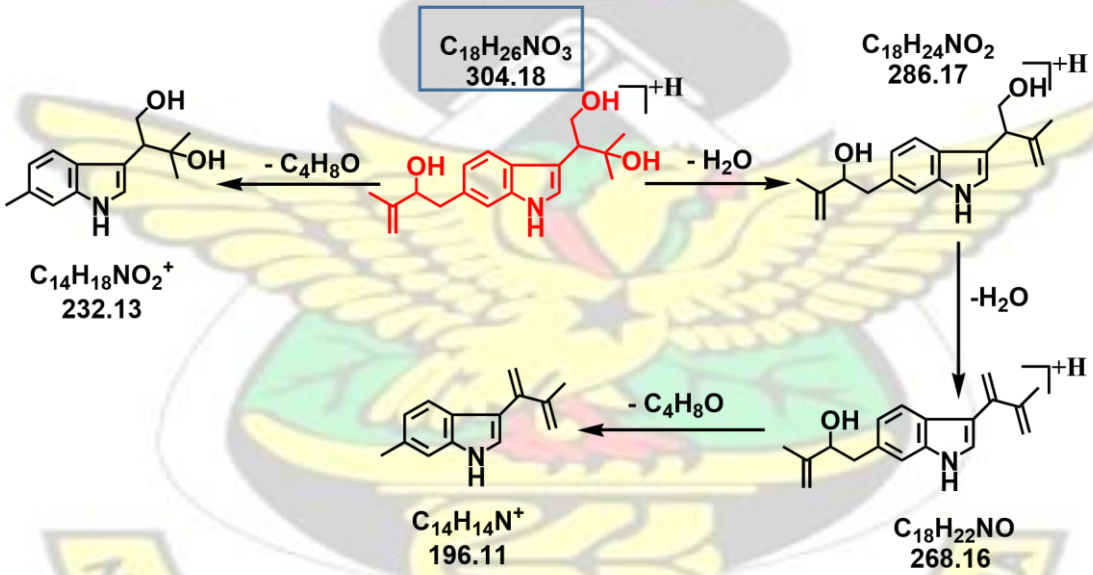

Fig. 4.41: Proposed $HRMS^2$ fragmentation pattern of compound **HM5**

Physicochemical properties of HM5: Colourless oil; [α] −15 ° (*c* 0.10; MeOH); CD: Δ ε_{230} – 2.2 (*c* = 3.30 x 10^{-4} $molL^{-1}$; in MeOH); UV: λ_{max} nm: 225 (in MeOH); IR: ν_{max} cm^{-1}: 3356 (> N-H, O-H), 2973

4.5.6: 3-(2′-Formyl-2′-methylpropyl)-6-(3"-methyl-2"-butenyl) indole (HM6new compound)

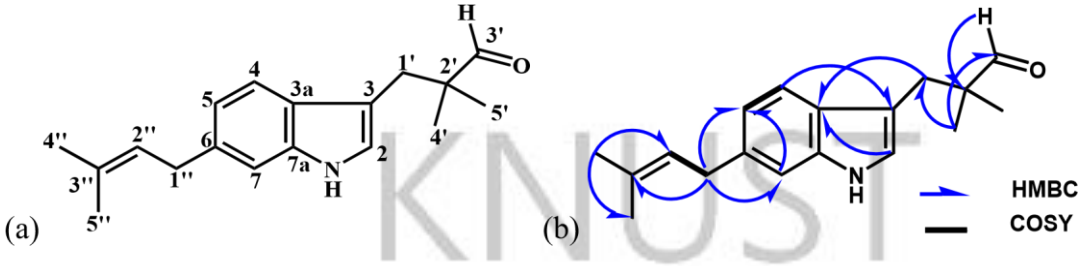

Fig. 4.42 (a): **HM6**; (b): HMBC & COSY correlations of **HM6**

The molecular formula of compound **6** was assigned as $C_{18}H_{23}ON$ as determined by its quassi-molecular ion peak at *m/z* 270.18527 $[M + H]^+$ (calculated for $C_{18}H_{24}ON$, 270.18524) in the HR-ESIMS experiment. From the ^1H and ^{13}C NMR (Table 4.24), signals for a 3,6-di-substituted indole were observed at their anticipated chemical shifts as earlier described for compounds **HM2** **HM5**. A characteristic proton signal for an aldehyde at δ 9.62 correlating with a carbonyl (δ 206.9) in the HSQC spectrum was observed. Analysis of 1D and 2D NMR spectrum revealed the C-6 substituent as 3-methyl-2-butenyl as described for compound **HM1**. The C-3 substituent was characterized as follows: HMBC cross peaks were observed from the methylene protons at δ 2.91 (s, H_2-1′) to δ 21.7, (CH_3-4′/5′), δ 47.3 (C-2′), δ 206.9 (C-3′), δ 111.2 (C-3) and δ 126.6 (C-3a) (Fig. 4.42b). Further HMBC correlations from the germinal methyl protons at δ 1.12 (CH_3- 4′/5′, s, 6H) to the methylene (δ 32.5, C-1′), the quaternary carbon (δ 47.3, C-2′) and the carbonyl (δ 206.9, C-3′) were observed. The aldehyde proton at δ 9.62 showed HMBC cross peaks with the quaternary carbon at δ 47.3 (C-2′) and the methyls at δ 21.7 (CH_3-4′/5′). This indicated the attachment of the aldehyde group at C-2 ′. The C-3 substituent was thus identified as 2-formyl-2-

methylpropyl (Achenbach and Löwel, 1995). Compound **6** was therefore characterized as 3-(2′-formyl-2′-methylpropyl)-6-(3″-methyl-2″-butenyl) indole (Fig. 4.42a).

Table 4.24: ^{1}H (500 MHz) and ^{13}C (125 MHz) NMR data of HM6

Position	**δ C** [a]	**δ H (mult, *J in Hz*)**
N-H	-	7.91, brs
2	122.8 (CH)	6.90, brd (2.0)
3	111.2 (C)	-
3a	126.6 (C)	-
4	118.9 (CH)	7.43-7.45, d (8.0)
5	120.6 (CH)	6.95-6.97, dd (8.5, 1.5)
6	136.1 (C)	-
7	110.2 (CH)	7.14, brs
7a	136.5 (C)	-
1′	32.5 (CH_2)	2.91, s
2′	47.3 (C)	-
3′	206.9 (C)	9.62, s
4′	21.7 (CH_3)	1.12, s
5′	21.7 (CH_3)	1.12, s
1″	34.5 (CH_2)	3.43-3.45, d (7.0)
2″	123.9, CH	5.39, tm
3″	132.1, C	-
4″	25.8, CH_3	1.75 , s
5″	17.8 CH_3	1.76 (3H, s)

Chemical shifts (ppm) are referenced to solvent ($CDCl_3$) peak (δ H 7.26); [a] *- signals assigned from HSQC spectrum*

In the HR-MS^2 analysis, a base peak at *m/z* 202.12 [M H 68] $^{+}$ indicated the loss of the C-6 prenyl side chain. Another peak at *m/z* 198.12 [M H 72] $^{+}$ for the C_4H_8O from the indole C-3 prenyl side chain was observed (Fig. 4.43).

Physicochemical properties of HM6: Pale yellow oil; UV: λ_{max} nm: 232 (In MeOH); IR: v_{max} cm^{-1}: 3394 (> N-H), 1723 (> C=O).

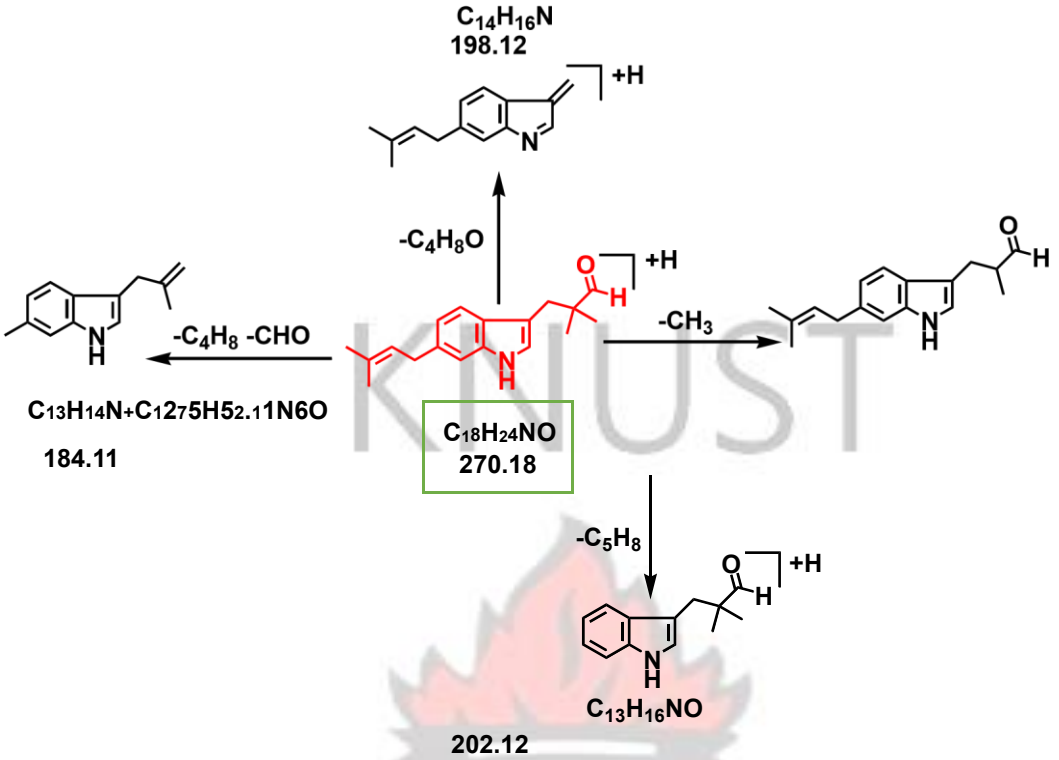

Fig. 4.43: Proposed fragmentation pattern of compound **HM6**

4.5.7: 3-(2′-methyl-3′-oxo butyl)-6-(3"-methyl-2"-butenyl) indole (HM7, new compound)

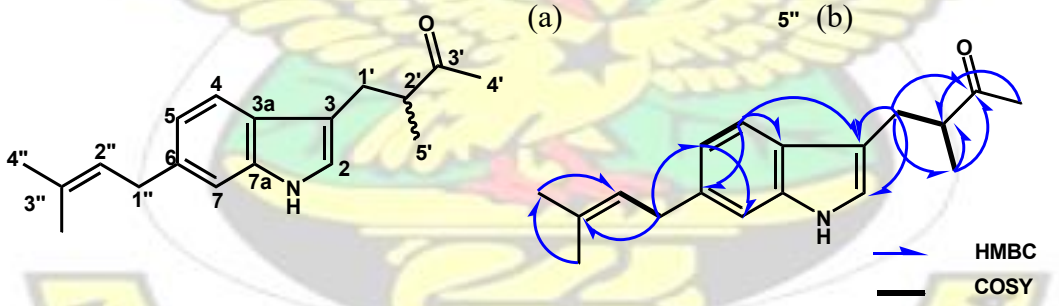

Fig. 4.44 (a): **HM7**; (b): HMBC & COSY correlations of **HM7** **HM7** was isolated as pale yellow oil. Its HR-ESIMS spectrum indicated the same molecular formula as compound **HM6** ($C_{18}H_{23}ON$). Careful analysis of ^{1}H and ^{13}C NMR data (Table 4.25) suggested a di-substituted indole nucleus with a 3-methyl-2butenyl moiety at the indole position C-6 as described for previous compounds (**HM2-HM4**). Further analysis by 2D NMR revealed the indole-C-3 substituent to be a 2-methyl-3-

oxobutyl moiety. Important correlations that led to this characterization included ^{1}H-^{1}H COSY correlations between the methylene protons (δ 2.71/3.10,

CH_2-1′), the methine proton at δ 2.95 (CH-2′) and methyl protons at δ 1.14 (CH_3-5′) which indicated that C-1, C-2 and C-5 were linked. Strong HMBC cross peaks from the methyl protons at δ 2.09 (H_3-4′) to the methine at δ 47.9 (C-2′) and the carbonyl at δ 213.3 (C-3′) indicated a ketone group at C-3′. HMBC correlations from the methylene, CH_2-1′ to C-2 (δ 121.9), C-3 (δ 113.8), C-3a (δ 125.8), C-3′ (δ 47.9), C-5′ (16.8) and the carbonyl at δ 213.3 (C-2′)confirmed the structure of the C-3 side chain as 2-methyl-3-oxobutyl (Fig. 4.44b). The methyl protons, δ 1.14(CH_3-5′) appeared as a doublet due to coupling with the CH-2′ methine proton. Compound **HM7** was thus characterized as 3-(2′-methyl-3′-oxobutyl)-6-(3"-methyl-2"-butenyl) indole (Fig. 4.44a). In the HR-MS^2 analysis, a base peak at *m/z* 198.12 [M H 72]$^+$ was observed for the loss of C_4H_8O from the C-3 prenyl chain. The loss of the C-6 prenyl side chain gave the peak at *m/z* 202.12 [M H 68]$^+$ (Fig. 4.45).

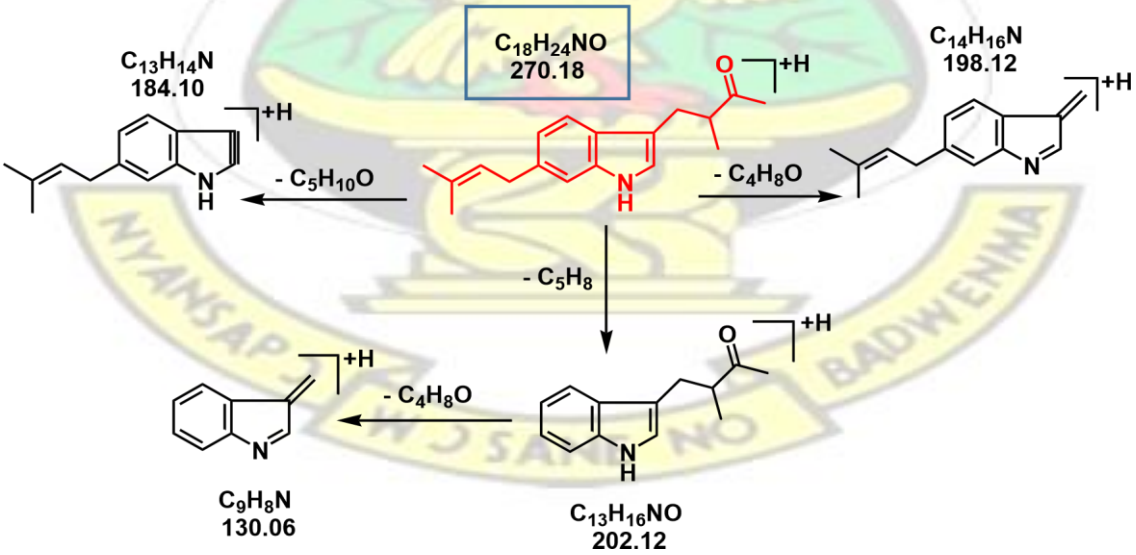

Fig. 4.45: Proposed HRMS^2 fragmentation pattern of compound **HM7**

Table 4.25: ^{1}H (500 MHz) and ^{13}C (125 MHz) NMR data of HM7

Position	δ C [a]	δ H (mult, *J in Hz)*
N-H	-	7.85, brs
2	121.9 (CH)	6.91, brd (1.5)
3	113.8 (C)	-
3a	125.8 (C)	-
4	118.7 (CH)	7.48-7.49, d (8.0)
5	120.6 (CH)	6.96-6.97, brd (8.0)
6	136.2 (C)	-
7	110.5 (CH)	7.15, brs
7a	136.9 (C)	-
1′	28.9 (CH_2)	2.71-2.72, dd (14.5, 7.5) 3.10-3.11, dd (14.5,7.0)
2′	47.9 (CH)	2.95-2.96, dd (14.0, 7.0)
3′	213.3 (C)	-
4′	28.8 (CH_3)	2.09, s
5′	16.8 (CH_3)	1.13-1.14, d (7.0)
1″	34.7 (CH_2)	3.44-3.45, d (7.0)
2″	124.1 (CH)	5.38, tm
3″	132.3 (C)	-
4″	26.0 (CH_3)	1.75, s
5″	18.0 (CH_3)	1.75, s

Chemical shifts (ppm) are referenced to solvent ($CDCl_3$) peak (δ H 7.26); *[a] -signals assigned from HSQC spectrum*

Physicochemical properties of HM7: Pale yellow oil; [α] +27 ° (*c* 0.10; MeOH); UV: λ_{max} nm: 226 (in MeOH); IR: v_{max} cm^{-1}: 3384 (> N-H), 1704 (> C=O).

4.5.8: 3-(1′, 3′-dihydroxy-3′-methyl-but-2′-yl)-6-(3″-methyl-2″-butenyl) indole (HM8)

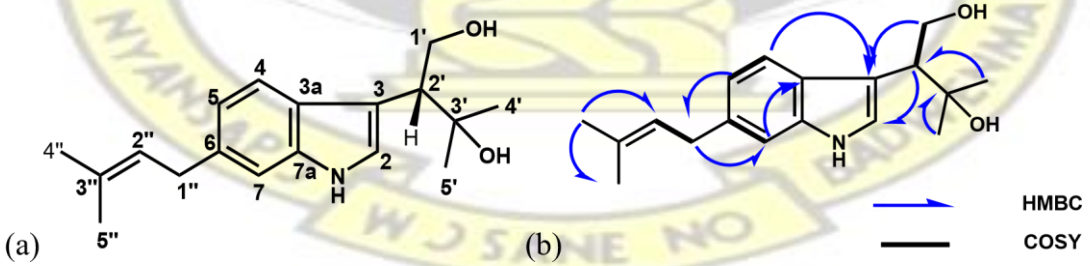

Fig. 4.46 (a): **HM8**; (b): HMBC & COSY correlations of **HM8 HM8** was isolated as colourless oil with the molecular formula $C_{18}H_{25}O_2N$ as indicated by its positive ion molecular peak at *m/z* 288.19 $[M + H]^+$ in the HRESIMS analysis. The 1D and 2D NMR data (Table 4.26, Fig. 4.46b) of **HM8** revealed signals for a di-

substituted indole nucleus (Achenbach *et al.*, 1995). From 2D NMR analysis, the indole C-6 substituent was identified as 3-methyl-2-butenyl as described for **HM1**. The indole C-3 substituent was characterized as 1, 3-dihydroxy3-methyl-but-2-yl based on comparison of NMR spectra to reported data in literature(Achenbach *et al.*, 1995). Compound **HM8** was thus identified as 3-(1′,3′dihydroxy-3′-methyl-but-2′-yl)-6-(3″-methyl-2″-butenyl)indole (Fig. 4.46a), a diprenylated indole isolated from *H. monopetalus* and *H. crispiflorus* (Achenbach *et al.*, 1995).

Table 4.26: ^{1}H (500 MHz) and ^{13}C (125 MHz) NMR data of HM8

Position	**δ C** [a]	**δ H (mult, *J in Hz*)**
N-H	-	8.23, brs
2	122.0 (CH)	7.12, brd (2.0)
3	113.7 (C)	-
3a	126.4 (C)	-
4	119.3 (CH)	7.52-7.53, d (7.0)
5	120.9 (CH)	6.97-6.99, dd (6.5, 1.0)
6	136.2 (C)	-
7	110.5 (CH)	7.17, br s
7a	136.4 (C)	-
1′	64.5 (CH_2)	4.07-4.10, m
2′	48.2 (CH)	3.26, t (5.0)
3′	74.6 (CH)	-
4′	29.4 (CH_3)	1.27, s
5′	27.2 (CH_3)	1.30, s
1″	34.6 (CH_2)	3.44-3.45, d (6.0)
2″	123.9 (CH)	5.38, tm
3″	132.4 (C)	-
4″	26.0 (CH_3)	1.75, s
5″	18.0 (CH_3)	1.75, s

Chemical shifts (ppm) are referenced to solvent ($CDCl_3$) peak (δ H 7.26)

4.5.9: 3-(2′,3′-dihydroxy-3′-methyl-but-2′-yl)-6-(3″-methyl-2″-butenyl) indole (HM9, known compound)

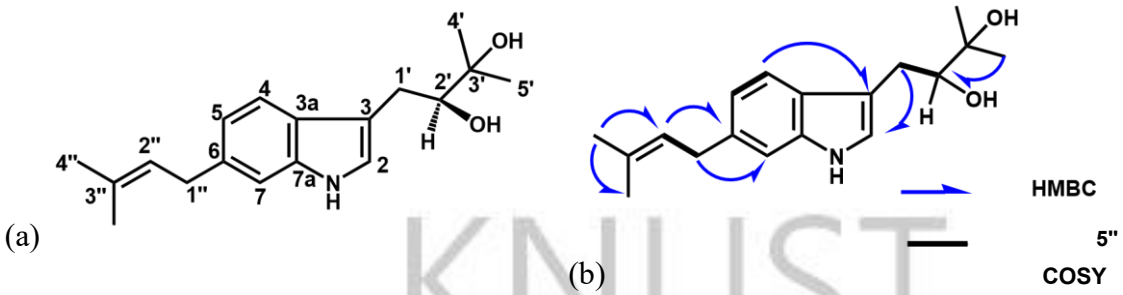

Fig. 4.47 (a):**HM9**; (b): HMBC & COSY correlations of **HM9**

The molecular formula of **HM9** was same as **HM8**. The 1D (Table 4.27) and 2D NMR gave signals for a 3, 6 di-substituted indole alkaloid with a 3-methyl but-2yl substituent at the indole C-6 as described for **HM8.** The indole C-3 substituent was characterized based on HMBC and COSY correlations (Fig. 4.47b) as follows: COSY correlation was observed between H-1′ and H-2′ as well as HMBC correlations from the methylene protons (H_2-1′) to the oxymethine (δ 77.6, CH-2′) and the carbon at δ 72.7 (C-3′). Compound **HM9** was therefore characterized as 3(2‘,3‘-dihydroxy-3‘-methyl-but-2‘-yl)-6-(3‘‘-methyl-2‘‘-butenyl) indole (Fig. 4.47a) previously isolated from *H. crispiflorus* (Achenbach *et al.*, 1995).

Table 4.27: ^{1}H (500 MHz) and ^{13}C (125 MHz) NMR data of HM9

Position	δ C [a]	δ H (mult, *J in Hz)*
N	-	7.95, brs
2	122.3 (CH)	7.06, brd (2.0)
3	112.4 (C)	-
3a	125.8 (C)	-
4	118.6 (CH)	7.50-7.52, d (8.0)
5	120.8 (CH)	6.97-6.99, dd (8.0, 1.0)
6	136.5 (C)	-
7	110.8 (CH)	7.18, brs
7a	137.3 (C)	-
1′	27.9 (CH_2)	2.73-2.76, dd (14.5, 11.0) 3.05-3.07, dd (14.5, 1.5)
2′	77.6 (CH)	3.72-3.75, dd (10.5, 2.0)
3′	72.7 (C)	-
4′	26.5 (CH_3)	1.35, s

5′	23.9 (CH_3)	1.32, s
1″	34.5 (CH_2)	3.44-3.46, d (7.0)
2″	123.9 (CH)	5.38, tm
3″	132.3 (C)	-
4″	26.0 (CH_3)	1.75, s
5″	17.9 (CH_3)	1.75, s

Chemical shifts referenced to $CDCl_3$ (δ H 7.26); [a] *signals assigned from HSQC spectrum*

By comparison of the optical rotations ($[\alpha]_D$) of compounds **HM2** **HM5** to those of similar compounds with known absolute configuration reported in literature (Achenbach and Löwel, 1995; Achenbach *et al.*, 1995), the configuration of C-2′ of the indole C-3 side chain is proposed to be *R* for compounds **3** **5** and *S* for compound **2**. The configuration at C-2′ of compounds **7** and at C-2″ of compound **5** could however not be determined due to paucity of samples obtained.

4.6 Discussion

The prenylated indole alkaloids are hybrid natural products derived from prenyl diphosphates and tryptophan or its precursors and are widely distributed in nature especially in fungi (Li, 2010). A number of naturally occurring mono and diprenylated indole alkaloids have also been reported from plants of the family Annonaceae (Achenbach and Raffelsberger, 1979; Achenbach *et al.*, 1995; Nkunya *et al.*, 2004) and rarely from Rutaceae (Wang *et al.*, 2005).

With regards to the biological activities, the prenylated indole alkaloids have been previously reported to exhibit antifungal (Achenbach *et al.*, 1995; Makangara *et al.*, 2004), antiviral (Wang *et al.*, 2005) and anti-plasmodial (Makangara *et al.*, 2004; Nkunya *et al.*, 2004) activities. From the results of the antimicrobial assay, the EtOAc fraction of *H. monopetalus* showed antimicrobial activity against *B. subtilis* and *S. pyogens* at MIC of 312 µg/mL. The isolated compounds however showed no

antimicrobial activity at 10 µg/mL against the plant pathogenic fungi, *Mucor miechei*, *Rhizoctonia solani* and *Pythium ultimum*. In previous antimicrobial studies, some prenyl indoles including the known compounds, **HM8** and **HM9** isolated from *H. crispiflorus* and *H. monopetalus* exhibited antifungal activity at 150 µg against the plant pathogenic fungi *Botrytis cinerea*, *Rhizoctonia solani* and *Saprolegnia asterophora* (Achenbach et al., 1995). In another study by Malebo et al., (2014), similar prenyl indoles isolated from *H. monopetalus* showed antifungal activity against *C. albicans* at 100 µg/mL. A comparison of these previous results with the current results suggests that the antimicrobial activity of the prenylated indole alkaloids may be organism specific and is only evident at high concentrations.

The crude MeOH extract also showed DPPH scavenging activity and was found to have a total phenolic content of 66.19 mg (tannic acid equivalent) per gram of dried extract.

4.6.1 Chemotaxonomic significance of the 'hexalobines'

The diprenylated indole alkaloids from the genus *Hexalobus* are usually called ‗hexalobines' due to their marked abundance in the genus. Moreover, this class of compounds have been exclusively isolated from certain genera in the family Annonaceae including *Hexalobus*, *Monodora*, *Isolona, Uvaria* and *Asteranthe*. This characteristic production of the prenylated indole alkaloids in specific genera confirms a molecular phylogenetic revision on the African Annonaceae which identified the genera *Hexalobus*, *Uvariastrum*, *Asteranthe*, *Isolona* and *Monodora* as one sub-clade in the African long-branch clade (ALBC) (Couvreur *et al.*, 2008; Botermans *et al.*, 2011). The prenylated indole alkaloids therefore represent an important class of compounds as their presence connote a chemotaxonomic relationship among the genera from which they are produced (Makangara *et al.*, 2004).

4.6.2 Proposed biogenesis of the prenylated indole alkaloids

The biogenesis of the prenylated indole alkaloids is proposed to result from the introduction of two C_5 units from the isoprene or mevalonate origin unto a tryptophan nucleus followed by the loss of serine or dehydroalanine (Kinoshita *et al.*, 1989; Achenbach *et al.*, 1995) in analogy to the biosynthesis of echinulin (Grundon *et al.*, 1980). Apart from Hexalobine A (Achenbach and Raffelsberger, 1979), the isopentenyl side chains in most prenylated indole alkaloids are present at various oxidation levels being an epoxide, a diol, ketone or aldehyde groups. Considering the pattern of the structures of the prenylated indole alkaloids, it could be proposed as also described for other prenylated natural products (Dreyer, 1967; Rodighiero *et al.*, 1979; Kinoshita *et al.*, 1989), that the first modification of the isopentenyl side chain is selective epoxidation of the terminal double bond to produce an epoxide. Acid catalysed hydrolysis of the epoxide then leads to the formation of the 1, 2-diol (**HM8**) as experimentally shown by Achenbach et al., (1995). A _pinacol-like‘ rearrangement (Snape, 2007) of the diol could account for the formation of the aldehyde or ketone derivatives (Fig. 4.48). This may occur by the migration of the β proton to give rise to the keto product or by migration of the C^{α}-C^{β} bond to give the formyl derivatives as described by Dreyer in 1967 (Dreyer, 1967). A simple biosynthetic relationship among some prenylated indoles is hereby proposed in Fig.

4.49 (Mireku *et al.*, 2016).

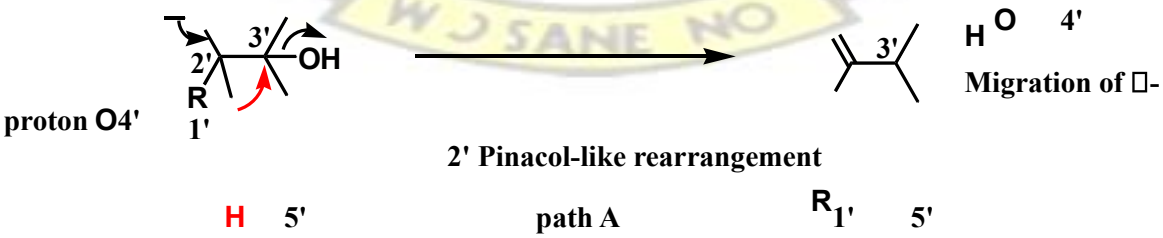

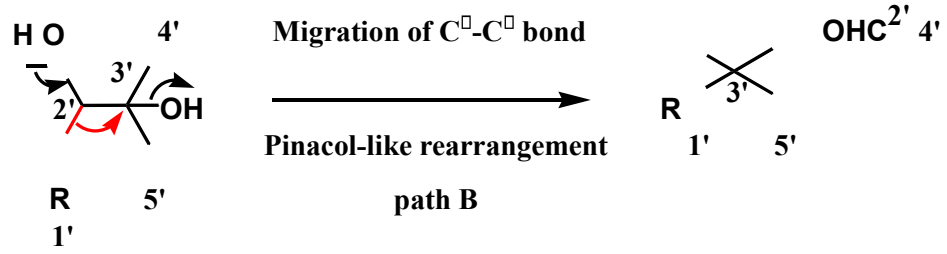

Fig. 4.48: The pinacol-like rearrangement
(Dreyer, 1967)

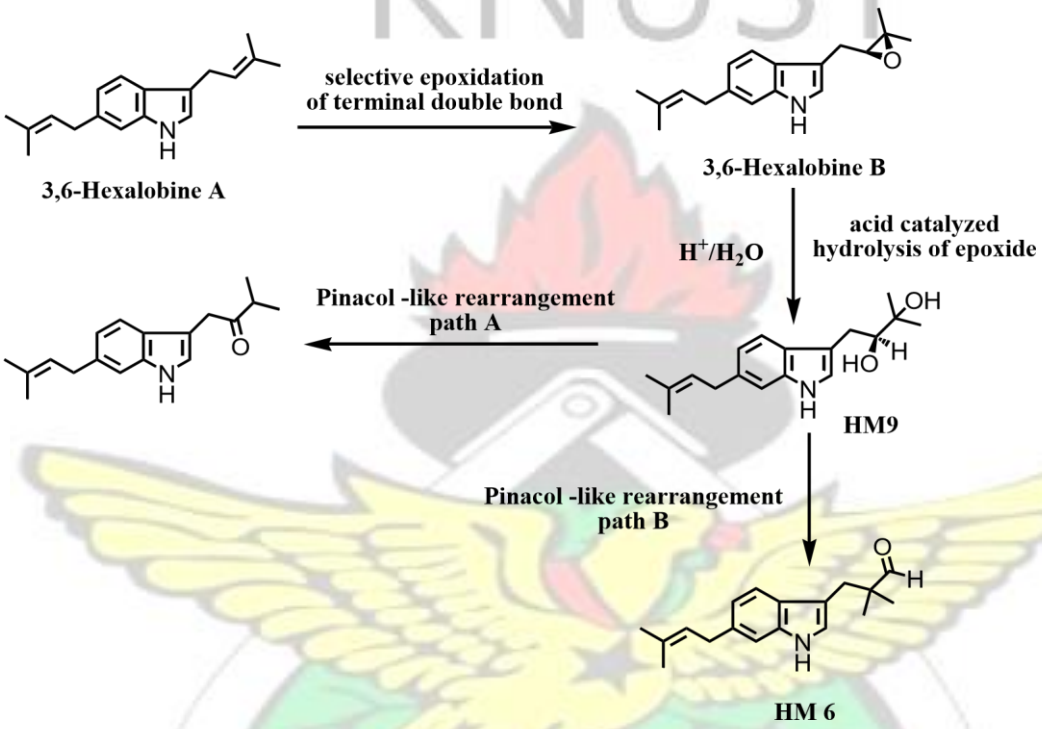

Fig. 4.49: Proposed biogenetic relationship among some prenylated indoles

4.7 Biological activities of roots of *Landolphia heudelotti*

4.7.1 Antimicrobial activity of L. heudelotti root fractions

The antimicrobial activity of the petroleum ether, EtOAc and MeOH fractions of *L. heudelotti* roots was investigated by the agar dilution assay. The results are stated in Table 4.28. *P. aeruginosa* was not inhibited by any of the test fractions. The petroleum ether fraction showed no antimicrobial activity against the organisms tested. The MeOH fraction showed the highest inhibitory effects against both Gram positive and

Gram negative bacteria and fungi, *C. albicans*. The highest activity was exhibited against *B. subtilis* and *S. pyogens* with MIC of 312 µg/mL.

Table 4.28: Antimicrobial activity of *L. heudelotti* root fractions

	Minimum inhibitory concentration (MIC); µg/mL				
	LHP	LHE	LHM	Ciprofloxacin	Ketoconazole
S. aureus	-	1250	625	0.25	-
B. subtilis	-	1250	312	0.10	-
S. pyogens	-	-	312	0.10	-
E. coli	-	>2500	1250	0.10	-
P. aeruginosa	-	-	-	0.10	-
S. typhi	-	>2500	1250	0.25	-
C. albicans	-	1250	625	-	5

LHP- petroleum ether fraction; LHE- EtOAc fraction, LHM-MeOH fraction

4.7.2 Antimicrobial activity of isolated compounds from L. heudelotti

(Refer to Section 4.8 for details on the isolated compounds from *L. heudelotti*)

Compounds **LH-1**, **LH-6**, **LH-7**, **LH-8**, **LH-10**, **LH-11**, **LH-12**, **LH-13** were tested for antimicrobial activity against *S. aureus*, *B. subtilis*, *E. coli* and *Acinetobacter species* at 100, 50, 25 and 12.5 µg/mL. Other isolated compounds could not be tested due to the paucity of sample obtained. All the tested compounds demonstrated antimicrobial activity. The results of the assay are given in Table 4.29.

Table 4.29: Antimicrobial activity of compounds from *L. heudelotti* roots

	Minimum inhibitory concentration (MIC); µg/mL								
	LH-1	**LH-6**	**LH-8**	**LH-10**	**LH-11**	**LH-12**	**LH-13**	**GM**	**SM**
S. aureus	-	-	100	100	50	50	50	1.0	5.0
B. subtilis	100	12.5	50	100	50	25	50	1.0	5.0
E. coli	-	50	25	50	50	25	12.5	1.0	1.0

Acineto bacter spp.	25	25	25	12.5	25	25	25	5.0	10.0

GM-Gentamycin; SM-streptomycin

4.7.3 Antioxidant Activity of the crude extract of L. heudelotti

4.7.3a DPPH Free radical Scavenging Assay

Different concentrations of the crude methanol extract of *L. heudelotti* roots were tested in the DPPH free radical scavenging assay. The results obtained showed a concentration-dependent scavenging effect of the extract (Fig. 4.50). The IC_{50} was determined as 6.956 ± 0.81 µg/mL for *L. heudelotti* root extract and 2.44 ± 0.0134 µg/mL for ascorbic acid as deduced from the log concentration versus % DPPH inhibition curve (Fig. 4.51).

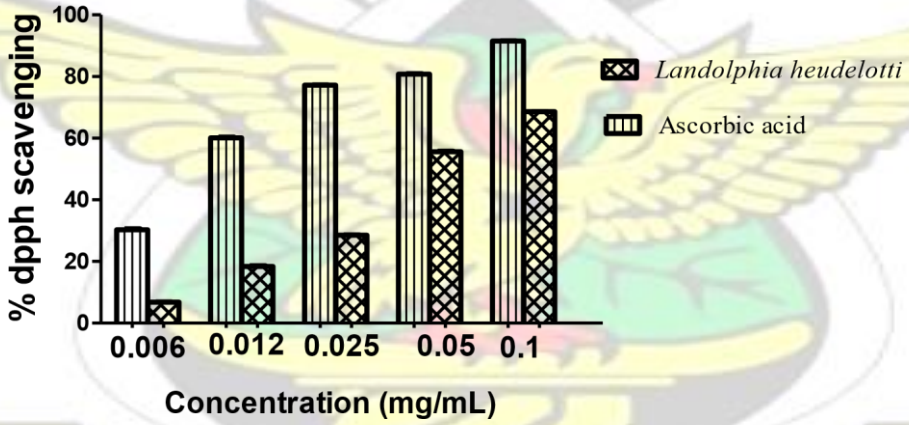

Fig. 4.50: Percentage DPPH scavenging of *L. heudelotti* root MeOH crude extract

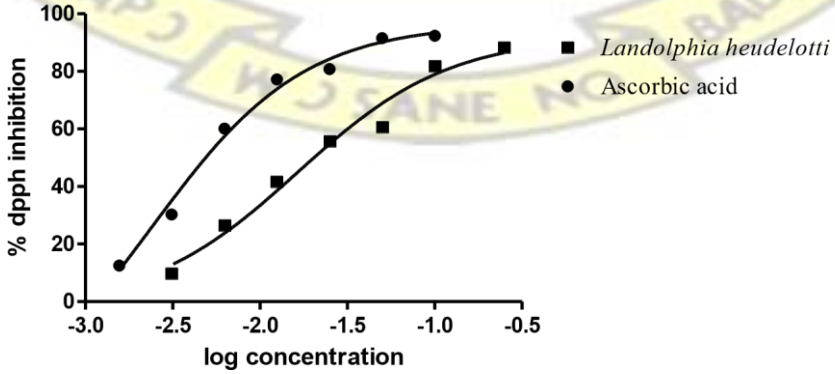

Fig. 4.51: Log concentration versus percentage DPPH scavenging effect of *L. heudelotti* root MeOH extract

4.7.2b Total Phenolic content and total antioxidant capacity

The crude MeOH extract of *L. heudelotti* roots was found to have a total phenolic content of 98.14 ± 14.70 mg TAE per gram of dried extract (standard curve of tannic acid, y = 23.92x + 0.01604, r^2 = 0.9996). The total antioxidant capacity of the extract was 108.8 ± 14.52 mg (AAE) per gram of dried extract (standard curve of ascorbic acid: y = 6.907 x + 0.04604, r^2 = 0.9832).

4.7.4 DPPH free radical scavenging activity of isolated compounds

The free radical scavenging effects of some of the isolated compounds was investigated at a concentration range between 0.5 and 0.01 mg/mL. **LH-2**, **LH-3**, **LH-4**, **LH-5**, **LH-9** could not be tested due to the paucity of samples obtained. The percentage scavenging effect of the lowest concentration (0.01 mg/mL) of each test sample is demonstrated Fig. 4.52. Pinoresinol (**LH-1**) exhibited the highest scavenging effects.

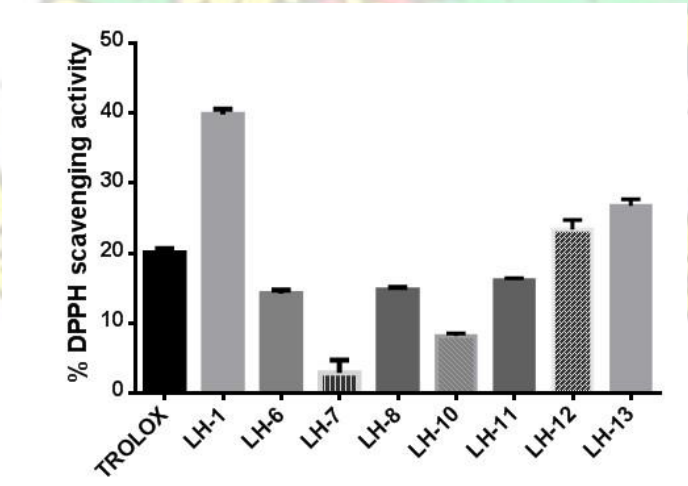

Fig. 4.52: Percentage DPPH free radical scavenging of compounds

4.8 Structural elucidation of isolated compounds of *L. heudelotti*

Repeated purification of the MeOH extract of *L. heudelotti* roots by silica gel, sephadex LH-20 and semi-preparative HPLC led to the isolation of fourteen known compounds including seven neolignans, four sesquilignans, a lignan, an aromadendrane and a coumarin (Fig. 4.53). The characterization of the compounds is discussed below. [All HR-ESIMS and NMR (1D and 2D) spectra for described compounds from *L. heudelotti* can be found in **Appendix C**].

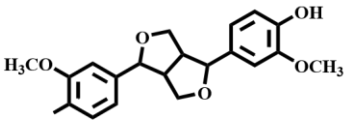

LH-1

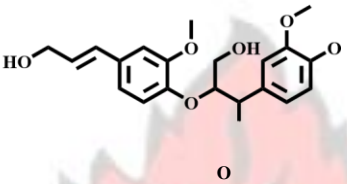

LH-2- *erythro* conformer
LH-3- *threo* conformer

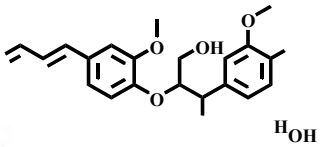

LH-4- *erythro* conformer
LH-5- *threo* conformer

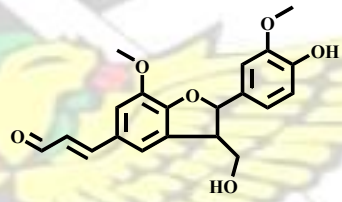

LH-6

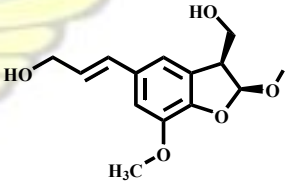

LH-7

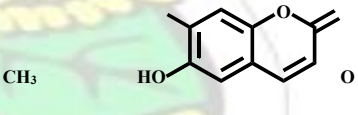

LH-8

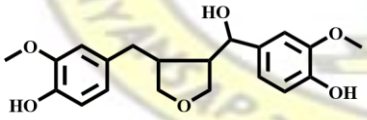

LH-9

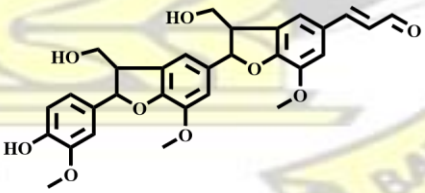

LH-10

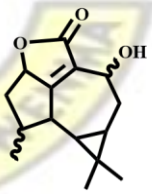

LH-14

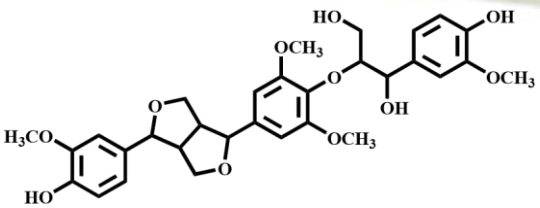

LH-11

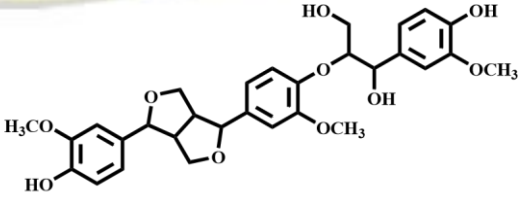

LH-12-*erythro* conformer
LH-13-*threo* conformer

Fig. 4.53: Isolated compounds from *L. heudelotti*

Structural elucidation of compounds

4.8.1: Pinoresinol (LH-1)

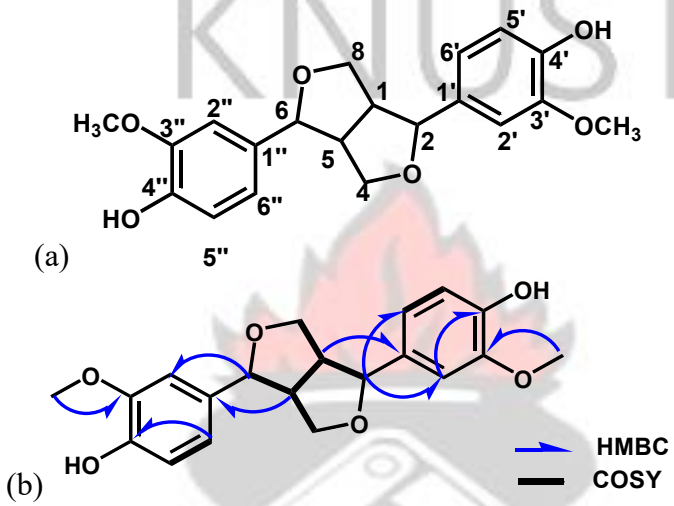

Fig. 4.54 (a): **LH-1**; (b): HMBC & COSY correlations of **LH-1**

LH-1 was isolated as yellow oil. The HR-MS analysis gave the molecular formula of **LH-1** as $C_{20}H_{22}O_6$ as determined from its pseudo-molecular ion peak at *m/z* 359.14 $[M + H]^+$ (calculated for $C_{20}H_{23}O_6$), a sodium adduct at *m/z* 381.13 $[M + Na]^+$ (calculated for $C_{20}H_{22}O_6Na$) and a major fragment ion at *m/z* 341.13 ($[M+H-H_2O]^+$, $C_{20}H_{21}O_5$). The ^1H NMR data (Table 4.30) displayed signals for three aromatic protons (δ 6.65-6.84) indicating a tri-substituted aromatic ring, a methoxy (δ 3.74, s), an oxymethylene group [δ 3.72 (dd, *J* = 3.8, 9.5) and 4.14 (dd, *J* = 2.1, 9.0)] and two methine protons [δ 4.60, (d, *J* = 4.3); 3.03, m]. From the ^{13}C NMR spectrum (Table 4.30), ten instead of twenty carbon signals were observed, clearly indicating the compound to be a symmetrically dimeric molecule. A comparison of the NMR data to reported literature (Jung *et al.*, 2010; During *et al.*, 2012) led to the characterization of

LH-1 as pinoresinol (Fig. 4.54a). The structure was confirmed by HMBC and COSY correlations as shown in Fig. 4.54b.

Table 4.30: ^{1}H and ^{13}C NMR data for compound LH-1

Position	$_{13}C$	^{1}H (mult, *J* in Hz)
1 (5)	55.6 (CH)	3.03, m
2 (6)	87.7 (CH)	4.60, d (4.3)
4 (8)	72.8 (CH_2)	4.12-4.14, dd (2.1, 9.0),3.72, dd (3.8, 9.5)
1′ (1″)	134.0 (C)	-
2′ (2″)	111.1 (CH)	6.84, d (1.6)
3′ (3″)	149.3 (C)	-
4′ (4″)	147.5 (C)	-
5′ (5″)	116.3 (CH)	6.65-6.67 d, (8.1)
6′ (6″)	120.3 (CH)	6.69-6.71, dd (1.3, 8.1)
O-CH_3	56.6	3.74, s

Chemical shifts (ppm) are referenced to solvent (CD_3OD, δ 4.78)

4.8.2: *Erythro*-guaiacylglycerol-8-*O*-4'-coniferyl alcohol ether (LH-2)

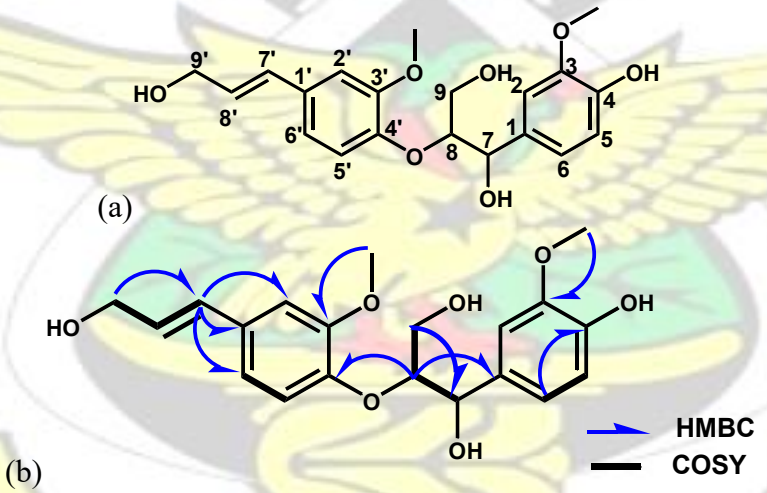

Fig. 4.55 (a): **LH-2**; (b): HMBC & COSY correlations of **LH-2**

The molecular formula of **LH-2**, a yellow oil was determined as $C_{20}H_{24}O_7$ based on its sodium adduct ion peak at *m/z* 399.14 $[M+Na]^+$ (calculated for $C_{20}H_{24}O_7Na$) and a fragment ion for the loss of two molecules of H_2O at *m/z* 341.13 (calculated for $C_{20}H_{21}O_5$) in the HR-MS spectrum.

The ^{1}H NMR spectral data (Table 4.31) showed signals for six aromatic protons, resonating between δ 6.61-δ 6.91 and two methoxyls, both resonating at δ 3.69 (s). Furthermore, two olefinic protons [δ 6.39 (brd, *J* = 15.6, H-7′) and δ 6.11-6.15 (dt, *J*= 5.7, 5.7, H-8′)], two oxymethylenes [δ 3.73 (dd, *J* = 5.8, 12.0, H-9α); δ 3.67 (dd, *J* = 3.6, 12.1, H-9β) and 4.08-4.09 (dd, *J* = 1.3, 5.8, H_2-9′)] and two oxymethines [δ 4.72 (d, *J* = 5.4, H-7) and δ 4.25, m, H-8] were assigned.

Based on long range COSY correlations between H-7/H-8 and H-8/H-9, a 1, 2, 3propane-triol chain (^{7}C–^{8}C–^{9}C) was identified and linked to C-1 by HMBC correlations from δ 4.72 (H-7) to C-2, C-6, C-8 and C-9 to give a guaiacylglycerol nucleus. A 3-propenol ($^{7'}$C–$^{8'}$C–$^{9'}$C) moiety was also assigned based on long range COSY correlations between H-7′/H-8′ and H-8′ /H-9′. Key HMBC correlations from H-7′ (δ 6.39) to C-1′, C-2′ and C-6′ of the benzene ring (Fig. 4.55b) led to the establishment of a coniferyl alcohol nucleus. HMBC cross peaks from H-8 of the guaiacylglycerol to C-4′ of the coniferyl alcohol confirmed an 8-*O*-4′ linkage to form a guaiacylglycerol-8-*O*-4'-coniferyl alcohol ether (Wang *et al.*, 2014). As described for 8-*O*-4′ neolignans in literature, a large or small coupling constant (*J* values) for H-7 and H-8 correspond to the *threo* or *erythro* forms respectively (Huang *et al.*, 2013). Moreover, the downfield shifts of H-8′ and H- 9′ are attributed to the erythro isomer, and the reverse for the threo isomer (Sakushima *et al.*, 2003). In the ^{1}H NMR spectra, a small *J* value ($J_{7,8}$ = 5.4 Hz) and a downfield shift of H-8 and H-9 suggested C-7/8 to be in the *erythro* configuration. Compound **LH-2** was thus identified as *erythro*-guaiacylglycerol-8-*O*-4'-coniferyl alcohol ether (Fig. 4.55a) previously isolated from *Melia toosendan* (Wang *et al.*, 2014), *Campylotropis hirtella* (Han *et al.*, 2008) and *Clematis armandii* (Xiong *et al.*, 2014).

Table 4.31: ^{1}H and ^{13}C NMR data for compound LH-2

Position	$_{13}C$	^{1}H (mult, *J* in Hz)
1	134.2(C)	-
2	112.0 (CH)	6.89-6.91, d (1.8)
3	148.9 (C)	-
4	147.2 (C)	-
5	115.8 (CH)	6.61-6.63, d (8.0)
6	121.2 (CH)	6.72, dd (2.0, 8.1)
7	74.3 (CH)	4.72, d (5.4)
8	86.5 (CH)	4.25, m
9	62.4 (CH_2)	3.73, dd (5.8, 12.0) , 3.67, dd (3.6, 12.1)
1′	133.2 (C)	-
2′	111.5 (CH)	6.89, brs
3′	152.1 (C)	-
4′	149.1 (C)	-
5′	119.0 (CH)	6.76, brs
6′	120.8 (CH)	6.76, brs
7′	131.7 (CH)	6.39, brd (15.6)
8′	128.6 (CH)	6.11-6.15, dt (5.7, 5.7)
9′	64.0 (CH_2)	4.08-4.09, dd (1.3, 5.8)
3-OCH_3	56.5	3.69, s
3′-OCH_3	56.7	3.69, s

Chemical shifts (ppm) are referenced to solvent (CD_3OD, δ 4.78)

4.8.3: *Threo*-guaiacylglycerol-8-*O*-4'-coniferyl alcohol ether (LH-3)

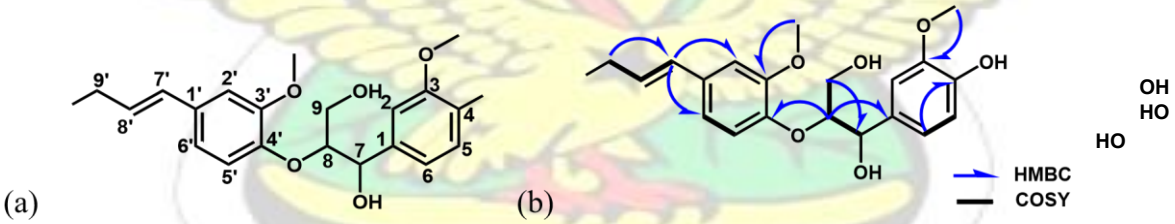

Fig. 4.56 (a): **LH-3**; (b): HMBC & COSY correlations of **LH-3**

LH-3 had the same molecular formula as **LH-2** (*m/z* 399.14, $C_{20}H_{24}O_7Na$). The NMR spectroscopic data (Table 4.32) showed similar pattern and chemical shifts to those of **LH-2**, suggesting the same planar structure as **LH-2**. However, a large coupling constant for H-7/8 ($J_{7,8}$ = 6.1 Hz) in the ^{1}H NMR of **LH-3** suggested a relative *threo* isomer. By comparison to reported literature, the spectral data of **LH-3** matched those reported for *threo*-guaiacylglycerol-8-*O*-4'-coniferyl alcohol ether (Fig. 4.56a). This

compound was previously isolated from *Melia toosendan* (Wang *et al.*, 2014) and *Clematis armandii* (Xiong *et al.*, 2014).

Table 4.32: ^{1}H and ^{13}C NMR data for compound LH-3

Position	$_{13}C$	^{1}H (mult, *J* in Hz)
1	133.9 (C)	-
2	111.8 (CH)	6.90, d (1.9)
3	149.0 (C)	-
4	147.4(C)	-
5	116.0 (CH)	6.62-6.63, d (8.1)
6	121.0 (CH)	6.77-6.79, dd (1.9, 8.4)
7	74.2 (CH)	4.75, d (6.1)
8	87.3 (CH)	4.16-4.17, m
9	62.1 (CH_2)	3.33, dd (5.3, 11.9); 3.60, dd (3.8, 11.8)
1′	133.3 (C)	-
2′	111.4 (CH)	6.93, d (1.9)
3′	151.9 (C)	-
4′	149.4 (C)	-
5′	119.0 (CH)	6.86-6.88, d (8.3)
6′	120.8 (CH)	6.72-6.74, dd (1.8, 8.1)
7′	131.6 (CH)	6.39-6.42, brd (15.7)
8′	128.8 (CH)	6.12-6.15, dt (5.7, 5.6)
9′	63.9 (CH_2)	4.07-4.08, dd (1.3, 5.9)
3-OCH_3	56.5	3.69, s
3′-OCH_3	56.7	3.75, s

Chemical shifts (ppm) are referenced to solvent (CD_3OD, δ 4.78)

4.8.4: *Erythro*-guaiacylglycerol-8-*O*-4′-coniferyl aldehyde ether (LH-4)

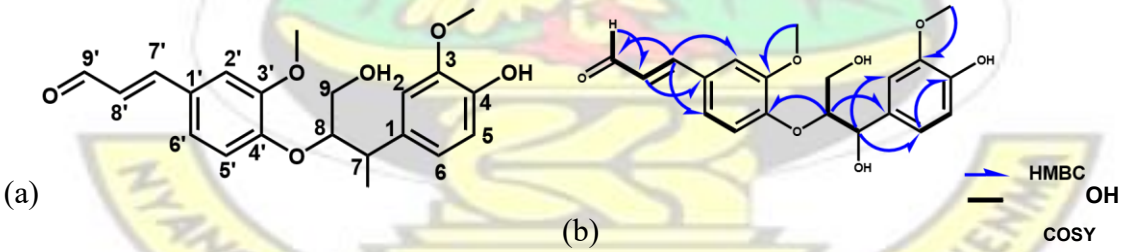

(a) (b)

Fig. 4.57 (a): **LH-4**; (b): HMBC & COSY correlations of **LH-4**

LH-4 was isolated as yellow oil with the molecular formula $C_{20}H_{22}O_7$ as derived from its sodium adduct (*m/z* 397.12 $[M + Na]^+$, $C_{20}H_{22}O_7Na$) ion peak in the positive HR-ESIMS analysis.

From the ^{1}HNMR spectral data (Table 4.33), six aromatic protons resonating between δ 6.59 and δ 7.12 and two methoxyls at δ 3.69 (s) and δ 3.72 (s)] were observed. A low field doublet signal at δ 9.47-9.48 (d, *J*= 8.0, H-9′) and two olefinic protons [δ 6.55 (dd, *J*= 7.9, 15.7, H-8′) and [δ 7.45-7.48 (d, *J* = 16.0, H-7′)] were also identified and linked by COSY correlations (H-7′/H-8′; H-8′/H-9′, Fig. 4.57b) to give the substructure $^{7'}$CH–$^{8'}$CH–$^{9'}$CHO (3-propenal). HMBC correlations from H-7′ (δ 7.45) to C- 1′, C-2′, C-6′ and C-9′ (Fig. 4.57b) led to the establishment of a coniferyl aldehyde nucleus. Furthermore, the ^{1}H NMR spectra gave signals for an oxymethylene [δ 3.73 (d, *J* = 4.8, H_2-9) and two oxymethine protons [δ 4.44 (m, H-8) and δ 4.70 (d, *J* = 5.0, H-7)] (Table 4.33). Based on long range COSY and HMBC correlations, a guaiacyl glycerol nucleus was assigned as described for **LH-2** and shown in Fig. 4.57b). HMBC cross peaks from H-8 of the guaiacylglycerol to C-4′ of the coniferyl aldehyde revealed an 8-*O*-4′ linkage to form a guaiacylglycerol-8-*O*-4'coniferyl aldehyde ether. The positions of the methoxyls were assigned by HMBC correlations (Fig. 4.57b). In the ^{1}H NMR spectra of **LH-4**, a small coupling constant for H-7/8 ($J_{7,8}$ = 5.0 Hz) suggested an *erythro* configuration at C-7/8. By comparison of data to reported literature, **LH-4** was unambiguously assigned as *erythro*guaiacylglycerol-8-*O*-4'-coniferyl aldehyde ether (Fig. 4.57a). This compound has been previously isolated from *Firmiana simplex* (Woo *et al.*, 2016).

Table 4.33: ^{1}H and ^{13}C NMR data for compound LH-4

Position	**$_{13}$C**	**^{1}H (mult, *J* in Hz)**
1	134.1 (C)	-
2	112.1 (CH)	6.93, d (1.8)
3	148.8 (C)	-
4	147.3(C)	-
5	115.7 (CH)	6.59, d (8.0)
6	121.3 (CH)	6.73, dd (1.9, 8.0)
7	74.2 (CH)	4.70, d (5.0)
8	85.5 (CH)	4.44, m

9	62.6 (CH_2)	3.73, d (4.8)
1′	129.4 (C)	-
2′	112.8 (CH)	7.11-7.12, d (2.0)
3′	152.0 (C)	-
4′	152.9 (C)	-
5′	117.2 (CH)	6.89-6.90, d (8.4)
6′	124.5 (CH)	7.05-7.06, dd (2.0, 8.5)
7′	155.7 (CH)	7.45-7.48, d (16.0)
8′	127.8 (CH)	6.55, dd (7.9, 15.7)
9′	196.3 (CH)	9.47-9.48 d (8.0)
3-OCH_3	56.4	3.69, s
3′-OCH_3	56.7	3.72, s

4.8.5: *Threo*-guaiacylglycerol-8-*O*-4'-coniferyl aldehyde ether (LH-5)

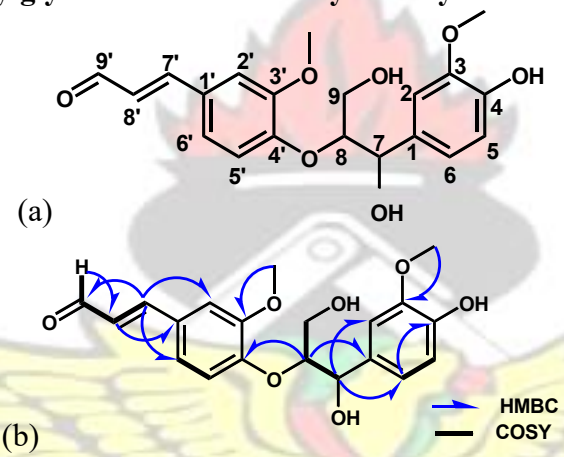

Fig. 4.58 (a): **LH-5**; (b): HMBC & COSY correlations of **LH-5**

LH-5 had the same molecular formula as **LH-4** (*m/z* 397.12 $[M + Na]^+$; $C_{20}H_{22}O_7Na$). The NMR spectroscopic data (Table 4.34) showed similar chemical shifts and pattern of signals to those of **LH-4,** suggesting that the same planar structure. However, the upfield shifts of H-8 and H- 9 relative to **LH-4**, led to the assignment of **LH-5** as the threo isomer of **LH-4**. (H-7 was overlapped by the solvent peak at δ 4.78 hence the coupling constant for H-7/8 could not be determined). ^1H and ^{13}C NMR chemical shifts also matched with the NMR data reported for *threo*-guaiacylglycerol-8-*O*-4'-coniferyl aldehyde ether in literature (Woo *et al.*, 2016).

Table 4.34: ^1H and ^{13}C NMR data for compound LH-5

Position	**$_{13}C$**	**^1H (mult, *J* in Hz)**

1	133.9 (C)	-
2	112.8 (CH)	7.19, d (1.9)
3	149.0 (C)	-
4	147.4(C)	-
5	116.0 (CH)	6.62-6.64, d (8.2)
6	120.8 (CH)	6.73-6.75, dd (1.9, 8.1)
7	74.1 (CH)	4.78, o
8	86.2 (CH)	4.38-4.40, m
9	62.2 (CH_2)	3.41-3.44, dd (6.0, 12.0), 3.65-3.68, dd (4.0, 12.0)
1′	129.5 (C)	-
2′	111.8 (CH)	6.92, d (1.9)
3′	151.9 (C)	-
4′	153.1 (C)	-
5′	117.3 (CH)	6.97-6.98, d (8.4)
6′	124.8 (CH)	7.09-7.10, dd (2.0, 8.9)
7′	155.7 (CH)	7.48-7.50, d (15.6)
8′	127.9 (CH)	6.56-6.60, dd (7.8, 15.8)
9′	196.3 (CH)	9.48-9.49, d (7.8)
3-OCH_3	56.5	3.70 s
3′-OCH_3	56.8	3.80, s

Chemical shifts (ppm) are referenced to solvent (CD_3OD, δ 4.78), o- overlapped

4.8.6: Balanophonin (LH-6)

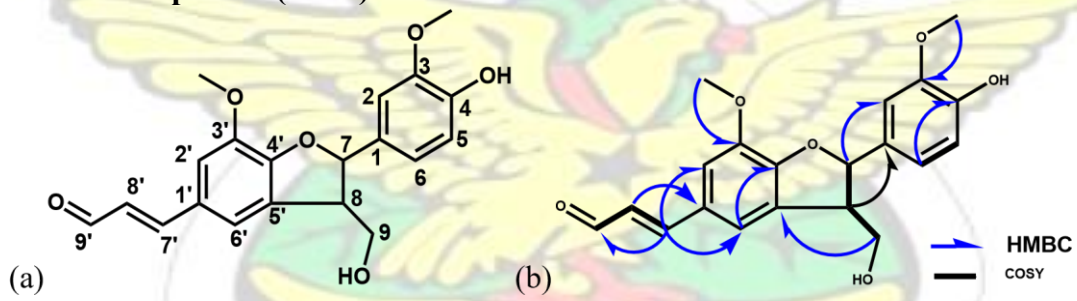

Fig. 4.59 (a): **LH-6**; (b): HMBC & COSY correlations of **LH-6**

LH-6 was isolated as yellow oil. Its molecular formula was determined to be $C_{20}H_{20}O_6$ based on its HR-ESIMS spectrum (*m/z* 357.13 $[M + H]^+$, 379.11 $[M + Na]^+$). The ^{1}H-NMR data (Table 4.35) exhibited five aromatic protons [resonating between δ 6.66 and δ 7.18], two methoxyls [δ 3.71, s; δ 3.81, s], an oxymethine [δ 5.50-5.10, (d, J = 6.5, H-7)] and an oxymethylene [δ 3.73-3.75 (dd, J = 1.9, 7.3, $H_2$9)]. Furthermore, an aldehyde proton [9.47-9.49 (d, J = 7.8, H-9′) and two olefinic protons [δ 7.51-7.53 (d, J =15.6, H-7′) and δ 6.56-6.60 (dd, J = 7.9, 15.7, H-8′)] were identified. From 2D NMR analysis, a di-substituted dihydrofuran skeleton was identified by the existence of

characteristic signals for two methine protons at δ 5.50 (H-7) and 3.45 (H-8) along with four carbon signals at δ 90.3 (C-7), δ 54.9 (C-8), δ

131.5 (C-5′), δ 153.2 (C-4′). The signals at δ 5.50 (H-7), δ 3.45 (H-8) and δ 3.74 (H9) were assigned to the substructure $^{7}CH–^{8}CH–^{9}CH_2OH$ based on $^{1}H–^{1}H$ COSY and HMBC correlations (Fig. 4.50b). A coniferyl aldehyde nucleus was assigned as described for **LH4** (Fig. 4.59b). HBMC correlations from H-9 to C-5′ and from H-8 to C-6′ established the fusion of the coniferyl aldehyde and dihydrofuran to form benzo-furan nucleus. Signals for a guaiacol nucleus (C-1 to C-6, Table 4.35) were identified and linked to the benzo-furan ring by HMBC correlations from H-7 to C-2 and C-6. The positions of the methoxyls were assigned by HMBC correlations (Fig.

4.59b). All these spectroscopic data for **LH-6** corresponded with those reported for balanophonin (Fig. 4.59a), a neolignan previously isolated from *Aquilaria sinensis* (Wang *et al.*, 2010).

Table 4.35: ^{1}H and ^{13}C NMR data for compound LH-6

Position	**$_{13}$C**	**^{1}H (mult, J in Hz)**
1	134.1 (C)	-
2	110.7 (CH)	6.84, d (1.8)
3	149.4 (C)	-
4	148.0 (C)	-
5	116.4 (CH)	6.66-6.68, d (8.2)
6	120.0 (CH)	6.71-6.73, dd (1.9, 8.2)
7	90.3 (CH)	5.50-5.10, d (6.5)
8	54.9 (CH)	3.45, dd (6.2, 12.2)
9	64.8 (CH_2)	3.73-3.75, dd (1.9, 7.3)
1′	129.8 (C)	-
2′	114.4 (CH)	7.13, brs
3′	146.2 (C)	-
4′	153.2 (C)	-
5′	131.5 (C)	-
6′	120.2 (CH)	7.18, brs
7′	156.3 (CH)	7.51-7.53, d (15.6)
8′	127.3 (CH)	6.56-6.60,dd (7.9, 15.7)
9′	196.4 (C)	9.47-9.49, d (7.8)
3-OCH_3	56.6	3.71, s
3′-OCH_3	57.0	3.81, s

4.8.7: 3-(α, 4-dihydroxy-3-methoxybenzyl)-4-(4-hydroxy-3-methoxy benzy1) tetrahydrofuran (LH-7)

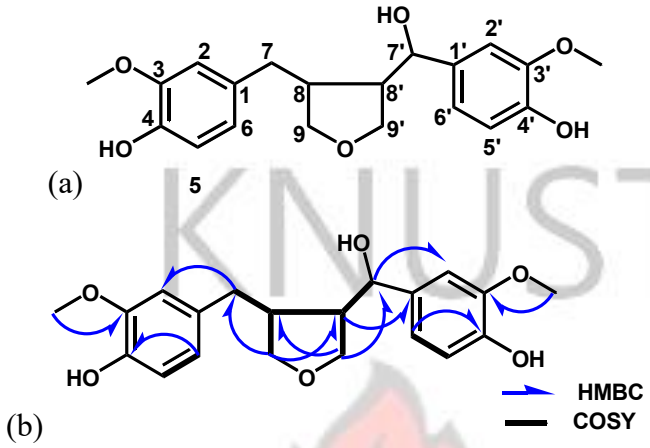

Fig. 4.60 (a): **LH-7**; (b): HMBC & COSY correlations of **LH-7**

The elemental and mass spectral data of **LH-7** gave the molecular formula $C_{20}H_{24}O_6$ (*m/z* 383.14, calculated for $C_{20}H_{24}O_6Na$). An intense fragment ion peak at *m/z* 219.10 (calculated for $C_{13}H_{15}O_3$) signified the loss of a molecule of water (H_2O) and a guaiacol nucleus ($C_7H_8O_2$). From the ^{1}H NMR data (Table 4.36), two methoxyls [δ 3.72, s and δ 3.74, s] and six aromatic protons [resonating between δ 6.53 and 6.80] were observed. Multiplets at δ 2.24-2.29 and δ 2.62 integrating for one proton each, and two double doublets at δ 2.36 (*J* =11.2, 13.2) and δ 2.83 (*J* = 4.8, 13.8) were attributed to H-8′, H-8 and H_2-7_A/7_B respectively. Signals for the two oxymethylene protons at H-9 and H-9′ were also identified (Table 4.36). The doublet at δ 4.63 (*J* = 7.01) was assigned to the oxymethine, H-7′. All 1D and 2D NMR spectral data analysis (Fig. 4.60b) corresponded with those reported for 3-(α,4-dihydroxy-3methoxybenzyl)-4-(4-hydroxy-3-methoxy benzy1) tetrahydrofuran (Fig. 4.60a) previously isolated from *Bupleurum salicifolium* (Estévez-Braun *et al.*, 1995).

Table 4.36: ^{1}H and ^{13}C NMR data for compound LH-7

Position	**$_{13}$C**	**^{1}H (mult, *J* in Hz)**

1	133.7 (C)	-
2	113.6 (CH)	6.69, d (1.9)
3	149.2 (C)	-
4	146.0 (C)	-
5	116.4 (CH)	6.60, d (8.0)
6	122.4 (CH)	6.53-6.54, dd (1.8, 8.0)
7	33.9 (CH_2)	2.36-2.40, dd (11.2, 13.2),2.81-2.83, dd (4.8, 13.4)
8	44.1 (CH)	2.62, m
9	73.7 (CH_2)	3.62, dd (5.9, 8.4), 3.88, dd (6.5, 8.4)
1′	135.9 (C)	-
2′	110.8 (CH)	6.80, d (1.3)
3′	149.2 (C)	-
4′	147.3 (C)	-
5′	116.2 (CH)	6.66, d (1.6)
6′	120.0 (CH)	6.65, brs
7′	84.2 (CH)	4.63, d (7.01)
8′	54.3 (CH)	2.24-2.29, m
9′	60.6 (CH_2)	3.52, dd (6.4, 11.0), 3.72, m
3-OCH_3	56.5	3.74, s
3′-OCH_3	56.5	3.72, s

4.8.8: Scopoletin (LH-8)

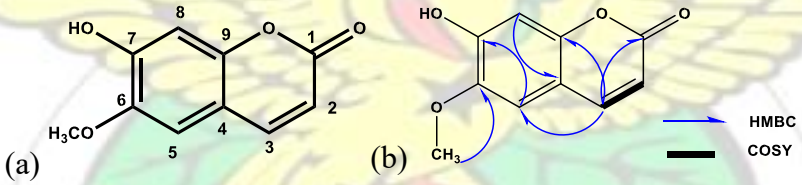

(a) (b)

Fig. 4.61 (a): **LH-8**; (b): HMBC & COSY correlations of **LH-8** **LH-8** was obtained as yellow crystalline needles. The molecular formula was determined to be $C_{10}H_8O_4$ from its positive ion peak at *m/z* 193.04 $[M+H]^+$. The ^1H and ^{13}C NMR data showed signals for a methoxyl (δ_C 57.0, δ_H 3.80, s), two olefinic methines [δ_C 112.7, δ_H 6.09 (d, *J*= 9.1, CH-2) and δ_C 146.3, δ_H 7.74 (d, *J* = 9.1, CH-3)] and two aromatic signals [δ_C 110.1, δ_H 7.00, s (CH-5) and δ_C 104.2, δ_H 6.66, s (CH-8)] (Table 4.37). All mass and NMR spectral data (Table 4.37) corresponded with that for scopoletin (7-hydroxy-6-methoxy coumarin) reported in literature (Valle *et al.*, 1997).

Table 4.37: ^{1}H and ^{13}C NMR data for compound LH-8

Position	$_{13}C$	^{1}H (mult, *J* in Hz)
1	164.3 (C)	-
2	112.7 (CH)	6.09, d (9.1)
3	146.3 (CH)	7.74; d (9.1)
4	112.7 (C)	-
5	110.1 (CH)	7.00, s
6	147.3 (C)	-
7	153.3 (C)	-
8	104.2 (CH)	6.66, s
9	151.7 (C)	-
O-CH_3	57.0	3.8, s

Chemical shifts (ppm) are referenced to solvent (CD_3OD, δ 4.78)

4.8.9 Capstemol (LH-9)

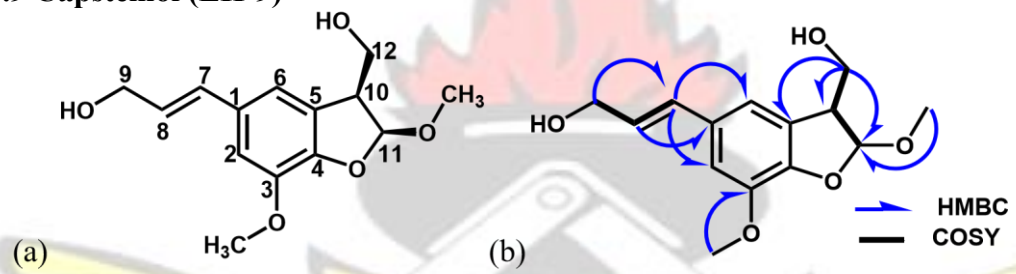

Fig. 4.62 (a): **LH-9**; (b): HMBC & COSY correlations of **LH-9**

LH-9 was isolated as colourless oil with the molecular formula $C_{14}H_{18}O_5$ as deduced from its sodium adduct ion peak at *m/z* 289.10 $[M + Na]^+$ in its HR-ESIMS spectrum.

The ^{1}H NMR spectral data (Table 4.38) showed signals for two methoxyls [δ 3.74, s and 3.39, s], two olefinic [δ 6.41 (dt, *J* = 1.5, 1.5, H-7) and 6.09, (dt, *J* = 5.8, 5.8, H-8)], two oxy-methylenes [δ 4.07, (dd, *J* = 1.5, 6.0, H_2-9) and δ 3.86, (dd, *J* = 7.9, 11.8, H_α12); 3.78, (dd, *J* = 4.3, 6.2, H_β-12)] and two aromatic protons [δ 6.78 (brs, H-2) and δ 6.85 (brs, H-6)] suggesting a tetra substituted benzene ring. A low field oxymethine proton at δ 5.54 (d, *J* = 6.3, H-11) was also observed.

From 2D NMR, ^{1}H-^{1}H COSY correlations were observed between δ 3.86/ 33.78 (H_2-

12) and δ 3.47 (H-10) and between δ 3.47 (H-10) and δ 5.54 (H-11) establishing the substructure, $^{12}CH_2OH$-^{10}CH-^{11}CH. HMBC cross peaks from δ 5.54 (H-11) to δ 147.7 (C-4), δ 130.6 (C-5) and δ 60.7 (C-12) confirmed the presence of a five membered ring. Long range ^1H-^1H COSY and HMBC correlations led to the assignment of the substructure $^9CH_2OH$-^8CH=^7CH (3-propenol) as described for LH2. The 3-propenol was linked to C-1 of the benzene ring based on key HMBC correlations from δ 6.41 (H-7) to δ 133.1 (C-1), δ 112.3 (C-2) and δ 116.2 (C-6). The positions of two methoxyl groups were determined based on HMBC correlations from δ 3.39 to δ 146.0 (C-3) and from δ 3.74 to δ 110.2 (C-11) (Fig. 4.62b). All spectral data of **LH-9** matched those reported for capstemol (Fig. 4.62a) previously isolated from *Capsicum annum var. angulosum*. Capsetmol exhibited inhibitory effects against *Helicobacter pylori* in a previous report (Ochi *et al.*, 2005).

Table 4.38: ^1H and ^{13}C NMR data for compound LH-9

Position	$_{13}C$	^1H (mult, *J* in Hz)
1	133.1 (C)	-
2	112.3 (CH)	6.78, brs
3	146.0 (C)	-
4	147.7 (C)	-
5	130.6 (C)	-
6	116.2 (CH)	6.85, brs
7	132.2 (CH)	6.41, dt (1.5, 1.5)
8	127.9(CH)	6.09, dt (5.8, 5.8)
9	64.0 (CH_2)	4.07, dd (1.5, 6.0)
10	49.9 (CH)	3.47, m
11	110.2 (CH)	5.54, d (6.3)
12	60.7 (CH_2)	3.86, dd (7.9, 11.8); 3.78, dd (4.3, 6.2)
13 (O-CH_3)	57.0	3.74, s
14 (O-CH_3)	56.9	3.39, s

Chemical shifts (ppm) are referenced to solvent (CD_3OD, δ 4.78) **4.8.10:**

Picrasmalignan (LH-10)

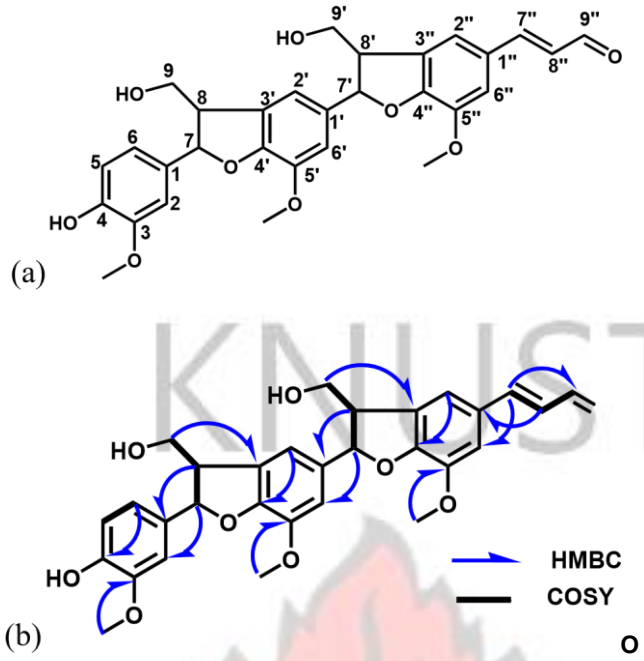

Fig. 4.63 (a): **LH-10**; (b): HMBC & COSY correlations of **LH-10**

LH-10 was isolated as white powder. Its HR-ESIMS displayed a positive molecular ion peak at *m/z* 535.19 $[M + H]^+$ for the molecular formula $C_{30}H_{30}O_9$. Based on detailed 1D and 2D NMR analysis as shown in Table 4.39 and Fig. 4.63b, **LH-10** was identified as the dihydrobenzofuran-type neolignan, picrasmalignan A (Fig. 4.63a), previously isolated from *Picrasma quassioides* Bennet (Jiao *et al.*, 2011) and *Cirsium eriophorum* (Sólyomváry *et al.*, 2015). Picrasmalignan A has been shown to possess potent anti-inflammatory effects (Zhao *et al.*, 2013).

Table 4.39: ^1H and ^{13}C NMR data for compound LH-10

Position	$_{13}C$	^1H (mult, *J*, Hz)	Position	$_{13}C$	^1H (mult, *J*,Hz)
1	133.1 (C)	-	**7′**	88.8 (CH)	5.55, dd (1.5, 6.5)
2	118.3 (CH)	6.71, dt (1.5, 8.2)	**8′**	53.3 (CH)	3.50, m
3	147.7 (C)	-	**9′**	63.2(CH_2)	3.76, m
4	146.2 (C)	-	**1″**	128.3 (C)	-
5	114.8 (CH)	6.66, dd (2.0, 8.2)	**2″**	118.6 (CH)	7.19, brs
6	109.1 (CH)	6.84, o	**3″**	129.8 (C)	-
7	87.9 (CH)	5.43, dd (4.4, 6.2)	**4″**	151.5 (C)	-
8	53.8 (CH)	3.39, dd (6.3, 11.8)	**5″**	144.6 (C)	-
9	63.3 (CH_2)	3.68, m	**6″**	112.8 (CH)	7.14, brs

1′	134.6 (C)	-	**7″**	154.7 (CH)	7.52-7.54, dd (2.0, 15.6)
2′	114.4 (CH)	6.84, o	**8″**	125.8 (CH)	6.59, qd (1.6, 7.8, 15.6)
3′	129.1 (C)	-	**9″**	194.7 (CH)	9.49, dd (1.5, 8.0)
4′	148.1 (C)	-	**3-OCH_3**	55.0	3.71, d (1.6)
5′	144.2 (C)	-	**5′OCH_3**	55.4	3.75, brs
6′	110.4 (CH)	6.83, brs	**5″OCH_3**	55.3	3.82, d (4.10)

Chemical shifts (ppm) are referenced to solvent (CD_3OD, δ 4.78) o- overlapping

4.8.11: Hedyotol C/ Buddlenol E (LH-11)

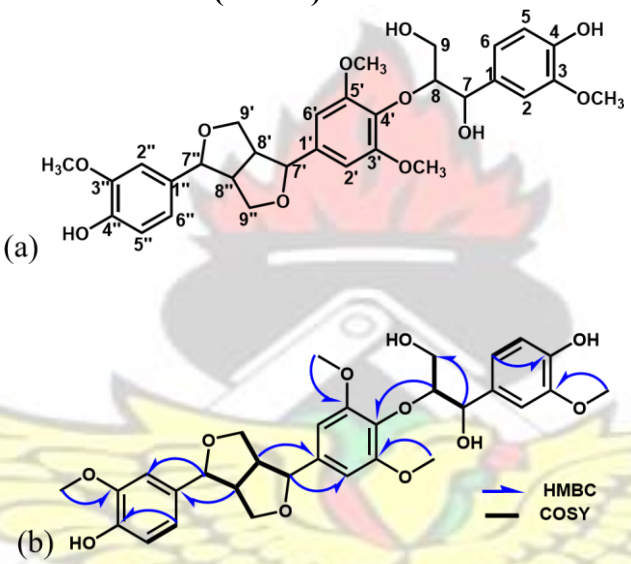

Fig. 4.64 (a): **LH-11**; (b): HMBC & COSY correlations of **LH-11** Compound

LH-11 was isolated as pale yellow gum. Its molecular formula was determined to be $C_{31}H_{36}O_{11}$ as determined from its sodium adduct ion peak at *m/z* 607.21 ($C_{31}H_{36}O_{11}Na$) in the HR-ESIMS analysis. The ^1H NMR spectral data (Table 44) showed characteristic signals for 8 aromatic [resonating between δ 6.64 and δ 6.84] and 4 methoxyl protons [δ 3.71, δ 3.72, δ 3.68, and δ 3.74]. From ^1H and ^{13}C NMR data (Table 4.40), chemical shifts corresponding to pinoresinol (compound **LH-1**, Section 4.11.1) with an additional methoxyl group at C-5′ were identified. The position of the C-5′ methoxyl was assigned by HMBC correlations (Fig. 4.64b). Further, signals corresponding to a guaiacylglycerol moiety (C^1-C^9 on Table 4.40)

were identified from 1D and 2D NMR analysis as described for **LH-2**. Strong HMBC correlation from H-8 of the guaiacylglycerol to C-4′ was observed (Fig. 4.64b). Detailed comparison of the data obtained to reported literature revealed compound **LH-11** as Hedyotol C (Buddlenol E) (Fig. 4.64a) isolated from *Hedyotis lawsoniae* (Satoko *et al.*, 1984) and *Buddleja davidii* (Houghton, 1985).

Table 4.40: ^{1}H and ^{13}C NMR data for compound LH-11

Position	**$_{13}C$**	**^{1}H (mult, *J* in Hz)**	**Position**	**$_{13}C$**	**^{1}H (mult, *J* in Hz)**
1	133.9 (C)	-	**8′**	55.5 (CH)	3.02, m
2	111.5 (CH)	6.84, brs	**9′**	73.1 (CH_2)	4.15, m; 3.77, m
3	148.8 (C)	-	**1″**	133.9 (C)	-
4	147.0 (C)	-	**2″**	111.1 (CH)	6.83, brs
5	115.8 (CH)	6.65, brs	**3″**	149.3 (C)	-
6	120.9 (CH)	6.64, d (8.0)	**4″**	147.5 (C)	-
7	74.2 (CH)	4.77, o	**5″**	116.2 (CH)	6.66, brs
8	87.4 (CH)	4.13, m	**6″**	120.2 (CH)	6.70, dd (2.0, 8.3)
9	61.9 (CH_2)	3.46, m; 3.76, m	**7″**	87.6 (CH)	4.61, d (4.0)
1′	139.1 (C)	-	**8″**	55.9 (CH)	3.02, m
2′	104.3 (CH)	6.56, brs	**9″**	72.9 (CH_2)	4.15, m; 3.77, m
3′	154.7 (C)	-	**3-OCH_3**	56.4	3.71, d (2.3)
4′	136.1 (C)	-	**3′-OCH_3**	56.8	3.72, s
5′	154.7 (C)	-	**5′-OCH_3**	56.8	3.68, d (2.3)
6′	104.3 (CH)	6.56, brs	**3″-OCH_3**	56.5	3.74, s
7′	87.5 (CH)	4.64, m			

Chemical shifts (ppm) are referenced to solvent (CD_3OD, δ 4.78) o- overlapping

4.8.12: *Erythro*- guaiacylglycerol-8-*O*-4'-pinoresinol ether(LH-12)

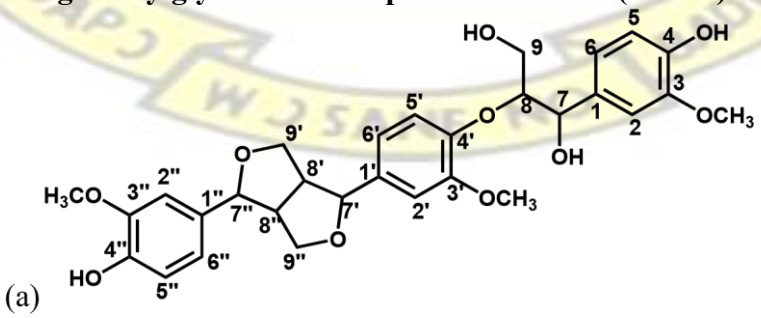

(a)

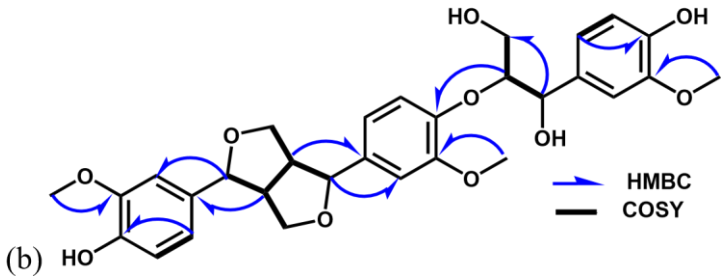

Fig. 4.65 (a): **LH-12**; (b): HMBC & COSY correlations of **LH-12**

The HR-ESIMS spectrum of **LH-12** gave a molecular ion peak at *m/z* 577.20 [M + Na] $^{+}$ for the sodium adduct of the compound and suggested the molecular formula $C_{30}H_{34}O_{11}$. Analysis of 1D and 2D NMR data (Table 4.41) revealed characteristic signals for pinoresinol (**LH-1**, Section 4.11.1) and guaiacylglycerol moiety. The structure of pinoresinol was assigned as described for **LH-1** and that of the guaiacylglycerol was assigned as described for **LH-2**. HMBC correlation from H-8 (δ 4.24) of guaiacylglycerol unit to C-4′ (δ 147.4) of pinoresinol (Fig. 4.65b) confirmed a linkage between the two moieties to give guaiacylglycerol-8-*O*-4′pinoresinol ether (Fig. 4.65a). From ^{1}H NMR spectrum, the coupling constant of H7/8 was determined as 5.3 suggesting an *erythro* form of the compound. This compound has been previously isolated from *Picea abies* (Willför *et al.*, 2004).

Table 4.41: ^{1}H and ^{13}C NMR data for compound LH-12

Position	**$_{13}$C**	**^{1}H (mult, *J* in Hz)**	**Position**	**$_{13}$C**	**^{1}H (mult, *J* in Hz)**
1	133.9 (C)	-	**7′**	87.4 (CH)	4.60, t (4.5)
2	111.8 (CH)	6.87, dd (1.9, 9.0)	**8′**	55.6 (CH)	3.03, m
3	149.0 (C)	-	**9′**	72.9 (CH_2)	3.76, o, 4.12, m
4	147.4 (C)	-	**1″**	134.0 (CH)	-
5	116.0 (CH)	6.57-6.59, dd (5.2, 8.0)	**2″**	111.1 (CH)	6.83, d (1.9)
6	120.9 (CH)	6.70, m	**3″**	149.3 (C)	-
7	74.2 (CH)	4.67, d (5.3)	**4″**	147.5 (C)	-
8	87.4 (CH)	4.24, m	**5″**	116.3 (CH)	6.64, d (8.2)
9	62.1 (CH_2)	3.67, o, 3.73, m	**6″**	120.3 (CH)	6.69, m
1′	137.0 (C)	-	**7″**	87.7 (CH)	4.58, m
2′	111.7 (CH)	6.81, t (1.6)	**8″**	55.7 (CH)	3.03, m

3′	152.0 (C)	-	**9″**	72.8 (CH_2)	3.74, o, 4.15, m
4′	149.0 (C)	-	**3-OCH_3**	56.7	3.66, d (4.5)
5′	119.1 (CH)	6.76-6.77, dd (1.9, 8.2)	**3′-OCH_3**	56.5	3.67, d (3.9)
6′	120.1 (CH)	6.71, m	**3″-OCH_3**	56.6	3.74, s

Chemical shifts (ppm) are referenced to solvent (CD_3OD, δ 4.78) o- overlapping signals

4.8.13: *Threo*-guaiacylglycerol-8-O-4′-pinoresinol ether (LH-13)

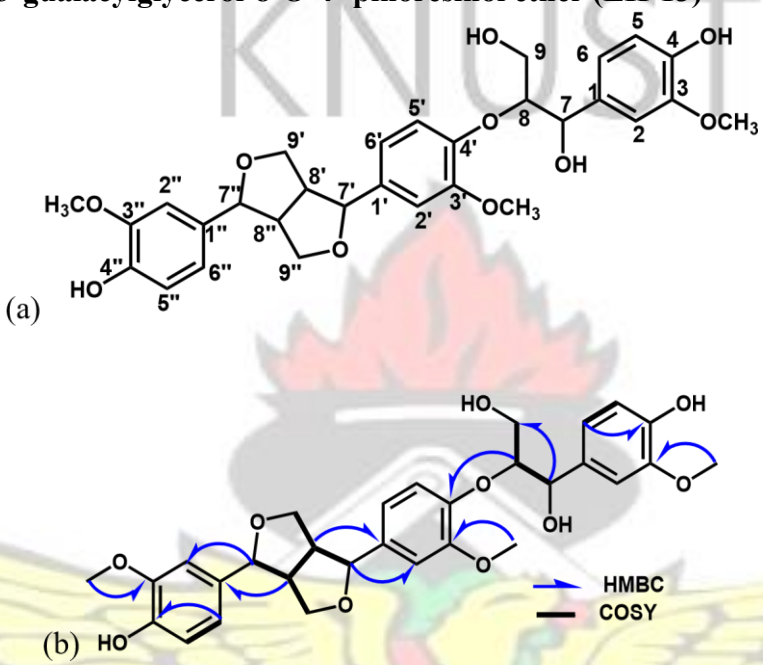

Fig. 4.66 (a): **LH-13**; (b): HMBC & COSY correlations for **LH-13**

The HR-ESIMS spectrum of **LH-13** had the same molecular formula ($C_{30}H_{34}O_{11}$) as **LH-12**. The 1D and 2D NMR spectral data of **LH-13** (Table 4.42) revealed the same pattern and chemical shifts as **LH-12** and thus proposed the same planar structure. From ^{1}H NMR spectrum however, the coupling constant of H-7/8 ($J_{7/8}$) was determined to be 6.3 suggesting a *threo* form of the same compound.

Table 4.42: ^{1}H and ^{13}C NMR data for compound LH-13

Position	$_{13}$C	^{1}H (mult, *J* in Hz)	Position	$_{13}$C	^{1}H (mult, *J* in Hz)
1	133.8 (C)	-	**7′**	87.3 (CH)	4.62, d (3.0)
2	111.8 (CH)	6.89, brs	**8′**	55.5 (CH)	3.02, m
3	148.8 (C)	-	**9′**	72.8 (CH_2)	3.73, m; 4.12, m
4	147.2 (C)	-	**1″**	133.9 (C)	-
5	115.9 (CH)	6.61, m	**2″**	111.1 (CH)	6.83, brs

6	120.8 (CH)	6.72, d (8.1)	**3″**	149.2 (C)	-
7	74.1 (CH)	4.75, d (6.3)	**4″**	147.4 (C)	-
8	87.4 (CH)	4.17, dd (5.1, 10.2)	**5″**	116.2 (CH)	6.64, d (8.2)
9	62.0 (CH_2)	3.35, m; 3.61, dd (3.9, 11.6)	**6″**	120.1 (CH)	6.69, dd (1.5, 8.5)
1′	137.0 (C)	-	**7″**	87.7 (CH)	4.58, d (4.0)
2′	111.6 (CH)	6.89, brs	**8″**	55.7 (CH)	3.02, m
3′	152.0 (C)	-	**9″**	72.9 (CH_2)	3.73, m; 4.12, m
4′	149.2 (C)	-	**3-OCH_3**	56.4	3.69, s
5′	119.0 (CH)	6.90, brs	**3′-OCH_3**	56.7	3.75, s
6′	119.9 (CH)	6.75, m	**3″-OCH_3**	56.5	3.74, s

Chemical shifts (ppm) are referenced to solvent (CD_3OD, δ 4.78)

4.8.14: 2,9-dihydroxy-1(10)-aromadendren-14-oic acid 2, 14-lactone (LH-14)

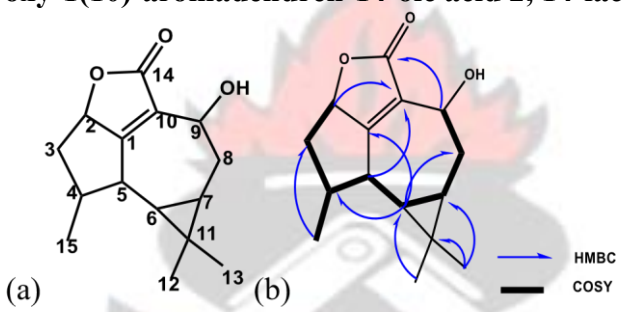

Fig. 4.67 (a): **LH-14**; (b) HMBC & COSY correlations for **LH-14**

LH-14 was isolated as colourless oil. Its HR-ESIMS data showed a pseudo molecular ion peak at *m/z* 271.13 $[M + Na]^+$ for its sodium adduct ion and suggested the molecular formula $C_{15}H_{20}O_3$. From the ^1H NMR data (Table 4.43), signals for two tertiary methyls (δ 1.05 and 0.98, s, CH_3-12/13), a doublet at 1.03 (J =7.0) for the secondary methyl (CH_3-15) and two oxymethine protons [δ 4.92, (dd, J = 6.5, 11.1, H-2) and δ 4.28 (brd, J = 11.0, H-9)] were observed. The ^{13}C NMR data (Table 4.43) gave signals for all 15 carbons. All proton and carbon resonances as well as HMBC and COSY NMR analysis (Fig. 4.67b) for **LH-14** corresponded with those reported for 2,9-dihydroxy-1(10)-aromadendren-14-oic acid-2,14-lactone (Fig. 4.67a), previously isolated from *Landolphia dulcis* (Stærk *et al.*, 2004).

Table 4.43: ^1H and ^{13}C NMR data for compound LH-14

Position	$_{13}C$	^{1}H (mult, *J* in Hz)
1	177.1 (C)	-
2	84.7 (CH)	4.92, dd (6.5, 11.1)
3	38.1 (CH_2)	2.17, m 1.09, m
4	38.4 (CH)	2.57, m
5	37.6 (CH)	2.73, t (8.7)
6	29.9 (CH)	0.68, t (9.0)
7	24.6 (CH)	0.44, m
8	32.4 (CH_2)	2.09, dt (3.89, 3.89); 1.33, dd (12.4, 12.8)
9	66.3 (CH)	4.28 brd (11.0)
10	128.3 (C)	-
11	22.6 (C)	-
12	28.7 (CH_3)	0.98, s
13	16.1 (CH_3)	1.05, s
14	181.6 (C)	-
15	15.2 (CH_3)	1.03, d (7.0)

Chemical shifts (ppm) are referenced to solvent (CD_3OD, δ 4.78)

4.9 Discussion

In the current study, the antimicrobial activity of the crude fractions and isolated compounds from *L. heudelotti* roots was investigated. The total phenolic content of the crude extract as well as the free radical scavenging effect was also determined.

From the results obtained, the root extracts exhibited considerable antimicrobial activity at a concentration range between 312-1250 µg/mL (Table 4.48). The highest activity was exhibited by the MeOH fraction against *B. subtilis* and *S. pyogens*. The crude MeOH extract showed a concentration dependent DPPH radical scavenging effect (Fig. 4.50a) with an IC_{50} of 6.956 ± 0.81 µg/mL. The extract was found to have a total phenolic content of 98.14 mg TAE per gram of dried plant extract.

In the genus *Landolphia,* the species *Landolphia owariensis* has been extensively studied for biological activity. With regards to antimicrobial activity, the leaf and root extracts of *L. owariensis* were reported to inhibit growth of *Staphylococcus aureus*, *E. coli* and *Proteus mirabilis* with an MIC range from 20 to 2000 µg/mL (Nwaogu *et al.*,

2007). In another study, the root extract of *L. owariensis* exhibited significant DPPH, hydroxyl and superoxide radical scavenging as well as inhibition of lipid peroxidation (Awah *et al.*, 2012). These bioactivities were attributed to the presence of phenolic compounds and alkaloids identified in preliminary phytochemical screening of the root extract (Okonkwo *et al.*, 2016).

Phytochemical investigations to identify the specific bioactive constituent present in the roots of *L. heudelotti* led to the isolation and characterization of 14 known compounds including lignans, neolignans, sesquilignans, an aromadendrane and a coumarin. These compounds are being reported for the first time from *L. heudelotti* and from the genus *Landolphia* to the best of my knowledge. The isolated compounds exhibited antimicrobial activity against selected Gram positive and Gram negative bacteria at a concentration range from 12.5-100 µg/mL (Table 4.29). The soil bacteria *Acinetobacter spp*. was the most susceptible to all tested compounds at a fairly low concentration range (12.5-25 µg/mL).The compounds also showed DPPH free radical scavenging activity. The highest activity was exhibited by **LH-1** which scavenged 40 % of DPPH free radicals at 0.01 mg/mL.

The identification of bioactive lignans and neolignans in the root extracts of *L. heudelotti* gives evidence that the observed activity may be due to the presence of these compounds. Plant lignans and similar analogues are reported to possess a variety of biological effects including anti-inflammatory, antimicrobial and antioxidant effects (Teponno *et al.*, 2016).

Among the isolated lignans, pinoresinol (**LH-1**) and picrasmalignan A (**LH-10**) have been previously shown to exhibit potent anti-inflammatory activity. In a study by During *et al*. in 2012, pinoresinol significantly reduced the pro-inflammatory mediator, interleukin 6 (IL6) in IL-1β stimulated cells by 65 %. Further, this compound

decreased COX-2 derived PGE_2 levels in stimulated cells by 62 % (During *et al.*, 2012). Picrasmalignan A (**LH-10**) also suppressed LPS-induced NO production and pro-inflammatory mediators such as TNF-α and IL6 in a dose dependent manner. COX-2 expression was also inhibited by 50 % in the presence of 5 μM of picrasmalignan A (Zhao *et al.*, 2013). These results suggest that pinoresinol and picrasmalignan A have a high potential as lead compounds for anti-inflammatory drug development. The threo and erythro guaiacylglycerol-8-*O*-4'-coniferyl alcohol ether isomers (**LH-4** and **LH-5**) have also been listed as phytochemicals with significant nitric oxide inhibitory effects (Woo *et al.*, 2016). All together, the results of biological activity screening and phytochemical investigation of *L. heudelotti* root extract give scientific justification to the use of this plant in traditional medicine.

CHAPTER 5

CONCLUSION AND RECOMMENDATIONS

5.1 Conclusion

Herbal medicines play an important role in the health care for a majority of the population of developing countries. Therefore analysing herbal medicines on scientific basis gives the opportunity to develop locally used plant medicines into the primary health care systems of a nation.

The present study has demonstrated that the extracts of the stem barks of *A. klaineana* and *H. monopetalus* and the roots of *L. heudelotti* possess considerable antimicrobial, antioxidant and anti-inflammatory properties, thereby justifying the use of these plants in traditional medicine. The antioxidant activity observed for all plants may account

for the wide range of ethno-medicinal uses claimed for the plants since oxidative stress is the underlying cause of most non-communicable diseases (chronic diseases).

Phytochemical studies led to the isolation and characterization of twelve compounds from *A. klaineana*, nine compounds from *H. monopetalus* and fourteen compounds from *L. heudelotti*, thereby highlighting the potential of medicinal plants as important sources of bioactive compounds.

Six limonoids, five tirucallane triterpenes and one protolimonoid were isolated from the EtOAc fraction of *A. klaineana*. Methyl angolensate (**AK1**) and 3,23-dioxo tirucalla-7,24-diene-21-oic acid (**AK6**) showed significant competitive inhibitory effects of PGE_2 indicating their plausible anti-inflammatory effect. All compounds also demonstrated significant antioxidant activity. This was the first report on the investigation of biological activity and phytochemical constituents from *A. klaineana* (Mireku *et al.*, 2014; Mireku *et al.*, 2015).

Nine prenylated indole alkaloids including seven novel compounds were isolated from the EtOAc fraction of *H. monopetalus* stem bark. The compounds showed no antimicrobial activity against selected pathogenic microorganisms at 10 µg/mL though the crude extract showed some activity. This observation supports the view that segregation of plants constituents into individual compounds may result in a loss of activity as the overall effect may be by synergy among constituents. The prenylated indole alkaloids are also recognized as important chemotaxonomic markers for the genus *Hexalobus* and closely related genera (Mireku *et al.*, 2016).

Fourteen known compounds including neolignans, lignans, aromadendranes and coumarins were isolated from the MeOH root extract of *L. heudelotti*. The compounds showed remarkable antimicrobial as well as DPPH radical scavenging effects. This

was the first investigation of biological activity and phytochemical constituents from *L. heudelotti*. The compounds isolated are being reported for the first time in the genus *Landolphia*.

The results of this study have given considerable evidence that plant extracts and purified phytochemicals have potential of being developed into agents that can be used in alternative medicine.

5.2 Recommendations

Further studies regarding the efficacy, safety and quantification of major active ingredients of the crude extracts will be important in order to develop the crude extracts into standardized dosage forms for clinical use in future.

It may be interesting to also establish in future studies, whether the crude extracts offer better therapeutic benefits, either alone or in combination with conventional therapies. With regards to the potential of the isolated compounds as leads for drug development, further biological assays and structure activity relationship studies are recommended. It is therefore necessary to undertake research focusing on the synthesis of bioactive plant constituents to enable the production of compounds in large quantities for further experiments.

Finally, it is important to note that several useful medicinal plants face extinction due to their widespread use and the extensive destruction of plant-rich habitats. A conservation action plan to cultivate highly patronized and endangered medicinal plant species in medicinal gardens will therefore be necessary to preserve important medicinal plants. It is recommended that other plant parts of *L. heudelotti* be investigated in future studies since the use of the roots is not sustainable.

REFERENCES

Abbiw, D. K. (1990). *Useful plants of Ghana: West African uses of wild and cultivated plants*. edn. Intermediate Technology Publications and The Royal Botanic Gardens.

Abdelgaleil, S. and Nakatani, M. (2003). Antifeeding activity of limonoids from *Khaya senegalensis* (Meliaceae). *Journal of applied entomology* **127**(4)**:** 236-239.

Abotsi, W. K. M., Ainooson, G. K. and Woode, E. (2012). Anti-inflammatory and antioxidant effects of an ethanolic extract of the aerial parts of *Hilleria latifolia* (Lam.) H. Walt.(Phytolaccaceae). *African Journal of Traditional, Complementary and Alternative Medicines* **9**(1)**:** 138-152.

Achenbach, H. (1986). Investigations on West African medicinal plants. *Pure and Applied Chemistry* **58**(5)**:** 653-662.

Achenbach, H. and Löwel, M. (1995). Constituents of *Isolona maitlandii*. *Phytochemistry* **40**(3)**:** 967-973.

Achenbach, H. and Raffelsberger, B. (1979). 3, 6-Bis (γ, γ-dimethylallyl)-indole from *Uvaria elliotiana*. *Tetrahedron Letters* **20**(28)**:** 2571-2574.

Achenbach, H., Renner, C. and Waibel, R. (1995). Constituents of tropical medicinal plants, LXIX. The hexalobines, diprenylated indoles from *Hexalobus crispiflorus* and *Hexalobus monopetalus*. *Liebigs Annalen* **1995**(7)**:** 1327-1337.

Agbovie, T., Amponsah, K., Crentsil, O., Dennis, F., Odamtten, G. and OfusoheneDjan, W. (2002). Conservation and sustainable use of medicinal plants in Ghana:
ethnobotanical survey. *Cambridge UK: UNEP-WCMC*.

Ahovuo‐Saloranta, A., Rautakorpi, U. M., Borisenko, O. V., Liira, H., Williams Jr, J. W. and Mäkelä, M. (2014). Antibiotics for acute maxillary sinusitis in adults. *The Cochrane Library*.

Akah, P. A. and Nwambie, A. I. (1994). Evaluation of Nigerian traditional medicines: 1. Plants used for rheumatic (inflammatory) disorders. *Journal of Ethnopharmacology* **42**(3)**:** 179-182.

Akihisa, T., Kimura, Y., Kokke, C. M. C. W., Takase, S. I., Yasukawa, K. and Tamura, T. (1996). Tirucalla-5, 24-dien-3β-ol [(13α, 14β, 17α, 20 S)-lanosta-5, 24dien-3β-ol] and three other Δ 5-unsaturated tirucallanes from the roots of *Bryonia dioica* Jacq.: the first naturally occurring C-10 methylated tetracyclic triterpene alcohols with a Δ 5-monounsaturated skeleton. *Journal of the Chemical Society, Perkin Transactions 1*(19)**:** 2379-2384.

Arbonnier, M. (2000). *Arbres, arbustes et lianes des zones sèches d'Afrique de l'Ouest Trees, shrubs and lianas of West Africa dry zones, Mali, Ouagadougou: Centre de Coopération Internationale en Recherche Agronomique pour le développement/Muséum national d'histoire naturelle/Union mondiale pour la nature*. CIRAD/MNHN/UICN.

Arnold, H.-J. and Gulumian, M. (1984). Pharmacopoeia of traditional medicine in Venda. *Journal of Ethnopharmacology* **12**(1)**:** 35-74.

Asase, A., Hesse, D. N. and Simmonds, M. S. (2012). Uses of multiple plants prescriptions for treatment of malaria by some communities in southern Ghana. *Journal of ethnopharmacology* **144**(2)**:** 448-452.

Atawodi, S. and Alafiatayo, A. (2007). Assessment of the phytochemical and antitrypanosomal properties of some extracts of leaves, stem and root bark of *Landolphia sp*., P. Beauv. *Journal of ethnopharmacology* **114**(2)**:** 207-211.

Awah, F. M., Uzoegwu, P. N., Ifeonu, P., Oyugi, J. O., Rutherford, J., Yao, X., Fehrmann, F., Fowke, K. R. and Eze, M. O. (2012). Free radical scavenging activity, phenolic contents and cytotoxicity of selected Nigerian medicinal plants. *Food Chemistry* **131**(4)**:** 1279-1286.

Balunas, M. J. and Kinghorn, A. D. (2005). Drug discovery from medicinal plants. *Life sciences* **78**(5)**:** 431-441.

Blokhina, O., Virolainen, E. and Fagerstedt, K. V. (2003). Antioxidants, oxidative damage and oxygen deprivation stress: a review. *Annals of botany* **91**(2)**:** 179-194.

Botermans, M., Sosef, M. S., Chatrou, L. W. and Couvreur, T. L. (2011). Revision of the African genus *Hexalobus* (Annonaceae). *Systematic Botany* **36**(1)**:** 33-48.

Bouquet, A. and Debray, M. (1974). Plantes médicinales de la Côte d'Ivoire. In: *Travaus et document de l'O.S.T.O.R.M* Vol. 32, pp 18-19. Paris.

Burkill, H. (1985). Entry for *Hexalobus monopetalus* (A. Rich) Engl. & Diels [Family Annonaceae]. The useful plants of West Tropical Africa. Edition 2. Vol. 1: families A-D. *Royal Botanical Gardens, Kew*.

Burkill, H. (1997). Entry for *Anopyxis klaineana* (Pierre) Engl. [family Rhizophoraceae]. The useful plants of West Tropical Africa. Volume 4, Families MR. *Royal Botanic Gardens, Kew, Richmond, United Kingdom*.

Chanda, S. and Dave, R. (2009). In vitro models for antioxidant activity evaluation and some medicinal plants possessing antioxidant properties: An overview. *African Journal of Microbiology Research* **3**(13)**:** 981-996.

Chi, Y. S., Jong, H. G., Son, K. H., Chang, H. W., Kang, S. S. and Kim, H. P. (2001). Effects of naturally occurring prenylated flavonoids on enzymes metabolizing arachidonic acid: Lipoxygenases and cyclooxygenases *Biochem Pharm* **62:** 1185-1191.

Chin, Y.-W., Balunas, M. J., Chai, H. B. and Kinghorn, A. D. (2006). Drug discovery from natural sources. *The AAPS Journal* **8**(2)**:** E239-E253.

Cho, J. Y., Kim, A. R. and Park, M. H. (2001). Lignans from the rhizomes of *Coptis japonica* differentially act as anti-inflammatory principles. *Planta medica* **67**(4)**:** 312-316.

Cipollone, F., Cicolini, G. and Bucci, M. (2008). Cyclooxygenase and prostaglandin synthases in atherosclerosis: recent insights and future perspectives. *Pharmacology & therapeutics* **118**(2)**:** 161-180.

Clark, J., Baldwin, R., Bayne, K., Brown, M., Gebhart, G., Gonder, J., Gwathmey, J., Keeling, M., Kohn, D. and Robb, J. (1996). Guide for the care and use of laboratory animals. *Washington, DC: Institute of Laboratory Animal Resources, National Research Council* **125**.

Couvreur, T., Richardson, J., Sosef, M., Erkens, R. and Chatrou, L. (2008). Evolution of syncarpy and other morphological characters in African Annonaceae: a posterior mapping approach. *Molecular Phylogenetics and Evolution* **47**(1)**:** 302-318.

Cowan, M. M. (1999). Plant products as antimicrobial agents. *Clinical microbiology reviews* **12**(4)**:** 564-582.

Cragg, G. M. and Newman, D. J. (2013). Natural products: a continuing source of novel drug leads. *Biochimica et Biophysica Acta (BBA)-General Subjects* **1830**(6)**:**

3670-3695.

Cragg, G. M., Newman, D. J. and Snader, K. M. (1997). Natural products in drug discovery and development. *Journal of Natural Products* **60**(1)**:** 52-60.

D'costa, V. M., King, C. E., Kalan, L., Morar, M., Sung, W. W., Schwarz, C., Froese, D., Zazula, G., Calmels, F. and Debruyne, R. (2011). Antibiotic resistance is ancient. *Nature* **477**(7365)**:** 457-461.

Da Silva, V. P., Oliveira, R. R. and Figueiredo, M. R. (2009). Isolation of Limonoids from seeds of *Carapa guianensis* Aublet (Meliaceae) by highspeed countercurrent chromatography. *Phytochemical Analysis* **20**(1)**:** 77-81.

Das, K., Tiwari, R. and Shrivastava, D. (2010). Techniques for evaluation of medicinal plant products as antimicrobial agent: Current methods and future trends. *Journal of medicinal plants research* **4**(2)**:** 104-111.

Dreyer, D. (1967). Chemotaxonomy of the Rutaceae—II: Extractives of *Severinia buxifolia* (Poir.) Ten. *Tetrahedron* **23**(12)**:** 4613-4622.

Ducancel, F., Mérienne, K., Fromen-Romano, C., Trémeau, O., Pillet, L., Drevet, P., Zinn-Justin, S., Boulain, J.-C. and Ménez, A. (1996). Mimicry between Receptors and Antibodies- Identification of snake toxin determinants recognized by the acetylcholine receptor and an acetylcholine receptor-mimicking monoclonal antibody. *Journal of Biological Chemistry* **271**(49)**:** 31345-31353.

During, A., Debouche, C., Raas, T. and Larondelle, Y. (2012). Among plant lignans, pinoresinol has the strongest antiinflammatory properties in human intestinal Caco-2 cells. *The Journal of nutrition* **142**(10)**:** 1798-1805.

Eldridge, G. R., Vervoort, H. C., Lee, C. M., Cremin, P. A., Williams, C. T., Hart, S. M., Goering, M. G., O'neil-Johnso, M. and Zeng, L. (2002). High-throughput method for the production and analysis of large natural product libraries for drug discovery. *Analytical chemistry* **74**(16)**:** 3963-3971.

Eleni, P. and Dimitra, H. L. (2003). Review in quantitative structure activity relationships on lipoxygenase. *Mini-Reviews in Medicinal Chemistry* **3:** 487-499.

Eloff, J. (1998). A sensitive and quick microplate method to determine the minimal inhibitory concentration of plant extracts for bacteria. *Planta medica* **64**(08)**:** 711713.

Emery, P. (2006). Treatment of rheumatoid arthritis. *BMJ: British Medical Journal* **332**(7534)**:** 152.

Estévez-Braun, A., Estevez-Reyes, R., González-Pérez, J. A. and Gonzalez, A. (1995). Busaliol and busalicifol, two new tetrahydrofuran lignans from *Bupleurum salicifolium*. *Journal of Natural Products* **58**(6)**:** 887-892.

Evans, W. C. (2002). *Trease and Evans Pharmacognosy,15th edition*. edn: W.B. Sanders, London.

Fabricant, D. S. and Farnsworth, N. R. (2001). The value of plants used in traditional medicine for drug discovery. *Environmental health perspectives* **109**(Suppl 1)**:** 69.

Fereidoni, M., Ahmadiani, A. and Samnanian, S. (2000). An accurate and simple method for measurement of paw oedema. *Journal of Pharmacology and Toxicological Methods* **43:** 11-14.

Frolov, A., Yang, L., Dong, H., Hammock, B. D. and Crofford, L. J. (2013). Antiinflammatory properties of prostaglandin E2: deletion of microsomal prostaglandin E synthase-1 exacerbates non-immune inflammatory arthritis in mice. *Prostaglandins, Leukotrienes and Essential Fatty Acids (PLEFA)* **89**(5)**:** 351-358.

Fürst, R. and Zündorf, I. (2014). Plant-derived anti-inflammatory compounds: hopes and disappointments regarding the translation of preclinical knowledge into clinical progress. *Mediators of inflammation* **2014**.

Gibbons, S. (2004). Anti-staphylococcal plant natural products. *Natural product reports* **21**(2)**:** 263-277.

Gibbons, S. (2005). Plants as a source of bacterial resistance modulators and antiinfective agents. *Phytochemistry Reviews* **4**(1)**:** 63-78.

Gill, R., Tsung, A. and Billiar, T. (2010). Linking oxidative stress to inflammation: Toll-like receptors. *Free Radical Biology and Medicine* **48**(9)**:** 1121-1132.

González-Lamothe, R., Mitchell, G., Gattuso, M., Diarra, M. S., Malouin, F. and Bouarab, K. (2009). Plant antimicrobial agents and their effects on plant and human pathogens. *International Journal of Molecular Sciences* **10**(8)**:** 3400-3419.

Gotzsche, P. C. (2000). Non-steroidal anti-inflammatory drugs. *British Medical Journal* **320**(7241)**:** 1058.

Grundon, M. F., Hamblin, M. R., Harrison, D. M., Logue, J. D., Maguire, M. and Mcgrath, J. A. (1980). Biosynthesis of aromatic isoprenoids. Part 5. The preparation of 1-(3, 3-dimethylallyl)-L-tryptophan and cyclo-L-aianyl-1-(3, 3-dimethylallyl)-Ltryptophan and their non-incorporation into echinulin. *Journal of the Chemical Society, Perkin Transactions 1***:** 1294-1298.

Guo, C., Wang, J.-S., Zhang, Y., Yang, L., Wang, P.-R. and Kong, L.-Y. (2012). Relationship of chemical structure to in vitro anti-inflammatory activity of tirucallane triterpenoids from the stem barks of *Aphanamixis grandifolia*. *Chemical and Pharmaceutical Bulletin* **60**(8)**:** 1003-1010.

Gurib-Fakim, A. (2006). Medicinal plants: traditions of yesterday and drugs of tomorrow. *Molecular aspects of Medicine* **27**(1)**:** 1-93.

Hammer, K. A., Carson, C. and Riley, T. (1999). Antimicrobial activity of essential oils and other plant extracts. *Journal of applied microbiology* **86**(6)**:** 985-990.

Han, H.-Y., Wang, X.-H., Wang, N.-L., Ling, M.-T., Wong, Y.-C. and Yao, X.-S. (2008). Lignans isolated from *Campylotropis hirtella* (Franch.) Schindl. decreased prostate specific antigen and androgen receptor expression in LNCaP cells. *Journal of agricultural and food chemistry* **56**(16)**:** 6928-6935.

Han, M.-L., Shen, Y., Wang, G.-C., Leng, Y., Zhang, H. and Yue, J.-M. (2013). 11βHSD1 Inhibitors from *Walsura cochinchinensis*. *Journal of Natural Products* **76**(7)**:** 1319-1327.

Happi, G. M., Kouam, S. F., Talontsi, F. M., Lamsh Ft, M., Z Hlke, S., Bauer, J. O., Strohmann, C. and Spiteller, M. (2015). Antiplasmodial and Cytotoxic Triterpenoids from the Bark of the Cameroonian Medicinal Plant *Entandrophragma congo nse*. *Journal of natural products* **78:** 604-614.

Hariram Nile, S. and Won Park, S. (2013). Optimized methods for in vitro and in vivo anti-inflammatory assays and its applications in herbal and synthetic drug analysis. *Mini reviews in medicinal chemistry* **13**(1)**:** 95-100.

Hensley, K., Robinson, K. A., Gabbita, S. P., Salsman, S. and Floyd, R. A. (2000). Reactive oxygen species, cell signaling, and cell injury. *Free Radical Biology and Medicine* **28**(10)**:** 1456-1462.

Hevesi, B., Houghton, P., Habtemariam, S. and Kéry, Á. (2009). Antioxidant and antiinflammatory effect of *Epilobium parviflorum* Schreb. *Phytotherapy Research* **23**(5)**:** 719-724.

Hold, G., El-Omar, Me. (2008). Genetic aspects of inflammation and cancer. *Biochem Journal* **1, 410(2):** 225-235.

Hostettmann, K. (1998). Strategy for the biological and chemical evaluation of plant extracts. *Pure and Applied Chemistry* **70**(11)**:** 23-27.

Hostettmann, K. and Marston, A. (2002). Twenty years of research into medicinal plants: results and perspectives. *Phytochemistry Reviews* **1**(3)**:** 275-285.

Houghton, P. J. (1985). Lignans and neolignans from *Buddleja davidii*. *Phytochemistry* **24**(4)**:** 819-826.

Hoye, T. R., Jeffrey, C. S. and Shao, F. (2007). Mosher ester analysis for the determination of absolute configuration of stereogenic (chiral) carbinol carbons. *Nature Protocols* **2**(10)**:** 2451-2458.

Hu, J., Song, Y., Li, H., Yang, B., Mao, X., Zhao, Y. and Shi, X. (2014). Cytotoxic and anti–inflammatory tirucallane triterpenoids from *Dysoxylum binectariferum*. *Fitoterapia* **99:** 86-91.

Huang, X.-X., Zhou, C.-C., Li, L.-Z., Li, F.-F., Lou, L.-L., Li, D.-M., Ikejima, T., Peng, Y. and Song, S.-J. (2013). The cytotoxicity of 8-O-4′ neolignans from the seeds of *Crataegus pinnatifida*. *Bioorganic & medicinal chemistry letters* **23**(20)**:** 5599-5604.

Ikeda, Y., Murakami, A. and Ohigashi, H. (2008). Ursolic acid: An anti-and proinflammatory triterpenoid. *Molecular nutrition & food research* **52**(1)**:** 26-42.

Ilodigwe, E., Igbokwe, E., Ajaghaku, D. and Ihekwereme, C. (2013). Aphrodisiac activity of ethanol root extract and fractions of *Landolphia dulcis* (Sabine) Pichon. *International Journal of Pharmaceutical Sciences and Research* **4**(2)**:** 813.

Itokawa, H., Morris-Natschke, S. L., Akiyama, T. and Lee, K.-H. (2008). Plantderived natural product research aimed at new drug discovery. *Journal of natural medicines* **62**(3)**:** 263-280.

Ivanov, A. I. and Romanovsky, A. A. (2004). Prostaglandin E2 as a mediator of fever: synthesis and catabolism. *Front Biosci* **9**(1-3)**:** 1977-1983.

Iwu, M. M. and Wootton, J. (2002). *Ethnomedicine and drug discovery*. edn, vol. 1. Elsevier Science BV: Netherlands.

Jabbour, H., Kelly, R. and Boddy, S. (2002). Autocrine/paracrine regulation of apoptosis in epithelial cells by prostaglandin E 2. *Prostaglandins, leukotrienes and essential fatty acids* **67**(5)**:** 357-363.

Jiao, W. H., Gao, H., Zhao, F., He, F., Zhou, G. X. and Yao, X. S. (2011). A New Neolignan and a New Sesterterpenoid from the Stems of *Picrasma quassioides* Bennet. *Chemistry & biodiversity* **8**(6)**:** 1163-1169.

Jung, H. W., Mahesh, R., Lee, J. G., Lee, S. H., Kim, Y. S. and Park, Y.-K. (2010). Pinoresinol from the fruits of *Forsythia koreana* inhibits inflammatory responses in LPS-activated microglia. *Neuroscience letters* **480**(3)**:** 215-220.

Kayode, J. and Kayode, G. (2008). Ethnomedicinal survey of botanicals used in treating sexually transmitted diseases in Ekiti State, Nigeria. *Ethnobotanical leaflets* **2008**(1)**:** 7.

Kerharo, J. and Adam, J. G. (1964). Plantes medicinales et toxiques des Peul et des Toucouleur du Senegal. *J. Agr. trop. Bot. appl* **11:** 384-444.

Khansari, N., Shakiba, Y. and Mahmoudi, M. (2009). Chronic inflammation and oxidative stress as a major cause of age-related diseases and cancer. *Recent patents on inflammation & allergy drug discovery* **3**(1)**:** 73-80.

Kim, H. P., Son, K. H., Chang, H. W. and Kang, S. S. (2004). Anti-inflammatory plant flavonoids and cellular action mechanisms. *Journal of pharmacological sciences* **96**(3)**:** 229-245.

Kinnula, V. L. and Crapo, J. D. (2004). Superoxide dismutases in malignant cells and human tumors. *Free Radical Biology and Medicine* **36**(6)**:** 718-744.

Kinoshita, T., Tatara, S., Ho, F.-C. and Sankawa, U. (1989). 3-Prenylindoles from *Murraya paniculata* and their biogenetic significance. *Phytochemistry* **28**(1)**:** 147151.

Koike, Y. O. K. and Ohmoto, T. (1994). Indole alkaloids from *Brucea mollis var. tonkinensis*. *Phytochemistry* **37**(2)**:** 575-578.

Langfield, R. D., Scarano, F. J., Heitzman, M. E., Kondo, M., Hammond, G. B. and Neto, C. C. (2004). Use of a modified microplate bioassay method to investigate

antibacterial activity in the Peruvian medicinal plant, *Peperomia galioides*. *Journal of ethnopharmacology* **94**(2)**:** 279-281.

Leclercq, P. A., Ayedoun, M. A., Sossou, P. V. and Houngnon, P. (1997). Essential oil of *Hexalobus monopetalus* (A. Rich) Engl. leaves from Benin: a new source of citral. *Journal of Essential Oil Research* **9**(1)**:** 97-99.

Li, B. Q., Fu, T., Gong, W.-H., Dunlop, N., Kung, H.-F., Yan, Y., Kang, J. and Wang, J. M. (2000). The flavonoid baicalin exhibits anti-inflammatory activity by binding to chemokines. *Immunopharmacology* **49**(3)**:** 295-306.

Li, G., Kusari, S., Lamsh Ft, M., Sch Ffler, A., Laatsch, H. and Spiteller, M. (2014). Antibacterial Secondary Metabolites from an Endophytic Fungus, *Eupenicillium sp*. LG41. *Journal of natural products* **77**(11)**:** 2335-2341.

Li, S.-M. (2010). Prenylated indole derivatives from fungi: structure diversity, biological activities, biosynthesis and chemoenzymatic synthesis. *Natural product reports* **27**(1)**:** 57-78.

Lin, B.-D., Yuan, T., Zhang, C.-R., Dong, L., Zhang, B., Wu, Y. and Yue, J.-M. (2009). Structurally diverse limonoids from the fruits of *Swietenia mahagoni*. *Journal of natural products* **72**(12)**:** 2084-2090.

Lin, C.-C. and Shieh, D.-E. (1996). The anti-inflammatory activity of *Scutellaria rivularis* extracts and its active components, baicalin, baicalein and wogonin. *The American journal of Chinese medicine* **24**(01)**:** 31-36.

Liu, Y. and Abreu, P. (2006). Tirucallane triterpenes from the roots of *Ozoroa insignis*. *Phytochemistry* **67**(13)**:** 1309-1315.

Lopchuk, J. M., Gribble, G. W. and Jasinski, J. P. (2013). Bruceolline D: 3, 3dimethyl-1H, 4H-cyclopenta [b] indol-2 (3H)-one. *Acta Crystallographica Section E: Structure Reports Online* **69**(7)**:** 1043-1043.

Lowy, F. D. (2003). Antimicrobial resistance: the example of *Staphylococcus aureus*. *The Journal of clinical investigation* **111**(9)**:** 1265-1273.

Mahdi, J. G. (2010). Medicinal potential of willow: A chemical perspective of aspirin discovery. *Journal of Saudi Chemical Society* **14**(3)**:** 317-322.

Makangara, J. J., Henry, L., Jonker, S. A. and Nkunya, M. H. (2004). The caulindoles: dimeric prenylindoles from *Isolona cauliflora*. *Phytochemistry* **65**(2)**:** 227-232.

Malebo, H. M., Jonker, S. A., Waibel, R. and Nkunya, M. H. H. (2014). "Diprenylated Indole Alkaloids from Fruits of *Hexalobus monopetalus*.". *Natural Products ans Bioprospecting* **4**(2)**:** 101-105.

Martin, K. W. and Ernst, E. (2003). Herbal medicines for treatment of bacterial infections: a review of controlled clinical trials. *Journal of Antimicrobial Chemotherapy* **51**(2)**:** 241-246.

Mathew, S. and Abraham, T. E. (2006). In vitro antioxidant activity and scavenging effects of *Cinnamomum verum* leaf extract assayed by different methodologies. *Food and chemical toxicology* **44**(2)**:** 198-206.

Mcchesney, J. D., Venkataraman, S. K. and Henri, J. T. (2007). Plant natural products: back to the future or into extinction? *Phytochemistry* **68**(14)**:** 2015-2022.

Mcdonald, S., Prenzler, P. D., Antolovich, M. and Robards, K. (2001). Phenolic content and antioxidant activity of olive extracts. *Food chemistry* **73**(1)**:** 73-84.

Mensah, T. and Amoh-Barimah, A. (2009). An Evaluation of the Anti-inflammatory, Antipyretic and Antinociceptive Effects of *Ficus exasperata* (Vahl) Leaf Extract. *Journal of pharmacology and Toxicology* **4**(4)**:** 138-151.

Meschino, J. P. (2001). Natural anti-inflammatory supplements: research status and clinical applications. *Dynamic Chiropractic* **1**(12).

Mireku, E. A., Kusari, S., Eckelmann, D., Mensah, A. Y., Talontsi, F. M. and Spiteller, M. (2015). Anti-inflammatory tirucallane triterpenoids from *Anopyxis klaineana* Pierre (Engl.),(Rhizophoraceae). *Fitoterapia* **106:** 84-91.

Mireku, E. A., Mensah, A. Y., Mensah, M. L. K., Tocher, D. A. and Habtemariam, S. (2014). Anti-inflammatory Properties of the Stem bark of *Anopyxis klaineana* and its Major Constituent, Methyl Angolensate. *Phytotherapy Research* **28:** 1855-1860.

Mireku, E. A., Mensah, M. L. and Mensah, A. Y. (2016). Prenylated indole alkaloids from the stem bark of *Hexalobus monopetalus*. *Phytochemistry Letters* **16:** 108-114.

Mohamad, K., Martin, M.-T., Litaudon, M., Gaspard, C., S venet, T. and Pa S, M.

(1999). Tirucallane triterpenes from *Dysoxylum macranthum*. *Phytochemistry* **52**(8)**:** 1461-1468.

Morris, C. J. (2003). Carrageenan-Induced Paw Edema in the Rat and Mouse. *Inflammation Protocols* **225:** 115-121.

Mshana, N., Abbiw, D., Addae-Mensah, I., Adjanohoun, E., Ahyi, M., Ekpere, J., Enow-Orock, E., Gbile, Z., Noamesi, G. and Odei, M. (2000). Traditional medicine and pharmacopoeia. *Contribution to the revision of ethnobotanical and floristic studies in Ghana. Organization of African Unity/Scientific, Technical & Research Commision, Accra*.

Murata, T., Miyase, T., Muregi, F. W., Naoshima-Ishibashi, Y., Umehara, K., Warashina, T., Kanou, S., Mkoji, G. M., Terada, M. and Ishih, A. (2008).

Antiplasmodial triterpenoids from *Ekebergia capensis*. *Journal of natural products* **71**(2)**:** 167-174.

Ncube, N., Afolayan, A. and Okoh, A. (2008). Assessment techniques of antimicrobial properties of natural compounds of plant origin: current methods and future trends. *African Journal of Biotechnology* **7**(12).

Necas, J. and Bartosikova, L. (2013). Carrageenan: a review. *Vet Med* **58**(4)**:** 187205.

Newman, D. J., Cragg, G. M. and Snader, K. M. (2003). Natural products as sources of new drugs over the period 1981-2002. *Journal of Natural Products* **66**(7)**:** 10221037.

Nick, A., Wright, A. D., Rali, T. and Sticher, O. (1995). Antibacterial triterpenoids from *Dillenia papuana* and their structure-activity relationships. *Phytochemistry* **40**(6)**:** 1691-1695.

Nimse, S. B. and Pal, D. (2015). Free radicals, natural antioxidants, and their reaction mechanisms. *RSC Advances* **5**(35)**:** 27986-28006.

Nkunya, M. H., Makangara, J. J. and Jonker, S. A. (2004). Prenylindoles from Tanzanian *Monodora* and *Isolona* species. *Natural product research* **18**(3)**:** 253-258.

Norrel, S. and Messley, K. E. (1997). *Microbiology Laboratory Manual Principles and Applicantions*. edn. Upper Saddle River, New Jersey: Prentice Hall.

Nostro, A., Germano, M., D'angelo, V., Marino, A. and Cannatelli, M. (2000). Extraction methods and bioautography for evaluation of medicinal plant antimicrobial activity. *Letters in Applied Microbiology* **30**(5)**:** 379-384.

Nsiama, T. K., Okamura, H., Hamada, T., Morimoto, Y., Doe, M., Iwagawa, T. and Nakatani, M. (2011). Rings D-seco and B, D-seco tetranortriterpenoids from root bark of *Entandrophragma angolense*. *Phytochemistry* **72**(14)**:** 1854-1858.

Nwaogu, L., Alisi, C., Ibegbulem, C. and Igwe, C. (2007). Phytochemical and antimicrobial activity of ethanolic extract of *Landolphia owariensis* leaf. *African Journal of Biotechnology* **6**(7).

Ochi, T., Takaishi, Y., Shibata, H., Higuti, T. and Kataoka, M. (2005). Chemical constituents of *Capsicum annuum L var. angulosum*, and anti *Helicobacter pylori* activity. *Natural Medicines* **59**(2)**:** 76-84.

Okeke, M. I., Iroegbu, C. U., Eze, E., Okoli, A. and Esimone, C. (2001). Evaluation of extracts of the root of *Landolphia owariensis* for antibacterial activity. *Journal of ethnopharmacology* **78**(2)**:** 119-127.

Okonkwo, T. J. and Osadebe, P. (2013). Isolation and characterization of potential bioactive compounds from *Landolphia owariensis* P. Beauv stringy seed pulp. *International Journal of Applied Research in Natural Products* **6**(3)**:** 28-38.

Okonkwo, T. J., Osadebe, P. O. and Proksch, P. (2016). Bioactive Phenylpropanoids, Phenolic Acid and Phytosterol from *Landolphia owariensis* P. Beauv Stringy Seed Pulp. *Phytotherapy Research* **30**(1)**:** 78-83.

Orisadipe, A. T., Adesomoju, A. A., D'ambrosio, M., Guerriero, A. and Okogun, J. I. (2005). Tirucallane triterpenes from the leaf extract of *Entandrophragma angolense*. *Phytochemistry* **66**(19)**:** 2324-2328.

Oteng-Amoako, A. A., Essien, C. (2011). *Anopyxis klaineana* (Pierre) Engl. In: *Plant Resources of Tropical Africa / Ressources végétales de l'Afrique tropicale*, Lemmens RHMJ, Louppe, D. & Oteng-Amoako, A.A. (ed). Wageningen, Netherlands.

Oubre, A., Carlson, T., King, S. and Reaven, G. (1997). From plant to patient: an ethnomedical approach to the identification of new drugs for the treatment of NIDDM. *Diabetologia* **40**(5)**:** 614-617.

Owoyele, B., Olaleye, S., Oke, J. and Elegbe, R. (2001). Anti-inflammatory and analgesic activities of leaf extracts of *Landolphia owariensis*. *African Journal of Biomedical Research* **4**(3).

Parekh, J., Karathia, N. and Chanda, S. (2006). Screening of some traditionally used medicinal plants for potential antibacterial activity. *Indian journal of pharmaceutical sciences* **68**(6)**:** 832.

Penido, C., Conte, F., Chagas, M., Rodrigues, C., Pereira, J. and Henriques, M. (2006). Anti-inflammatory effects of natural tetranortriterpenoids isolated from *Carapa guianensis* Aublet on zymosan-induced arthritis in mice. *Inflammation Research* **55**(11)**:** 457-464.

Persoon, J. (1992). *African species of Landolphia P. Beauv. series of revisions of Apocynaceae XXXIV*. edn. Agricultural University.

Posadas, I., Bucci, M., Roviezzo, F., Rossi, A., Parente, L., Sautebin, L. and Cirino, G. (2004). Carrageenan induced mouse paw oedema is biphasic, age weight dependent and displays differential nitric oxide cyclooxygenase‐2 expression. *British journal of pharmacology* **142**(2)**:** 331-338.

Prieto, P., Pineda, M. and Aguilar, M. (1999). Spectrophotometric quantitation of antioxidant capacity through the formation of a phosphomolybdenum complex: specific application to the determination of vitamin E. *Analytical biochemistry* **269**(2)**:** 337-341.

Ravangpai, W., Sommit, D., Teerawatananond, T., Sinpranee, N., Palaga, T., Pengpreecha, S., Muangsin, N. and Pudhom, K. (2011). Limonoids from seeds of Thai *Xylocarpus moluccensis*. *Bioorganic & medicinal chemistry letters* **21**(15)**:** 4485-4489.

Rice-Evans, C., Miller, N. and Paganga, G. (1997). Antioxidant properties of phenolic compounds. *Trends in plant science* **2**(4)**:** 152-159.

Rios, J. and Recio, M. (2005). Medicinal plants and antimicrobial activity. *Journal of ethnopharmacology* **100**(1)**:** 80-84.

Rishton, G. M. (2008). Natural products as a robust source of new drugs and drug leads: past successes and present day issues. *The American journal of cardiology* **101**(10)**:** S43-S49.

Roach, J. T. and Sufka, K. J. (2003). Characterization of the chick carrageenan response. *Brain research* **994**(2)**:** 216-225.

Rodighiero, P., Guiotto, A. and Manzini, P. (1979). Synthesis of Isoponcimarin. *Zeitschrift für Naturforschung B* **34**(7)**:** 1010-1014.

Rout, S. P., Choudary, K., Kar, D., Das, L. and Jain, A. (2009). Plants in traditional medicinal system-future source of new drugs. *Int J Pharm Pharm Sci* **1**(1)**:** 1-23.

Roy, A. and Saraf, S. (2006). Limonoids: overview of significant bioactive triterpenes distributed in plants kingdom. *Biological and Pharmaceutical Bulletin* **29**(2)**:** 191-201.

Sakushima, A., Ohno, K., Maoka, T., Coskun, M., Guvenc, A., Erdurak, C. S., Ozkan, A. M., Seki, K. I. and Ohkura, K. (2003). Guaiacylglycerol-7′-O-methyl 8′vanillic acid ether and related compounds from *Boreava orientalis*. *Phytochemical analysis* **14**(1)**:** 48-53.

Salie, F., Eagles, P. F. and Leng, H. M. (1996). Preliminary antimicrobial screening of four South African Asteraceae species. *Journal of Ethnopharmacology*

52: 27-33.

Salzano, S., Checconi, P., Hanschmann, E.-M., Lillig, C. H., Bowler, L. D., Chan, P., Vaudry, D., Mengozzi, M., Coppo, L. and Sacre, S. (2014). Linkage of inflammation and oxidative stress via release of glutathionylated peroxiredoxin-2, which acts as a danger signal. *Proceedings of the National Academy of Sciences* **111**(33)**:** 1215712162.

Santos, A. (2003). Anti-inflammatory compounds of plant origin. Part I. Action on arachidonic acid pathway, nitric oxide and nuclear factor κ B (NF-κB). *Planta Med* **69:** 973-983.

Santos, A. (2004). Anti-inflammatory compounds of plant origin. Part II. Modulation of pro-inflammatory cytokines, chemokines and adhesion molecules. *Planta Med* **70:** 93-103.

Sarigaputi, C., Sommit, D., Teerawatananond, T. and Pudhom, K. (2014). Weakly Anti-inflammatory Limonoids from the Seeds of *Xylocarpus rumphii*. *Journal of natural products* **77**(9)**:** 2037-2043.

Sato, A. (2012). Revealing the popularity of traditional medicine in light of multiple recourses and outcome measurements from a user's perspective in Ghana. *Health policy and planning* **27**(8)**:** 625-637.

Satoko, M., Kadota, S., Tai, T. and Kikuchi, T. (1984). Isolation and structures of hedyotisol A, B, and C, novel dilignans from *Hedyotis lawsoniae*. *Chemical and pharmaceutical bulletin* **32**(12)**:** 5066-5069.

Schmourlo, G., Mendonça-Filho, R. R., Alviano, C. S. and Costa, S. S. (2005). Screening of antifungal agents using ethanol precipitation and bioautography of medicinal and food plants. *Journal of Ethnopharmacology* **96**(3)**:** 563-568.

Schreck, R., Albermann, K. and Baeuerle, P. A. (1992). Nuclear factor kB: an oxidative stress-responsive transcription factor of eukaryotic cells (a review). *Free radical research communications* **17**(4)**:** 221-237.

Seifried, H. E., Anderson, D. E., Fisher, E. I. and Milner, J. A. (2007). A review of the interaction among dietary antioxidants and reactive oxygen species. *The Journal of nutritional biochemistry* **18**(9)**:** 567-579.

Seminerio, J., Mcgrath, K., Arnold, C. A., Voltaggio, L. and Singhi, A. D. (2014). Medication-associated lesions of the GI tract. *Gastrointestinal endoscopy* **79**(1)**:** 140150.

Sen, C. K. and Packer, L. (1996). Antioxidant and redox regulation of gene transcription. *The FASEB journal* **10**(7)**:** 709-720.

Shen, Y.-C., Chiou, W.-F., Chou, Y.-C. and Chen, C.-F. (2003). Mechanisms in mediating the anti-inflammatory effects of baicalin and baicalein in human leukocytes. *European journal of pharmacology* **465**(1)**:** 171-181.

Siemoneit, U., Koeberle, A., Rossi, A., Dehm, F., Verhoff, M., Reckel, S., Maier, T., Jauch, J., Northoff, H. and Bernhard, F. (2011). Inhibition of microsomal prostaglandin E2 synthase_1 as a molecular basis for the anti_inflammatory actions of boswellic acids from frankincense. *British journal of pharmacology* **162**(1)**:** 147-162.

Silva, M. T., Simas, S. M., Batista, T. G., Cardarelli, P. and Tomassini, T. C. (2005). Studies on antimicrobial activity, in vitro, of *Physalis angulata* L.(Solanaceae) fraction and physalin B bringing out the importance of assay determination. *Memorias do Instituto Oswaldo Cruz* **100**(7)**:** 779-782.

Singh, S. B. and Barrett, J. F. (2006). Empirical antibacterial drug discovery—foundation in natural products. *Biochemical pharmacology* **71**(7)**:** 1006-1015.

Singh, U. and Jialal, I. (2006). Oxidative stress and atherosclerosis. *Pathophysiology* **13**(3)**:** 129-142.

Snape, T. J. (2007). Recent advances in the semi-pinacol rearrangement of αhydroxy epoxides and related compounds. *Chemical Society Reviews* **36**(11)**:** 18231842.

Sólyomváry, A., Tóth, G., Komjáti, B., Horváth, P., Kraszni, M., Noszál, B., MolnárPerl, I. and Boldizsár, I. (2015). Identification and isolation of new neolignan and sesquineolignan species: Their acid-catalyzed ring closure and specific accumulation in the fruit wall of *Cirsium eriophorum* (L.) Scop. *Process Biochemistry* **50**(5)**:** 853858.

Sprague, T. and Boodle, L. (1909). Kokoti (*Anopyxis ealaensis*, Sprague.). *Bulletin of Miscellaneous Information (Royal Botanic Gardens, Kew)***:** 309-312.

Stærk, D., Skole, B., Jørgensen, F. S., Budnik, B. A., Ekpe, P. and Jaroszewski, J. W. (2004). Isolation of a Library of Aromadendranes from *Landolphia dulcis* and Its Characterization Using the VolSurf Approach. *Journal of natural products* **67**(5)**:** 799-805.

Stark, T. D., Mtui, D. J. and Balemba, O. B. (2013). Ethnopharmacological Survey of Plants Used in the Traditional Treatment of Gastrointestinal Pain, Inflammation and Diarrhea in Africa: Future Perspectives for Integration into Modern Medicine. *Animals* **3**(1)**:** 158-227.

Steentoft, M. (1988). *Flowering plants in west Africa*. edn. Cambridge University Press.

Stermitz, F. R., Lorenz, P., Tawara, J. N., Zenewicz, L. A. and Lewis, K. (2000). Synergy in a medicinal plant: antimicrobial action of berberine potentiated by 5′methoxyhydnocarpin, a multidrug pump inhibitor. *Proceedings of the National Academy of Sciences* **97**(4)**:** 1433-1437.

Suh, N., Honda, T., Finlay, H. J., Barchowsky, A., Williams, C., Benoit, N. E., Xie, Q.-W., Nathan, C., Gribble, G. W. and Sporn, M. B. (1998). Novel triterpenoids suppress inducible nitric oxide synthase (iNOS) and inducible cyclooxygenase (COX-2) in mouse macrophages. *Cancer research* **58**(4)**:** 717-723.

Tabi, M., Powell, M. and Hodnicki, D. (2006). Use of traditional healers and modern medicine in Ghana. *International nursing review* **53**(1)**:** 52-58.

Tan, Q.-G. and Luo, X.-D. (2011). Meliaceous limonoids: chemistry and biological activities. *Chemical reviews* **111**(11)**:** 7437-7522.

Teponno, R. B., Kusari, S. and Spiteller, M. (2016). Recent advances in research on lignans and neolignans. *Natural product reports*.

Transue, T. R., De Genst, E., Ghahroudi, M. A., Wyns, L. and Muyldermans, S. (1998). Camel single-domain antibody inhibits enzyme by mimicking carbohydrate substrate. *Proteins-Structure Function and Genetics* **32**(4)**:** 515-522.

Umeh, E., Oluma, H. and Igoli, J. (2005). Research communication-Antibacterial Screening of four local plants using an indicator-based microdilution technique. *African Journal of Traditional, Complementary and Alternative Medicines* **2**(3)**:** 238243.

Valle, T., López, J. L., Hernández, J. M. and Corchete, P. (1997). Antifungal activity of scopoletin and its differential accumulation in *Ulmus pumila* and *Ulmus campestris* cell suspension cultures infected with Ophiostoma ulmi spores. *Plant Science* **125**(1)**:** 97-101.

Vanden-Berghe, D. and Vlientinck, A. (1991). Screening Methods for Antibacterial and Antiviral Agents from Higher Plants. In: Hostettmann K (ed)^(eds). *Methods in Plant Biochemistry VI. Assays for Bioactivity*, edn. p^pp 47–69.

Vaziri, N. D. and Rodriguez-Iturbe, B. (2006). Mechanisms of disease: oxidative stress and inflammation in the pathogenesis of hypertension. *Nature Clinical Practice Nephrology* **2**(10)**:** 582-593.

Verhoff, M., Seitz, S., Paul, M., Noha, S. M., Jauch, J., Schuster, D. and Werz, O. (2014). Tetra-and Pentacyclic Triterpene Acids from the Ancient Anti-inflammatory Remedy Frankincense as Inhibitors of Microsomal Prostaglandin E2 Synthase-1. *Journal of natural products* **77**(6)**:** 1445-1451.

Vuorela, P., Leinonen, M., Saikku, P., Tammela, P., Wennberg, T. and Vuorela, H. (2004). Natural products in the process of finding new drug candidates. *Current medicinal chemistry* **11**(11)**:** 1375-1389.

Wallace, R. J. (2004). Antimicrobial properties of plant secondary metabolites. *Proceedings of the Nutrition Society* **63**(04)**:** 621-629.

Wang, J., Zheng, Y., Efferth, T., Wang, R., Shen, Y. and Hao, X. (2005). Indole and carbazole alkaloids from *Glycosmis montana* with weak anti-HIV and cytotoxic activities. *Phytochemistry* **66**(6)**:** 697-701.

Wang, L., Li, F., Yang, C.-Y., Khan, A.-A., Liu, X. and Wang, M.-K. (2014). Neolignans, lignans and glycoside from the fruits of *Melia toosendan*. *Fitoterapia* **99:** 92-98.

Wang, Q.-H., Peng, K., Tan, L.-H. and Dai, H.-F. (2010). Aquilarin A, a new benzenoid derivative from the fresh stem of *Aquilaria sinensis*. *Molecules* **15**(6)**:** 4011-4016.

Waris, G. and Ahsan, H. (2006). Reactive oxygen species: role in the development of cancer and various chronic conditions. *Journal of carcinogenesis* **5**(1)**:** 14.

Whiteley, P. E. and Dalrymple, S. A. (2001). Models of Inflammation: CarrageenanInduced Paw Edema in the Rat. *Current protocols in pharmacology* **54:** 541-543.

Who (2014). Antimicrobial resistance global report on surveillance: 2014 summary.

Willför, S., Reunanen, M., Eklund, P., Sjöholm, R., Kronberg, L., Fardim, P., Pietarinen, S. and Holmbom, B. (2004). Oligolignans in Norway spruce and Scots pine knots and Norway spruce stemwood. *Holzforschung* **58**(4)**:** 345-354.

Wolfender, J. L., Ndjoko, K. and Hostettmann, K. (2003). Liquid chromatography with ultraviolet absorbance–mass spectrometric detection and with nuclear magnetic resonance spectrometry: a powerful combination for the on-line structural investigation of plant metabolites. *Journal of Chromatography A* **1000**(1)**:** 437-455.

Woo, K. W., Suh, W. S., Subedi, L., Kim, S. Y., Kim, A. and Lee, K. R. (2016). Bioactive lignan derivatives from the stems of *Firmiana simplex*. *Bioorganic & medicinal chemistry letters* **26**(3)**:** 730-733.

Wu, J., Yang, S.-X., Li, M.-Y., Feng, G., Pan, J.-Y., Xiao, Q., Sinkkonen, J. and Satyanandamurty, T. (2010). Limonoids and tirucallane derivatives from the seeds of a Krishna mangrove, *Xylocarpus moluccensis*. *Journal of natural products* **73**(4)**:** 644-649.

Wu, S. J., Tsai, J. Y., Chang, S. P., Lin, D. L., Wang, S. S., Huang, S. N. and Ng, L. T. (2006). Supercritical carbon dioxide extract exhibits enhanced antioxidant and anti-

inflammatory activities of *Physalis peruviana*. *Journal of ethnopharmacology* **108**(3)**:** 407-413.

Xia, H.-M., Li, C.-J., Yang, J.-Z., Ma, J., Chen, X.-G., Zhang, D., Li, L. and Zhang, D.-M. (2014). A, D-seco-Limonoids from the Stems of *Clausena emarginata*. *Journal of natural products* **77**(4)**:** 784-791.

Xiong, J., Bui, V.-B., Liu, X.-H., Hong, Z.-L., Yang, G.-X. and Hu, J.-F. (2014). Lignans from the stems of *Clematis armandii* (—Chuan-Mu-Tong‖) and their antineuroinflammatory activities. *Journal of ethnopharmacology* **153**(3)**:** 737-743.

Yang, M.-H., Wang, J.-S., Luo, J.-G., Wang, X.-B. and Kong, L.-Y. (2011). Chisopanins A–K, 11 new protolimonoids from *Chisocheton paniculatus* and their anti-inflammatory activities. *Bioorganic & medicinal chemistry* **19**(4)**:** 1409-1417.

Yuan, C.-M., Tang, G.-H., Zhang, Y., Wang, X.-Y., Cao, M.-M., Guo, F., Li, Y., Di, Y.-T., Li, S.-L. and Hua, H.-M. (2013). Bioactive Limonoid and Triterpenoid Constituents of *Turraea pubescens*. *Journal of natural products* **76**(6)**:** 1166-1174.

Zeng, Q., Guan, B., Qin, J.-J., Wang, C.-H., Cheng, X.-R., Ren, J., Yan, S.-K., Jin, H.-Z. and Zhang, W.-D. (2012). 2, 3-Seco-and 3, 4-seco-tirucallane triterpenoid derivatives from the stems of *Aphanamixis grandifolia* Blume. *Phytochemistry* **80:** 148-155.

Zhao, F., Chen, L., Bi, C., Zhang, M., Jiao, W. and Yao, X. (2013). In vitro antiinflammatory effect of picrasmalignan A by the inhibition of iNOS and COX-2 expression in LPS-activated macrophage RAW 264.7 cells. *Molecular medicine reports* **8**(5)**:** 1575-1579.

Eicosanoids. http://tmedweb.tulane.edu/pharmwiki/doku.php/eicosanoids_draft, accessed on 24-07-2016

APPENDIX A

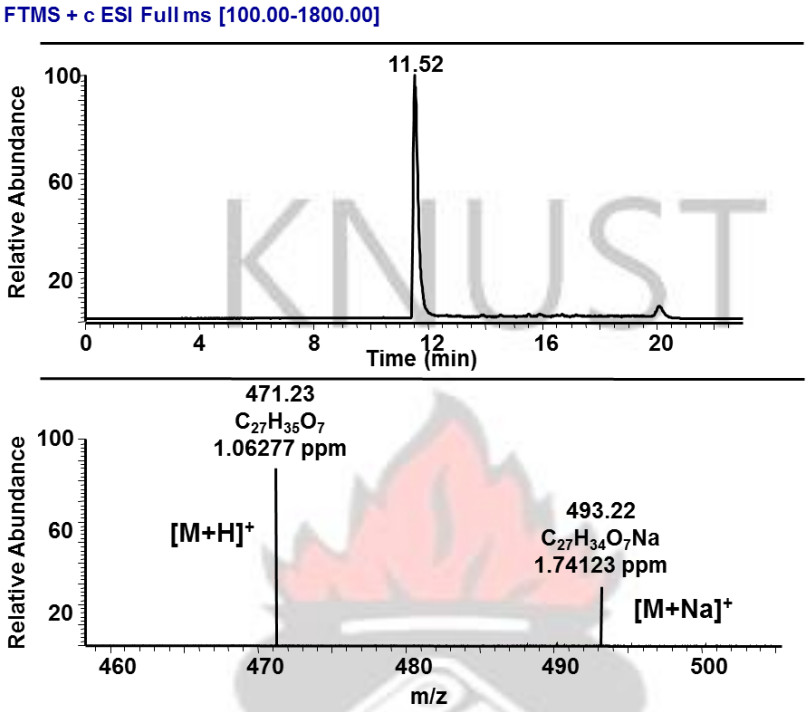

Fig. A-1 Full scan HR-MS spectrum of AK1

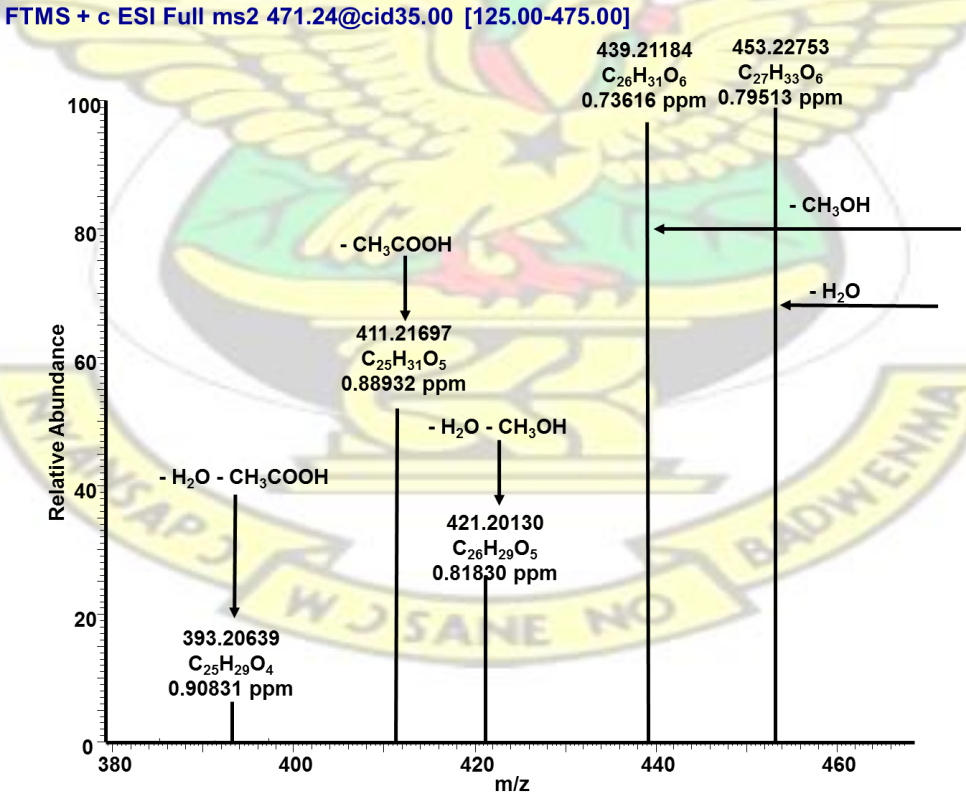

Fig. A-2 HR-MS^2 fragmentation spectrum of AK1

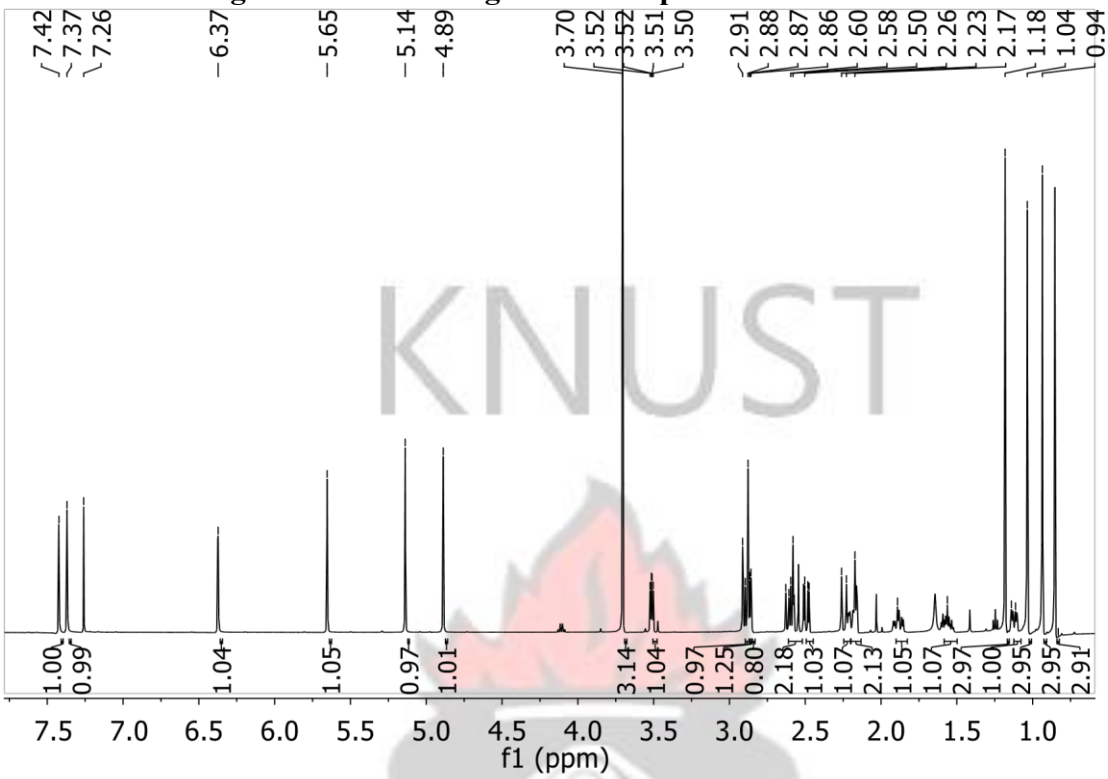

Fig. A-3 ^{1}H NMR spectrum of AK1

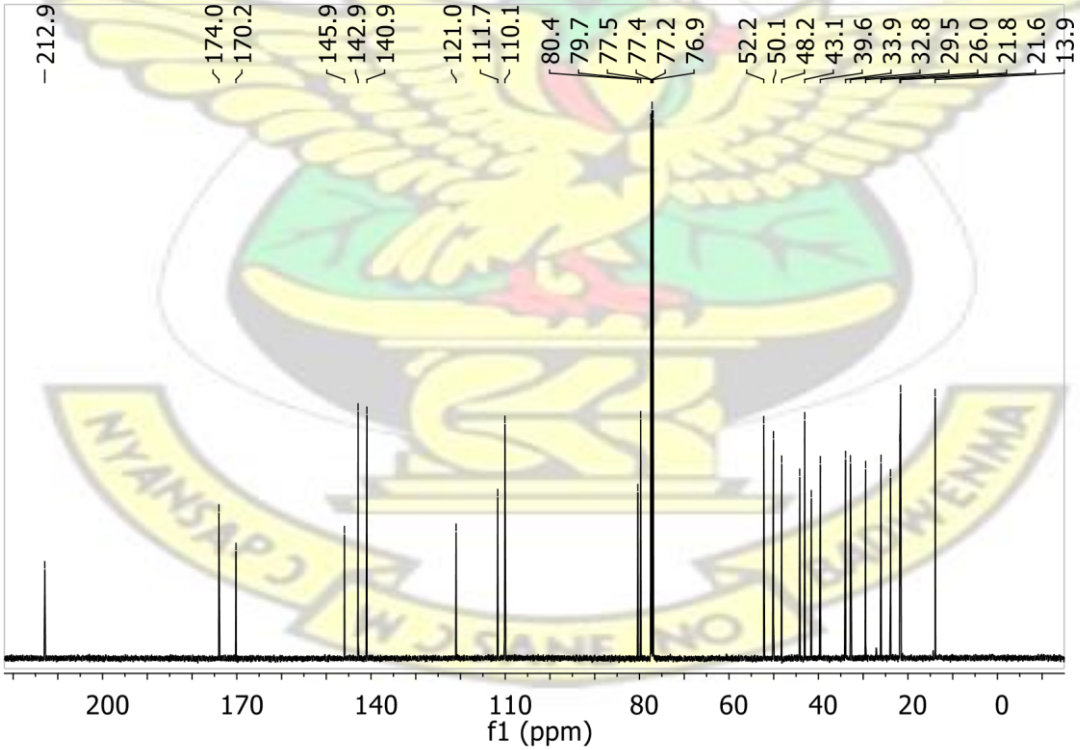

Fig. A-4 ^{13}C NMR spectrum of AK1

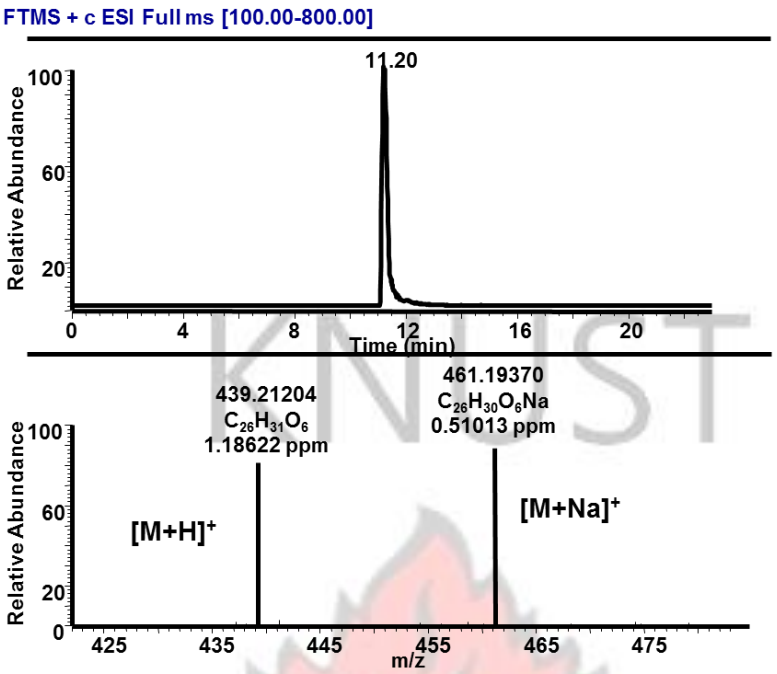

Fig. A-5 Full scan HR-MS spectrum of AK2

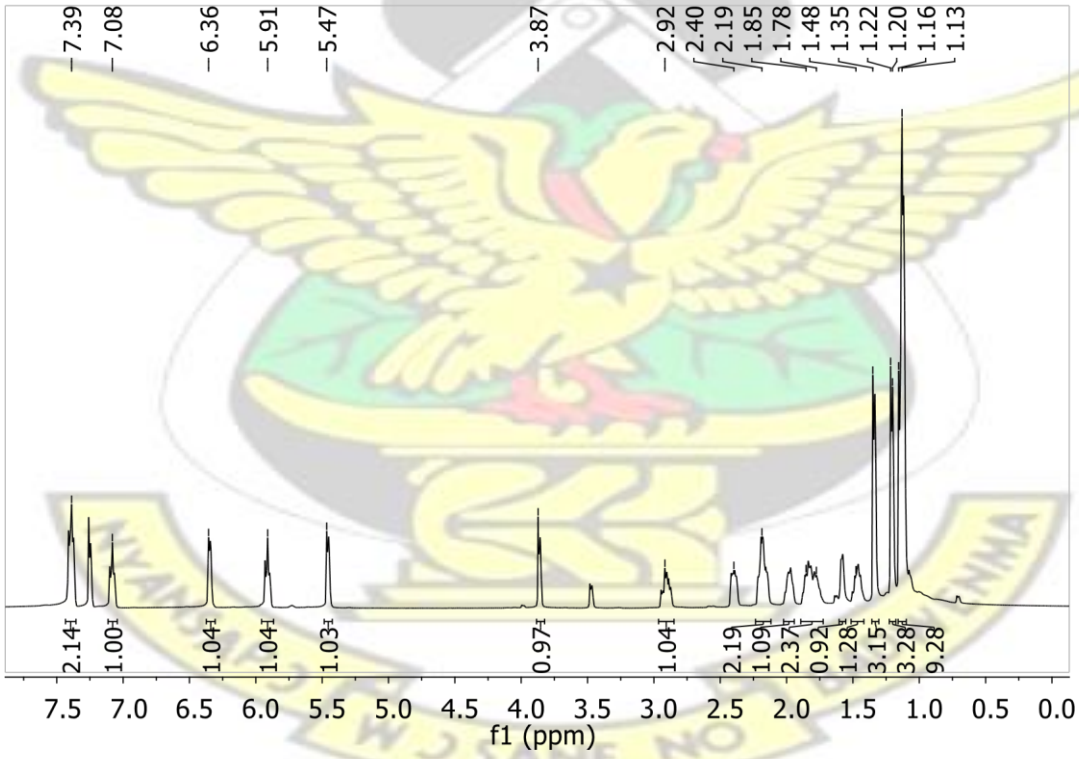

Fig. A-6 ^{1}H NMR spectrum of AK2

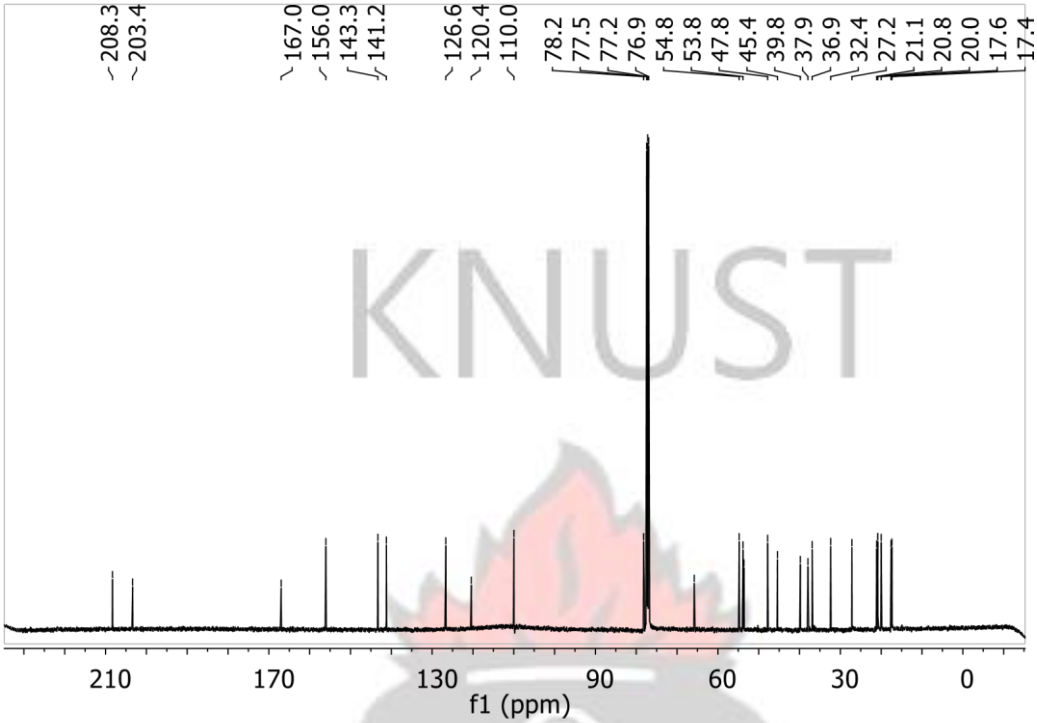

Fig. A-7 ^{13}C NMR spectrum of AK2

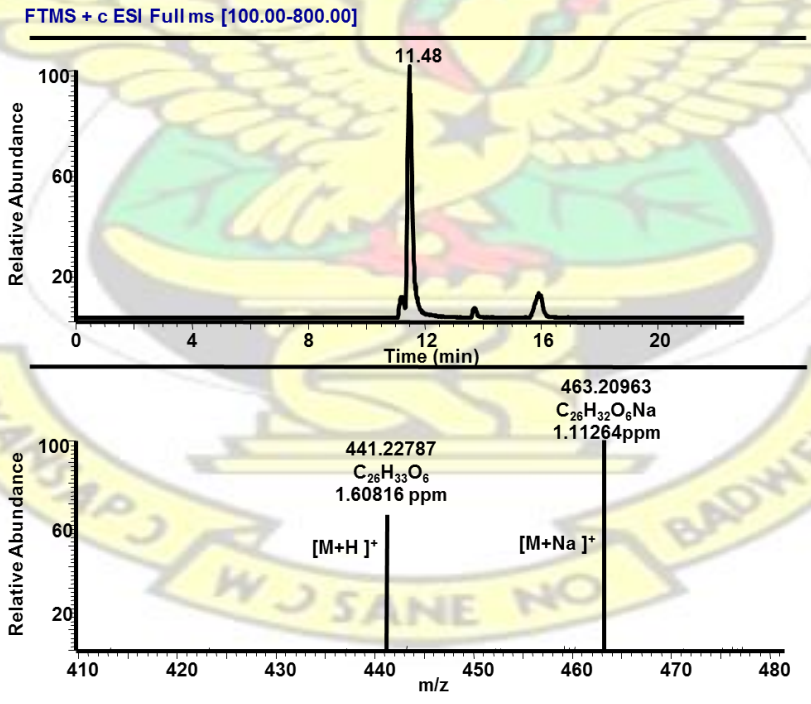

Fig. A-8 Full scan HR-MS spectrum of AK3

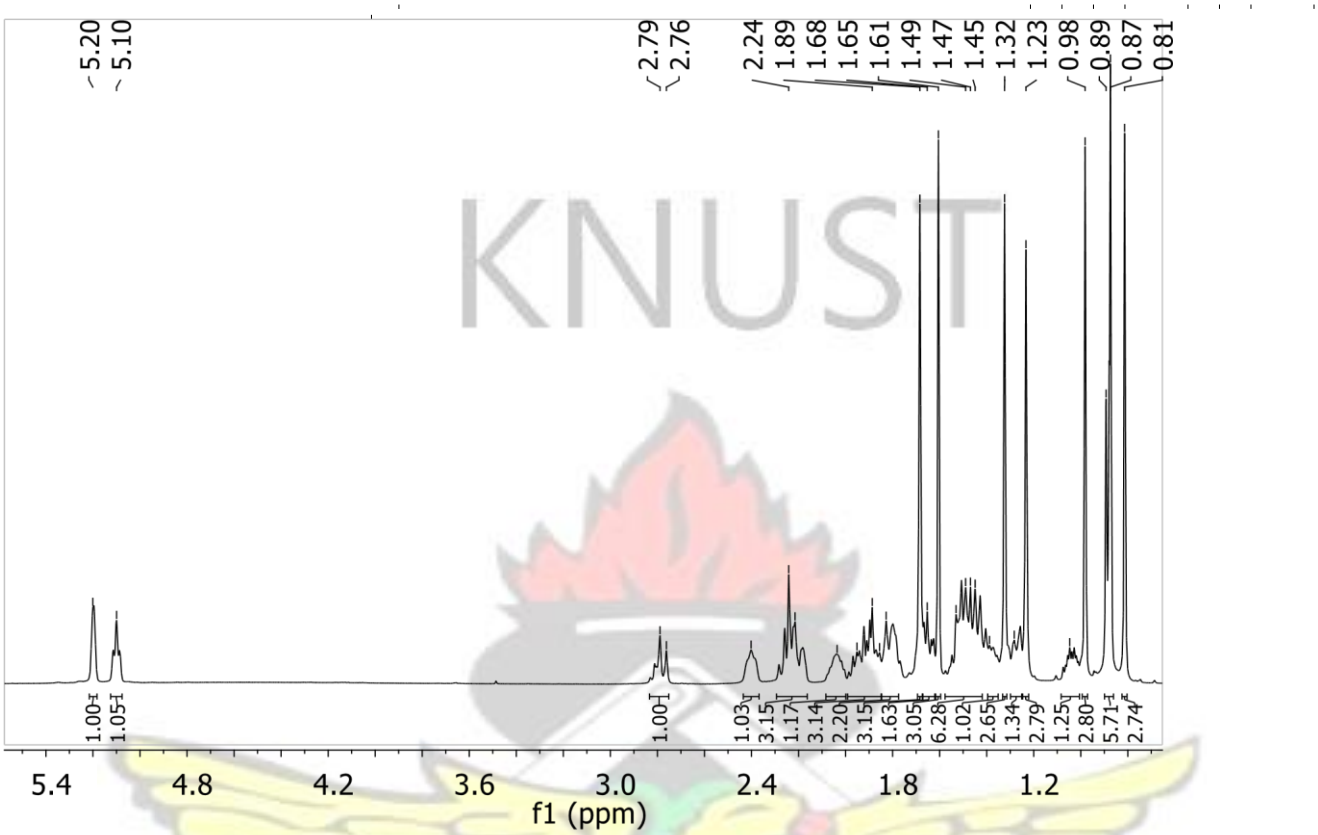

Fig. A-9 ^{1}H NMR spectrum of AK3

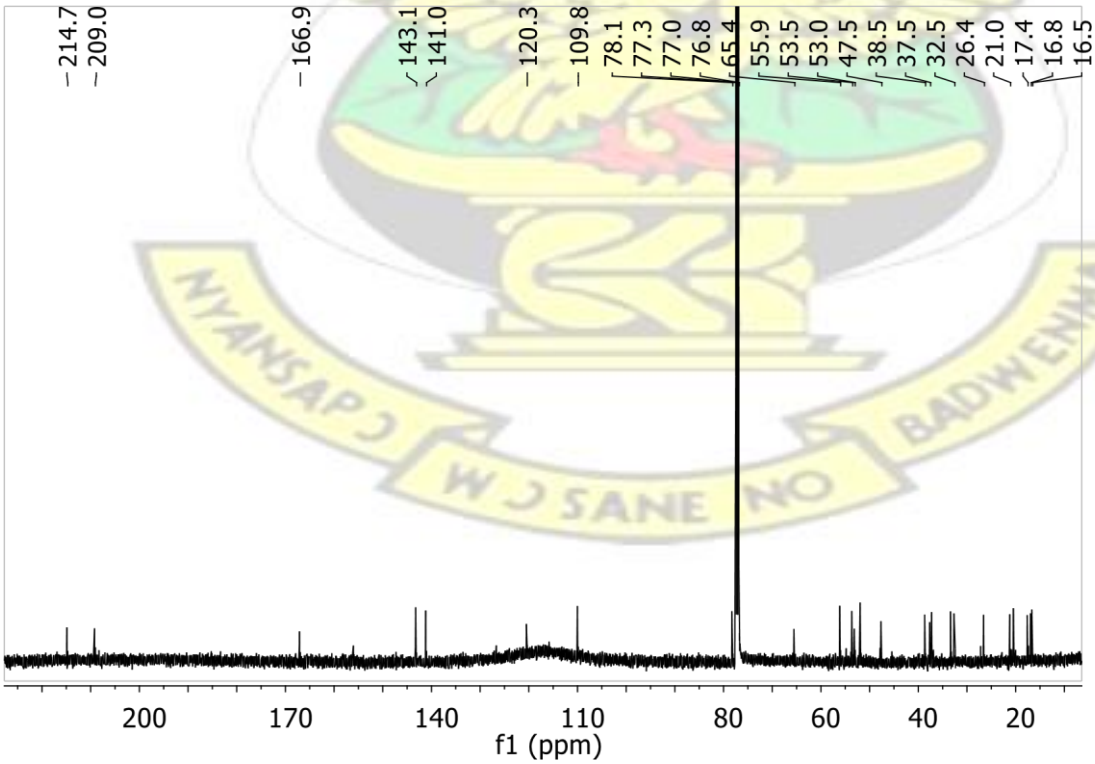

Fig. A-10 ^{13}C NMR spectrum of AK3

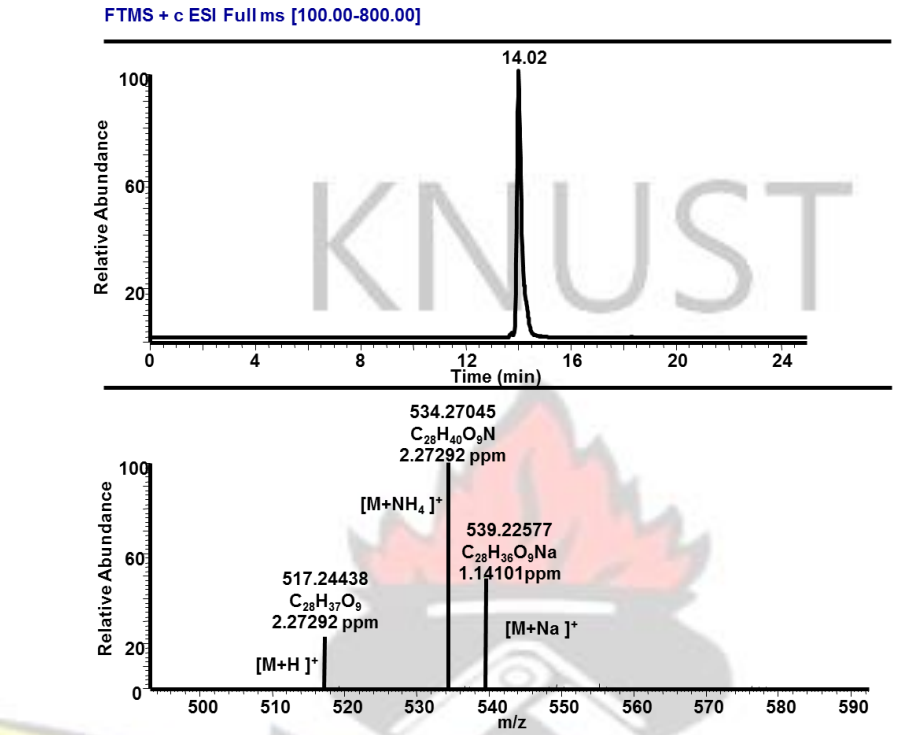

Fig. A-11 Full scan HR-MS spectrum of AK4

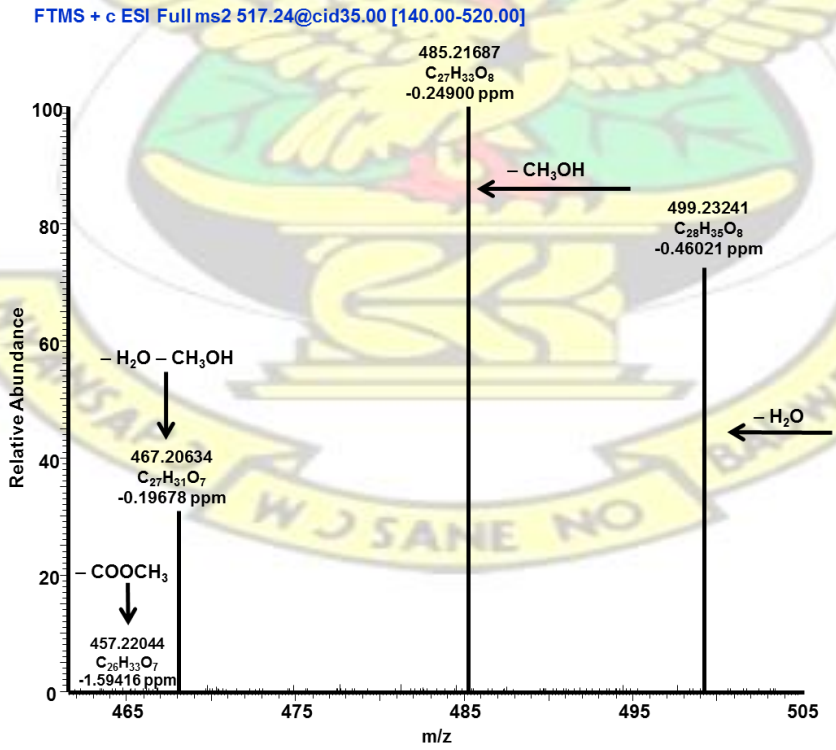

Fig. A-12 HR-MS^2 fragmentation spectrum of AK4

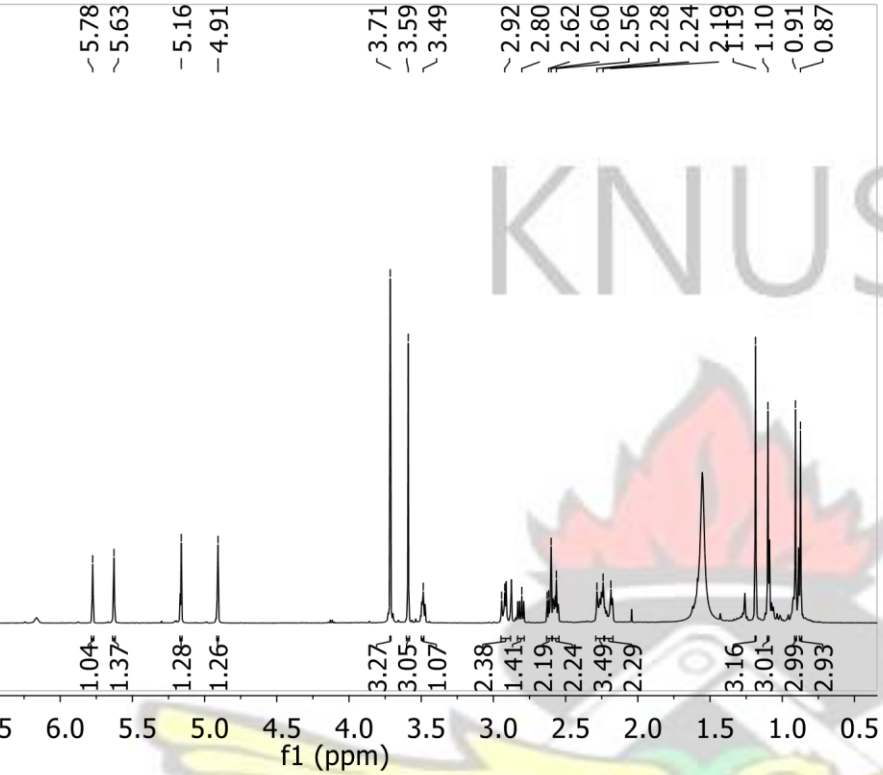

Fig. A-13 ^{1}H NMR spectrum of AK4

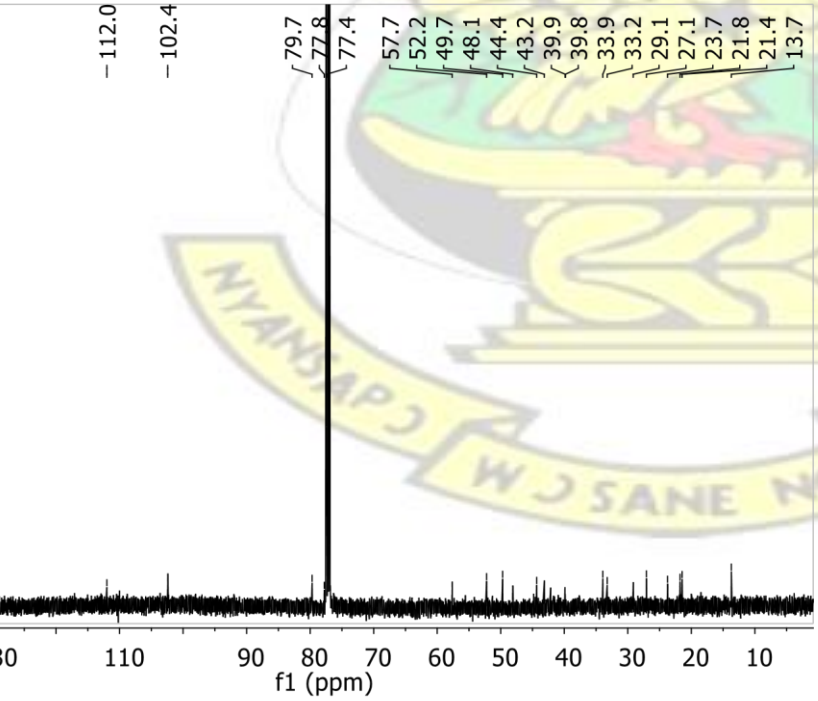

Fig. A-14 ^{13}C NMR spectrum of AK4

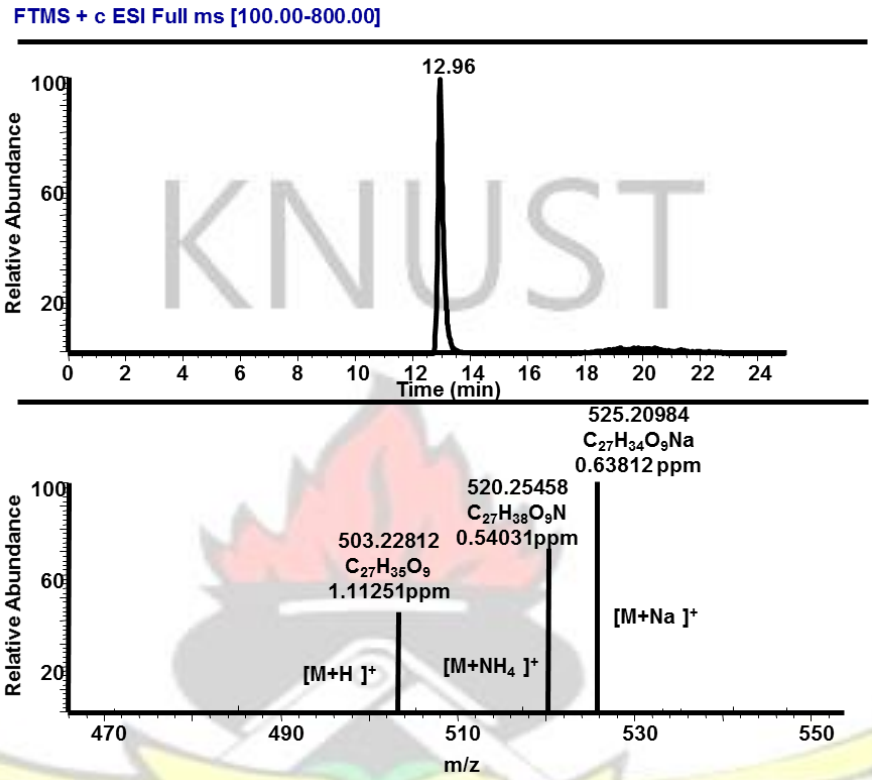

Fig. A-15 Full scan HR-MS spectrum of AK5a/b

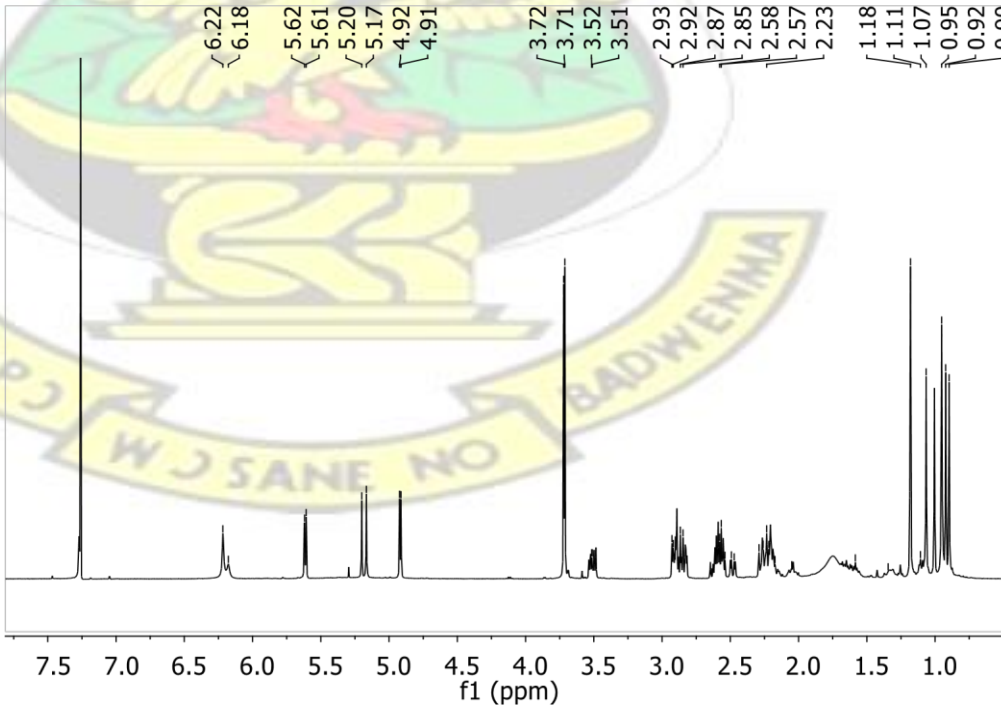

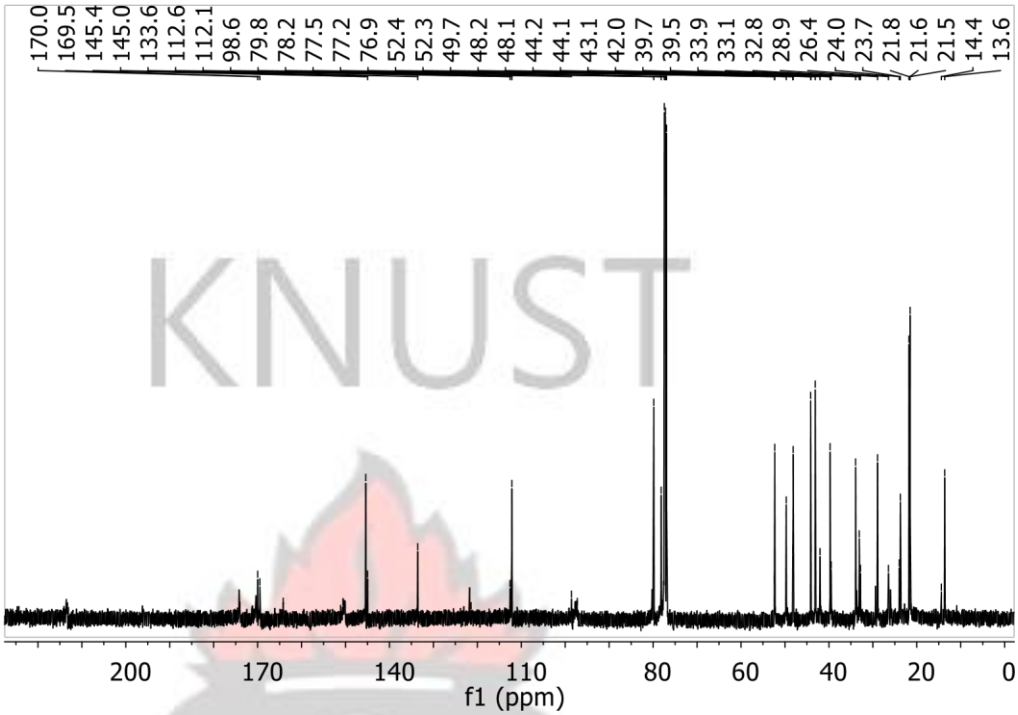

Fig. A-16 ^{1}H NMR spectrum of AK5a/b

Fig. A-17 ^{13}C NMR spectrum of AK5a/b

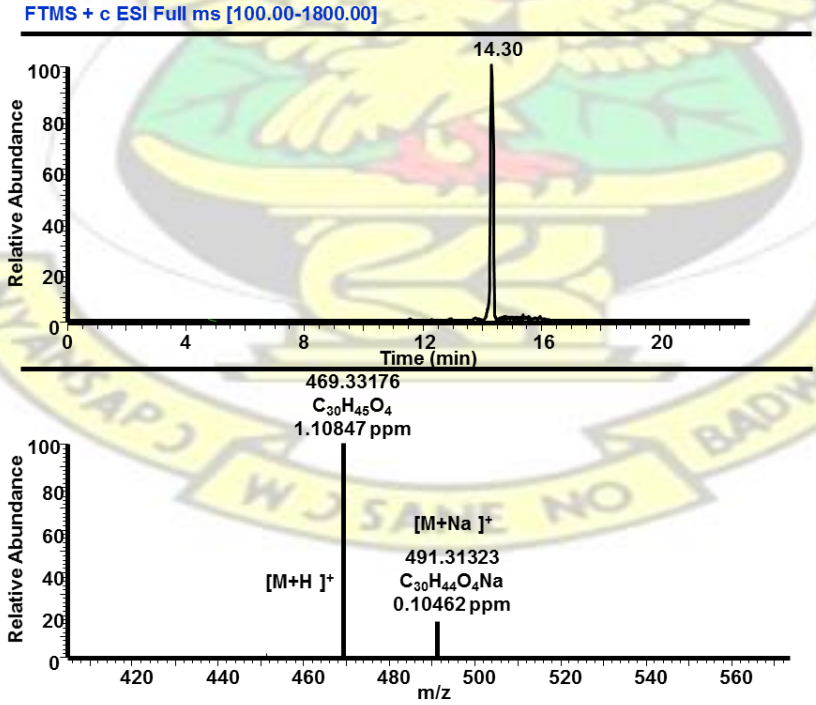

Fig. A-18 Full scan HR-MS spectrum of AK6

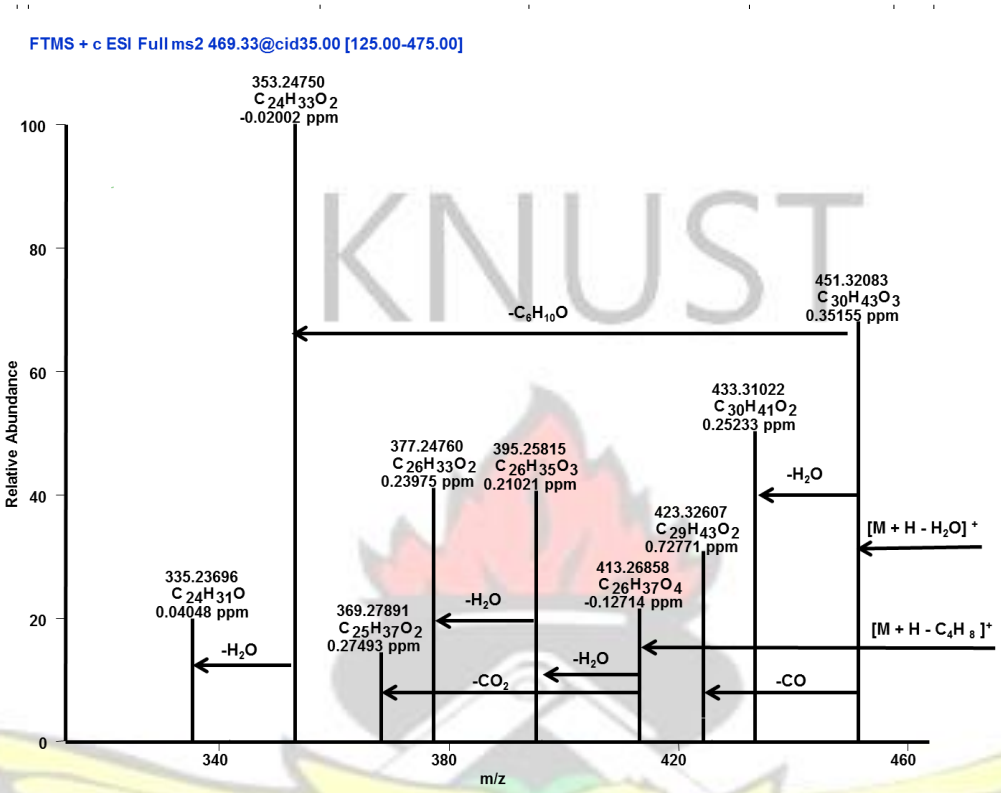

Fig. A-19 HR-MS^2 fragmentation spectrum of AK6

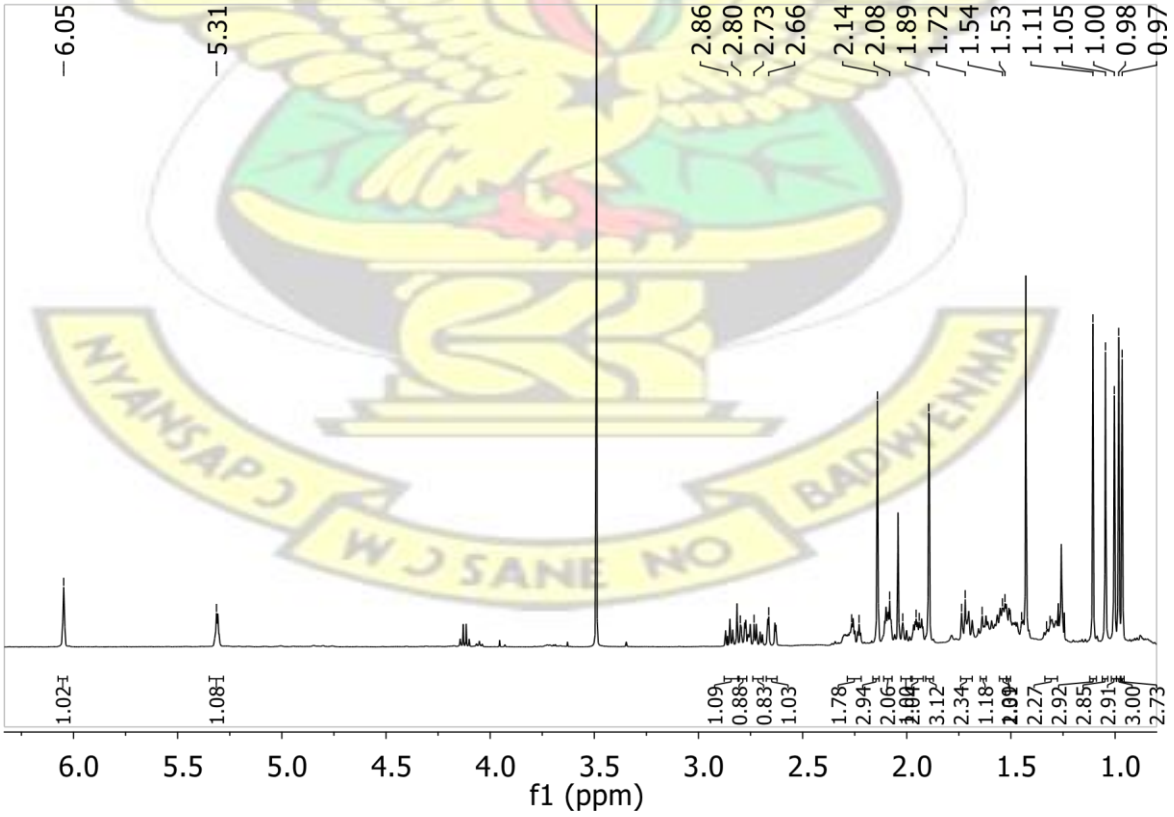

Fig. A-20 ^{1}H NMR spectrum of AK6

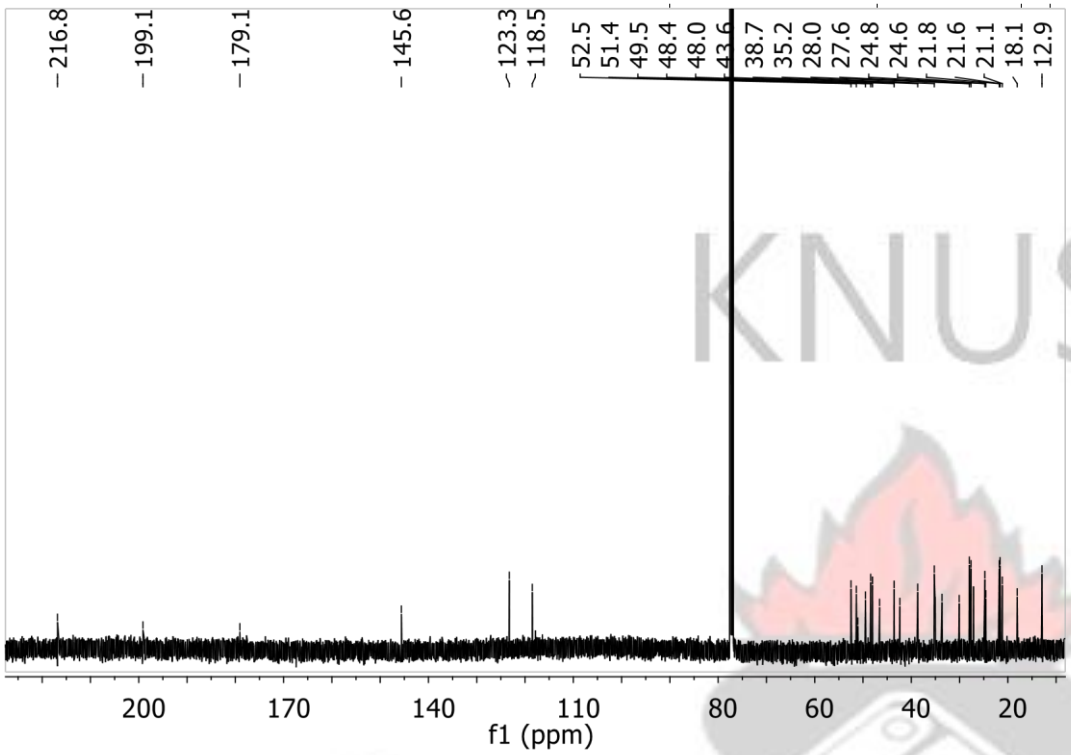

Fig. A-21 ^{13}C NMR spectrum of AK6

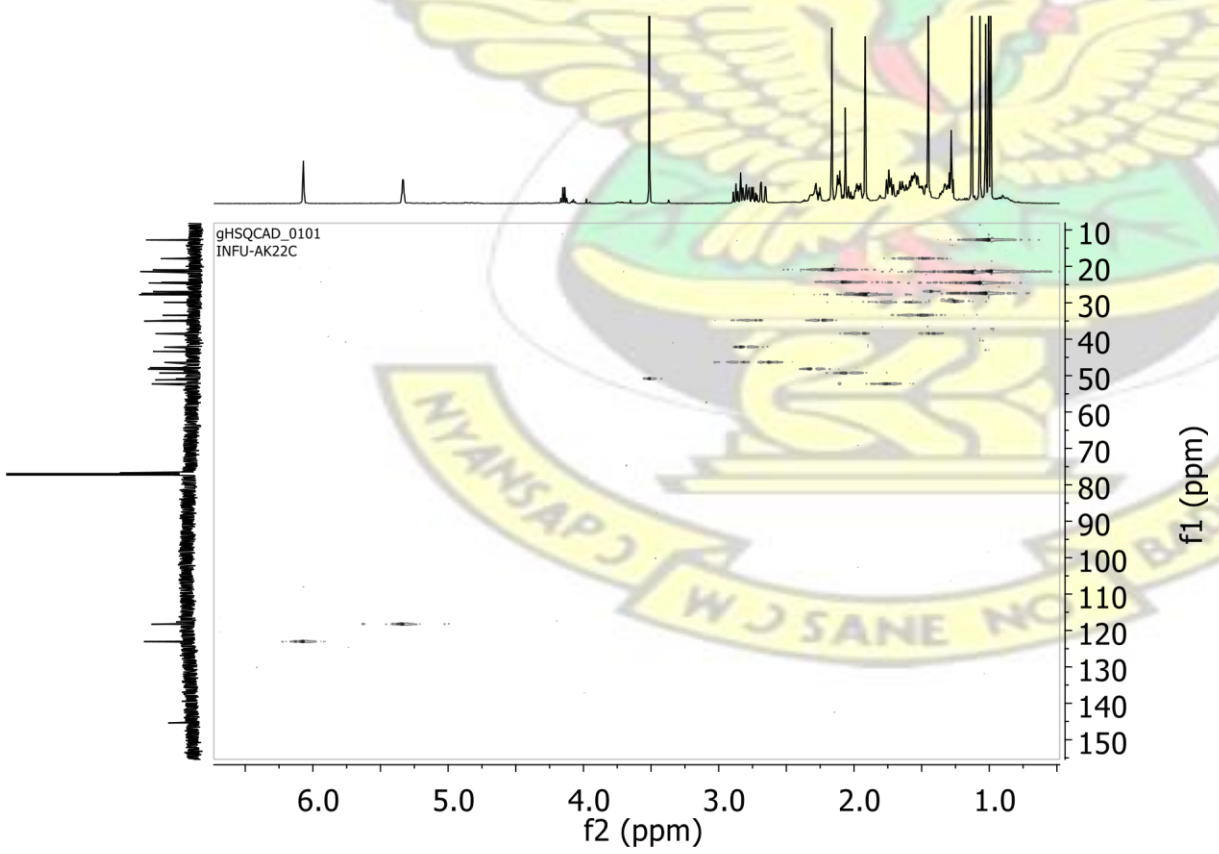

Fig. A-22 HSQC NMR spectrum of AK6

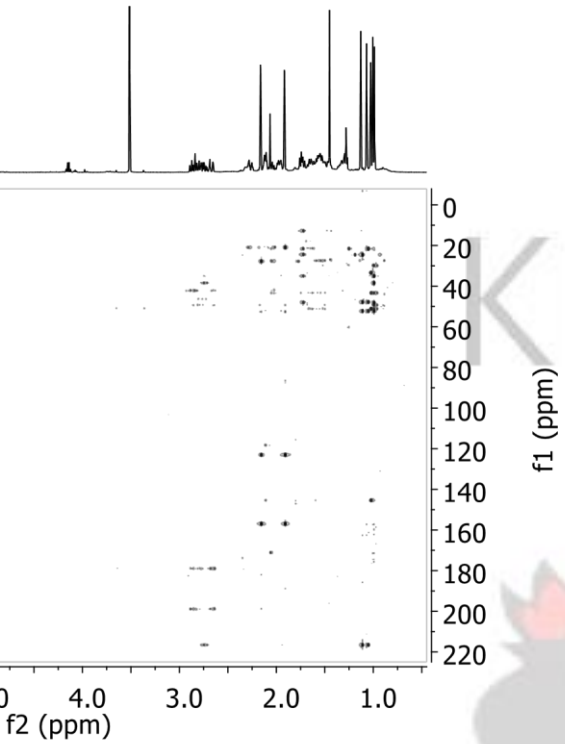

NMR spectrum of AK6

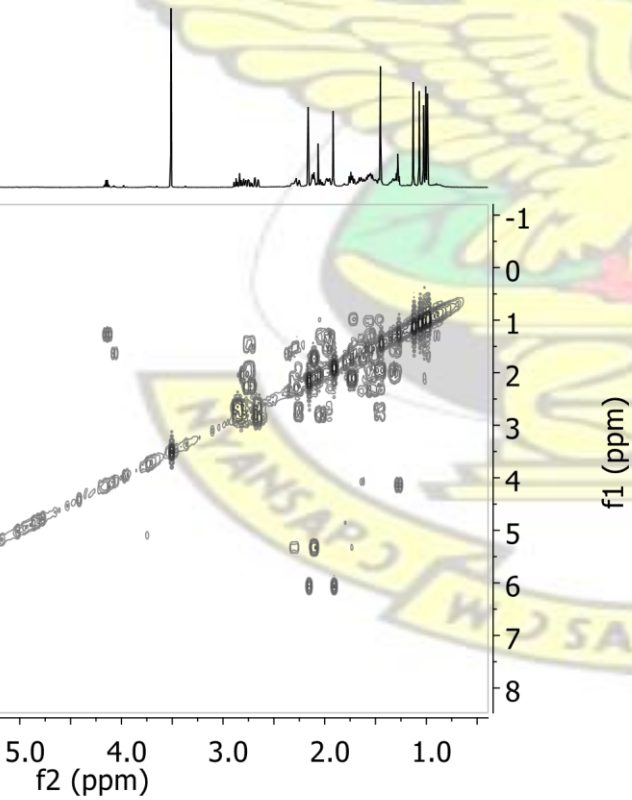

NMR spectrum of AK6

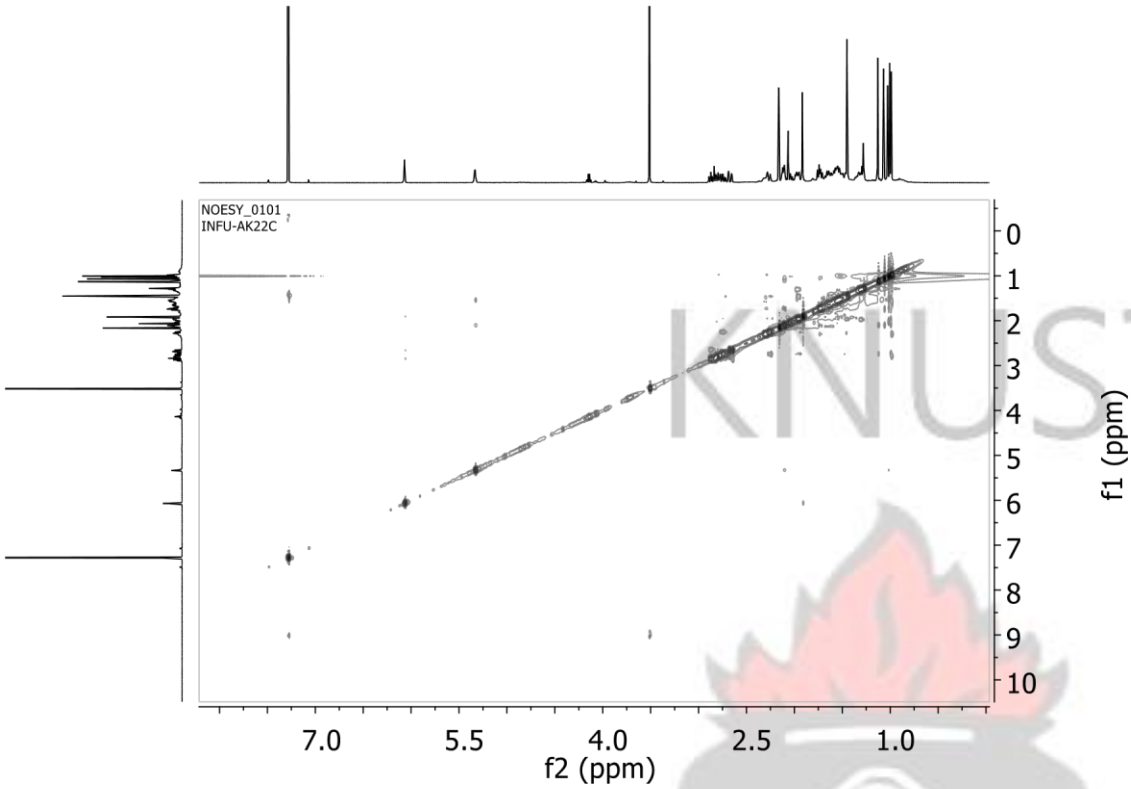

Fig. A-25 NOESY NMR spectrum of AK6

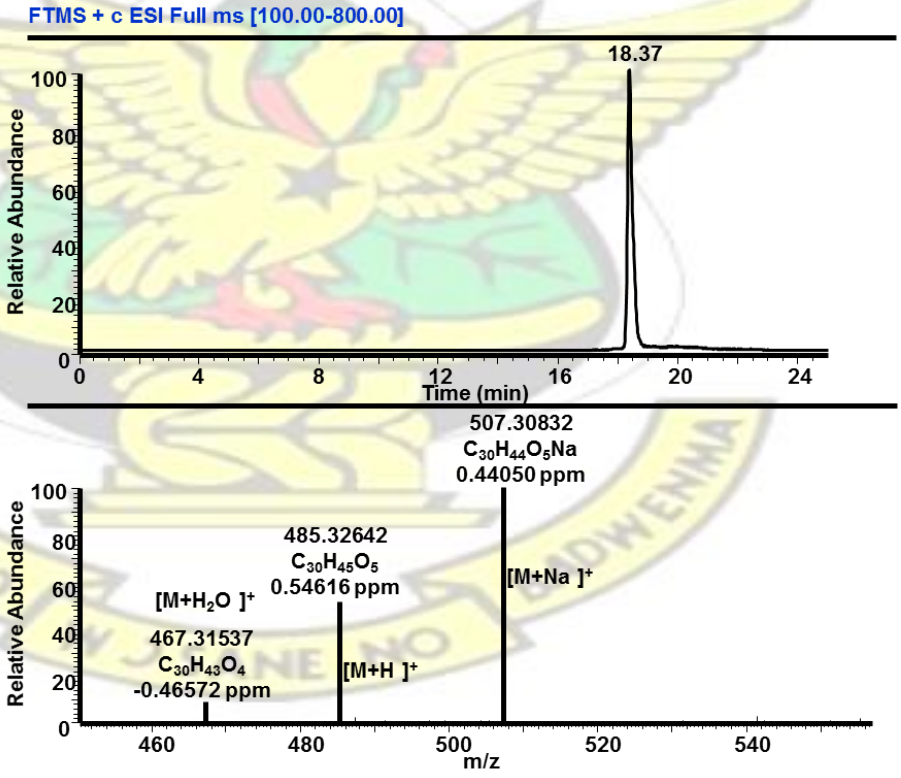

Fig. A-26 Full scan HR-MS spectrum of AK7

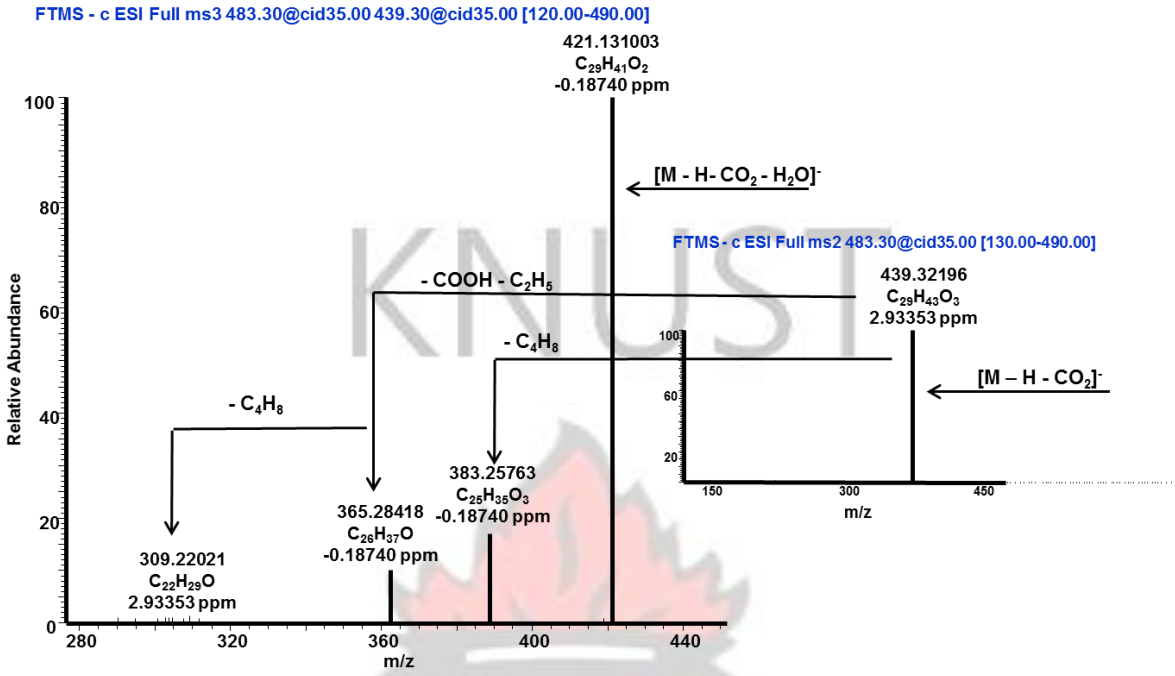

Fig. A-27 HR-MS^2 fragmentation spectrum of AK7

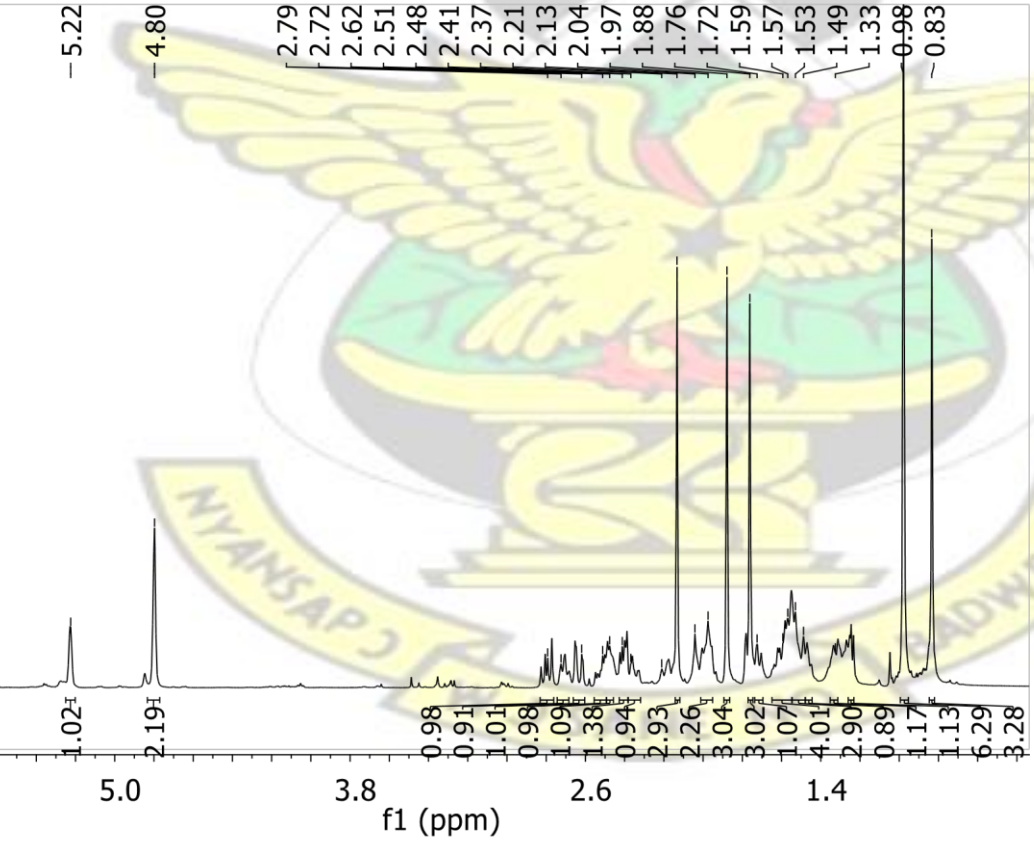

Fig. A-28 ^{1}H NMR spectrum of AK7

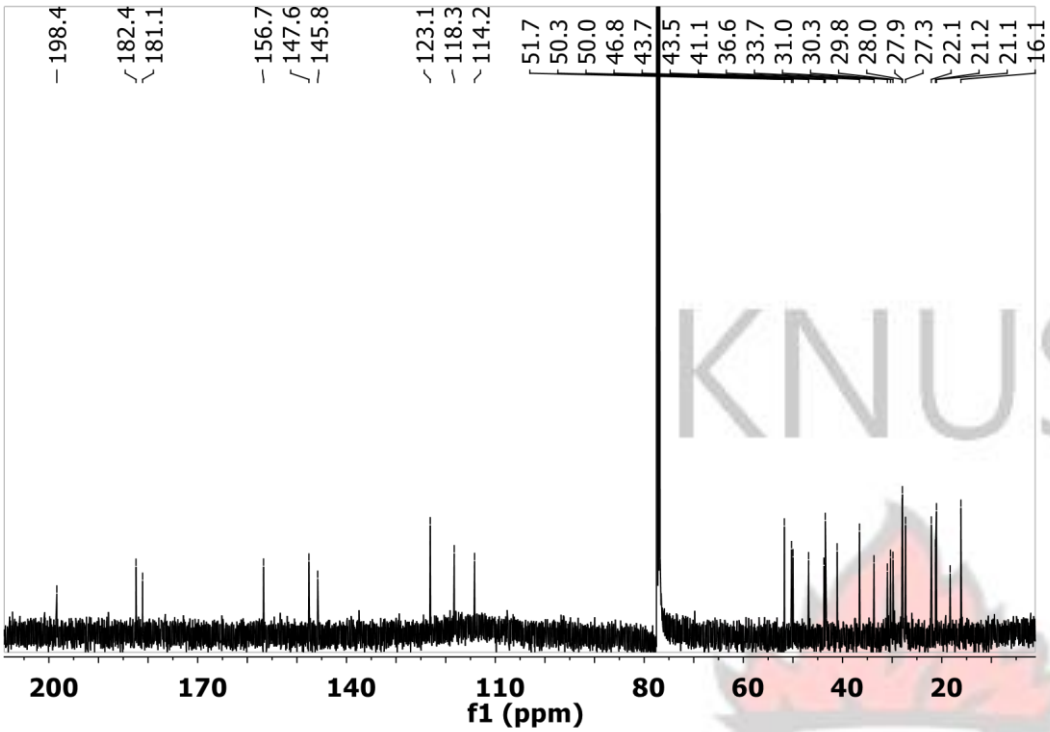

Fig. A-29 ^{13}C NMR spectrum of AK7

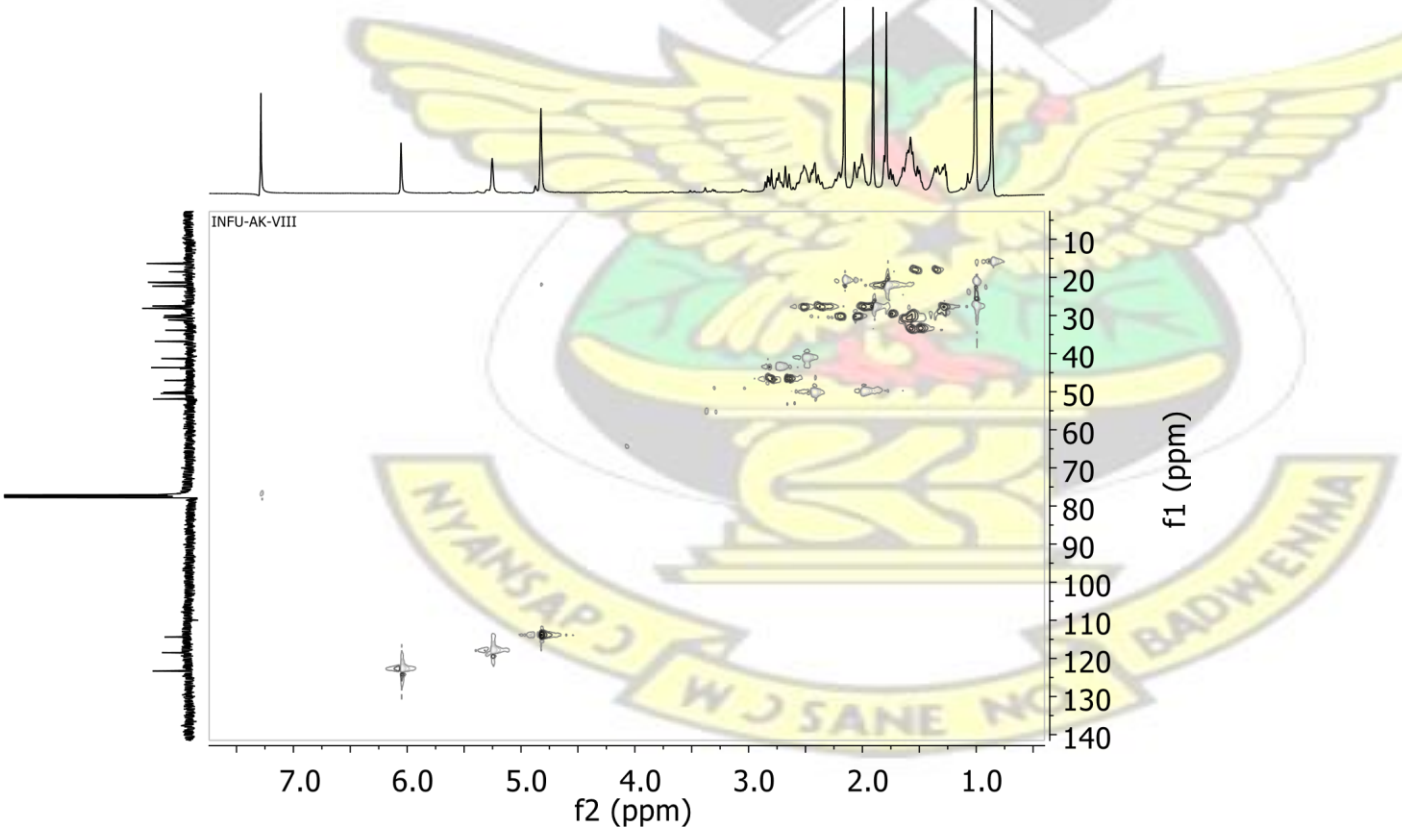

Fig. A-30 HSQC NMR spectrum of AK7

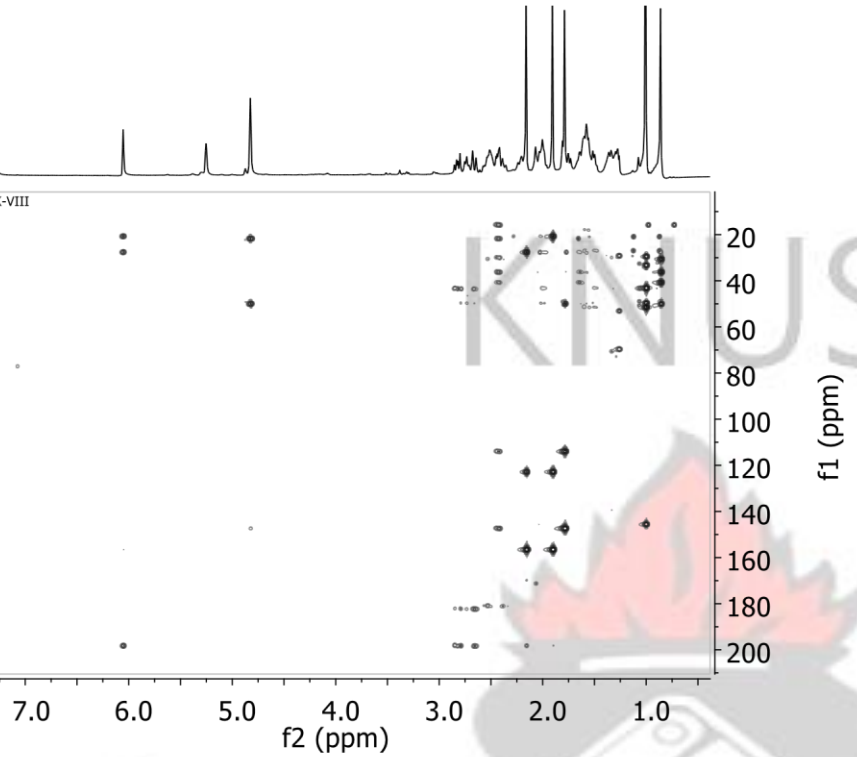

Fig. A-31 HMBC NMR spectrum of AK7

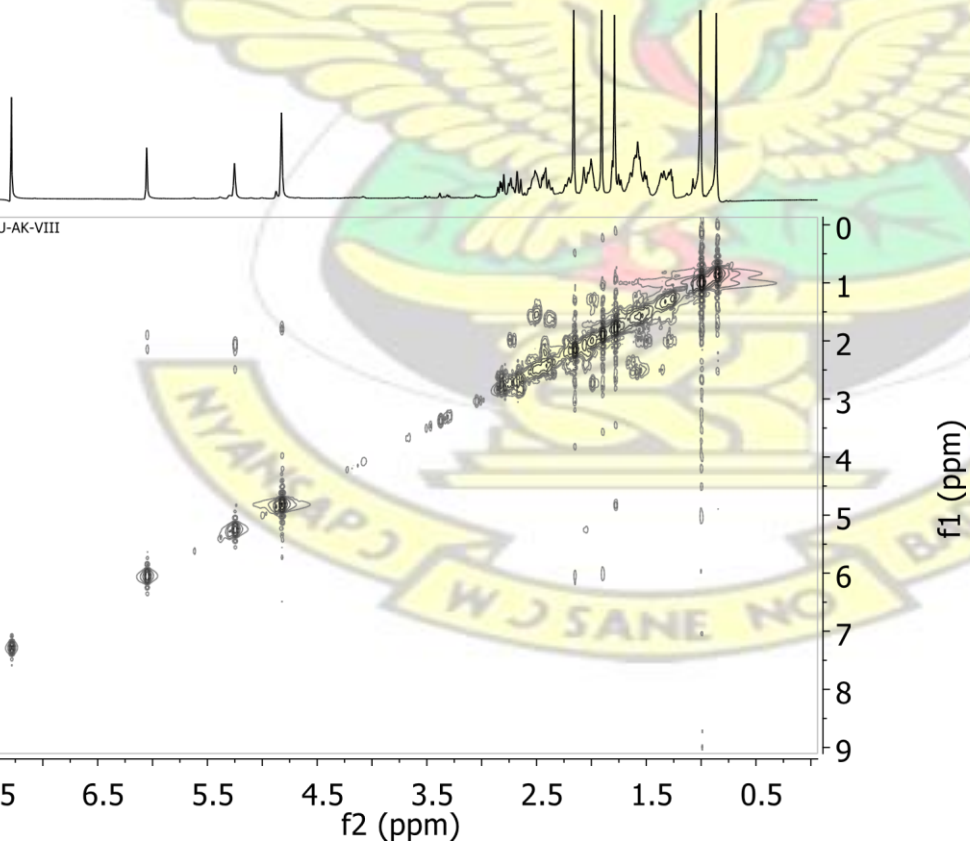

Fig. A-32 COSY NMR spectrum of AK7

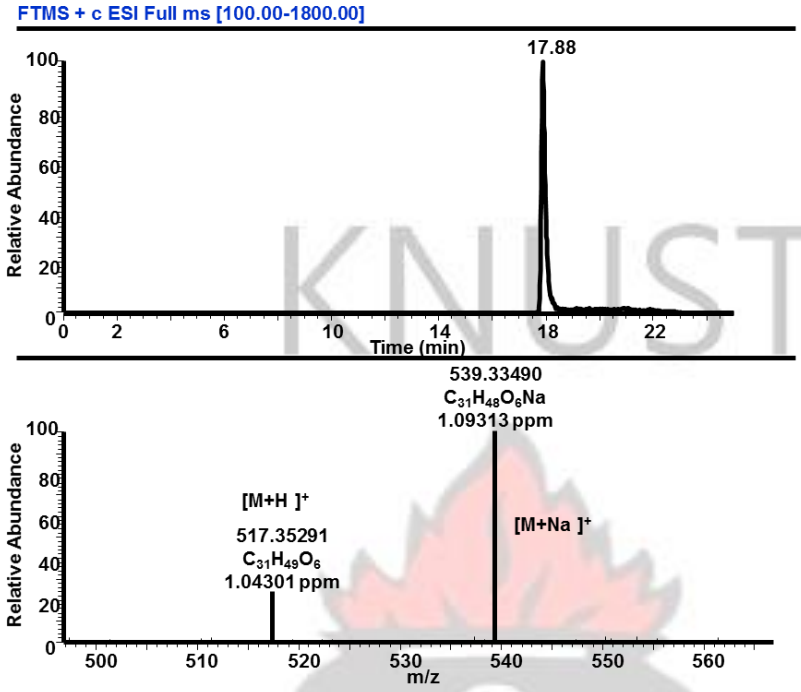

Fig. A-33 Full scan HR-MS spectrum of AK8

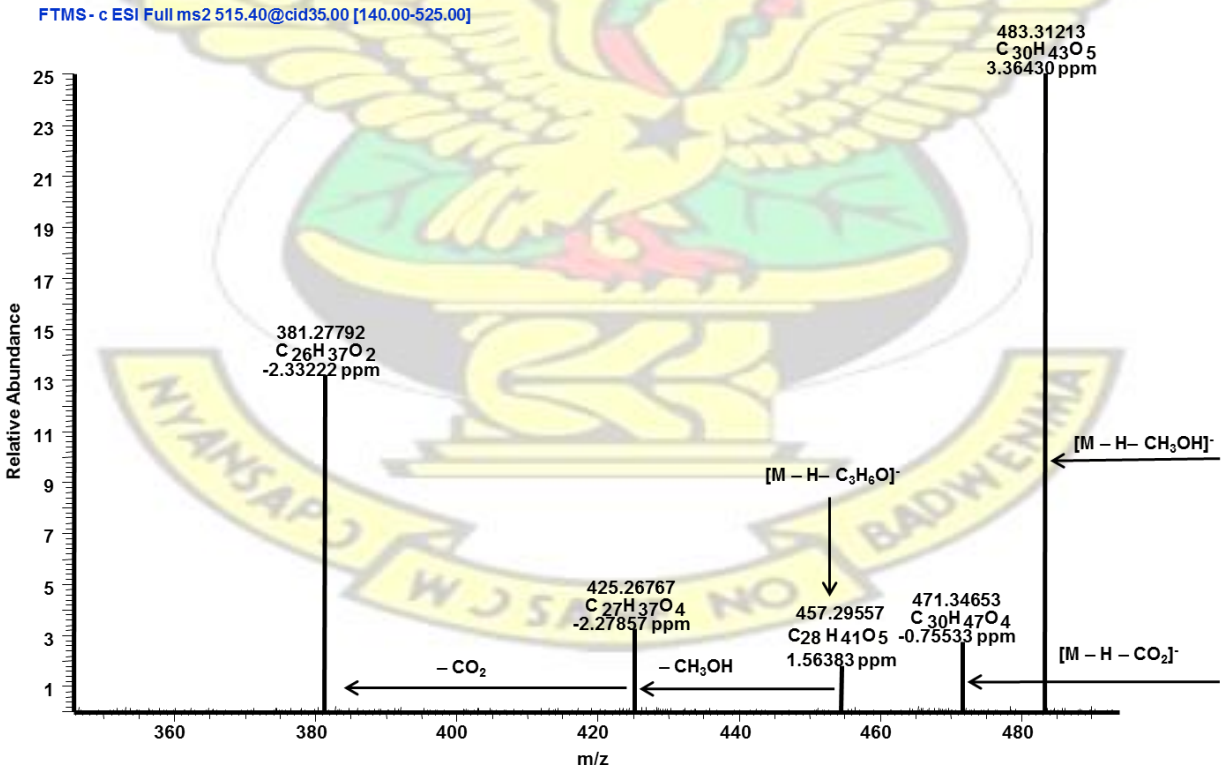

Fig. A-34 HR-MS^2 fragmentation spectrum of AK8

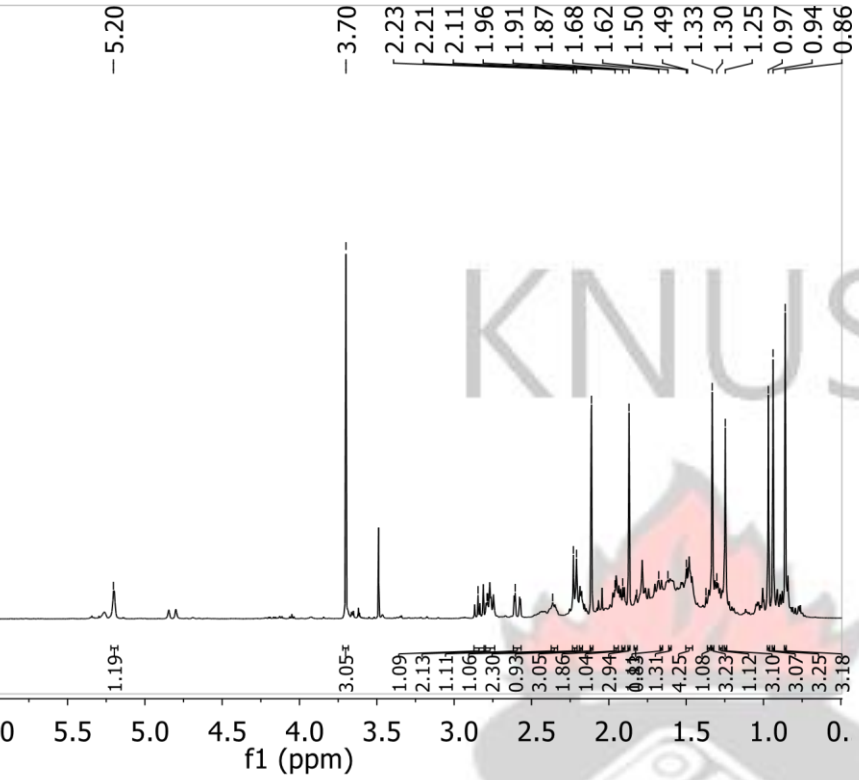

Fig. A-35 ^{1}H NMR spectrum of AK8

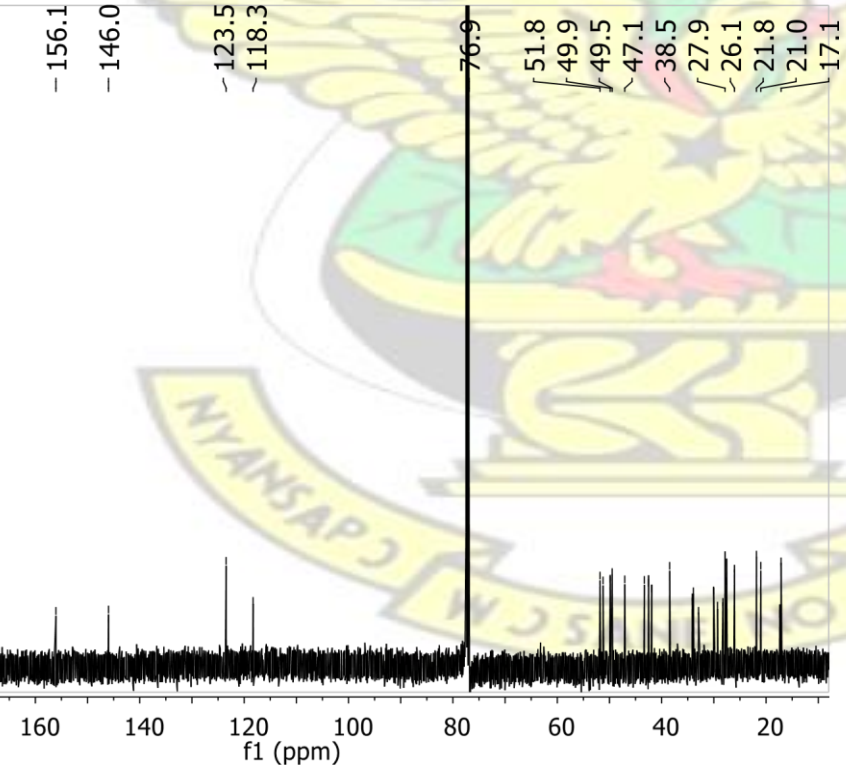

Fig. A-36 ^{13}C NMR spectrum of AK8

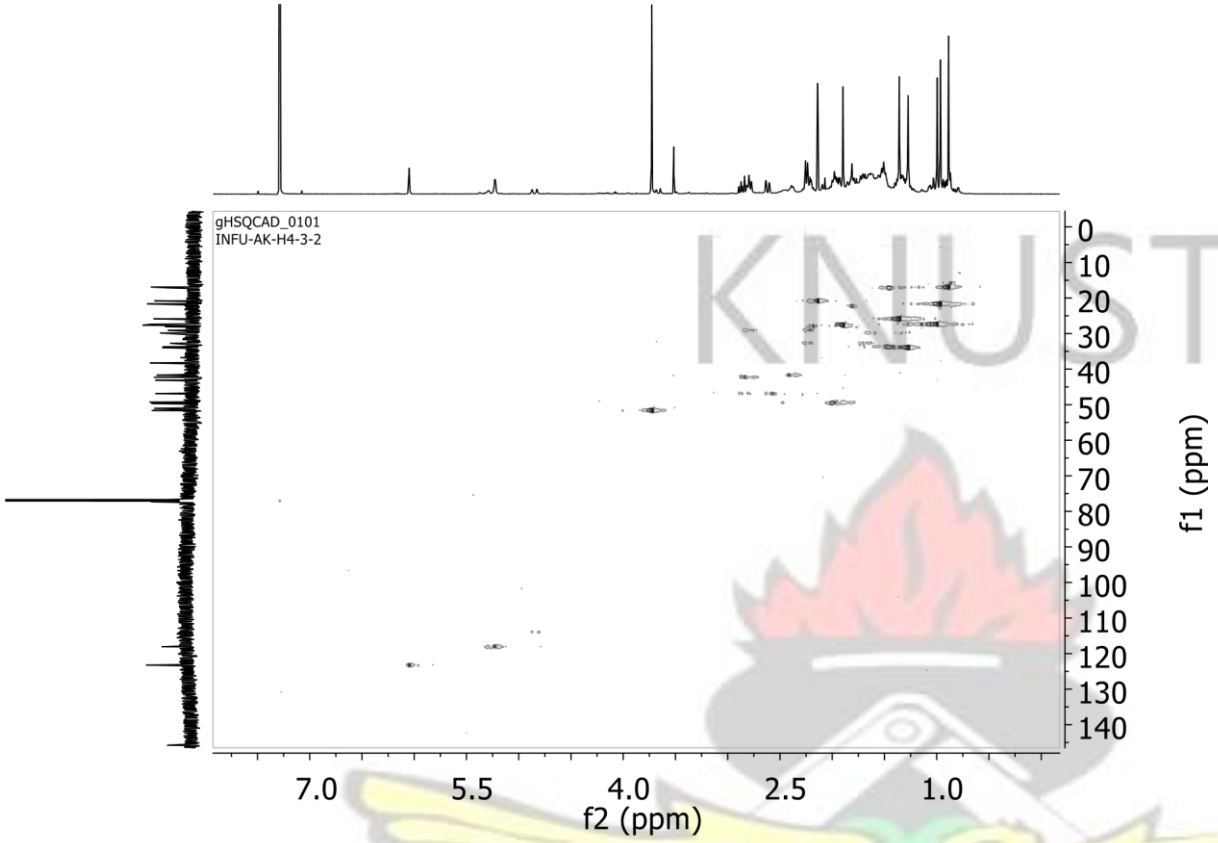

Fig. A-37 HSQC NMR spectrum of AK8

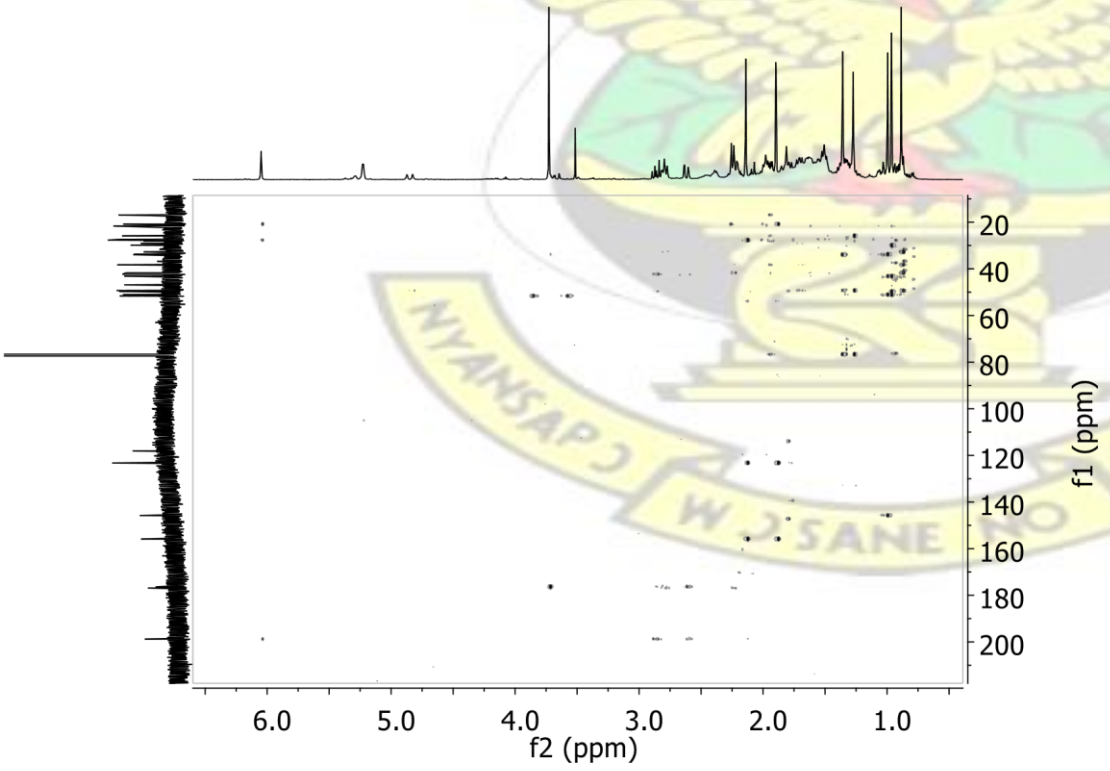

Fig. A-38 HMBC NMR spectrum of AK8

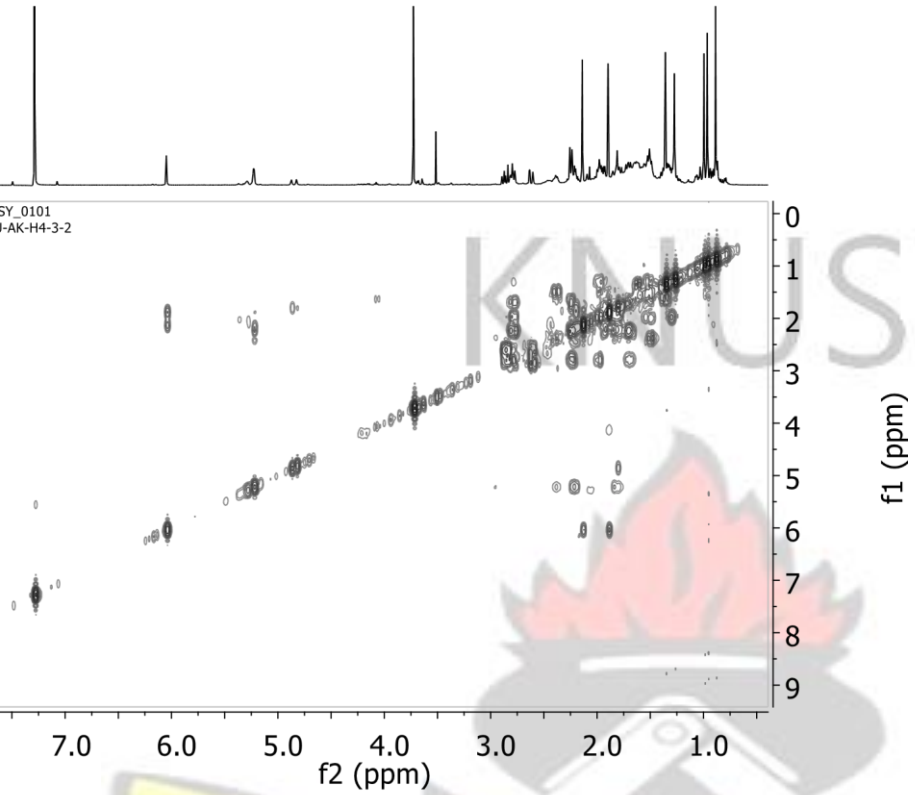

Fig. A-39 COSY NMR spectrum of AK8

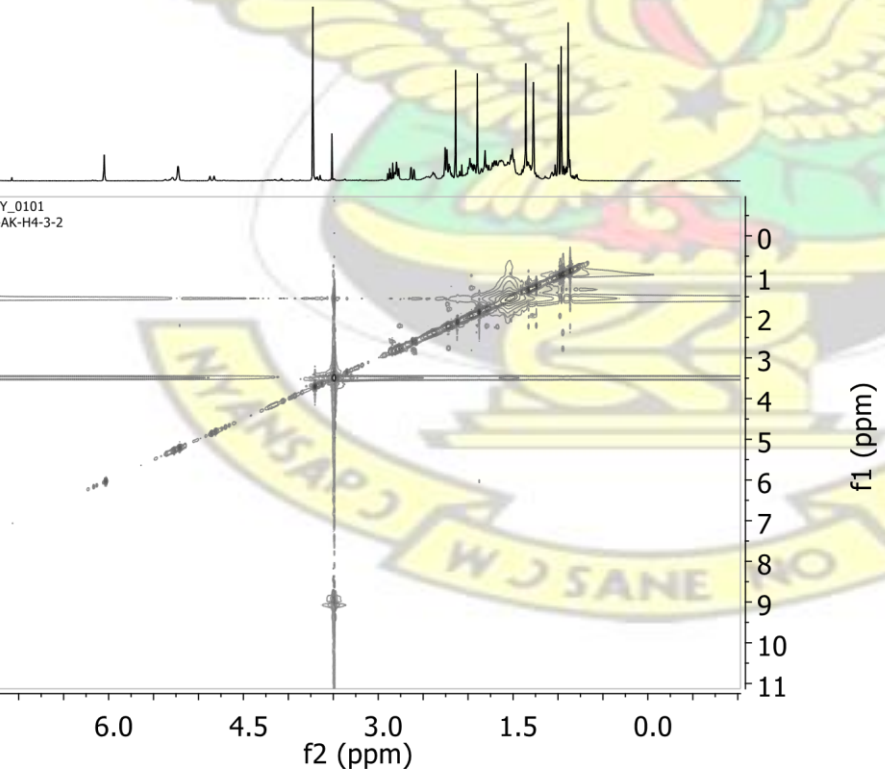

Fig. A-40 NOESY NMR spectrum of AK8

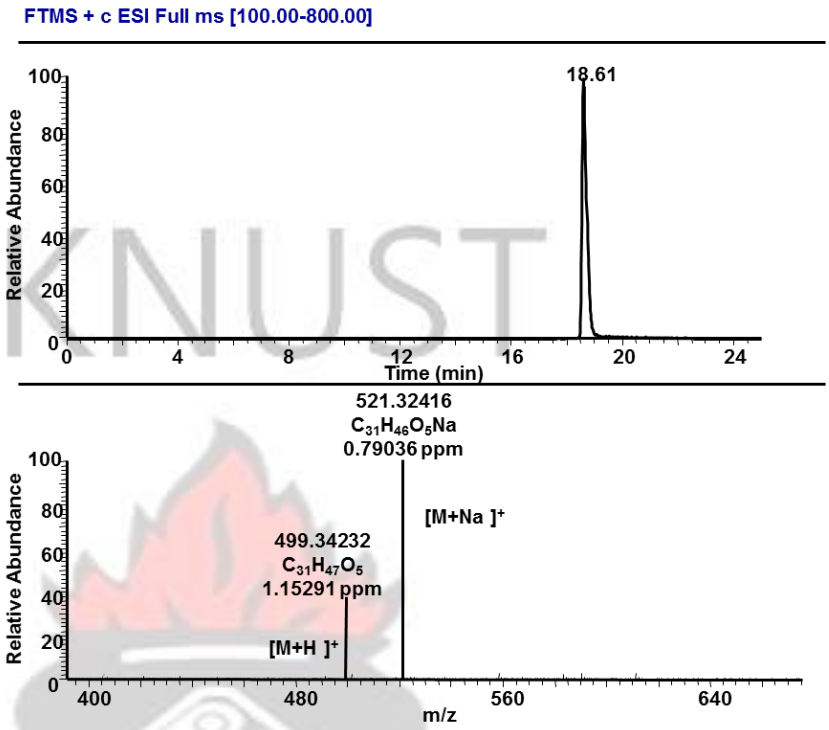

Fig. A-41 Full scan HR-MS spectrum of AK9

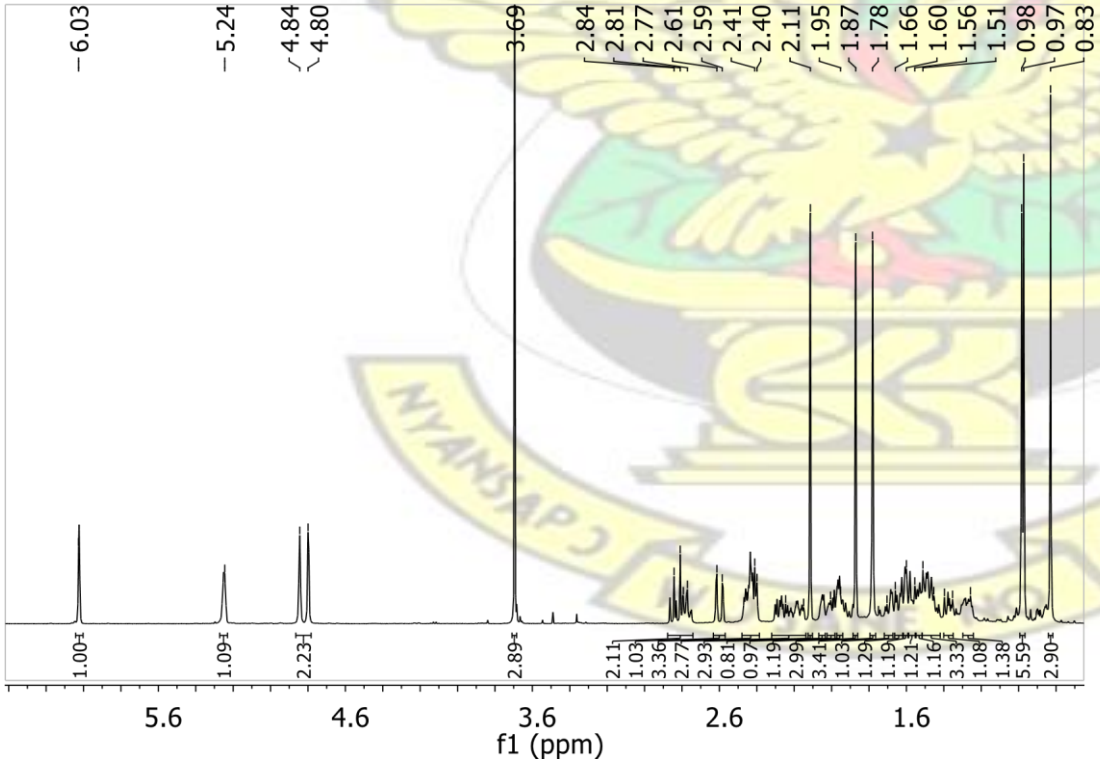

Fig. A-42 ^{1}H NMR spectrum of AK9

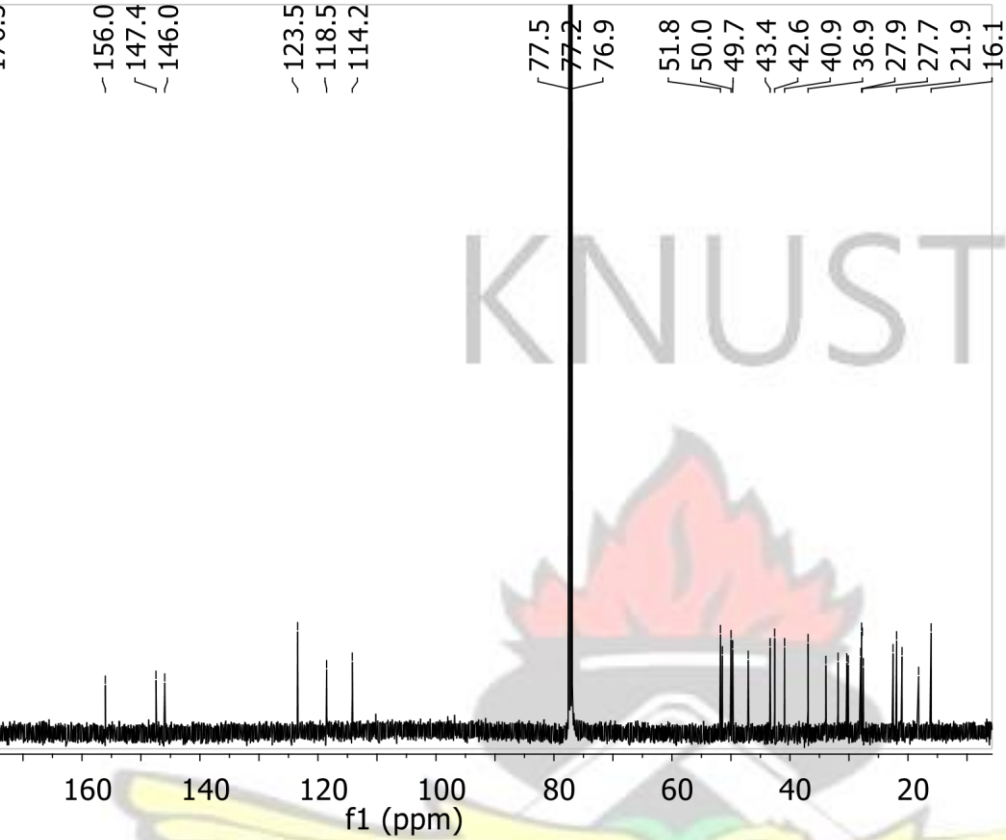

Fig. A-43 ^{13}C NMR spectrum of AK9

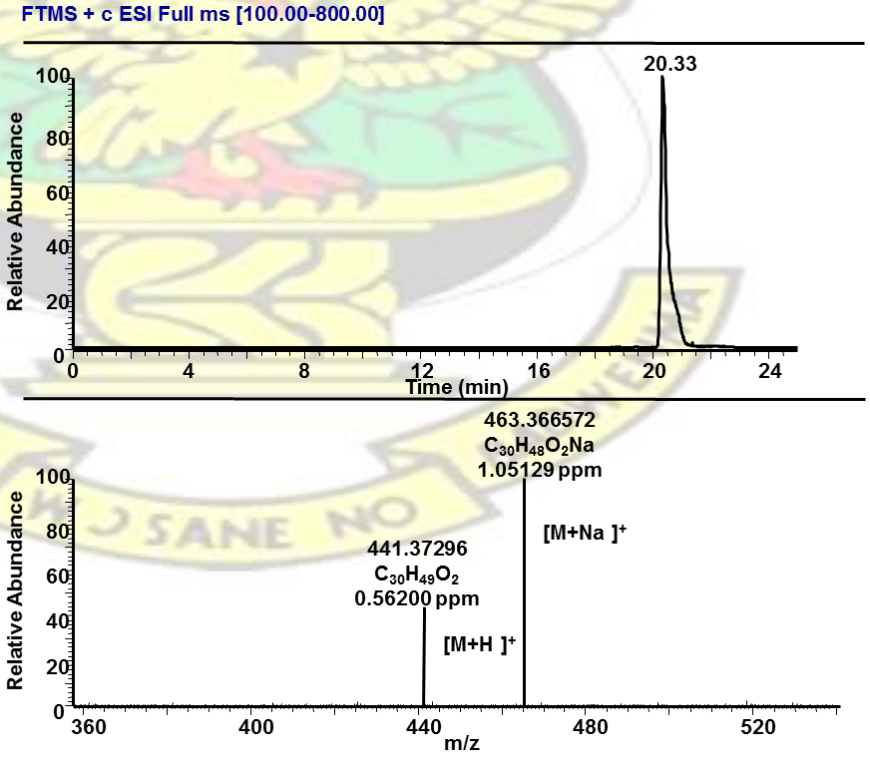

Fig. A-44 Full scan HR-MS spectrum of AK10

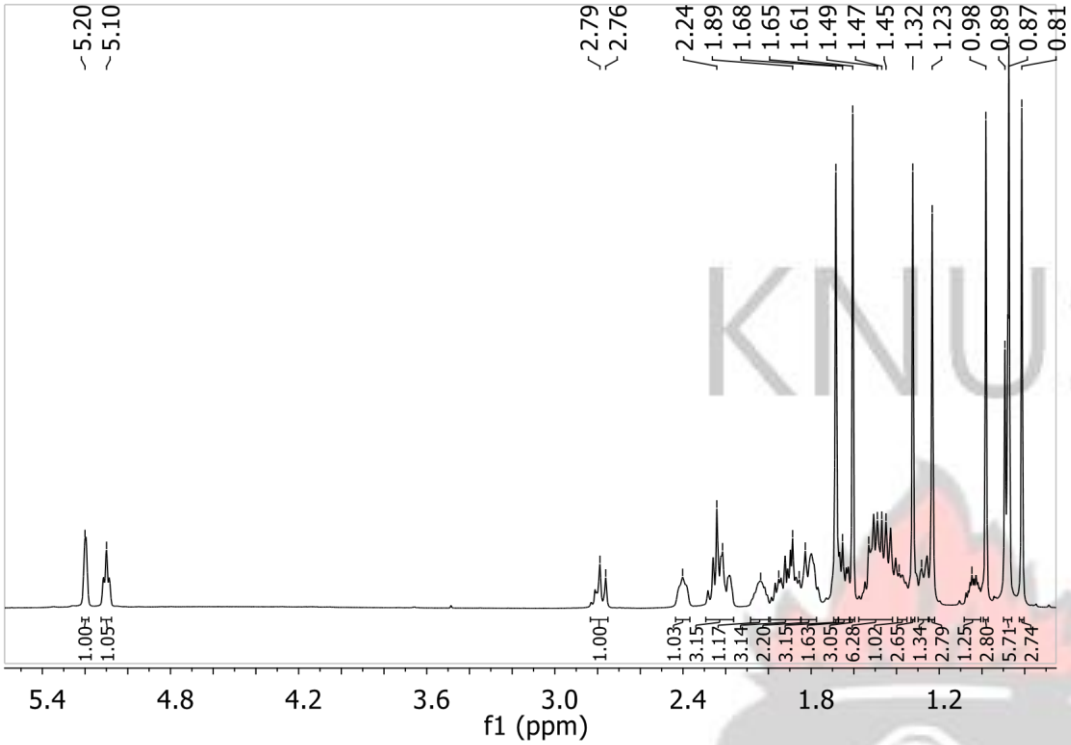

Fig. A-45 ^{1}H NMR spectrum of AK10

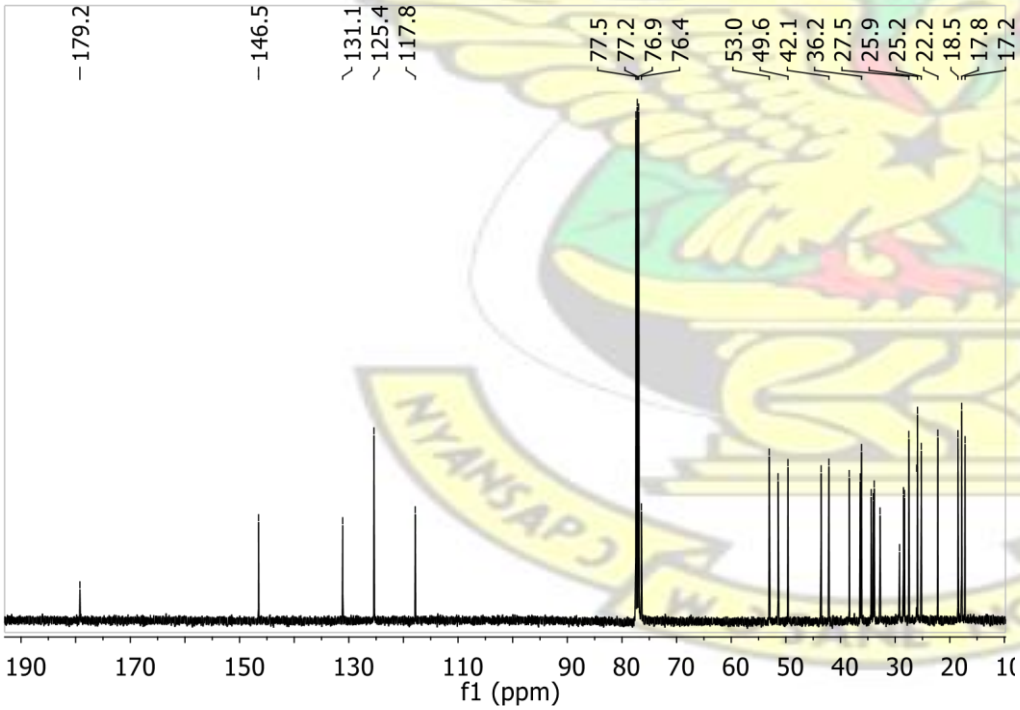

Fig. A-46 ^{13}C NMR spectrum of AK10

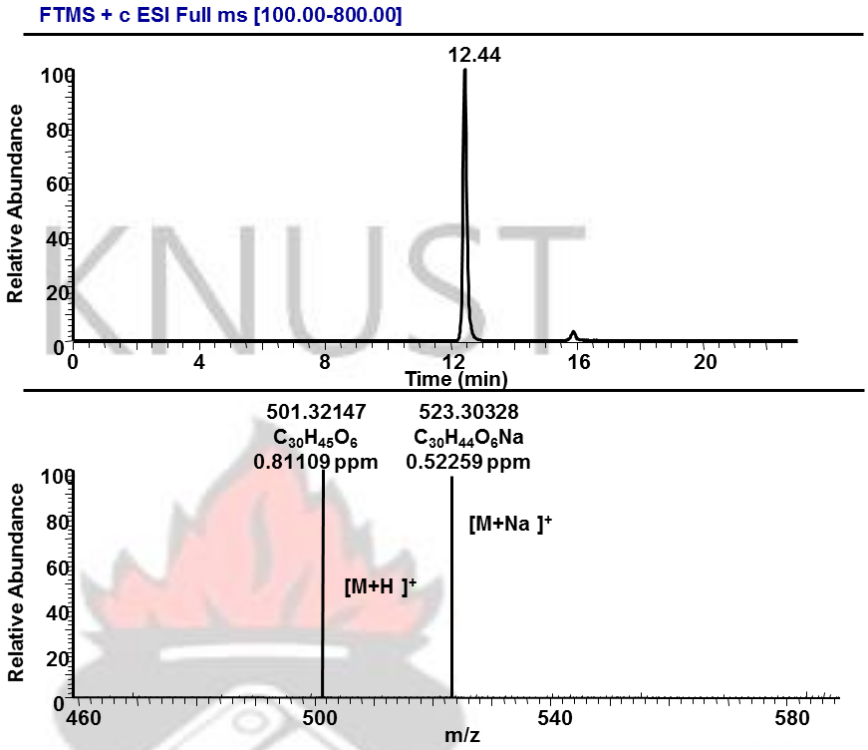

Fig. A-47 Full scan HR-MS spectrum of AK11

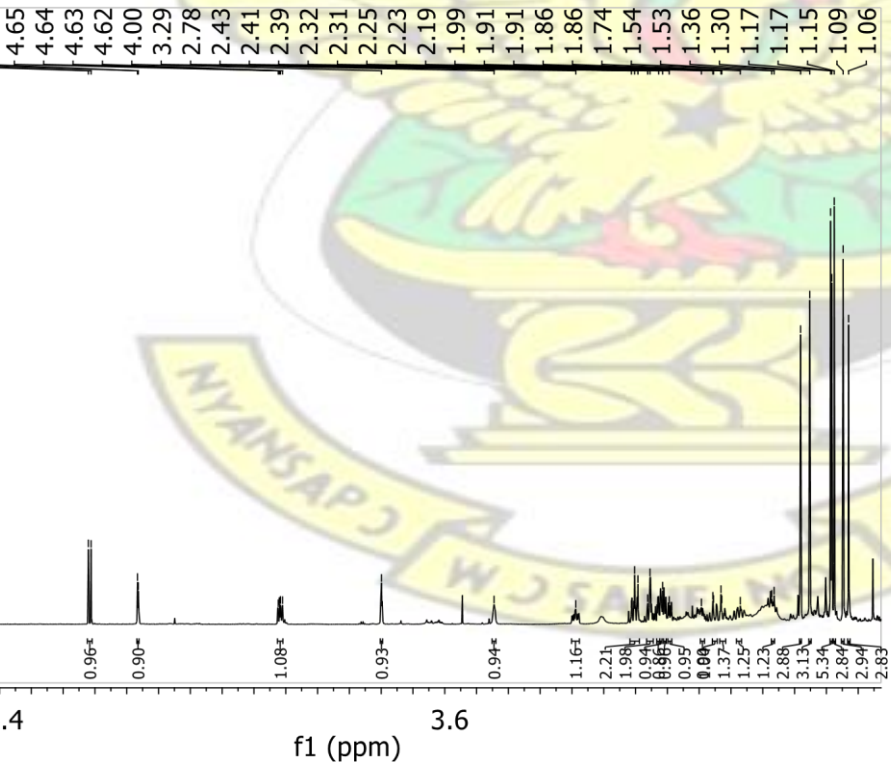

Fig. A-48 ^{1}H NMR spectrum of AK11

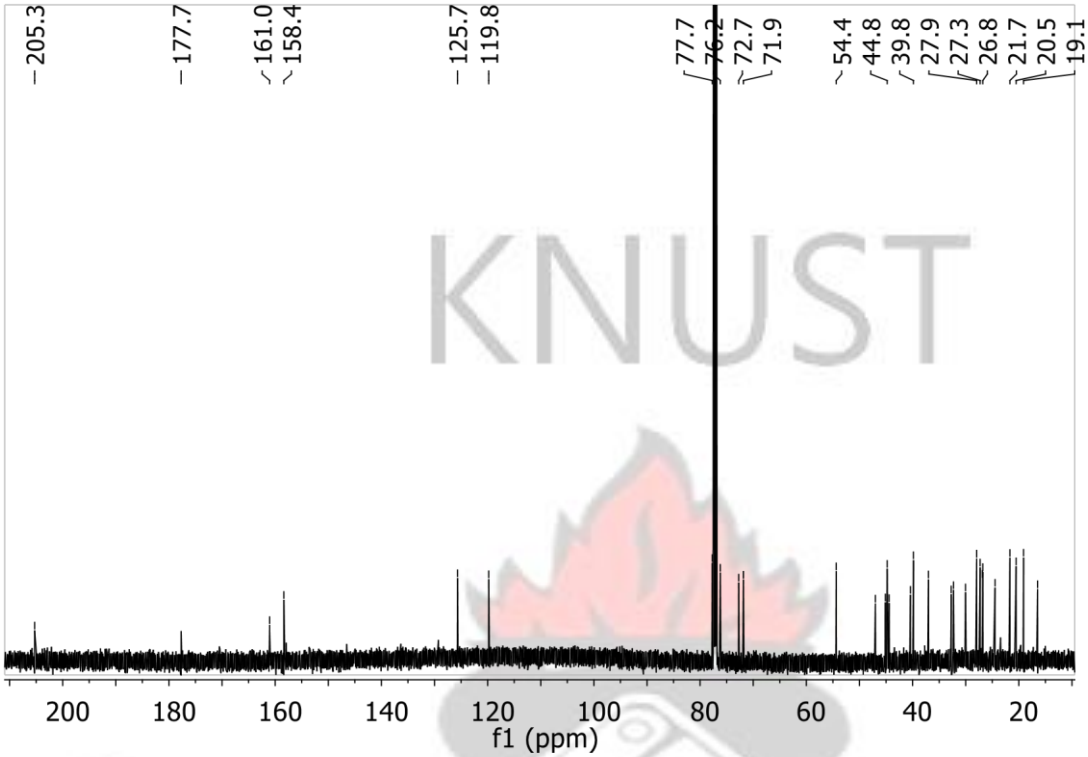

Fig. A-49 ^{13}C NMR spectrum of AK11 (125 MHz)

APPENDIX B

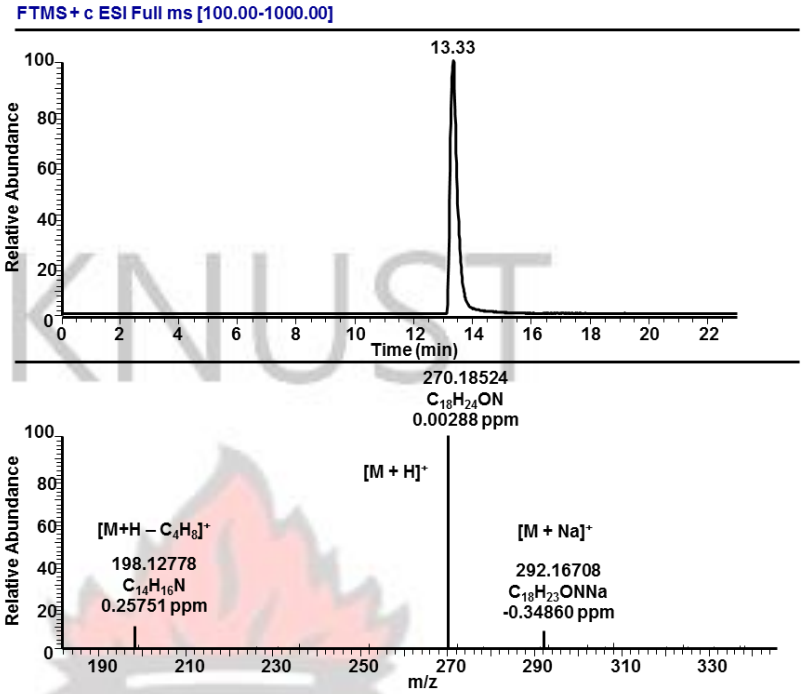

Fig. B-1 ull scan H M spectrum of HM1

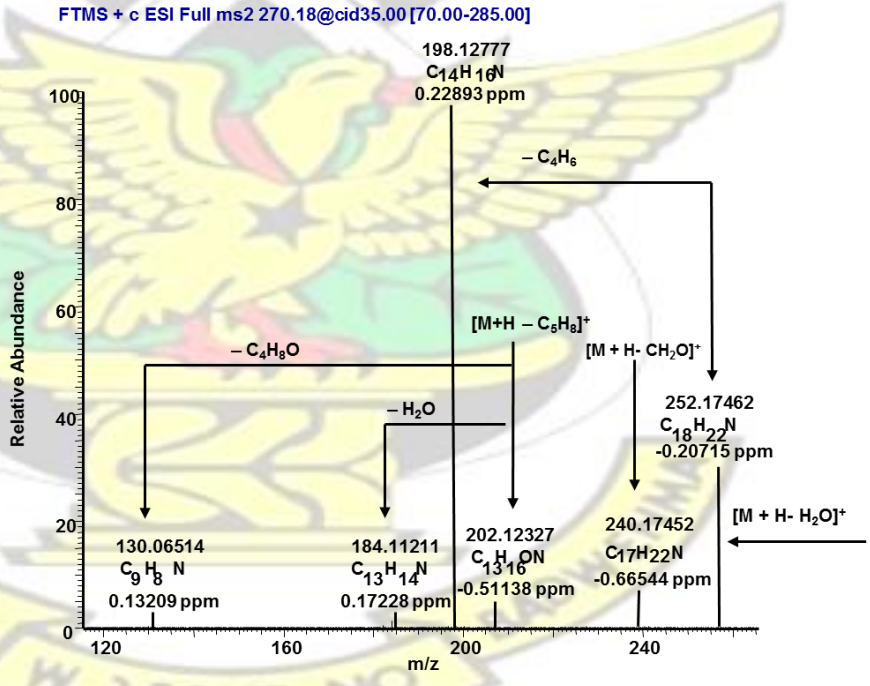

Fig. B-2 H M ^{2} fragmentation spectrum of HM1

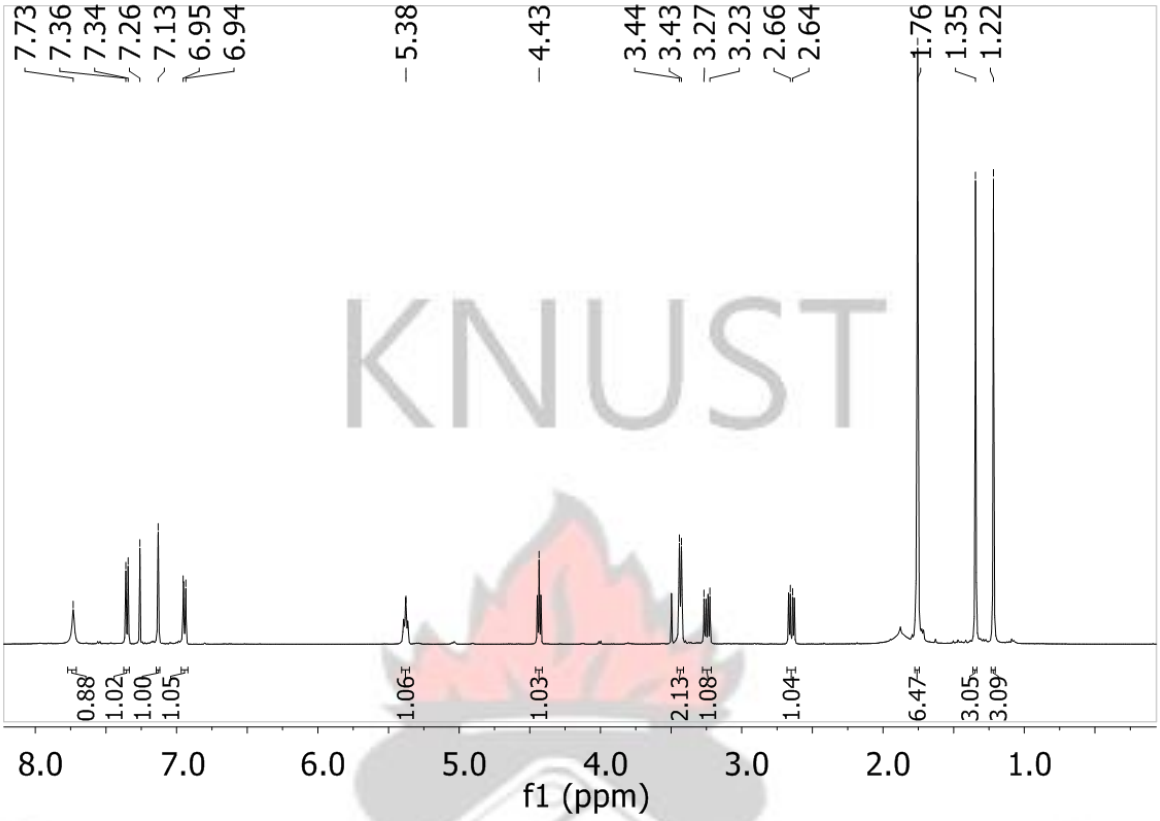

Fig. B-3: ^{1}H NMR spectrum of HM1 (500 MHz; $CDCl_3$)

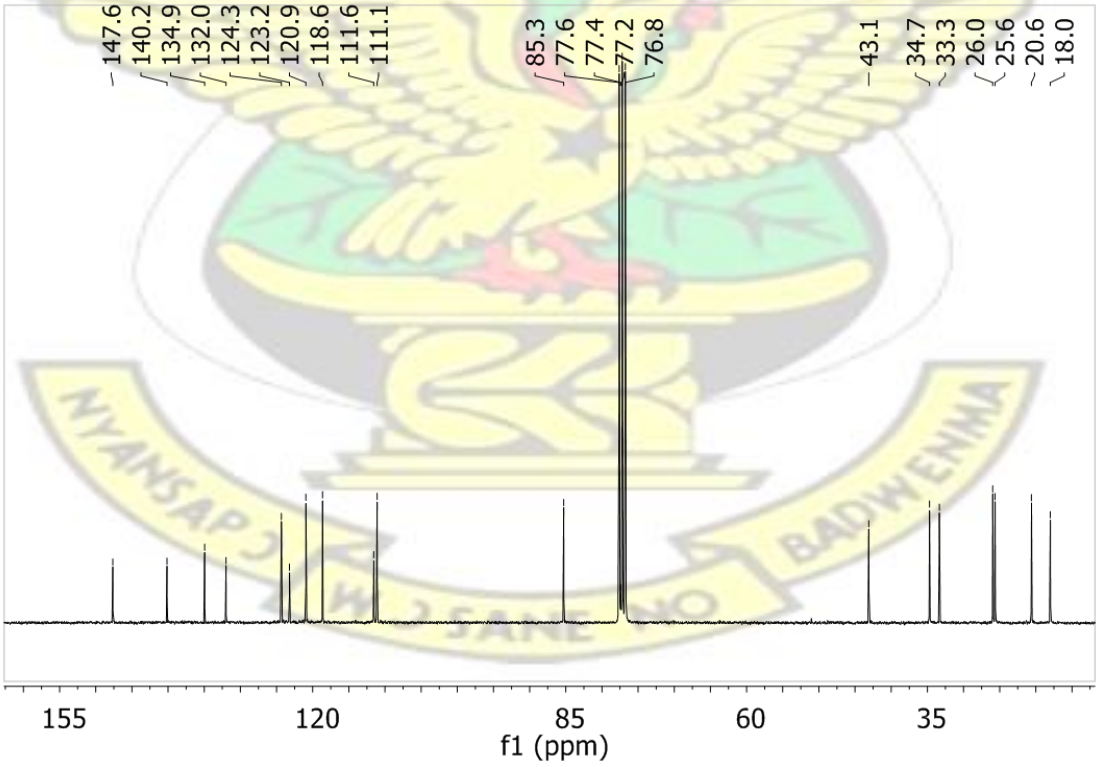

Fig. B-4: ^{13}C NMR spectrum of HM1 (125 MHz; $CDCl_3$)

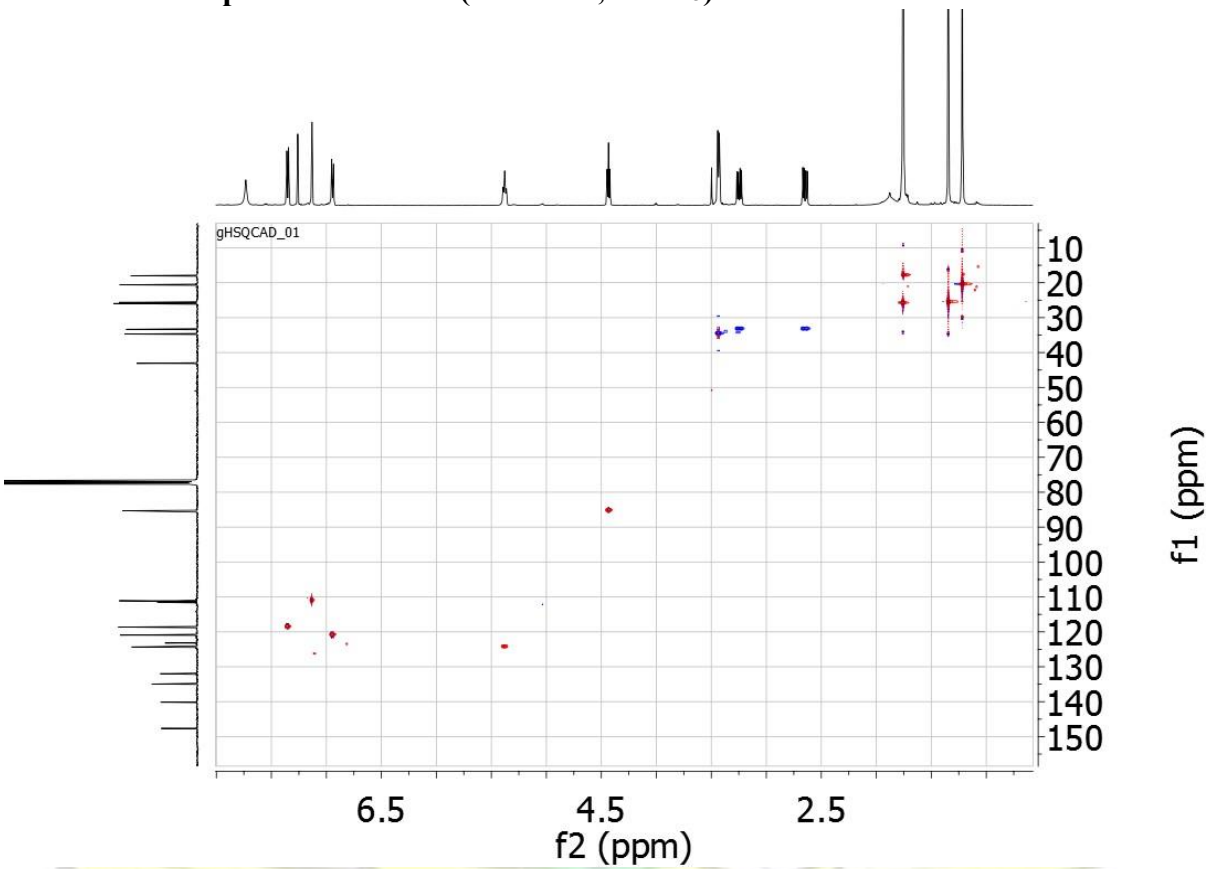

Fig. B-5: HSQC NMR spectrum of HM1 (500 MHz; $CDCl_3$)

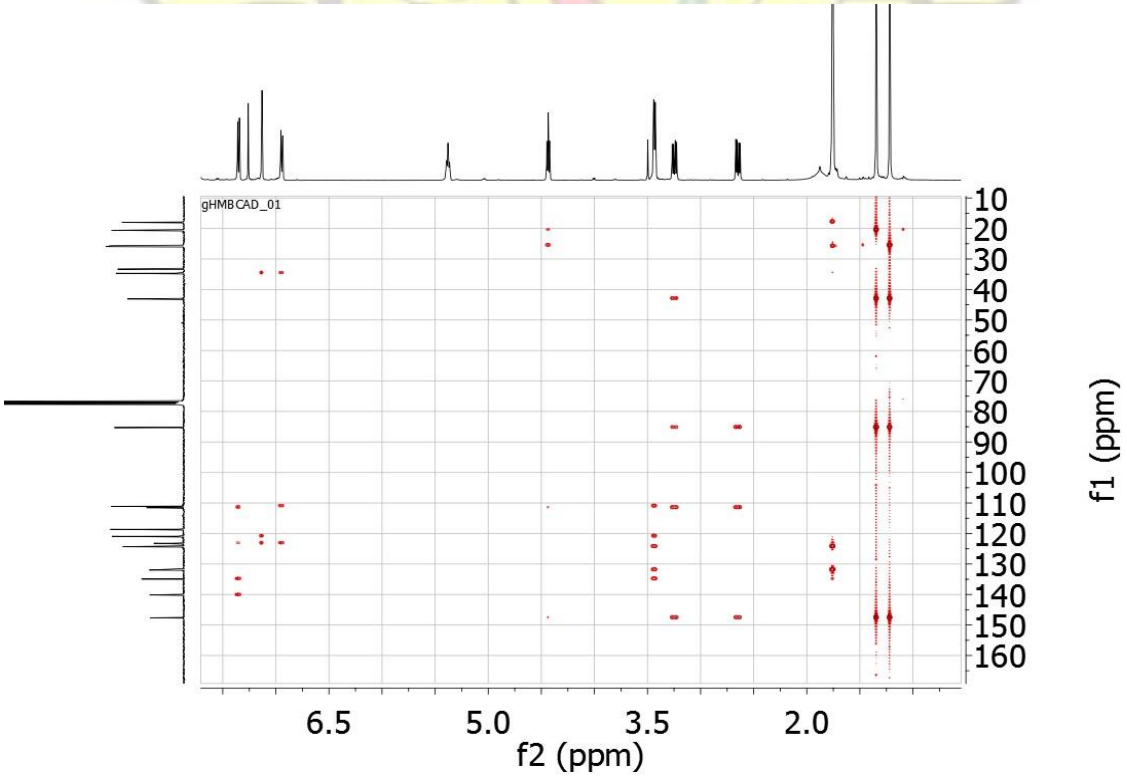

Fig. B-6: HMBC NMR spectrum of HM1 (500 MHz; $CDCl_3$)

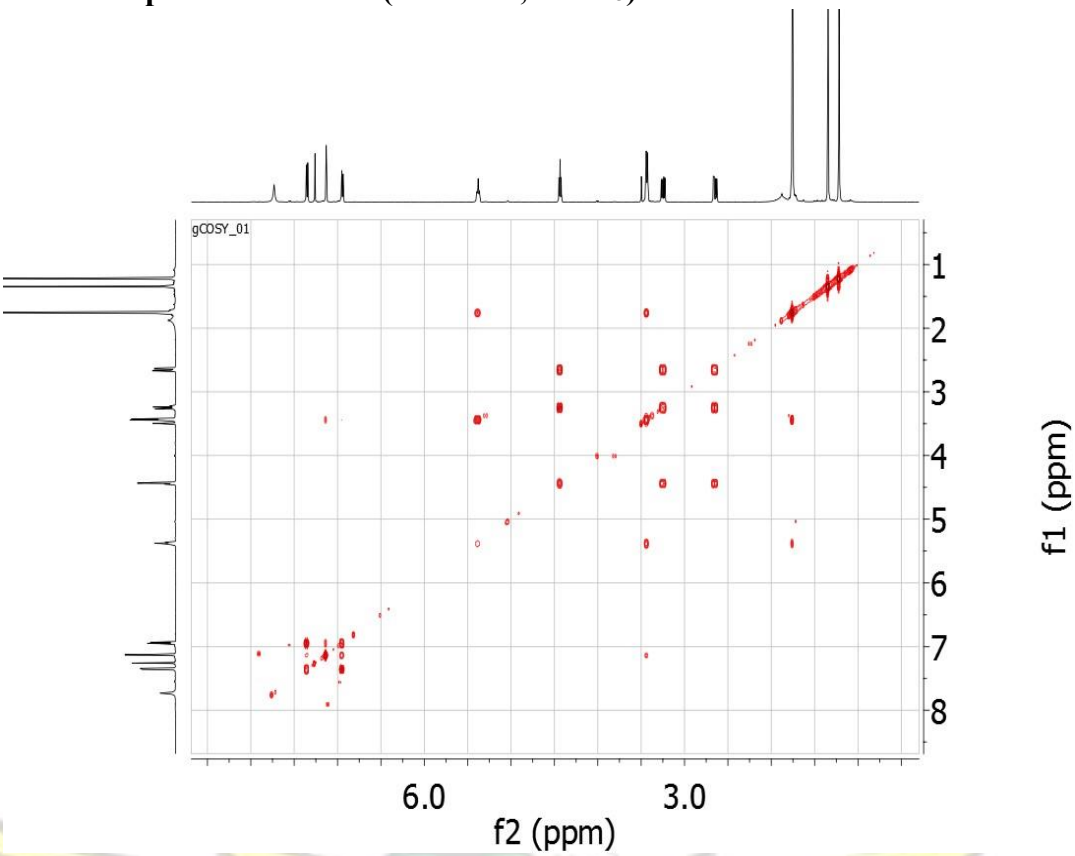

Fig. B-7: COSY NMR spectrum of HM1 (500 MHz; $CDCl_3$)

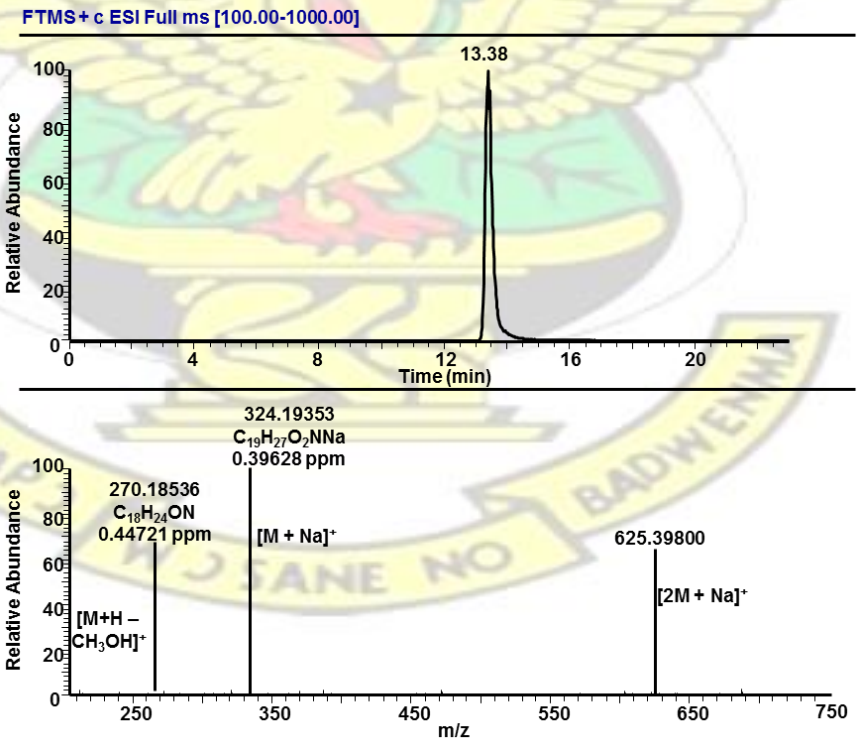

Fig. B-8 ull scan H M spectrum of HM2

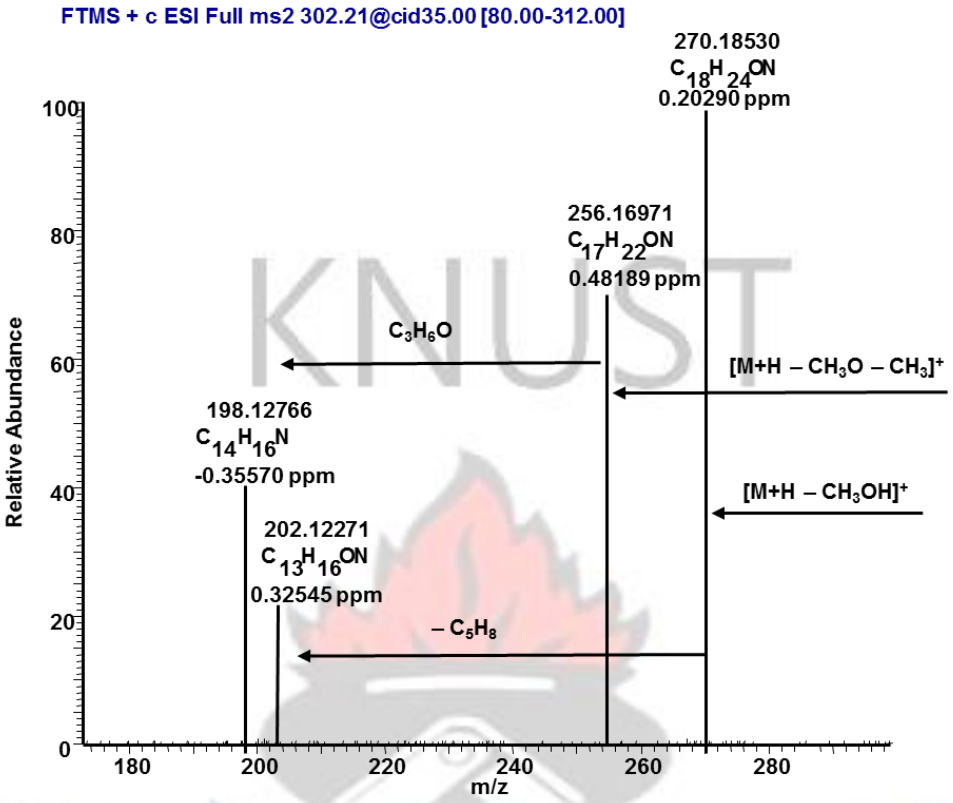

Fig. B-9 HR-ESI-MS^2 fragmentation spectrum of HM2

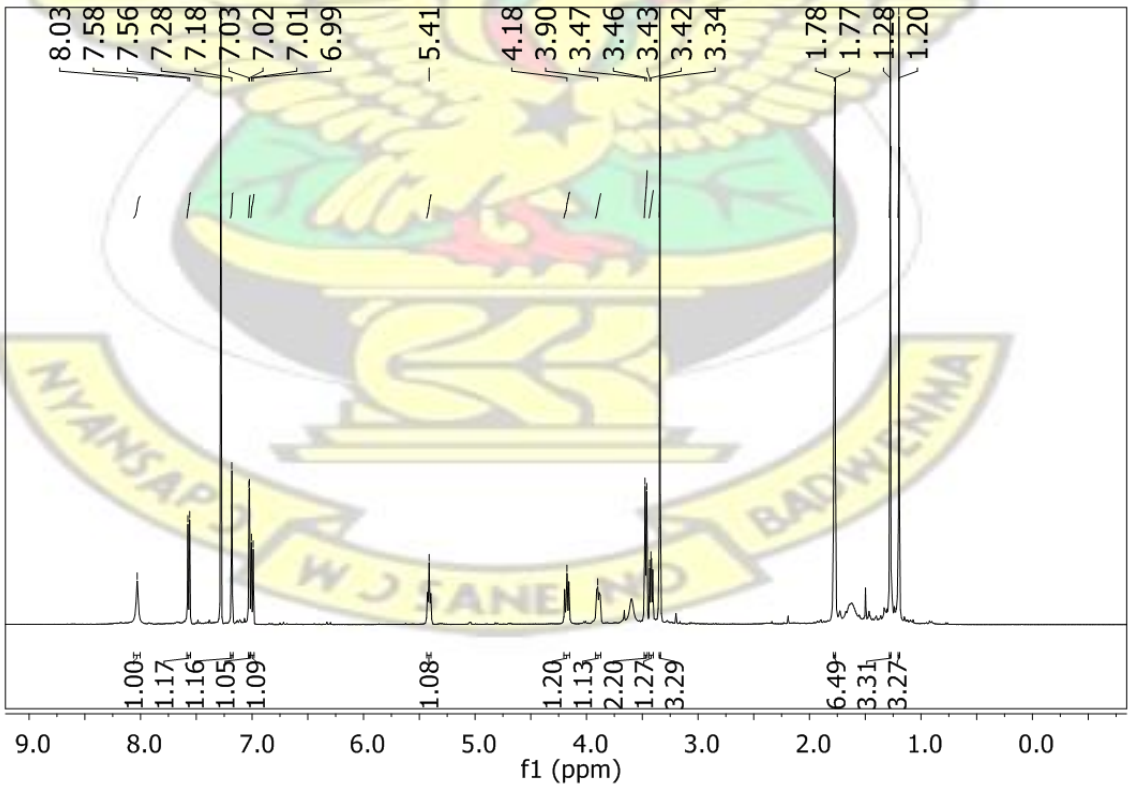

Fig. B-10: ^{1}H NMR spectrum of HM2 (500 MHz; $CDCl_3$)

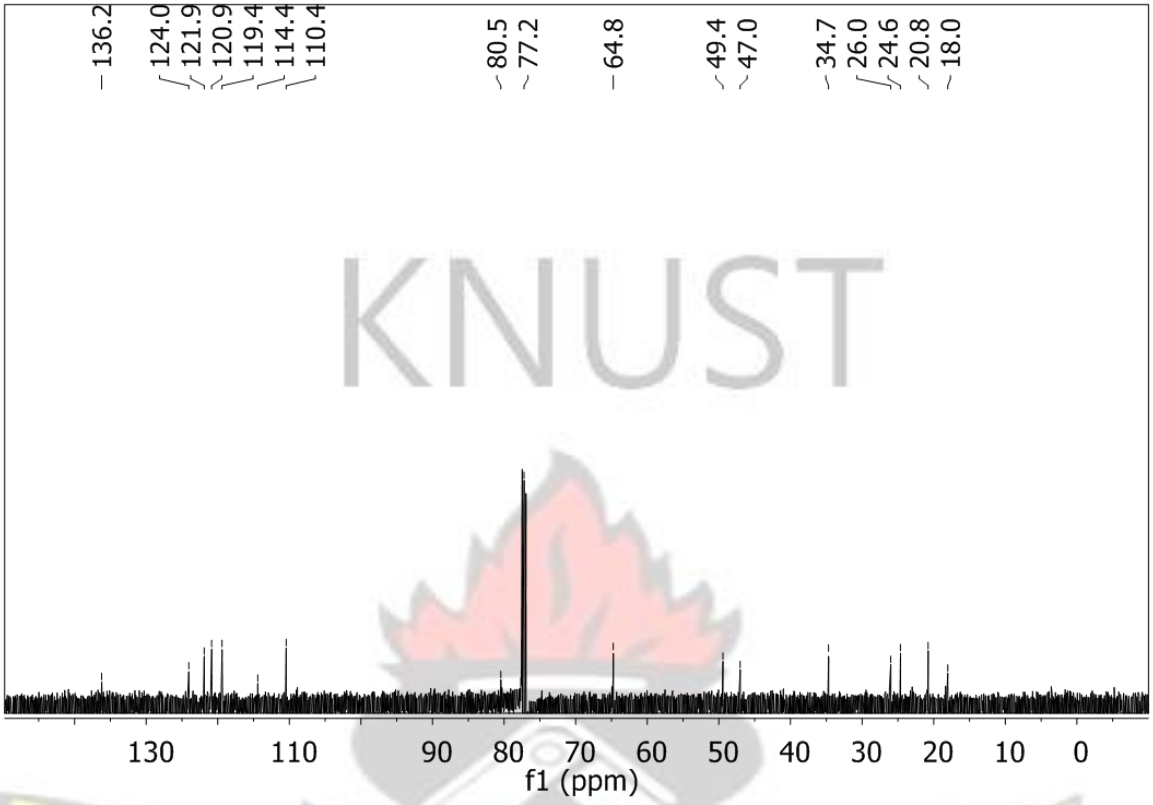

Fig. B-11: ^{13}C NMR spectrum of HM2 (125 MHz; $CDCl_3$)

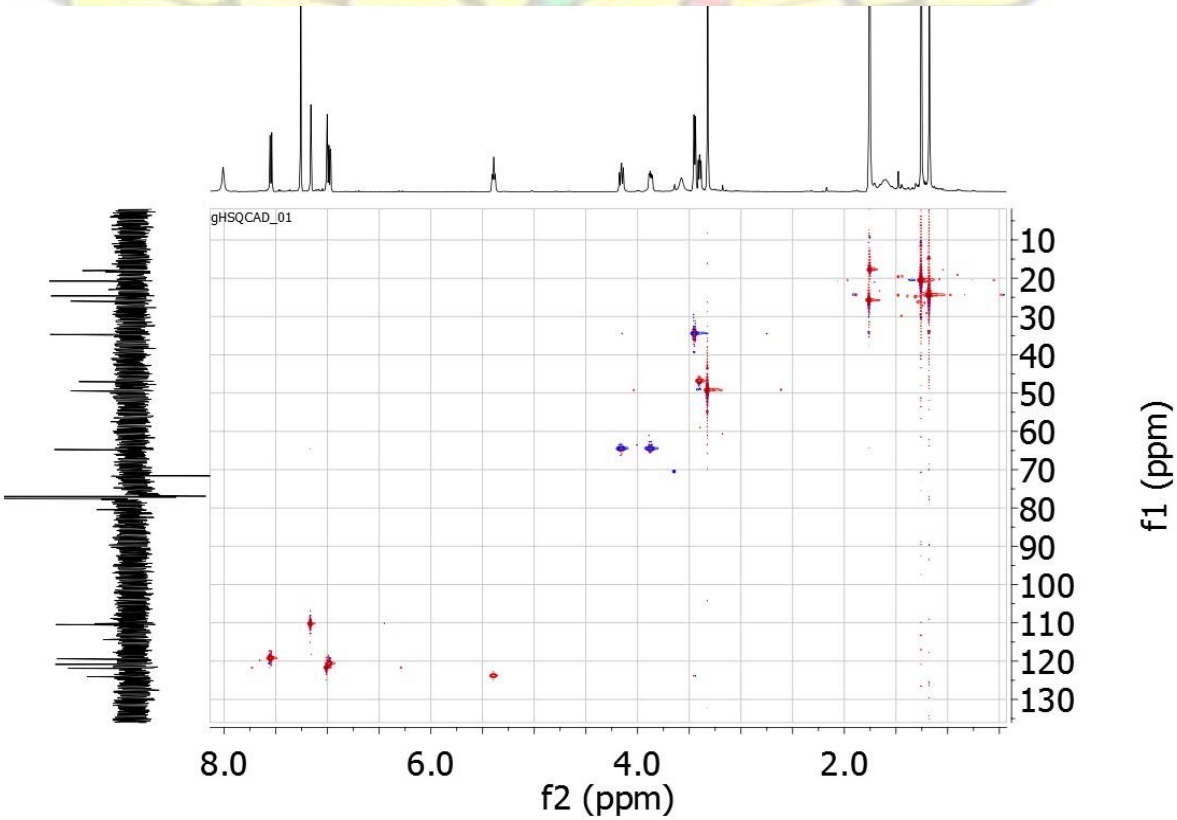

Fig. B-12: HSQC NMR spectrum of HM2 (500 MHz; $CDCl_3$)

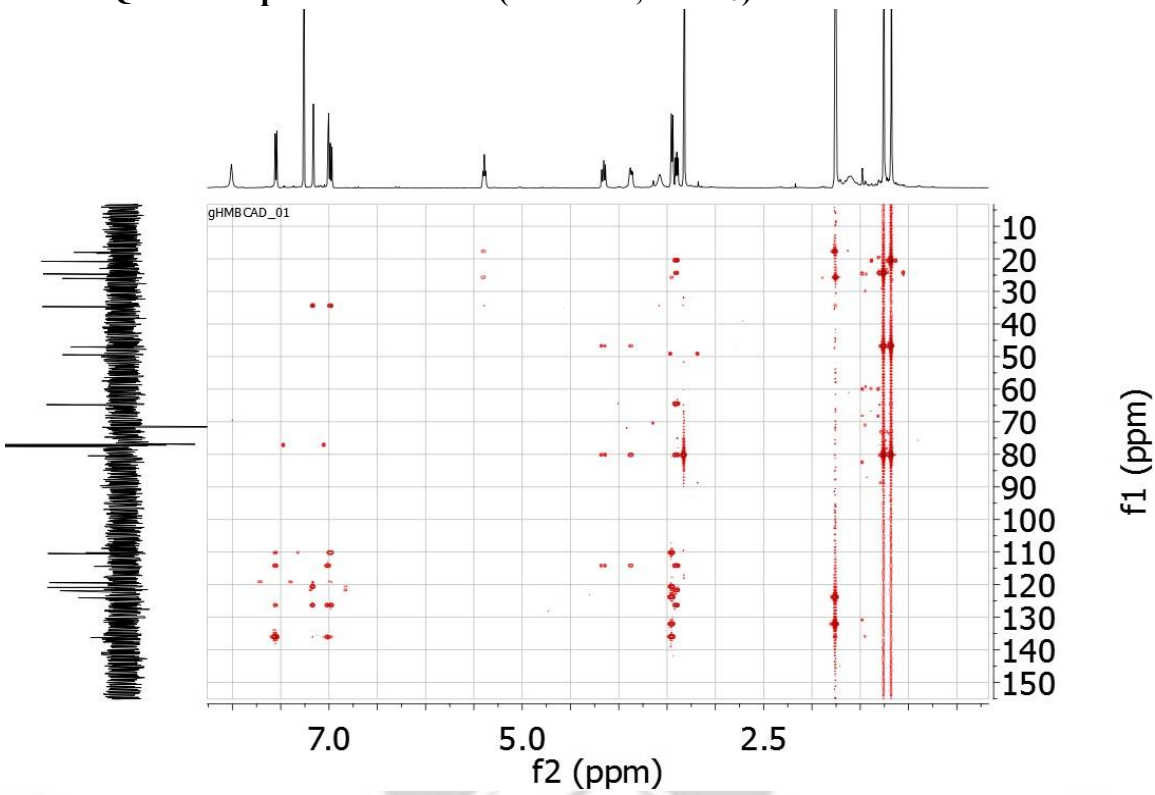

Fig. B-13: HMBC NMR spectrum of HM2 (500 MHz; $CDCl_3$)

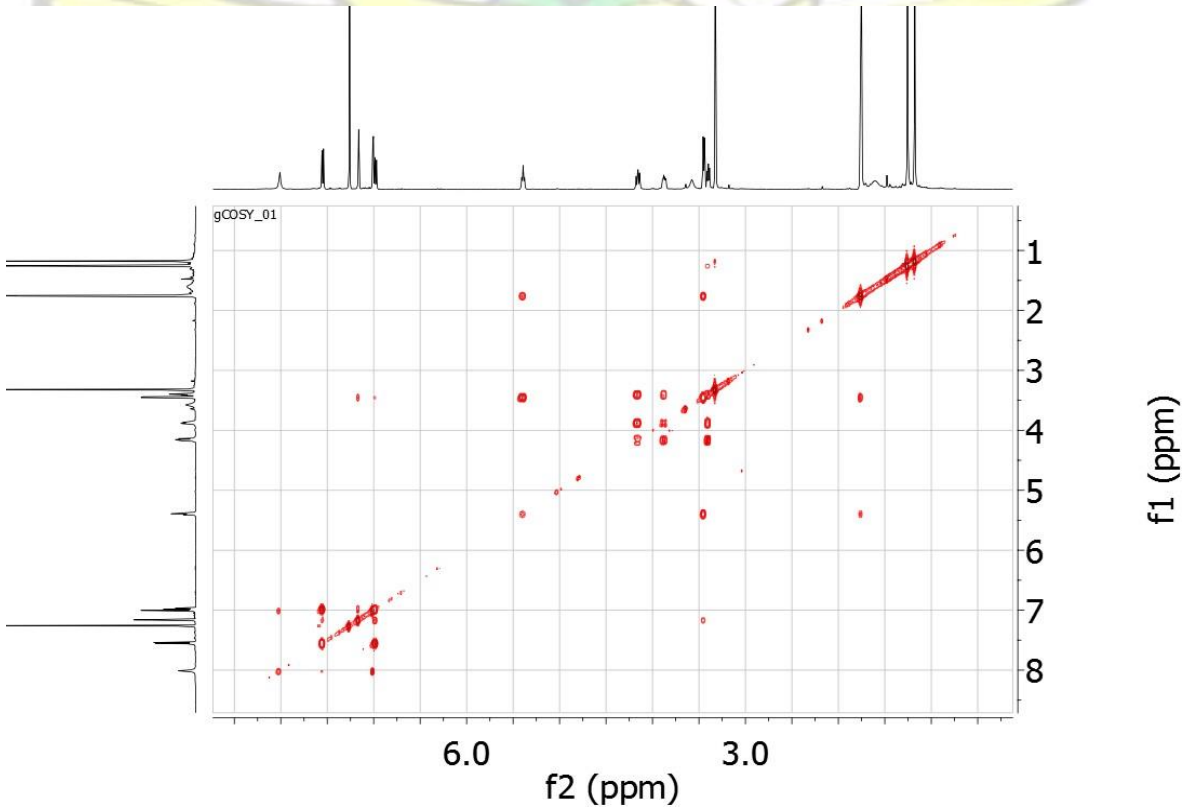

Fig. B-14: COSY NMR spectrum of HM2 (500 MHz; $CDCl_3$)

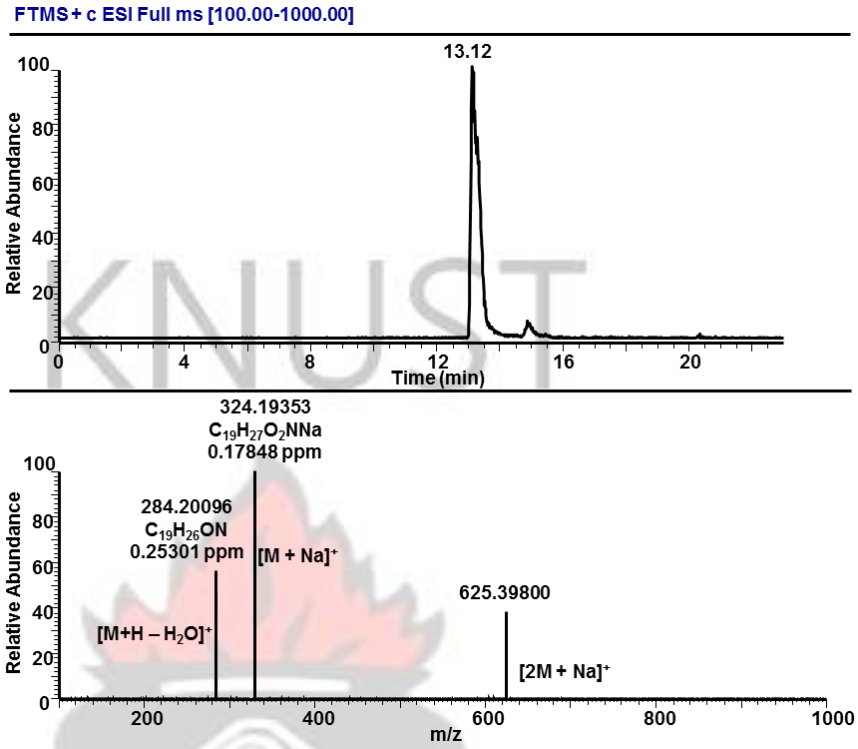

Fig. B-15 ull scan H M spectrum of HM3

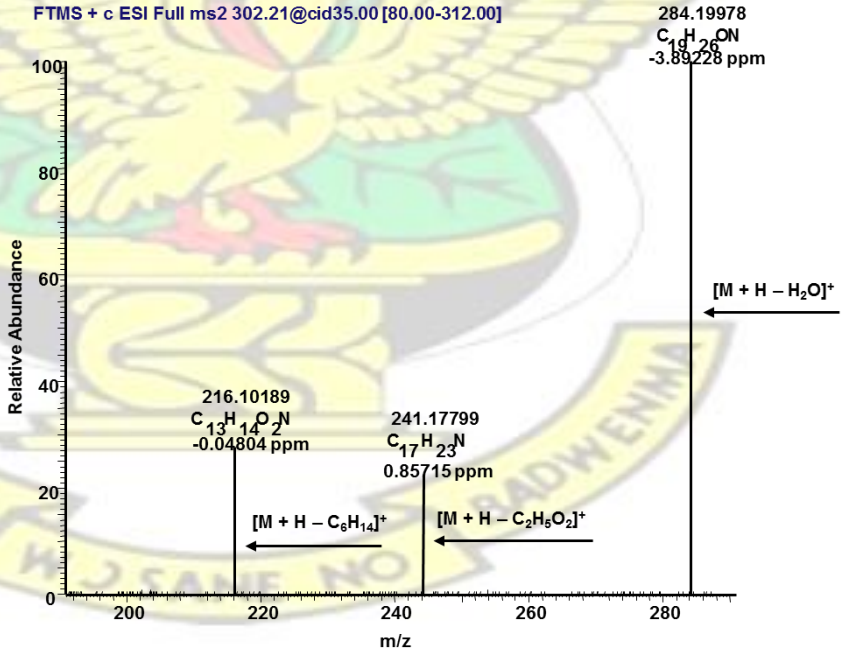

Fig. B-16 H M ^{2} fragmentation spectrum of HM3

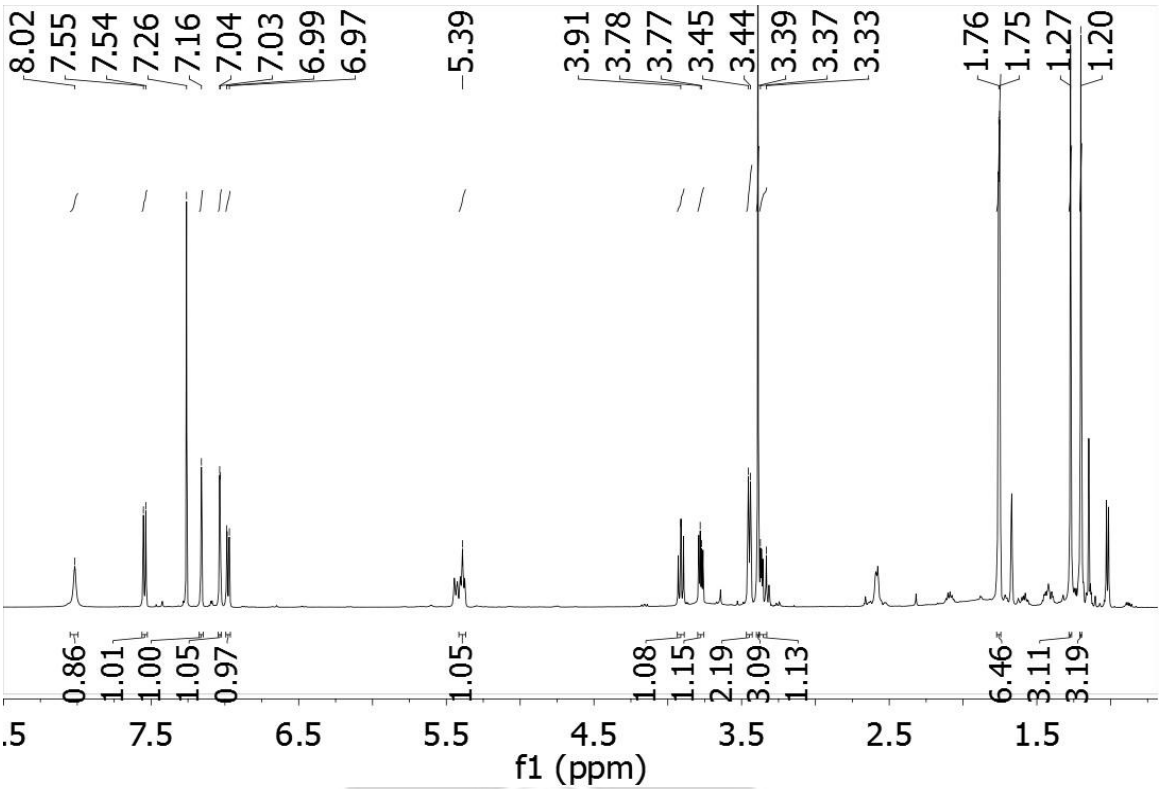

Fig. B-17: ^{1}H NMR spectrum of HM3 (500 MHz; $CDCl_3$)

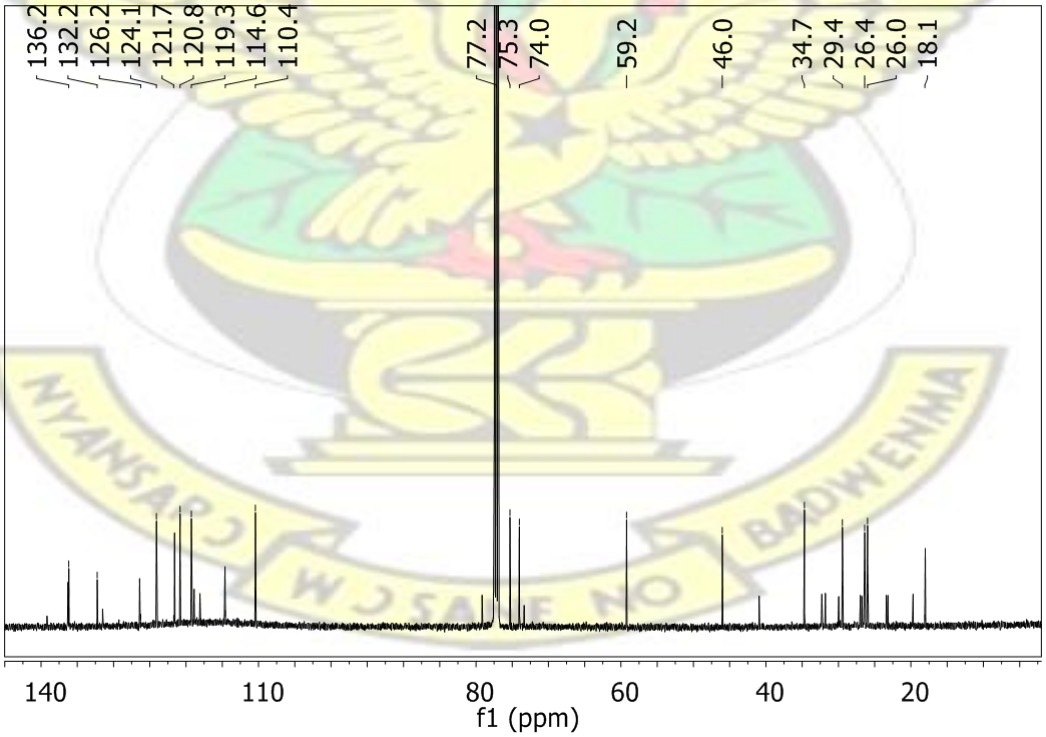

Fig. B-18: ^{13}C NMR spectrum of HM3 (125 MHz; $CDCl_3$)

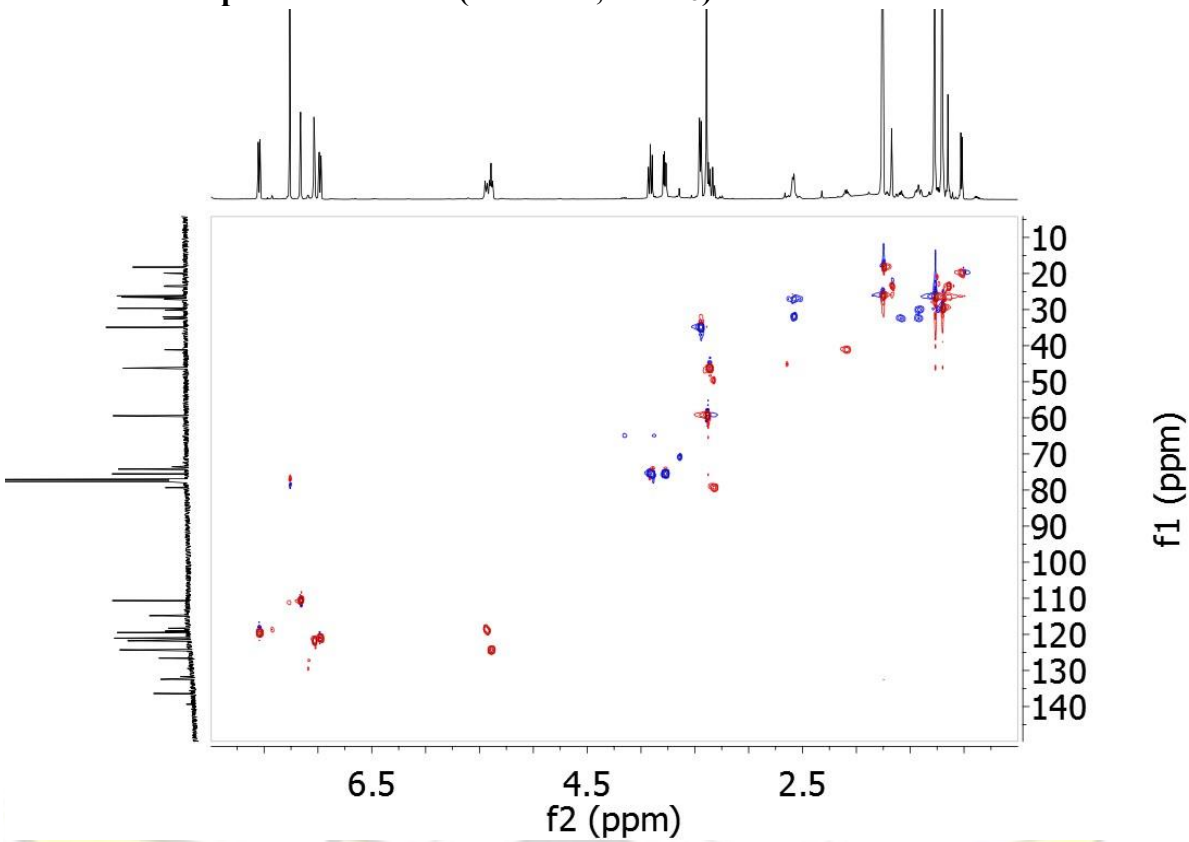

Fig. B-19: HSQC NMR spectrum of HM3 (500 MHz; $CDCl_3$)

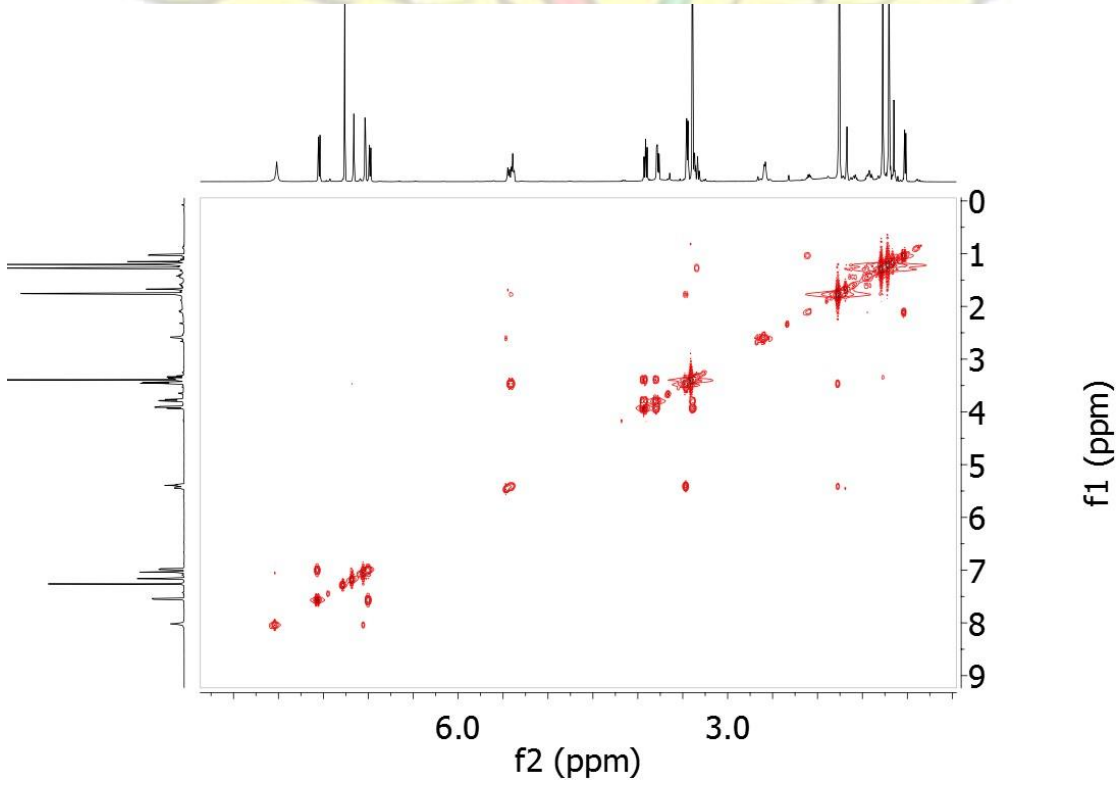

Fig. B-21: COSY NMR spectrum of HM3 (500 MHz; $CDCl_3$)

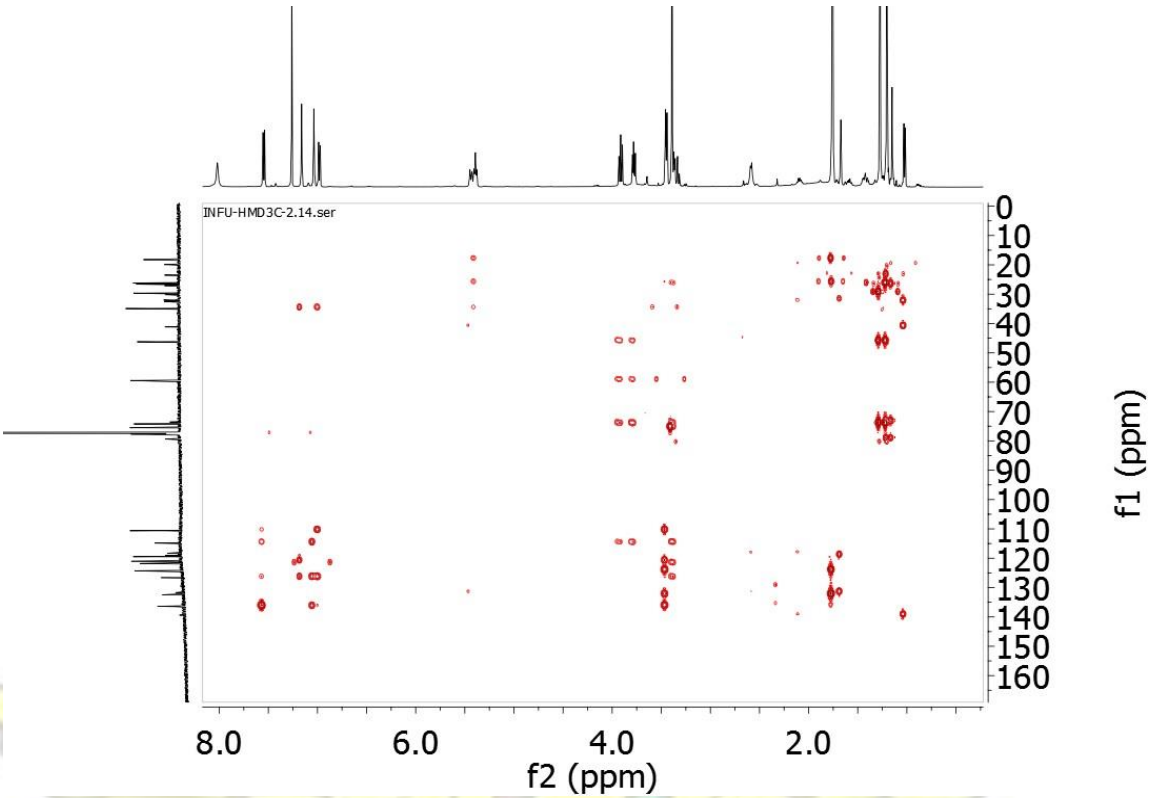

Fig. B-20: HMBC NMR spectrum of HM3 (500 MHz; $CDCl_3$)

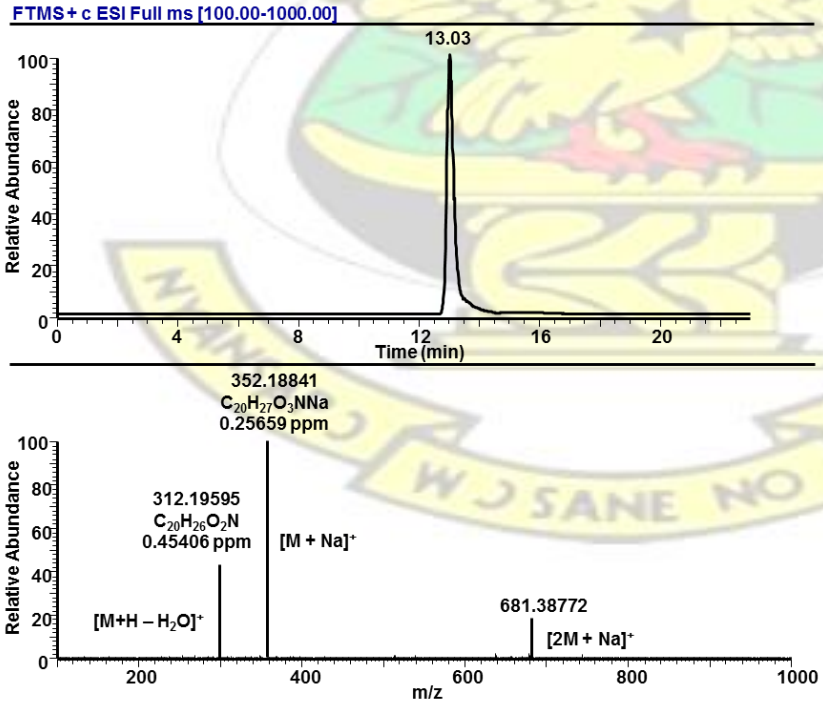

Fig. B-22 ull scan H M spectrum of HM4

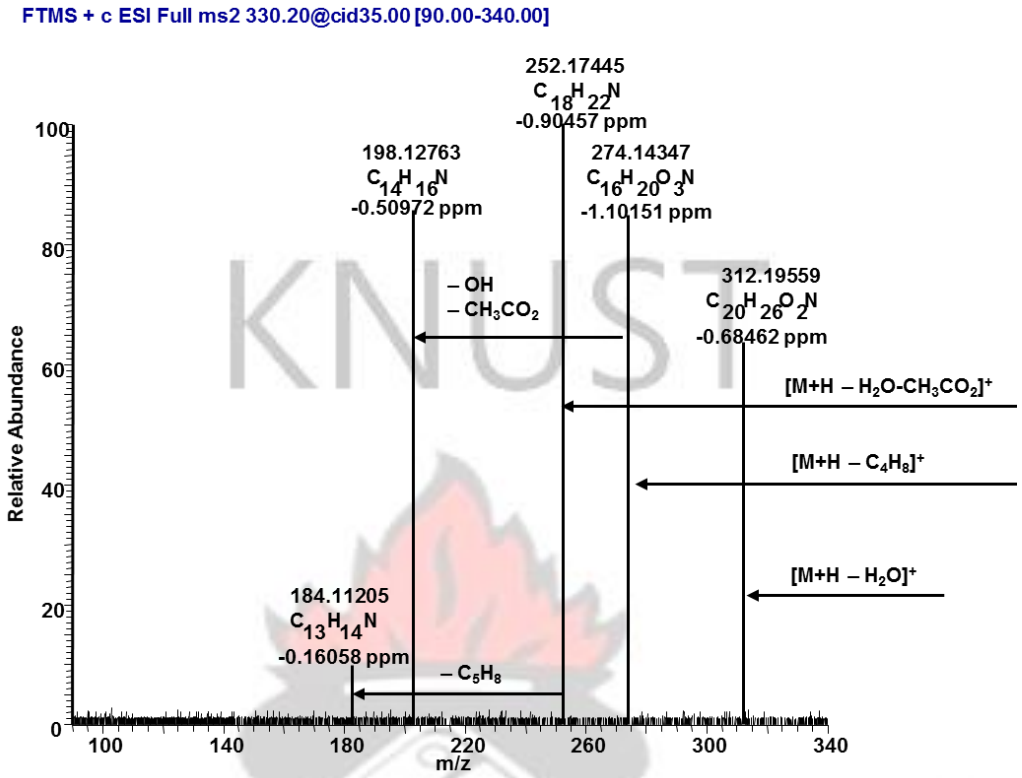

Fig. B-23 H M ^{2} fragmentation spectrum of HM4

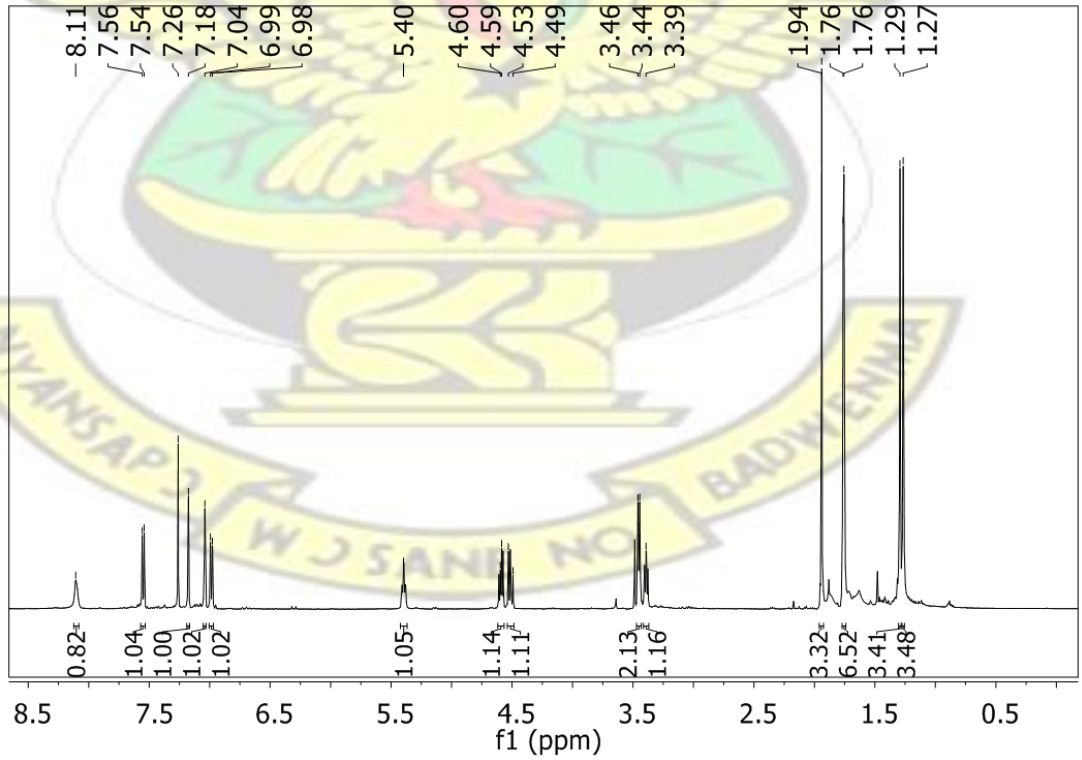

Fig. B-24: ^{1}H NMR spectrum of HM4 (500 MHz; $CDCl_3$)

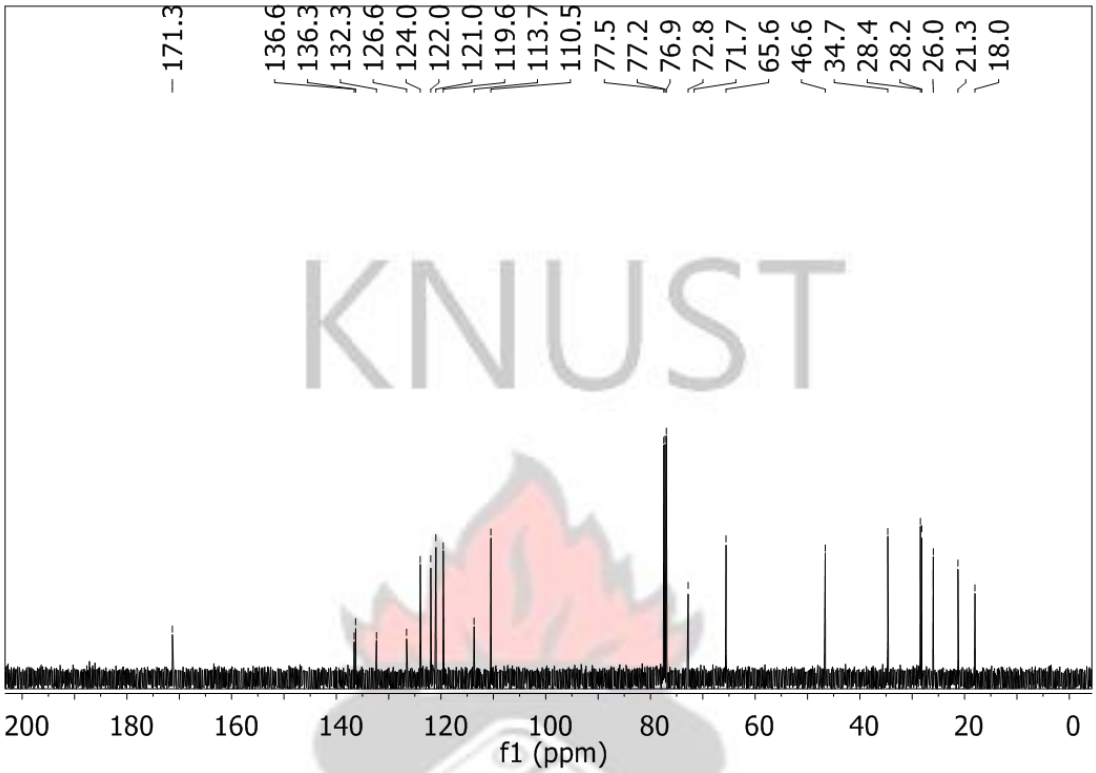

Fig. B-25: ^{13}C NMR spectrum of HM4 (150 MHz; $CDCl_3$)

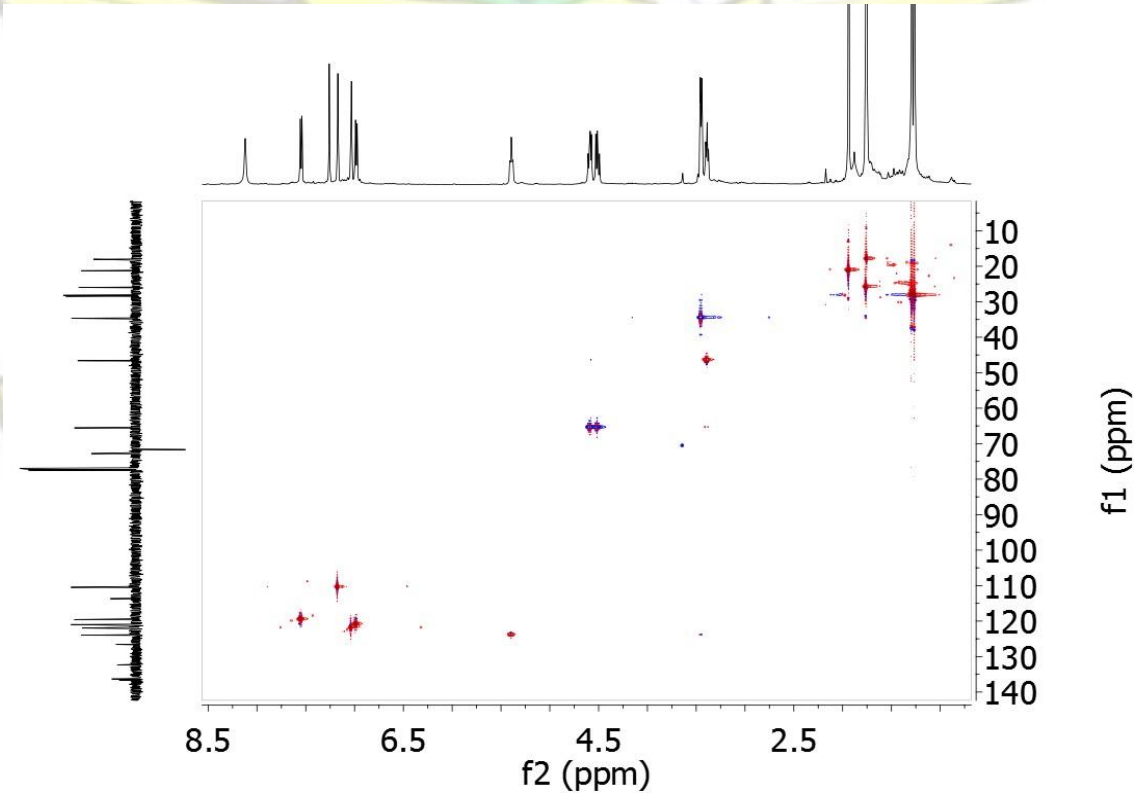

Fig. B-26: HSQC NMR spectrum of HM4 (500 MHz; $CDCl_3$)

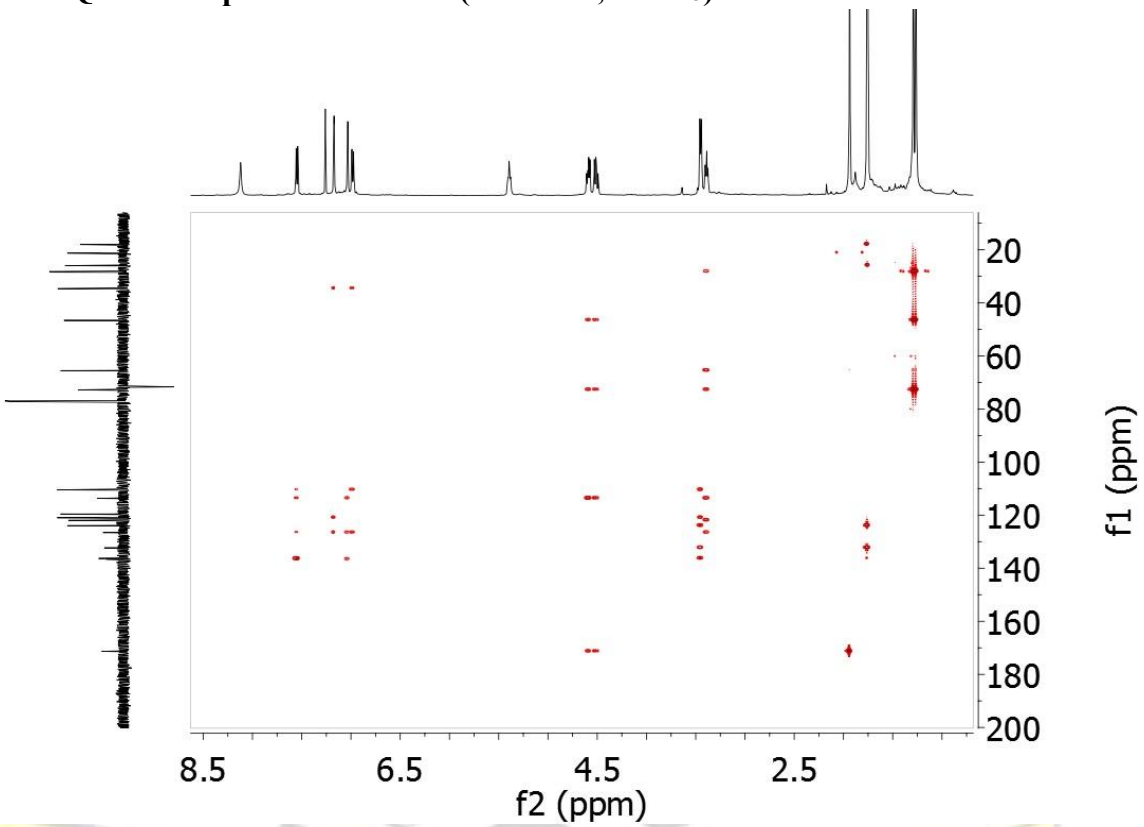

Fig. B-27: HMBC NMR spectrum of HM4 (500 MHz; $CDCl_3$)

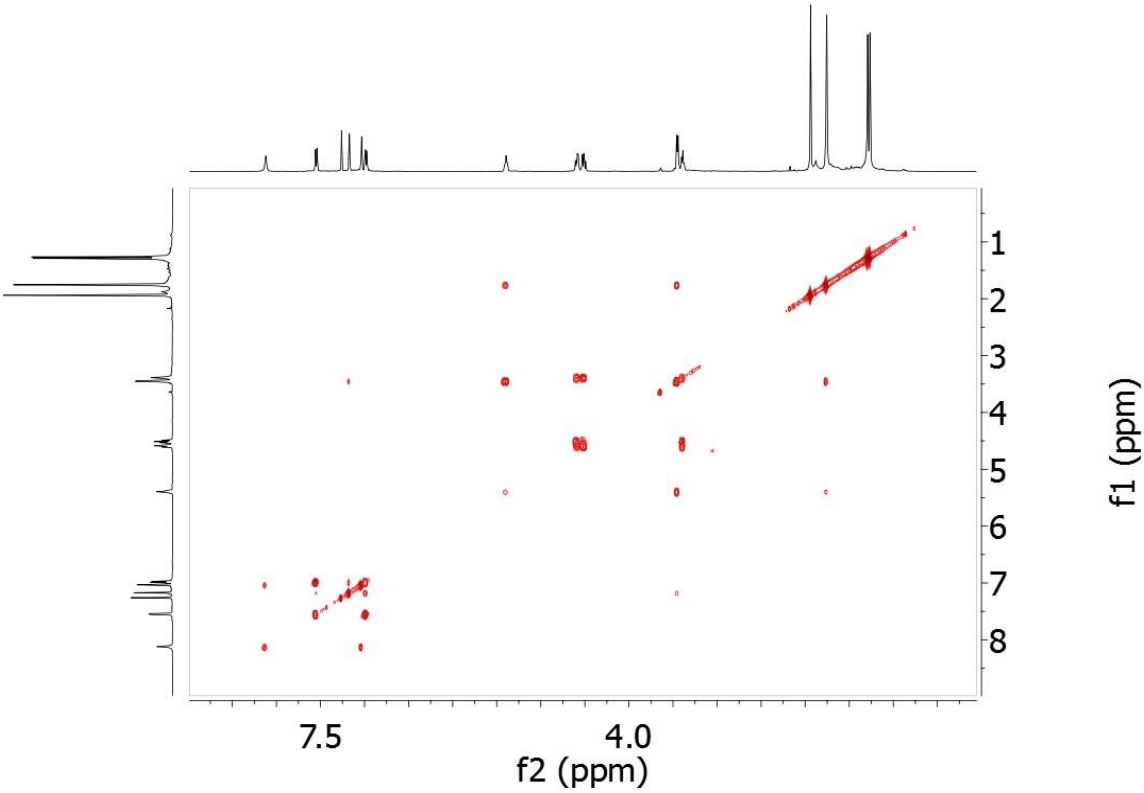

Fig. B-28: COSY NMR spectrum of HM4 (500 MHz; $CDCl_3$

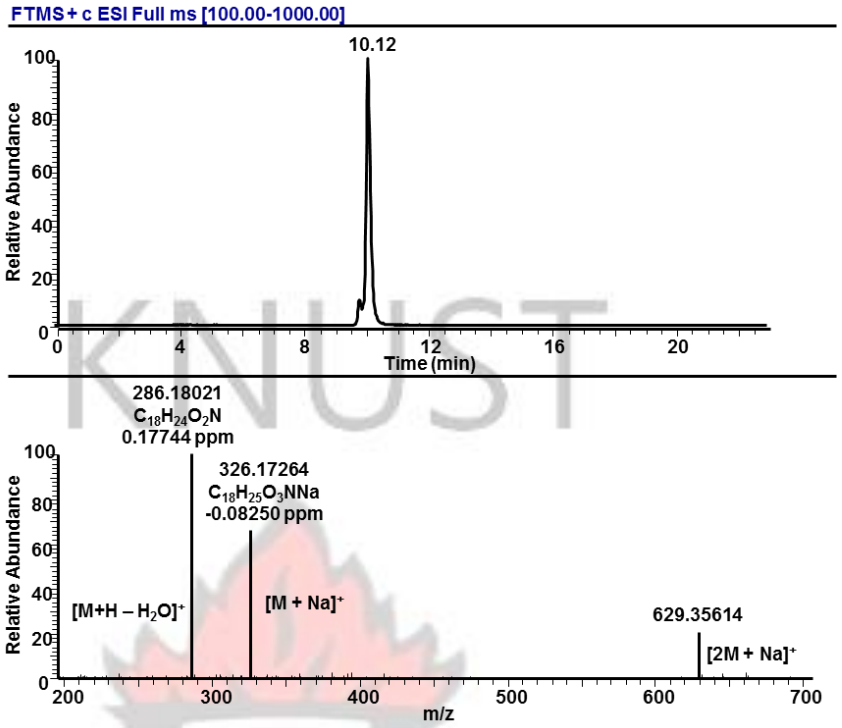

Fig. B-29: ull scan H M spectrum of HM5

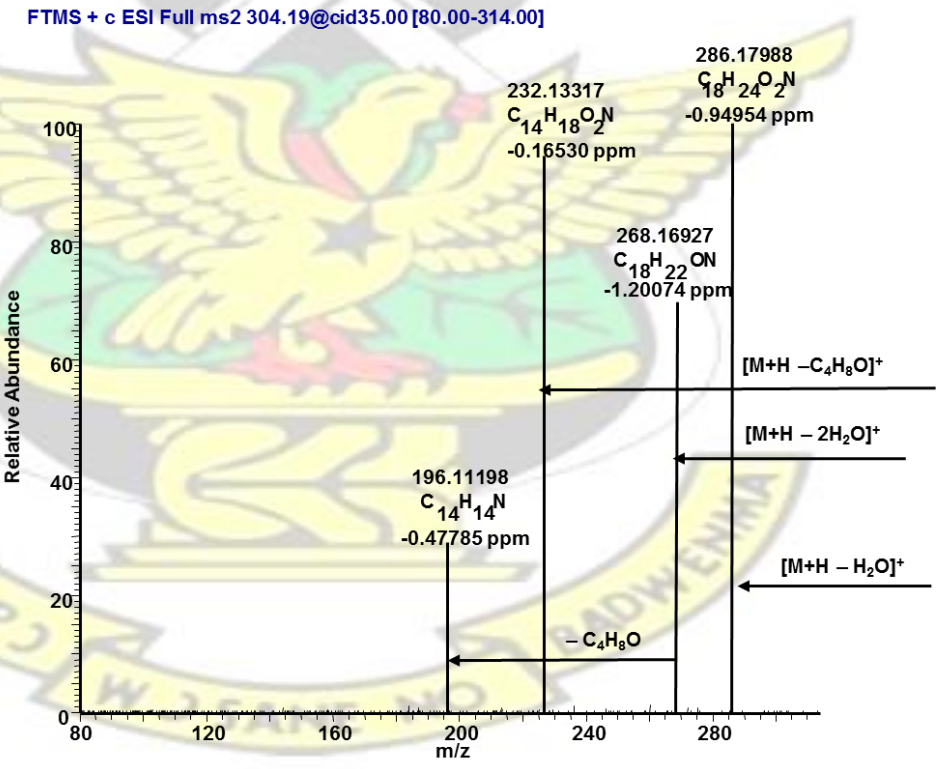

Fig. B-30: H M ^{2} fragmentation spectrum of HM5

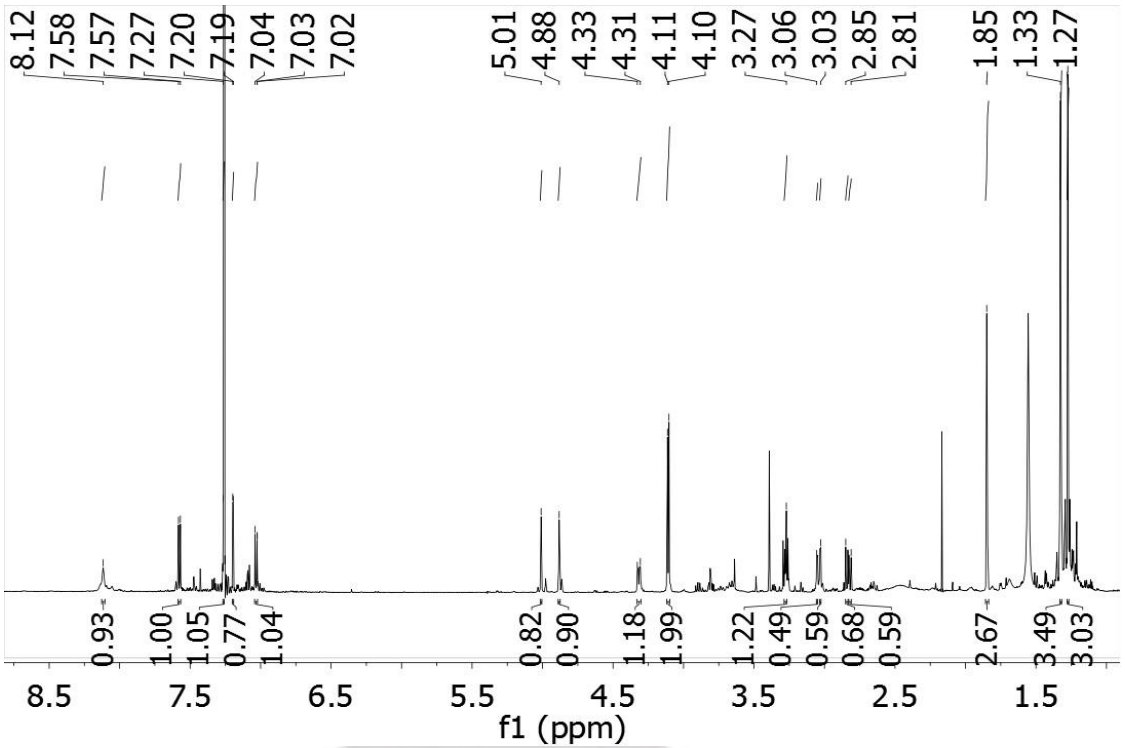

Fig. B-31: ^{1}H NMR spectrum of HM5 (500 MHz; $CDCl_3$)

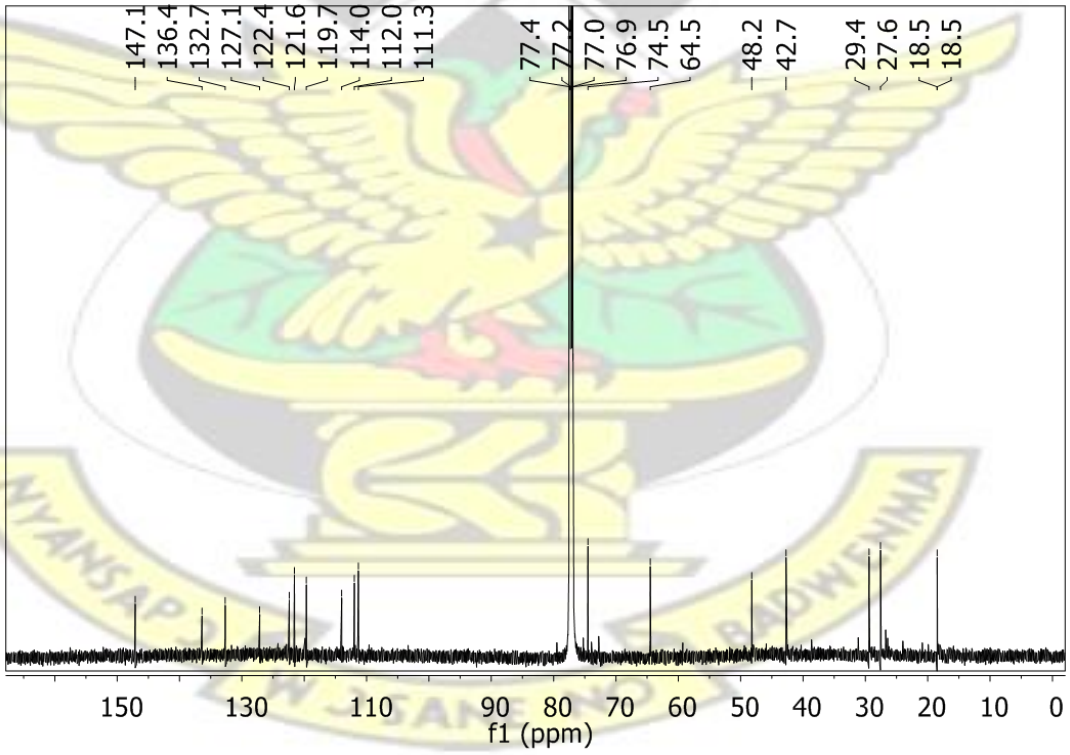

Fig. B-32: ^{13}C NMR spectrum of HM5 (150 MHz; $CDCl_3$)

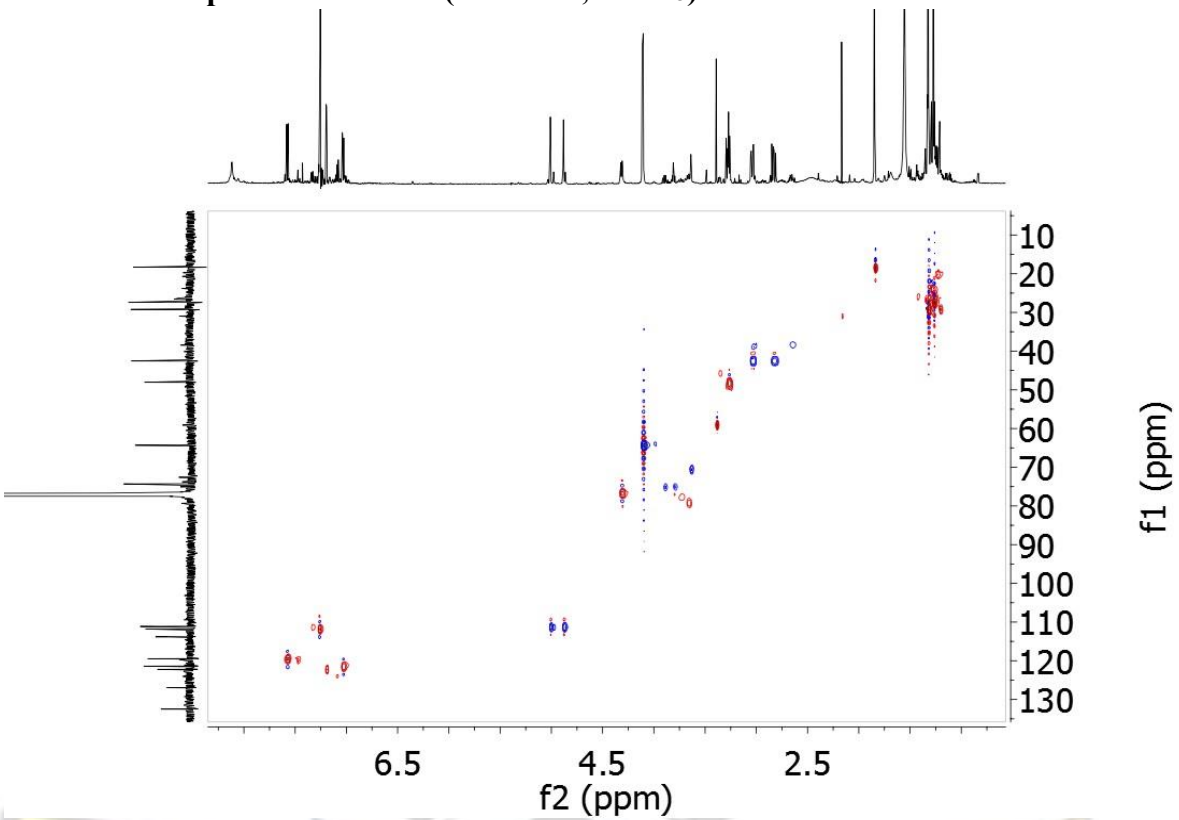

Fig. B-33: HSQC NMR spectrum of HM5 (500 MHz; $CDCl_3$)

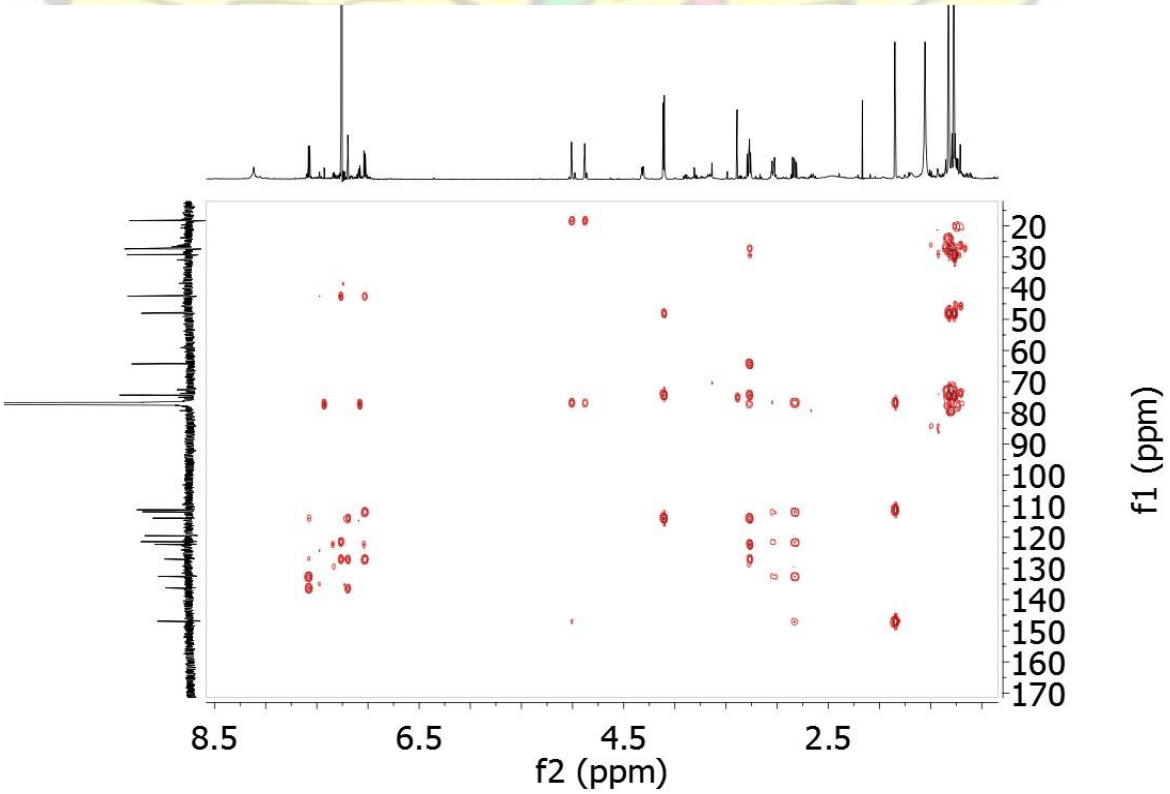

Fig. B-34: HMBC NMR spectrum of HM5 (500 MHz; $CDCl_3$)

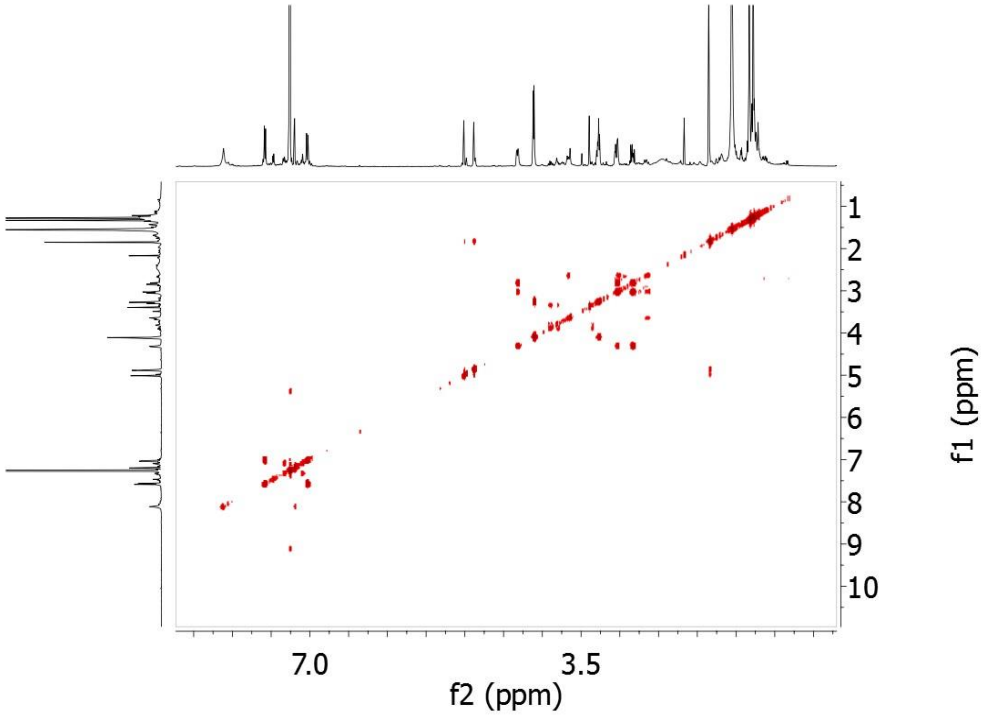

Fig. B-35: COSY NMR spectrum of HM5 (500 MHz; $CDCl_3$)

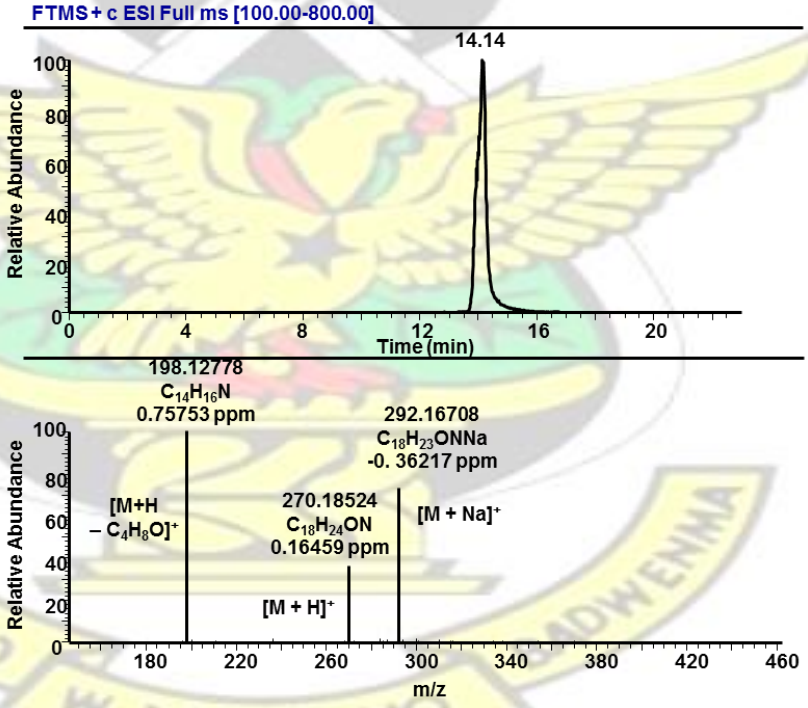

Fig. B-36: ull scan H M spectrum of HM6

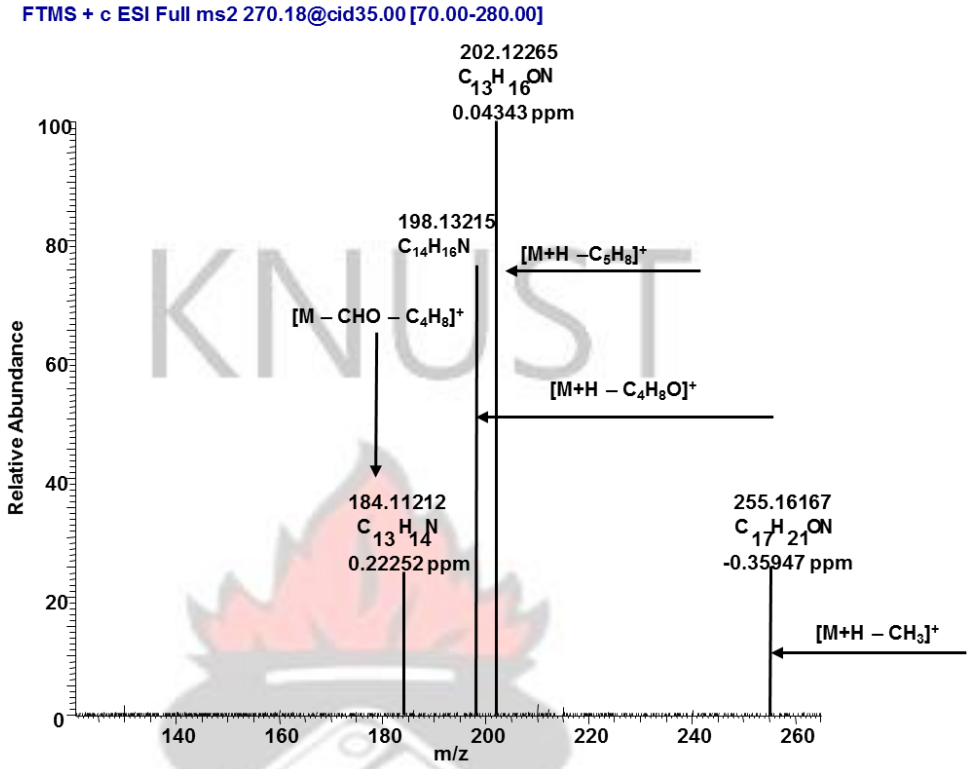

Fig. B-37: H M ^{2} fragmentation spectrum of HM6

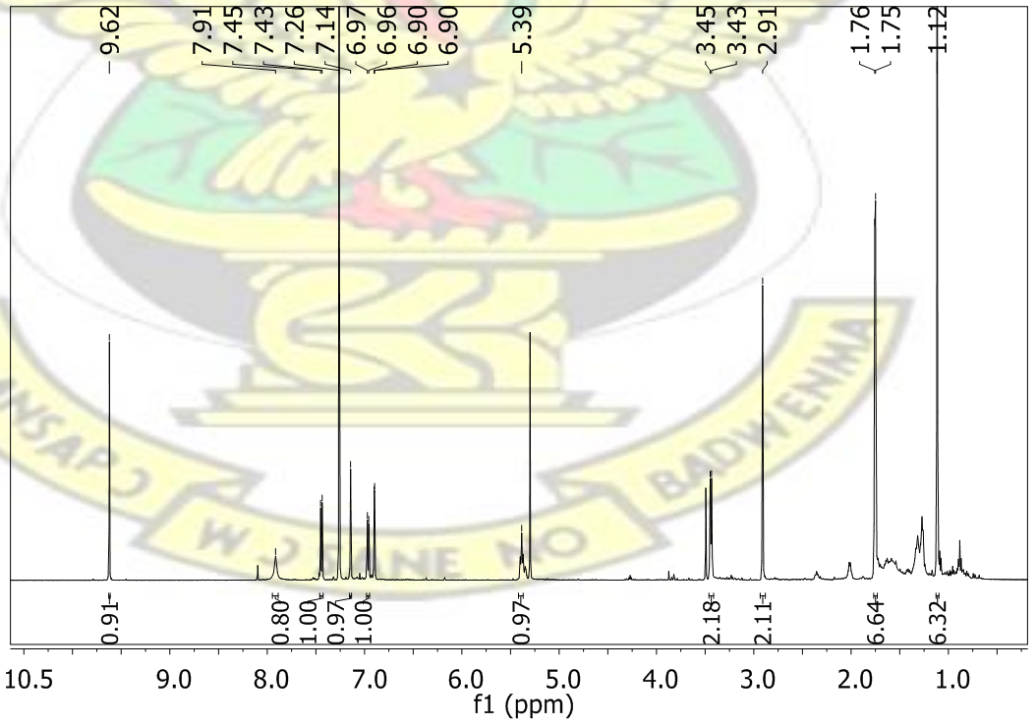

Fig. B-38: ^{1}H NMR spectrum of HM6 (500 MHz; $CDCl_3$)

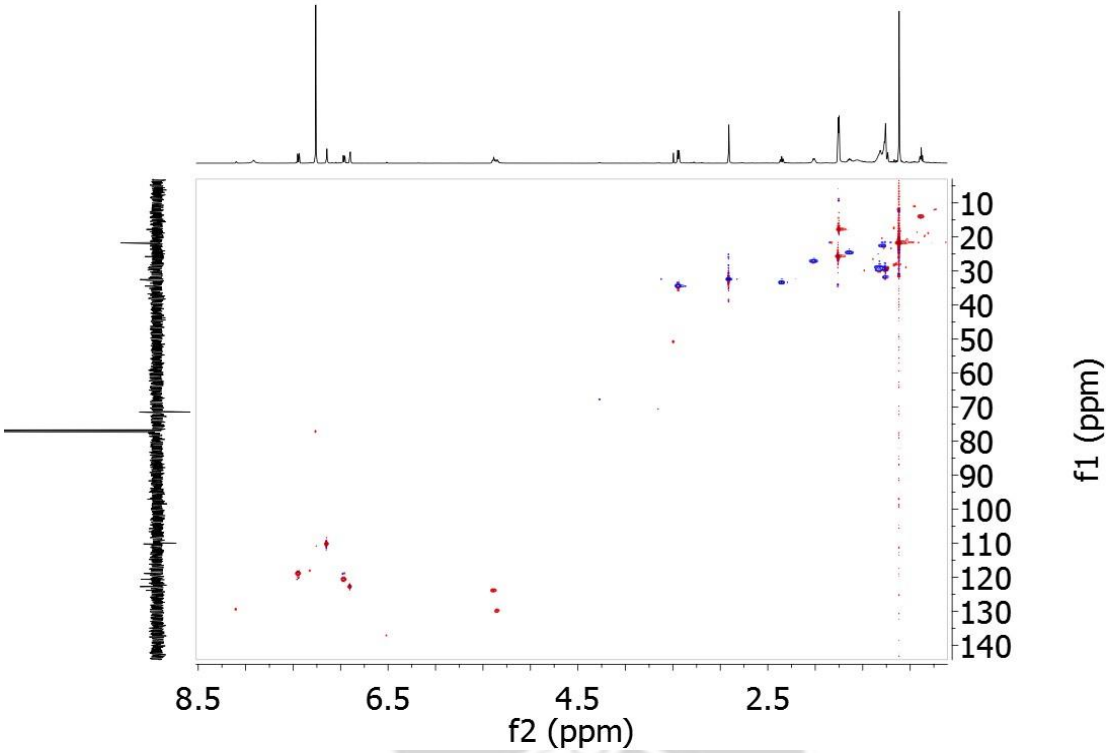

Fig. B-39: HSQC NMR spectrum of HM6 (500 MHz; $CDCl_3$)

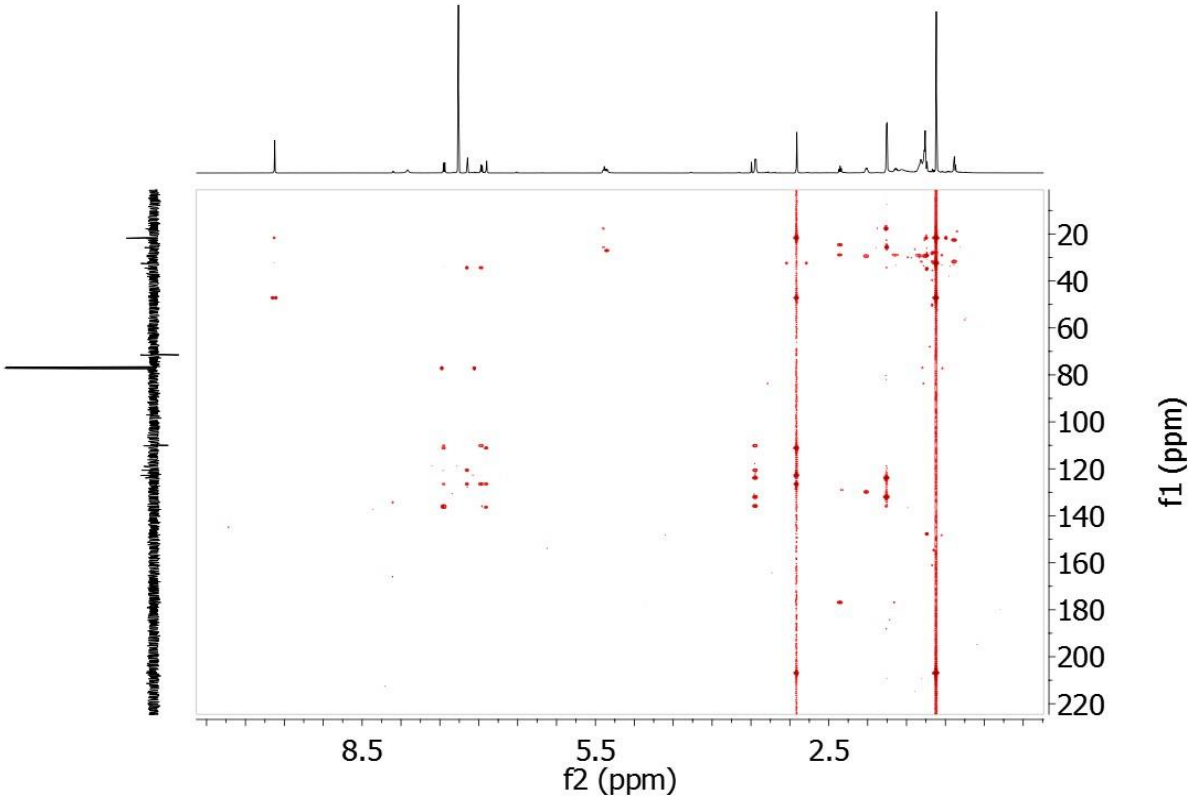

Fig. B-40: HMBC NMR spectrum of HM6 (500 MHz; $CDCl_3$)

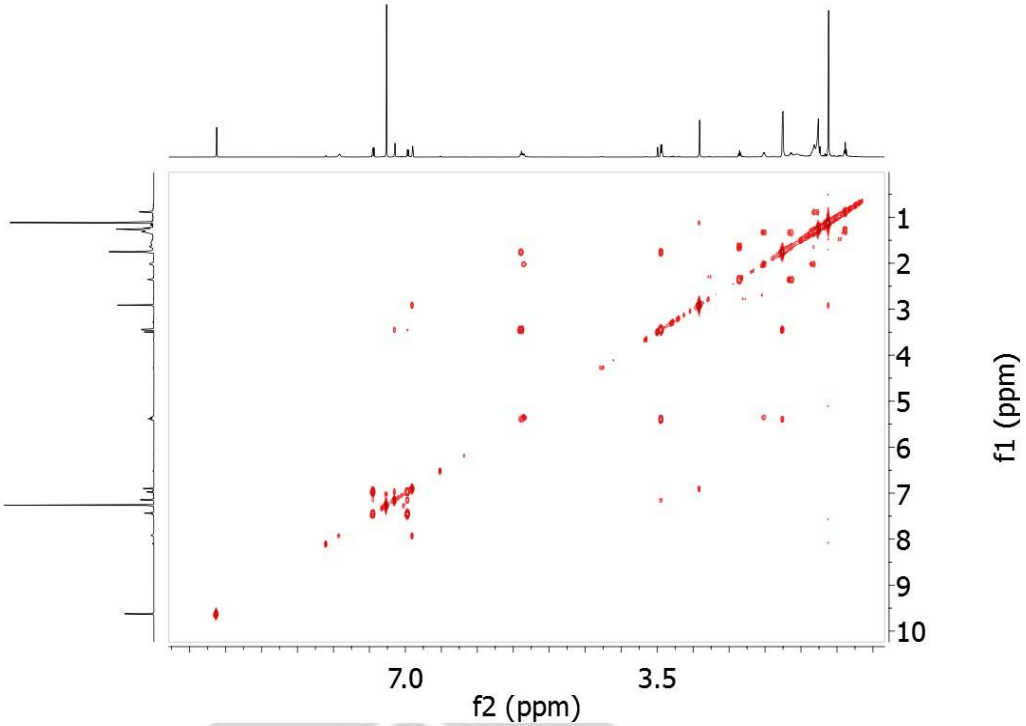

Fig. B-41: COSY NMR spectrum of HM6 (500 MHz; $CDCl_3$)

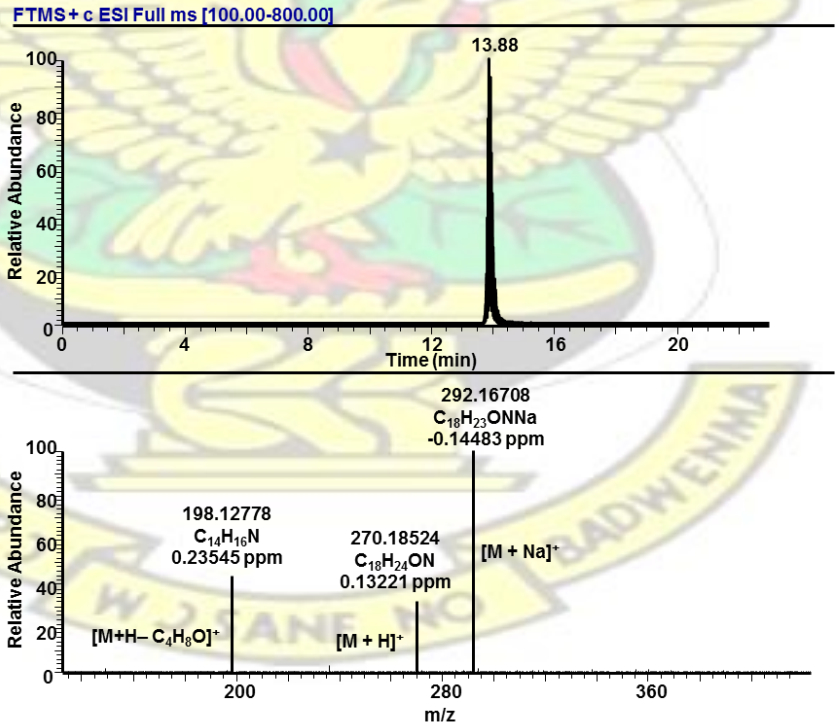

Fig. B-42: ull scan H M spectrum of HM7

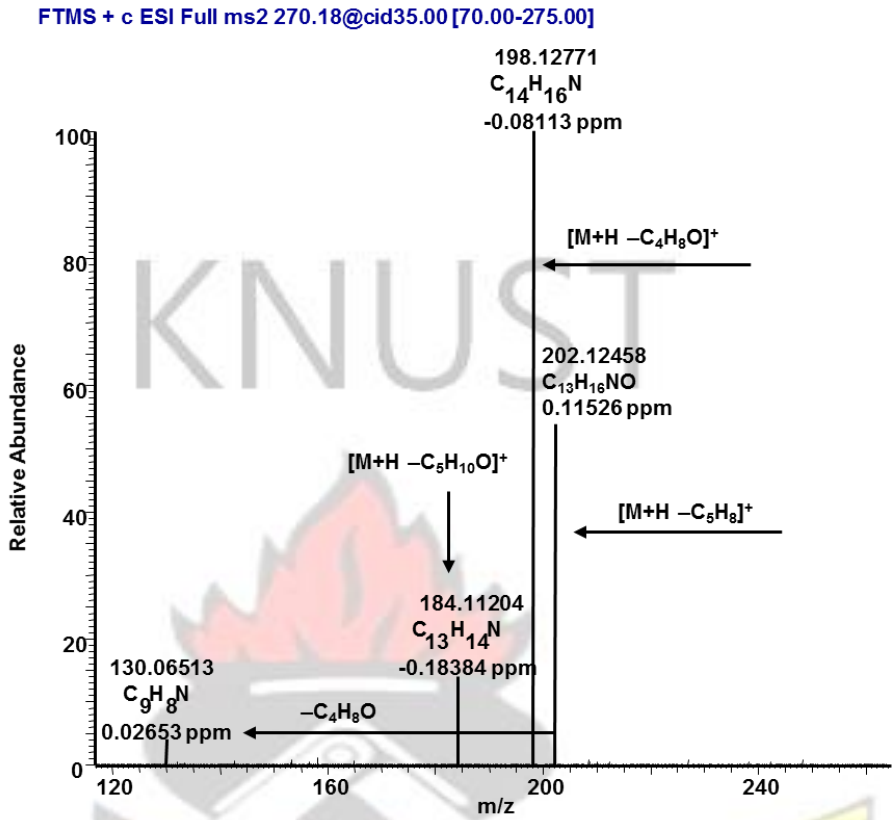

Fig. B-43 H M [2] fragmentation spectrum of HM7

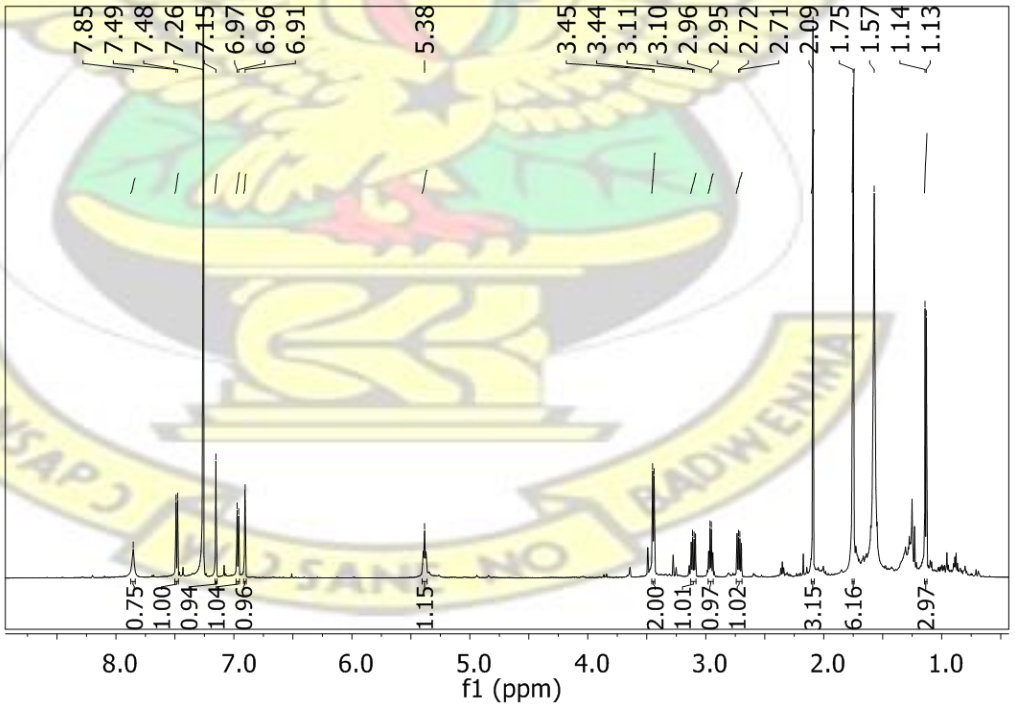

Fig. B-44: [1]H NMR spectrum of HM7 (500 MHz; $CDCl_3$)

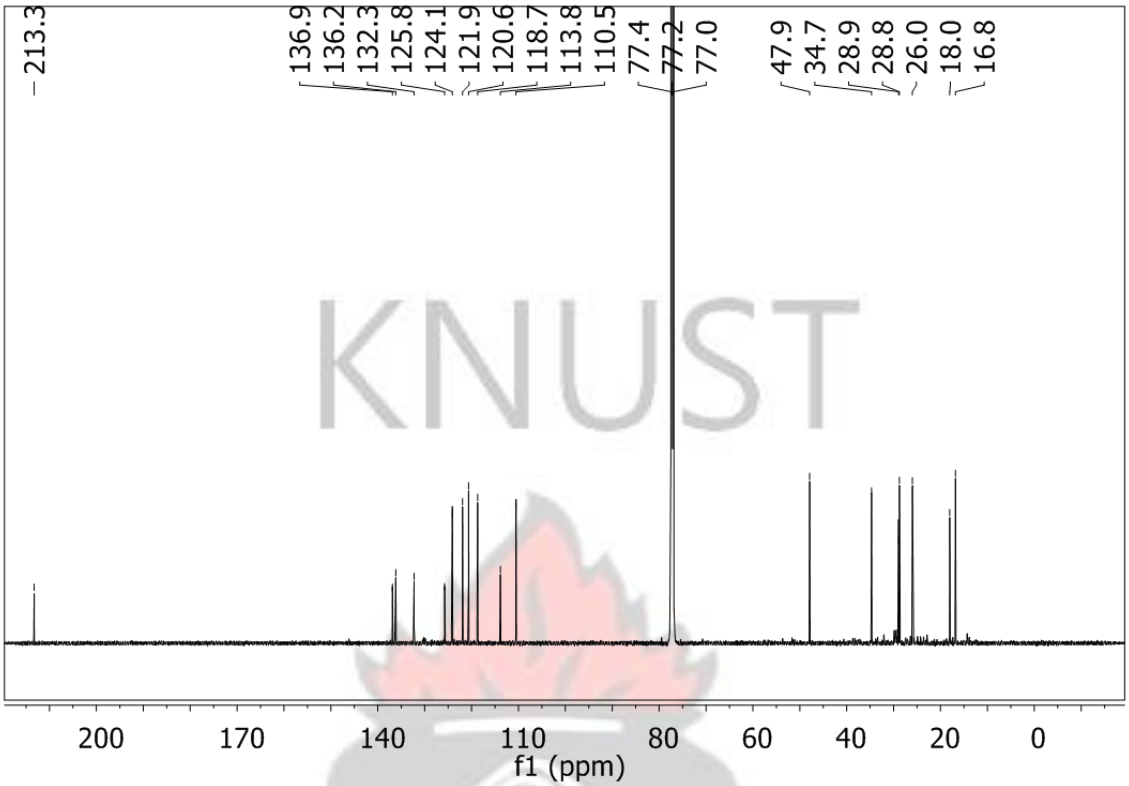

Fig. B-45: ^{13}C NMR spectrum of HM7 (150 MHz; $CDCl_3$)

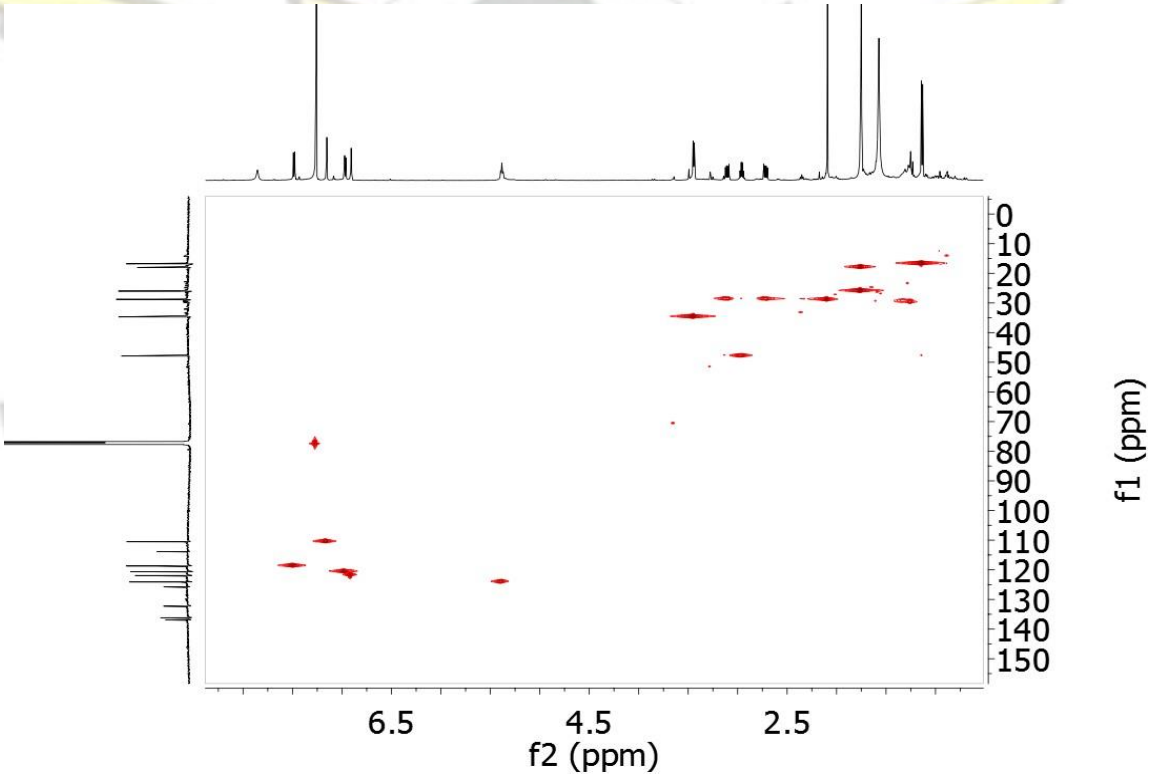

Fig. B-46: HSQC NMR spectrum of HM7 (500 MHz; $CDCl_3$)

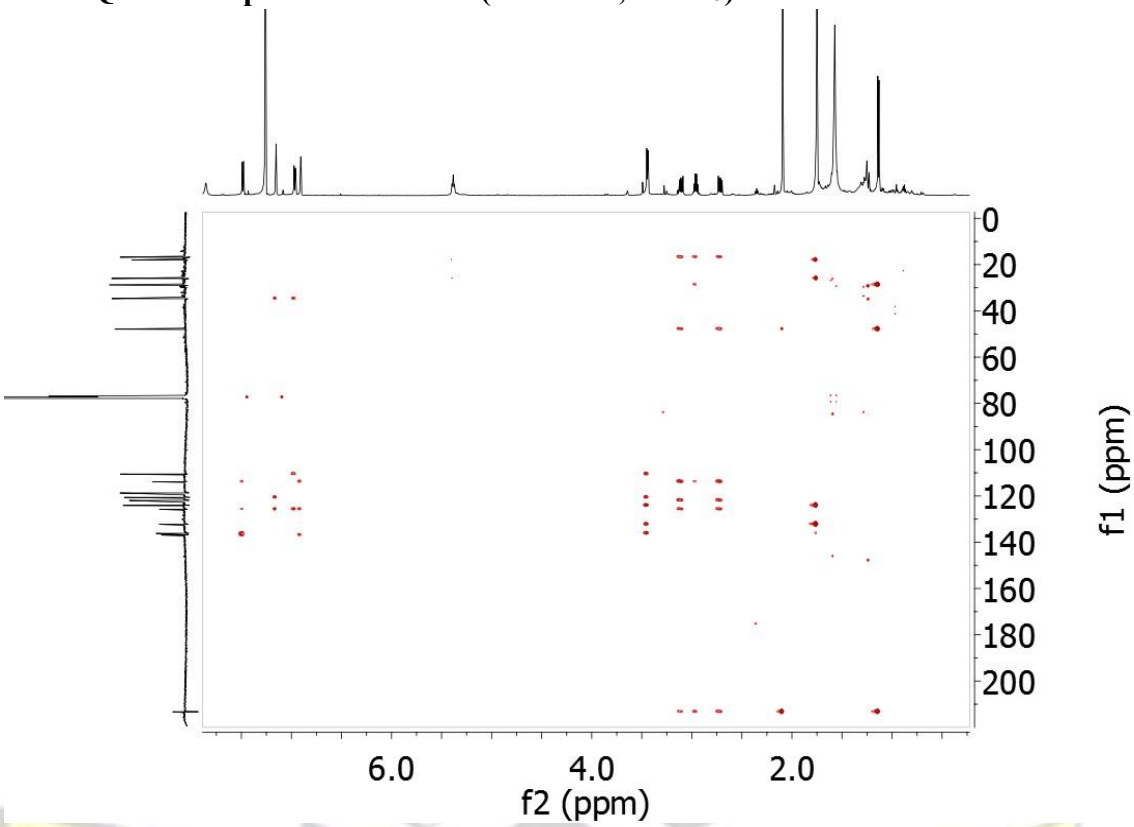

Fig. B-47: HMBC NMR spectrum of HM7 (500 MHz; $CDCl_3$)

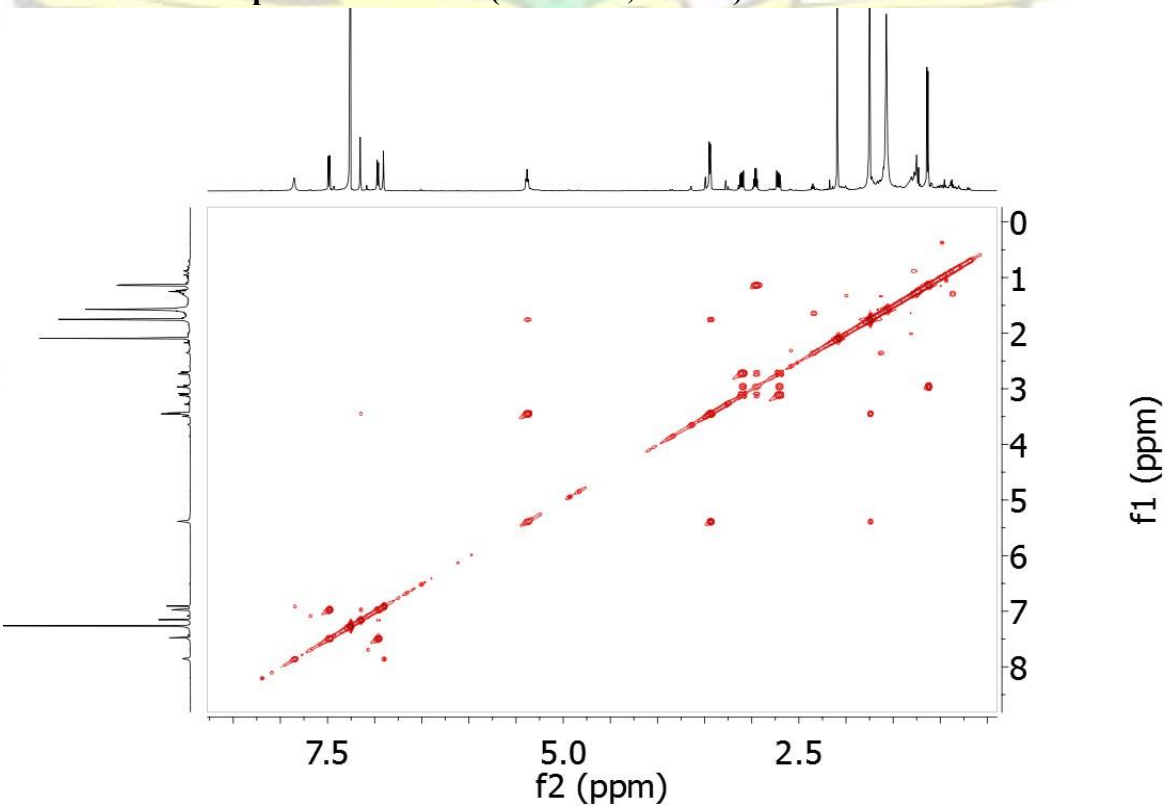

Fig. B-48: COSY NMR spectrum of HM7 (500 MHz; $CDCl_3$)

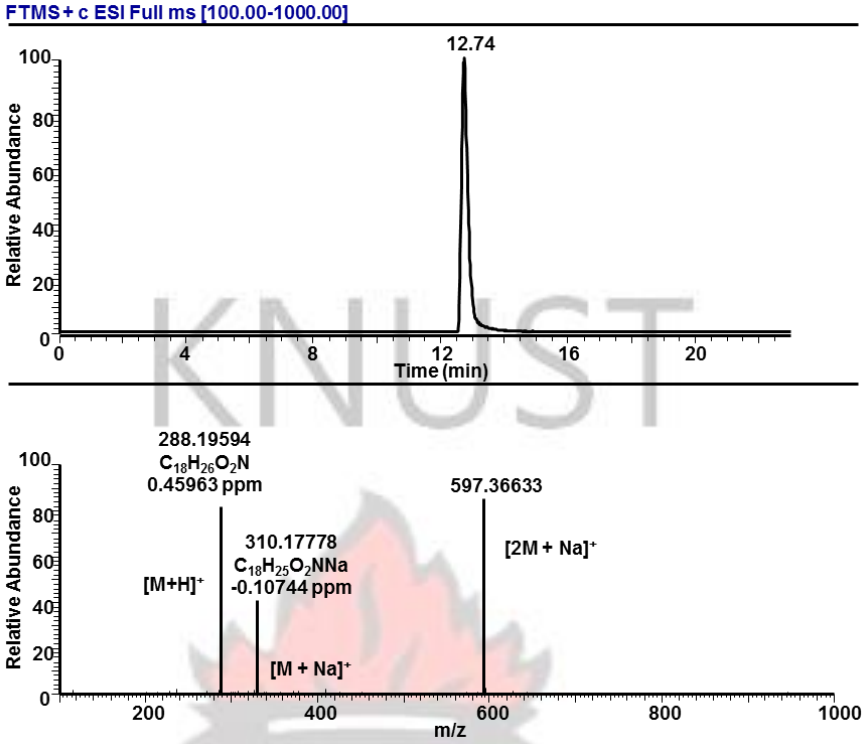

Fig. B-49 ull scan H M spectrum of HM8

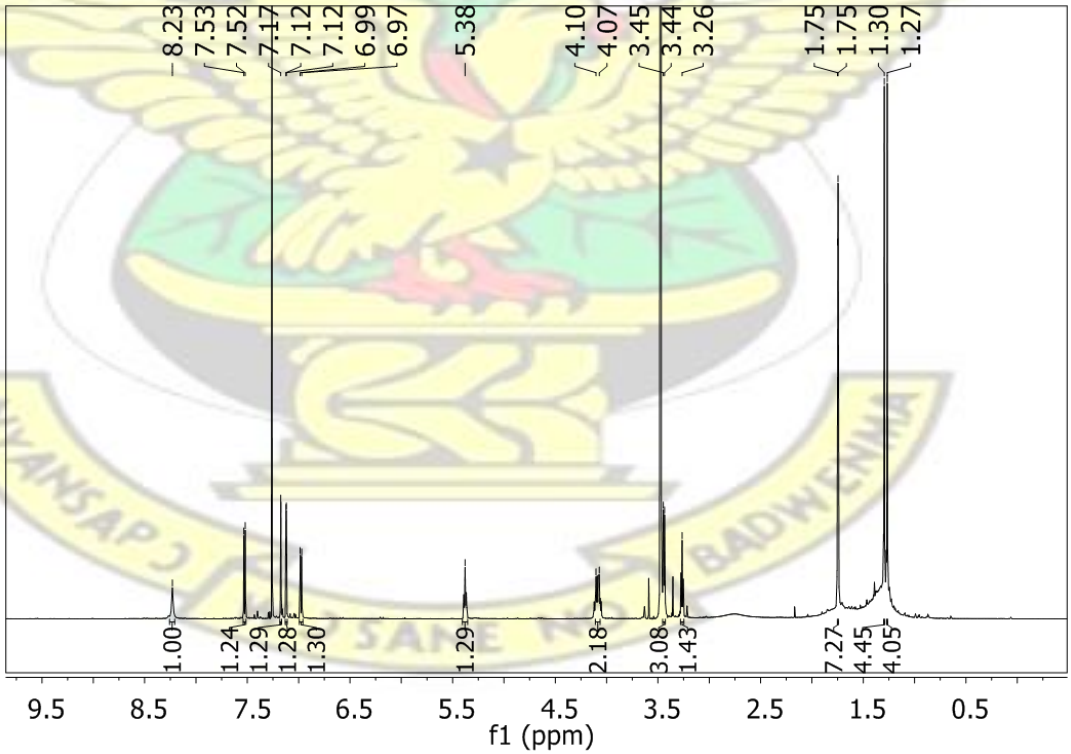

Fig. B-50 ^{1}H NMR spectrum of HM8 (500 MHz; $CDCl_3$)

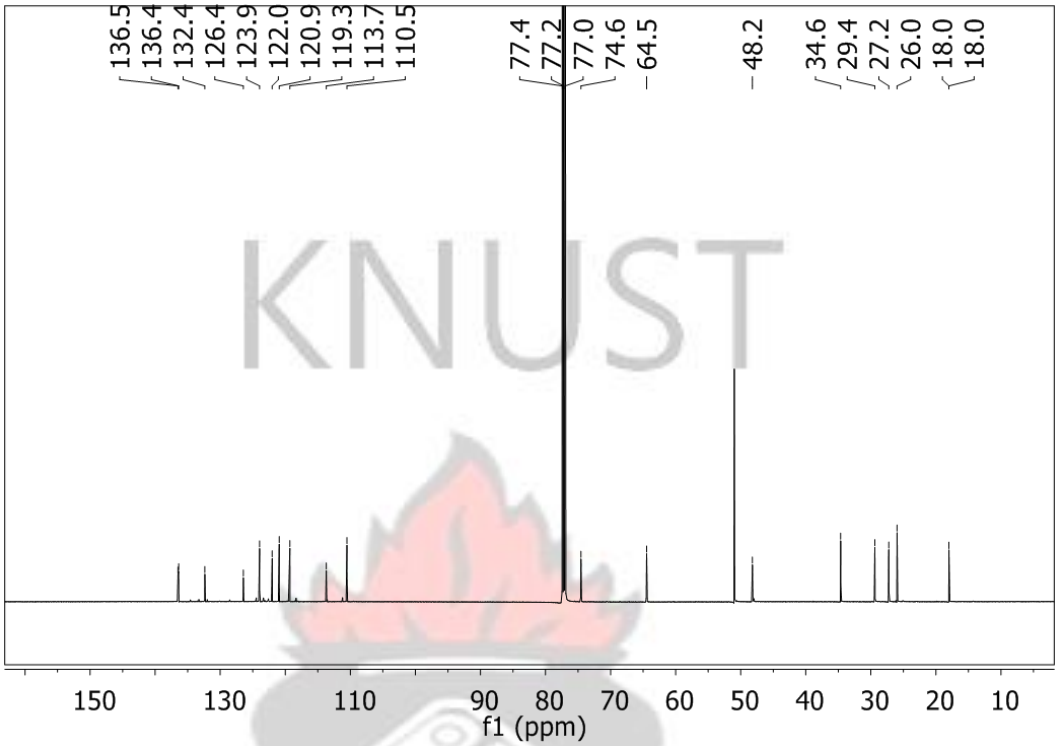

Fig. B-51 ^{13}C NMR spectrum of HM8 (125 MHz; $CDCl_3$)

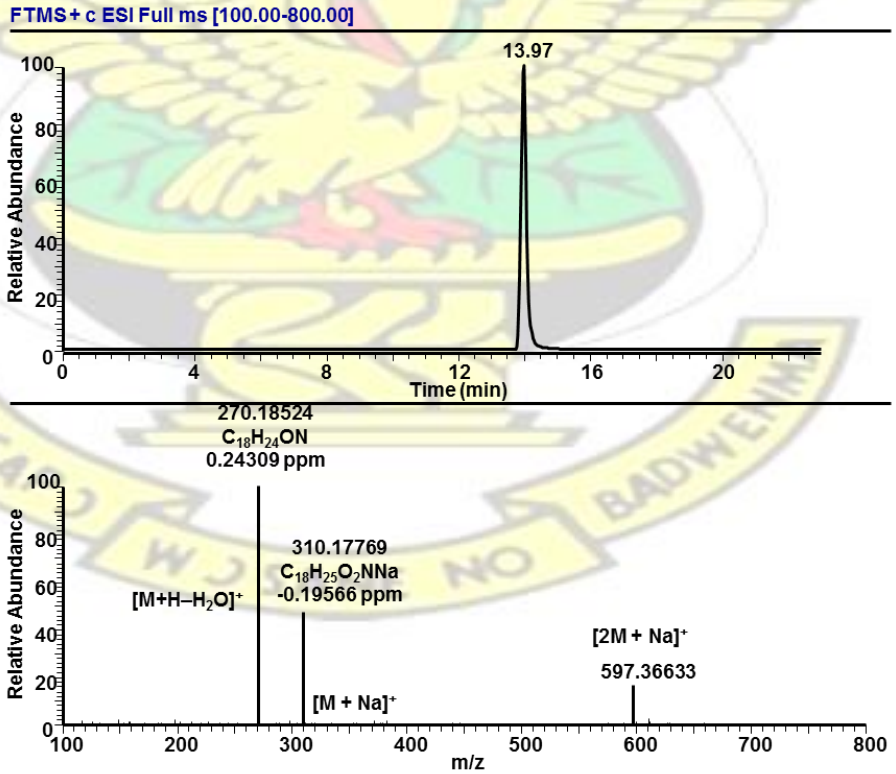

Fig. B-52 ull scan H M spectrum of HM9

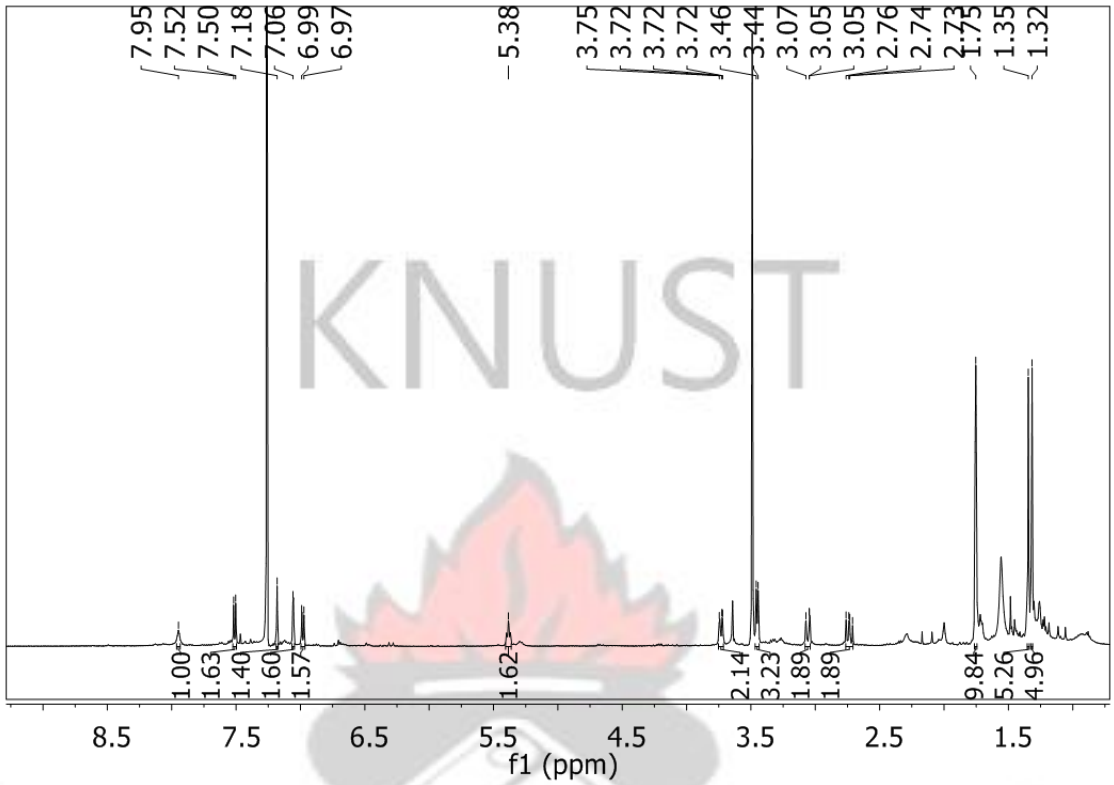

Fig. B-53: ^{1}H NMR spectrum of HM9 (500 MHz; $CDCl_3$)

APPENDIX C

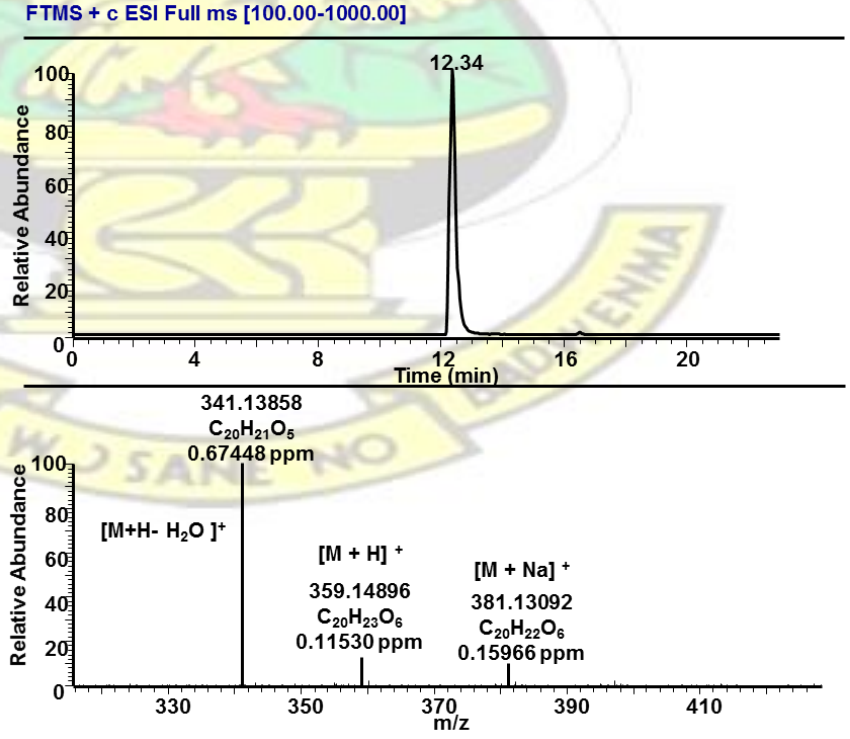

Fig. C-1 ull scan H M spectrum of H1

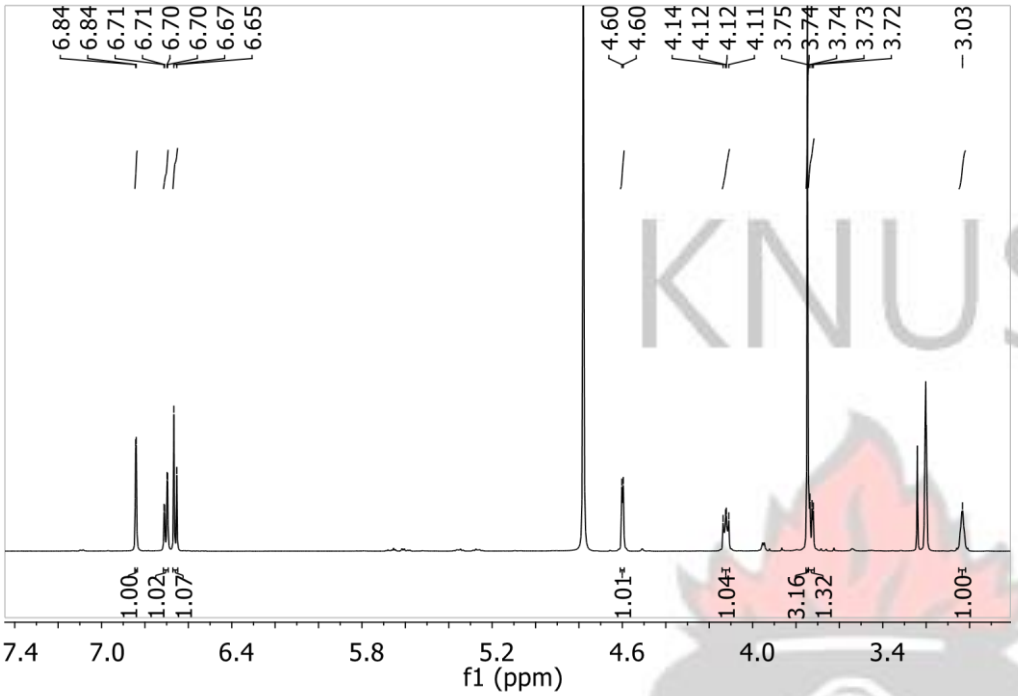

Fig. C-2[1]H NMR spectrum of LH1

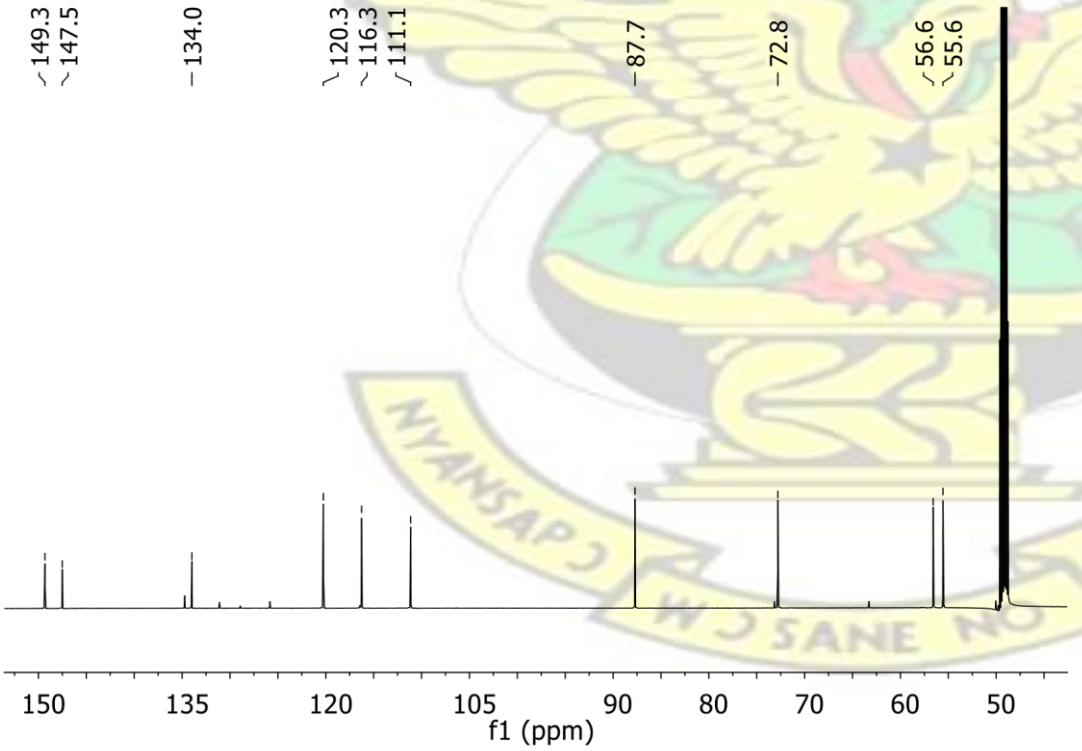

Fig. C-3[1]H NMR spectrum of LH1

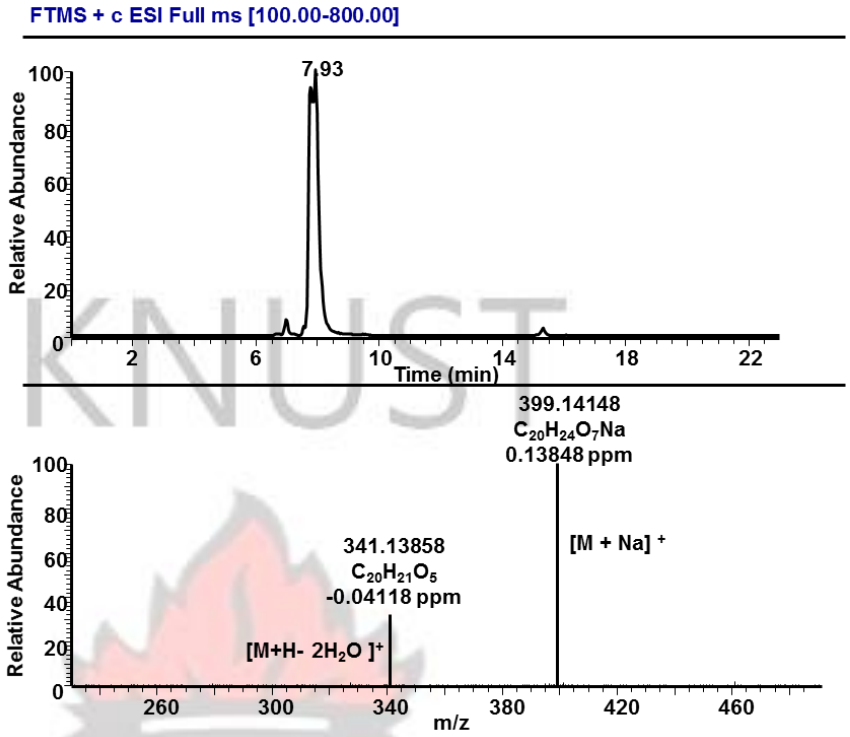

Fig. C-4 ull scan H M spectrum of H2

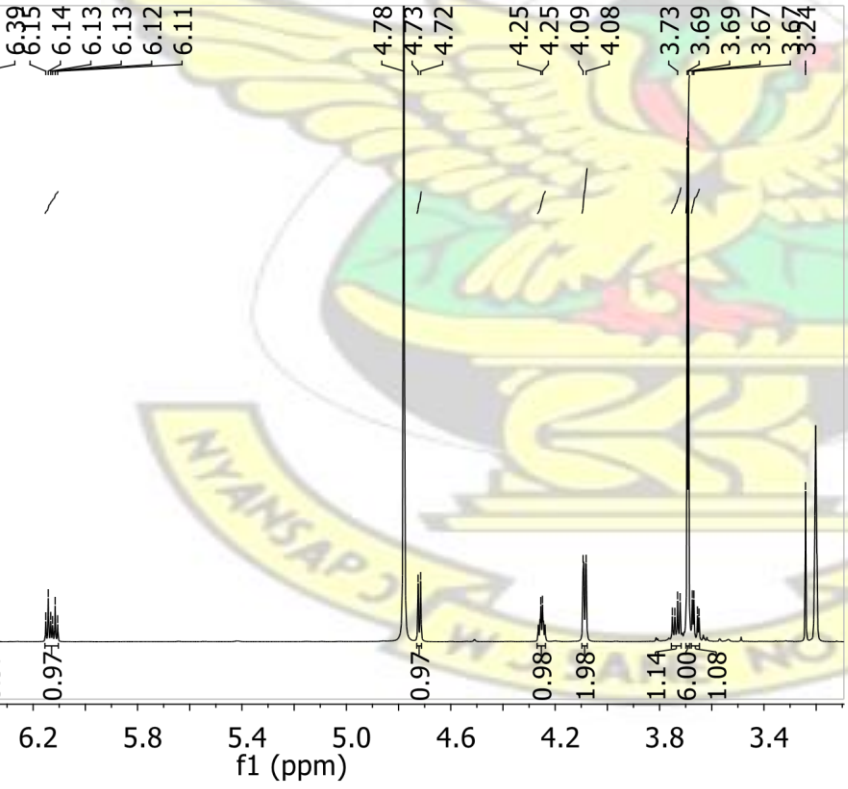

Fig. C-5 ^{1}H NMR spectrum of LH2

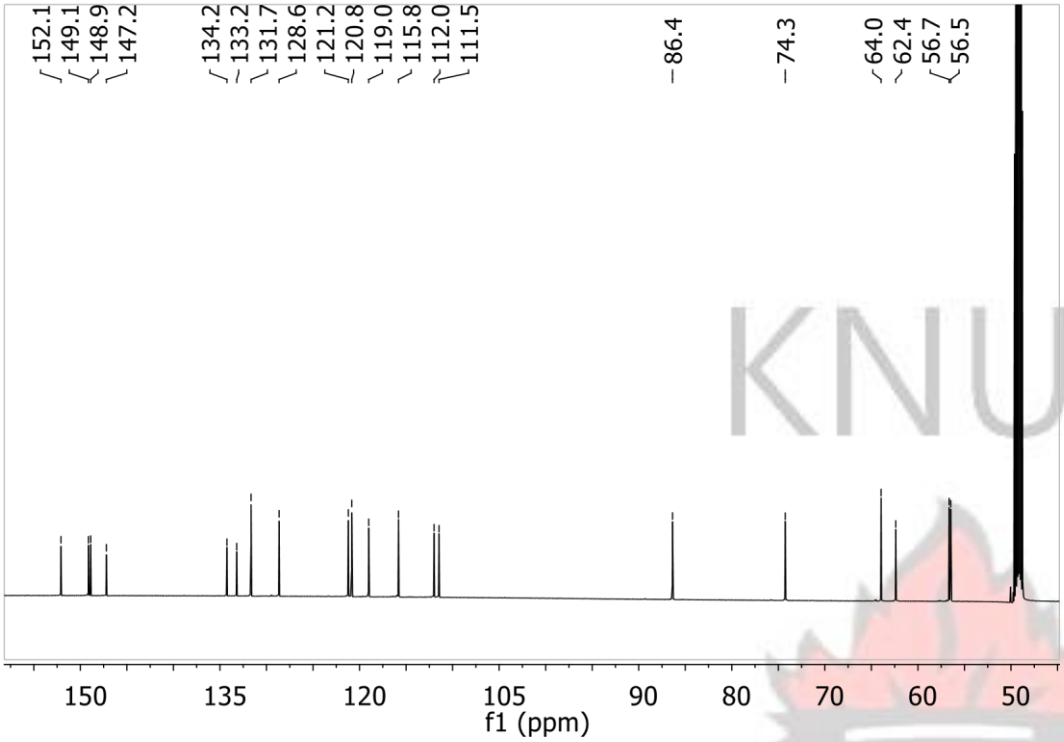

Fig. C-6^{13}C NMR spectrum of LH2

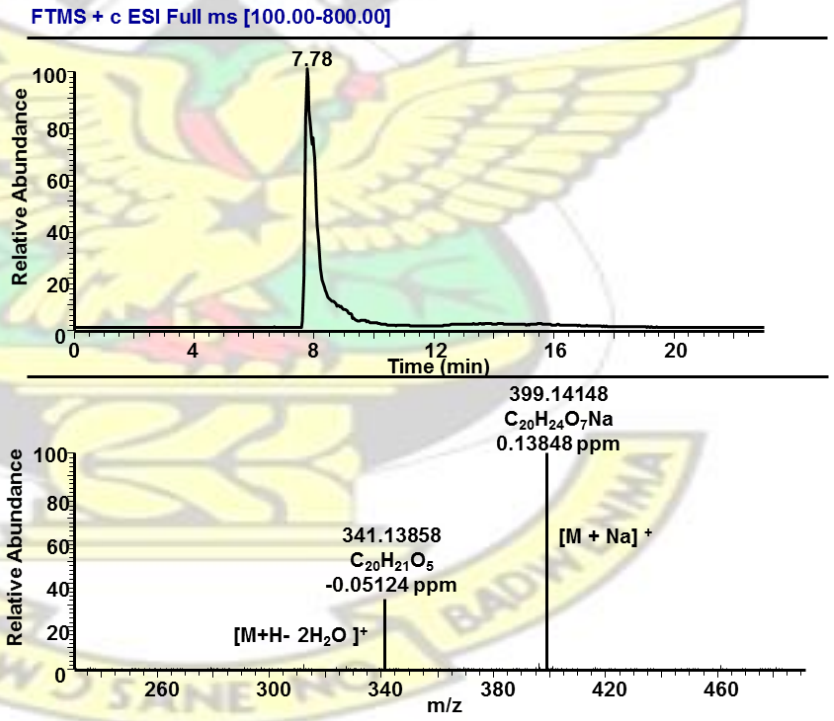

Fig. C-7 Full scan HR-MS spectrum of LH3

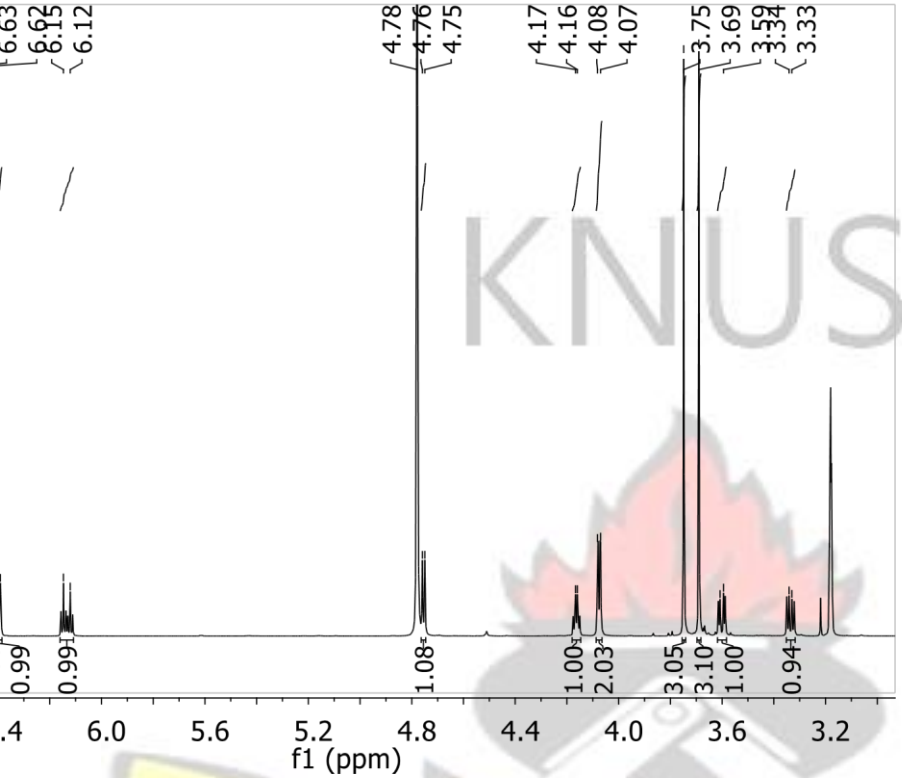

Fig. C-8[1]H NMR spectrum of LH3

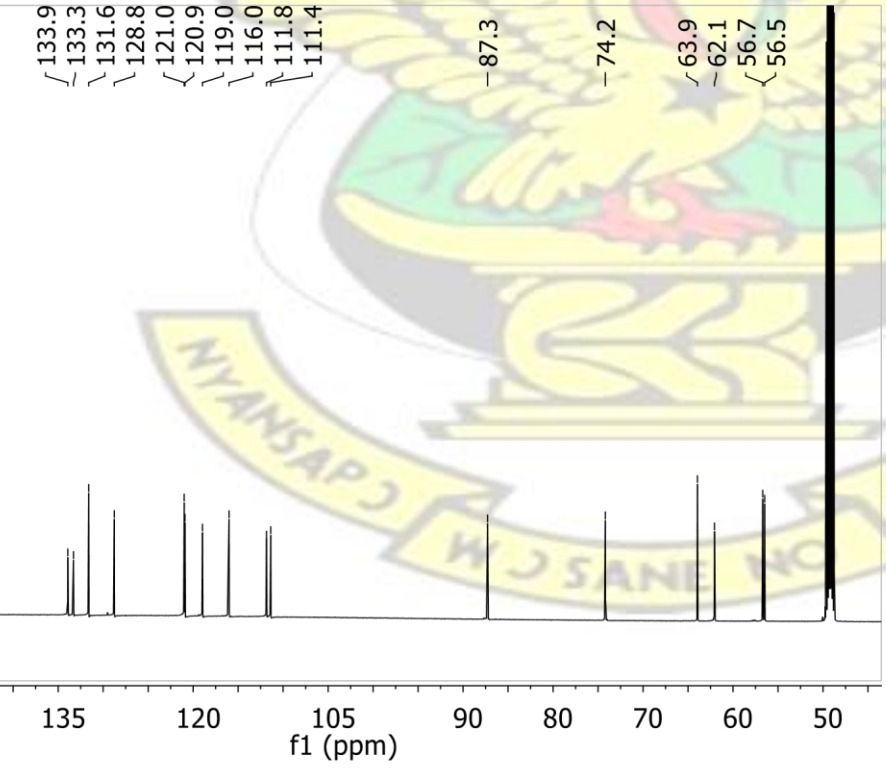

Fig. C-9[13]C NMR spectrum of LH3

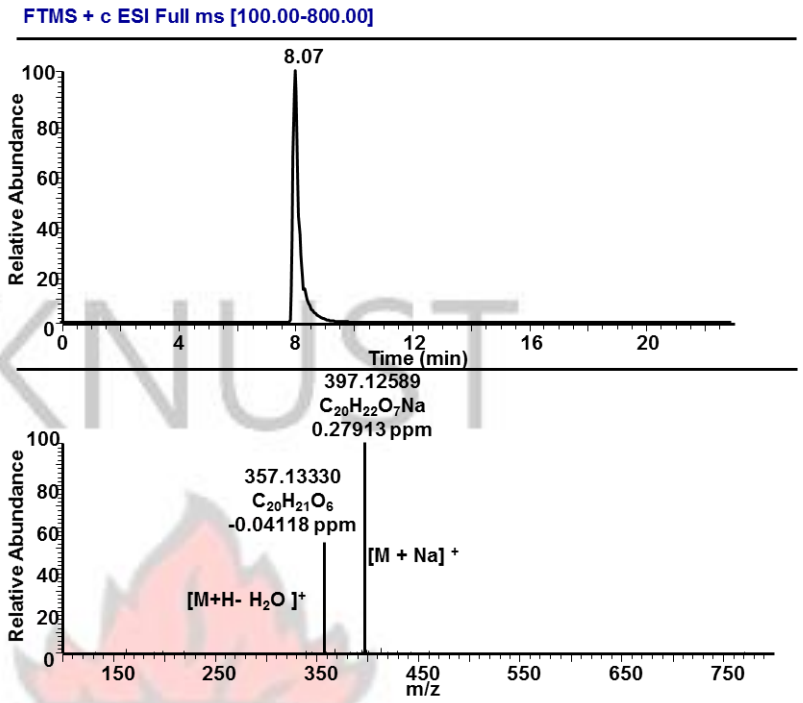

Fig. C-10 Full scan HR-MS spectrum of LH4

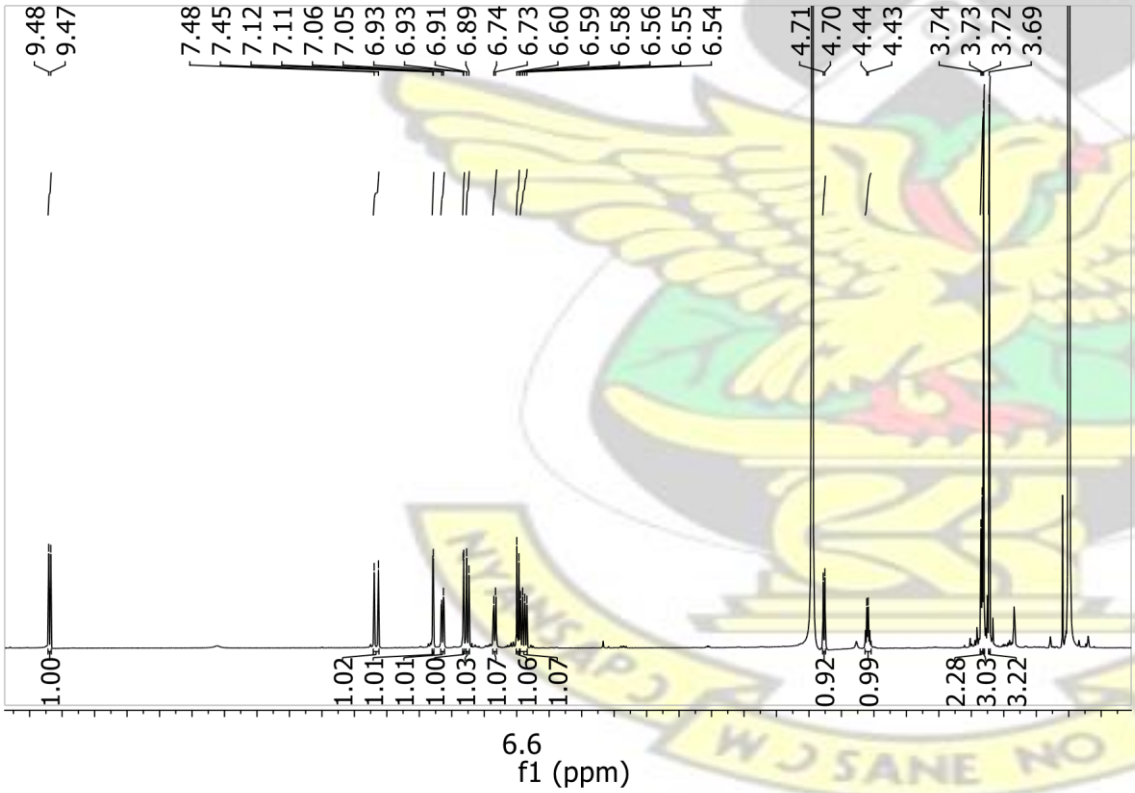

Fig. C-11 ^{1}H NMR spectrum of LH4

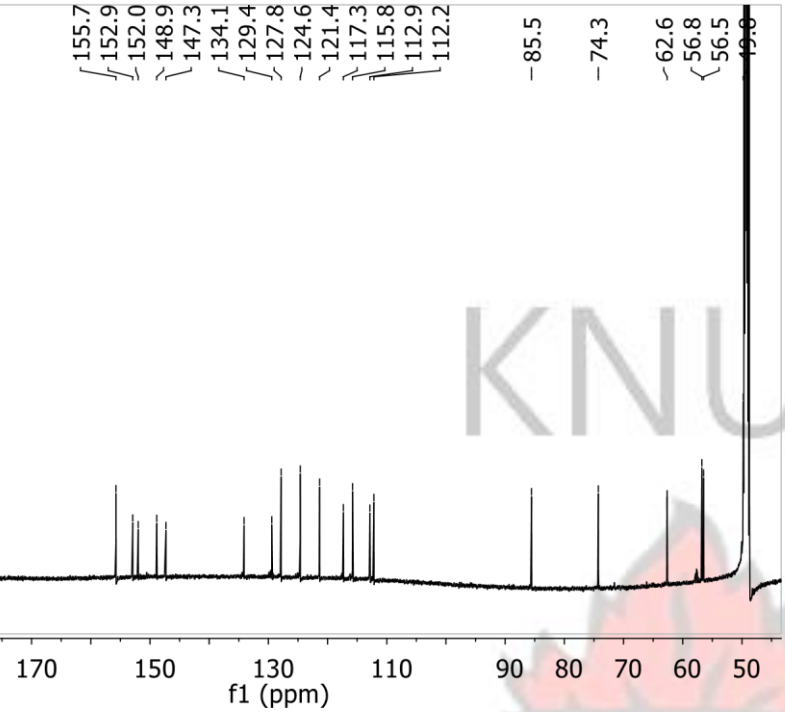

Fig. C-12^{13}C NMR spectrum of LH4

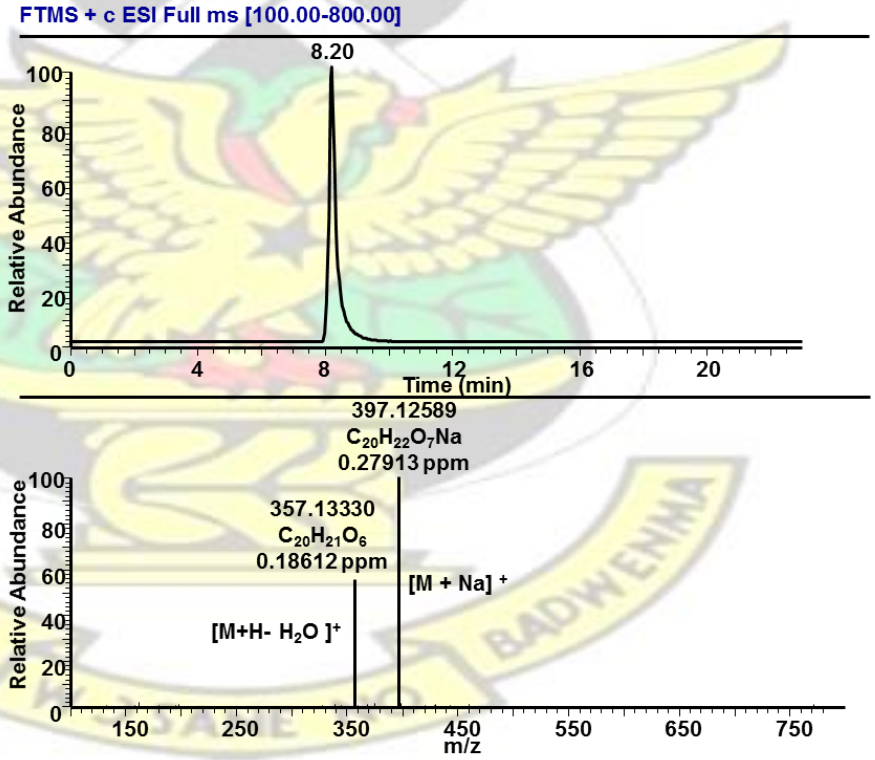

Fig. C-13 Full scan HR-MS spectrum of LH5

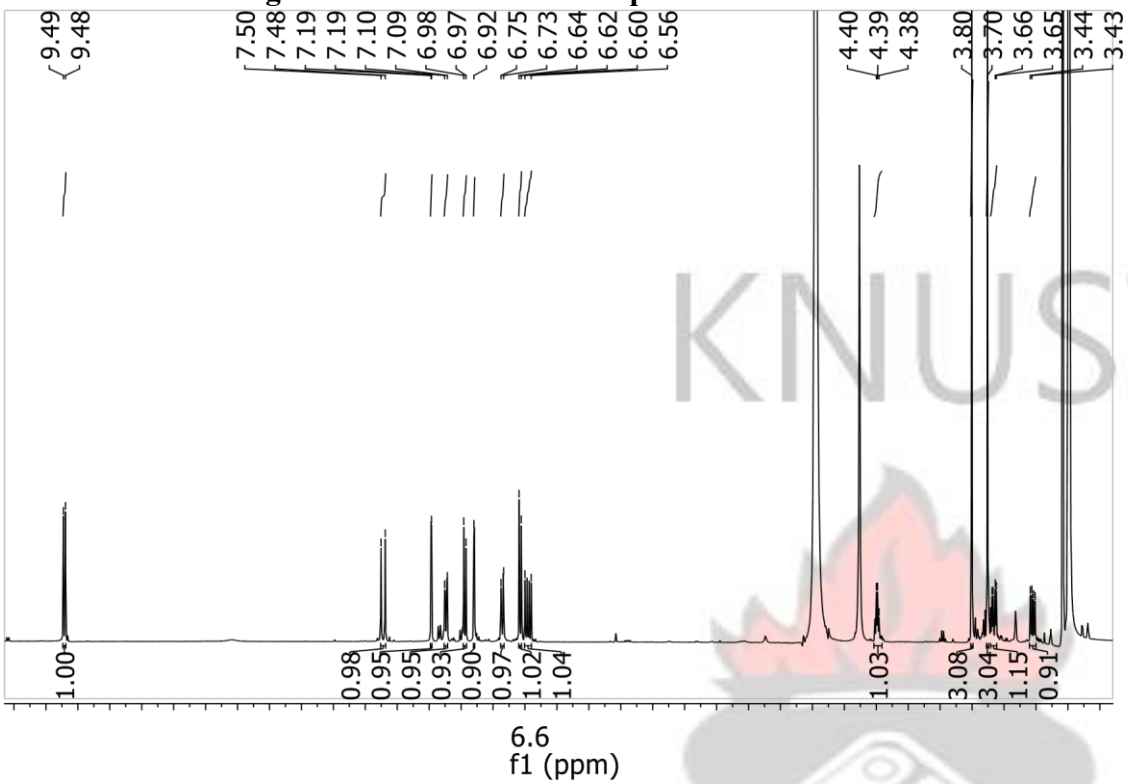

Fig. C-14 ^{1}H NMR spectrum of LH5

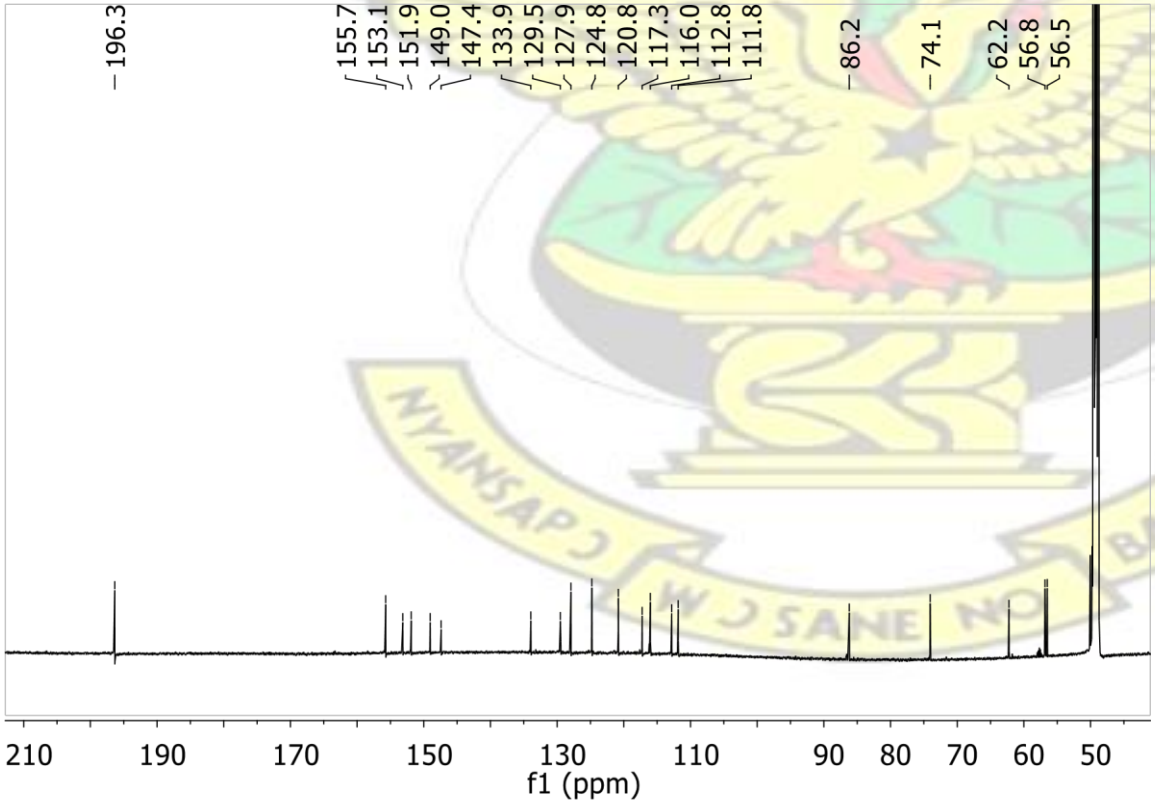

Fig. C-15 ^{13}C NMR spectrum of LH5

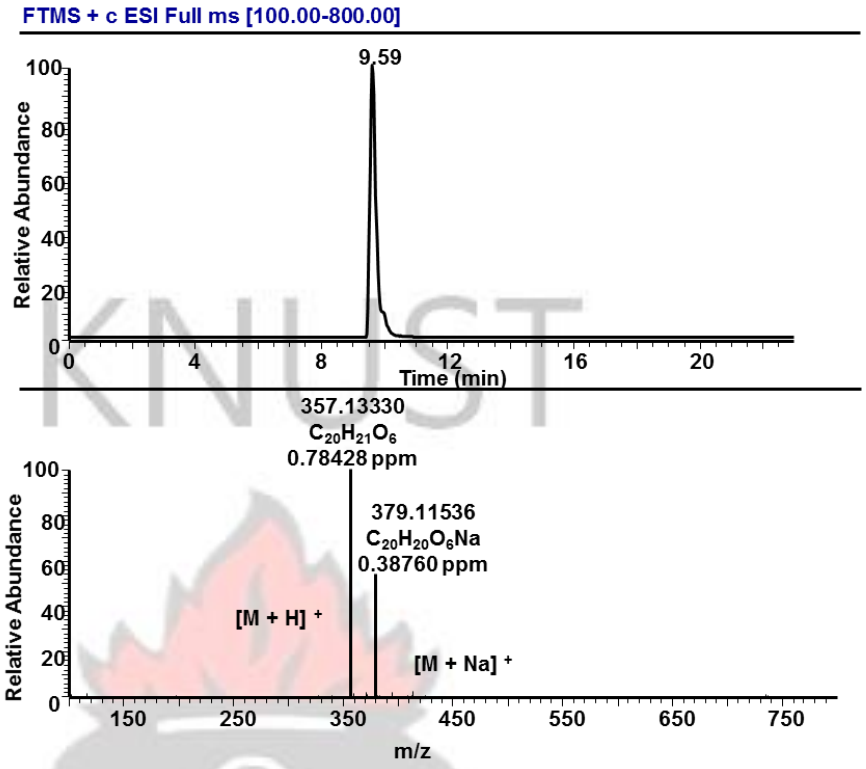

Fig. C-16 Full scan HR-MS spectrum of LH6

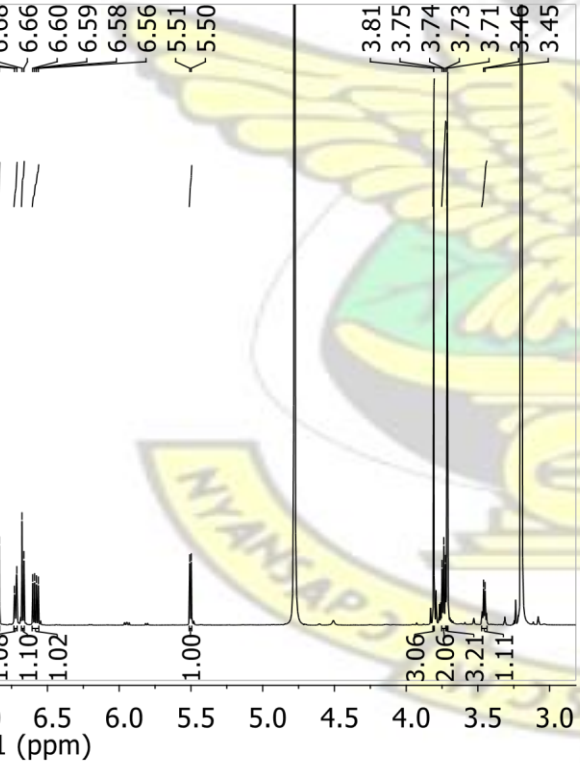

HR spectrum of LH6

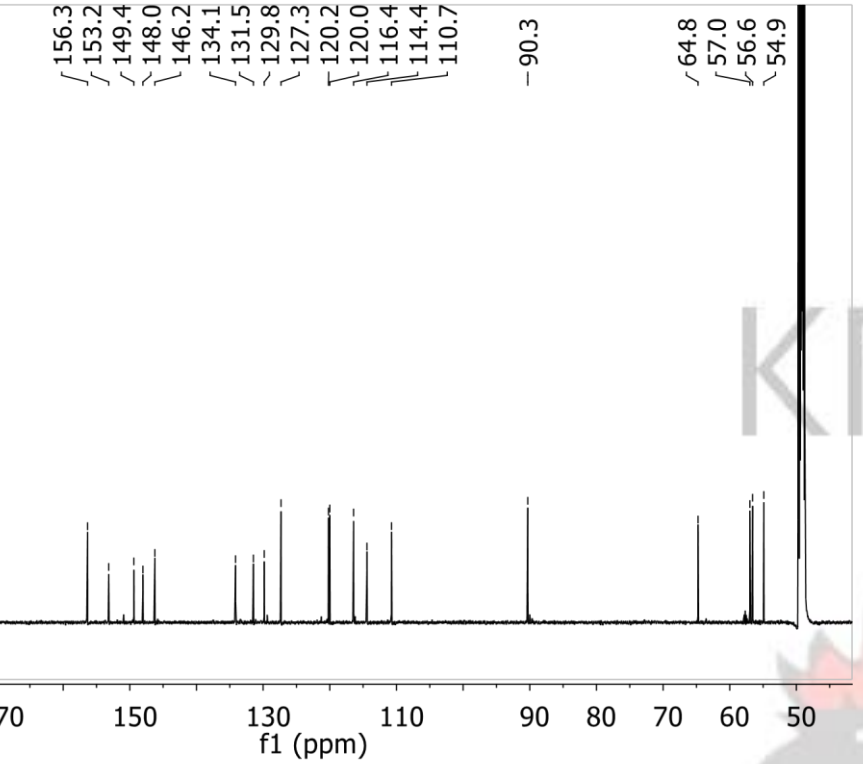

Fig. C-18 ^{13}C NMR spectrum of LH6

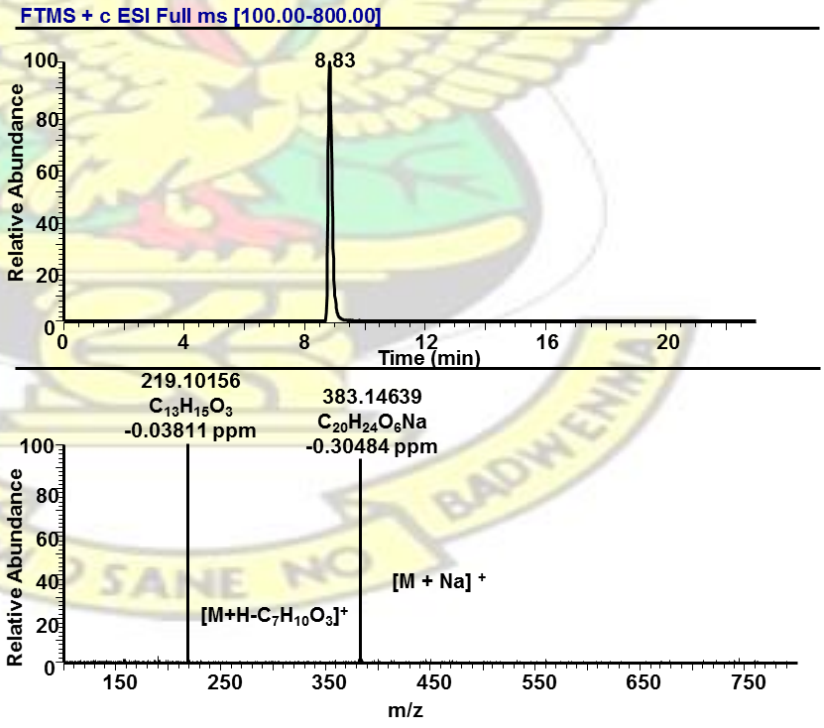

Fig. C-19 Full scan HR-MS spectrum of LH7

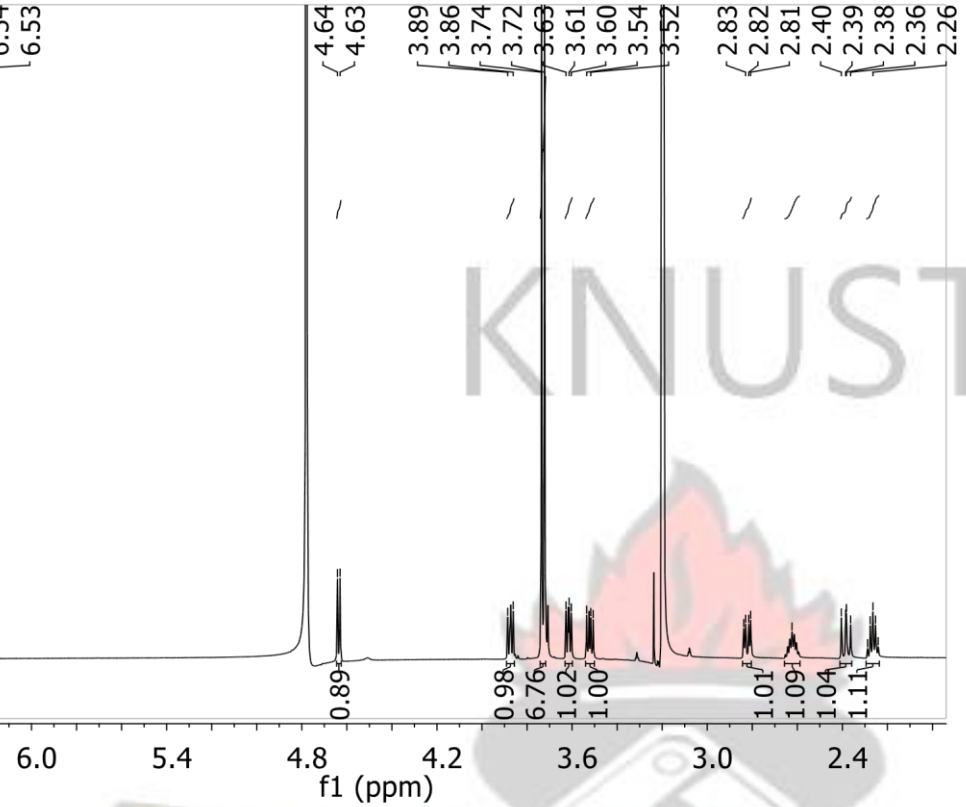

Fig. C-20 ^{1}H NMR spectrum of LH7

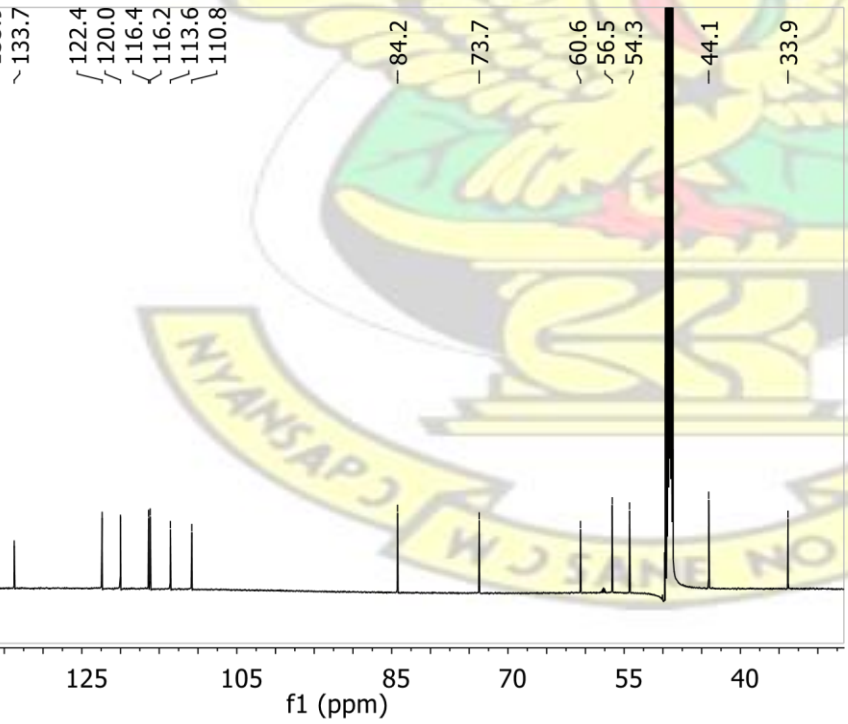

Fig. C-21 ^{13}C NMR spectrum of LH7

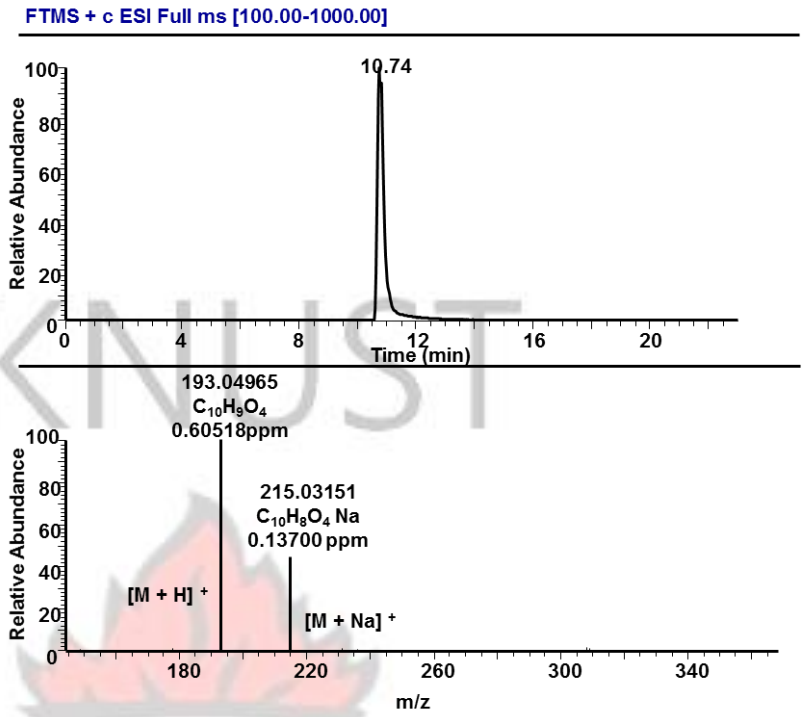

Fig. C-22 Full scan HR-MS spectrum of LH8

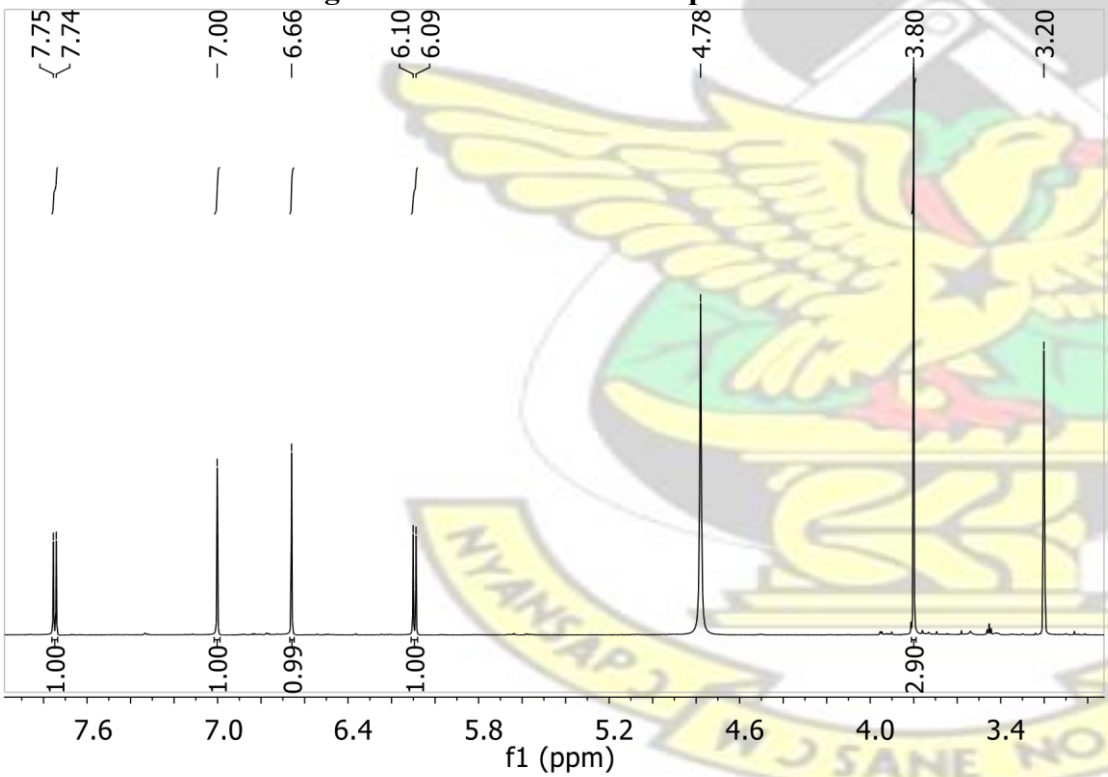

Fig. C-23 ^{1}H NMR spectrum of LH8

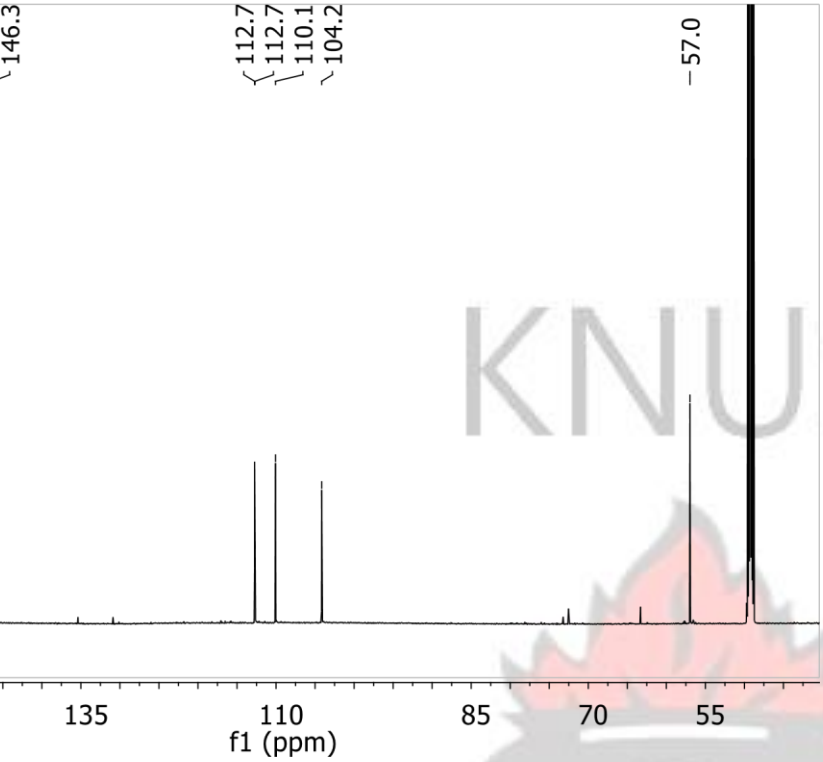

Fig. C-24^{13}C NMR spectrum of LH8

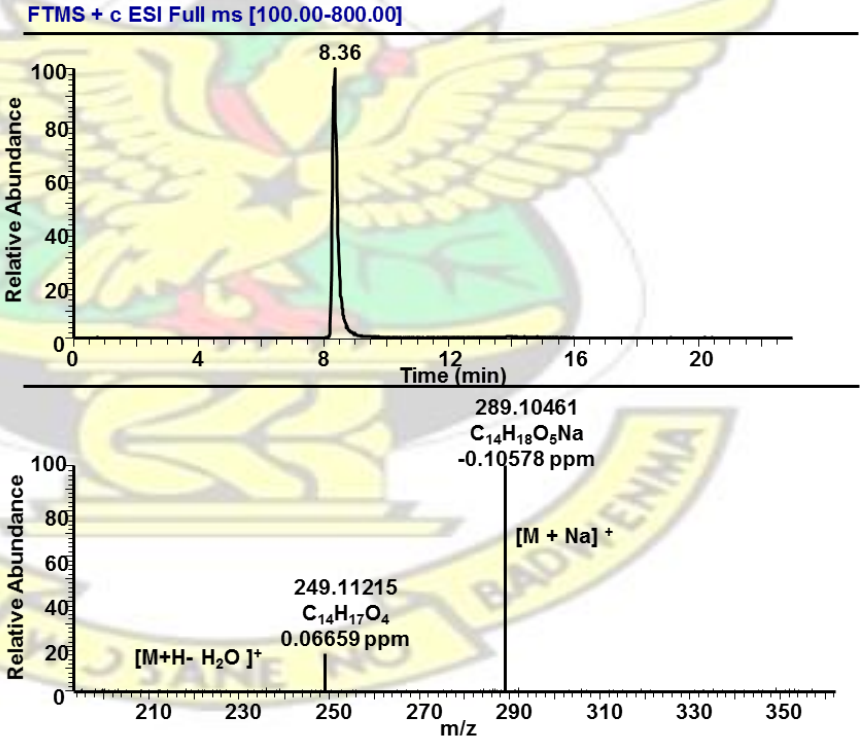

Fig. C-25 Full scan HR-MS spectrum of LH9

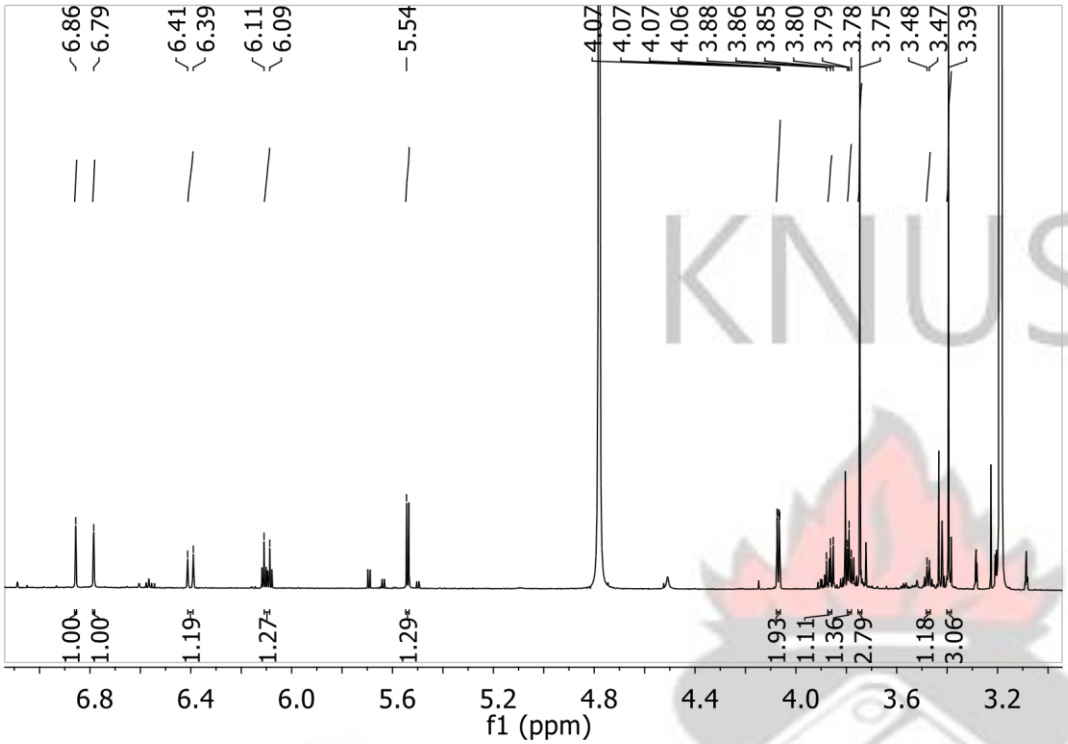

Fig. C-26 ^{1}H NMR spectrum of LH9

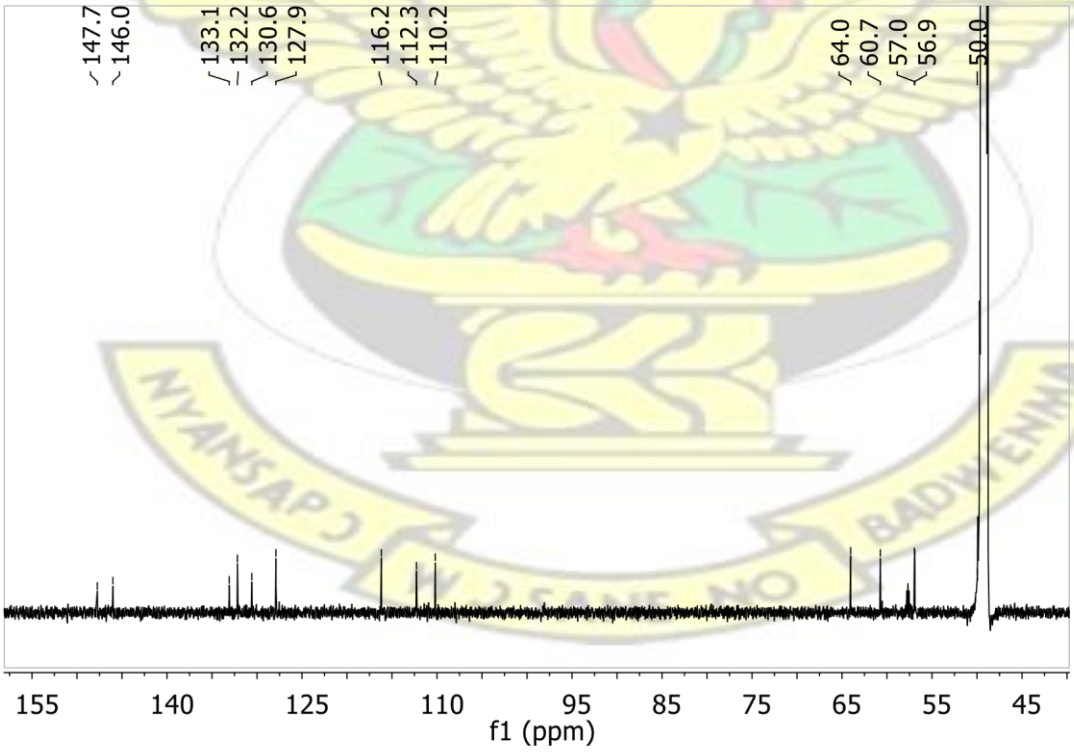

Fig. C-27 ^{13}C NMR spectrum of LH9

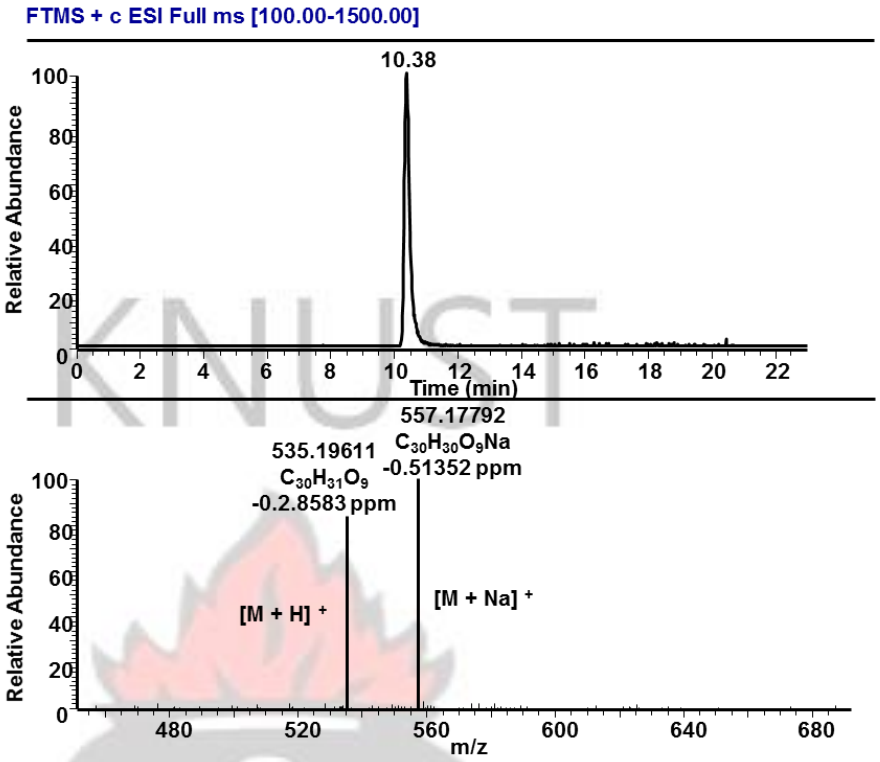

Fig. C-28 Full scan HR-MS spectrum of LH10

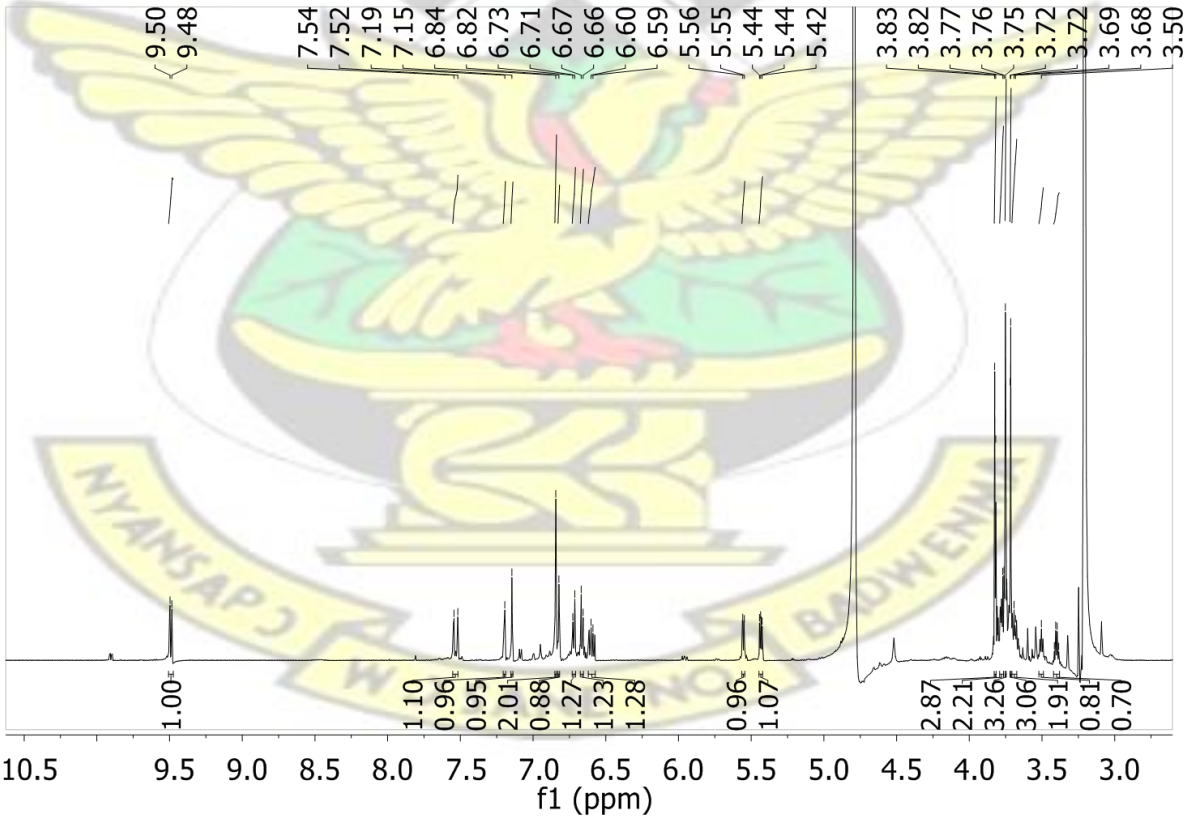

Fig. C-29 ^{1}H NMR spectrum of LH10

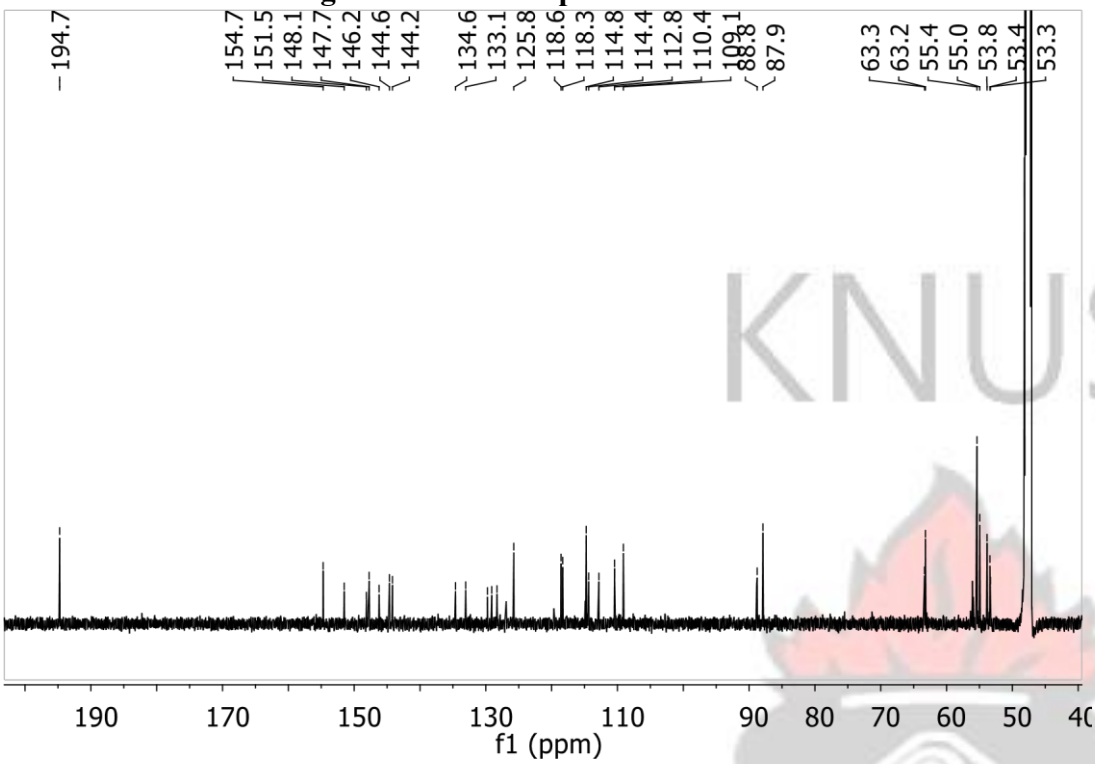

Fig. C-30 ^{13}C NMR spectrum of LH10

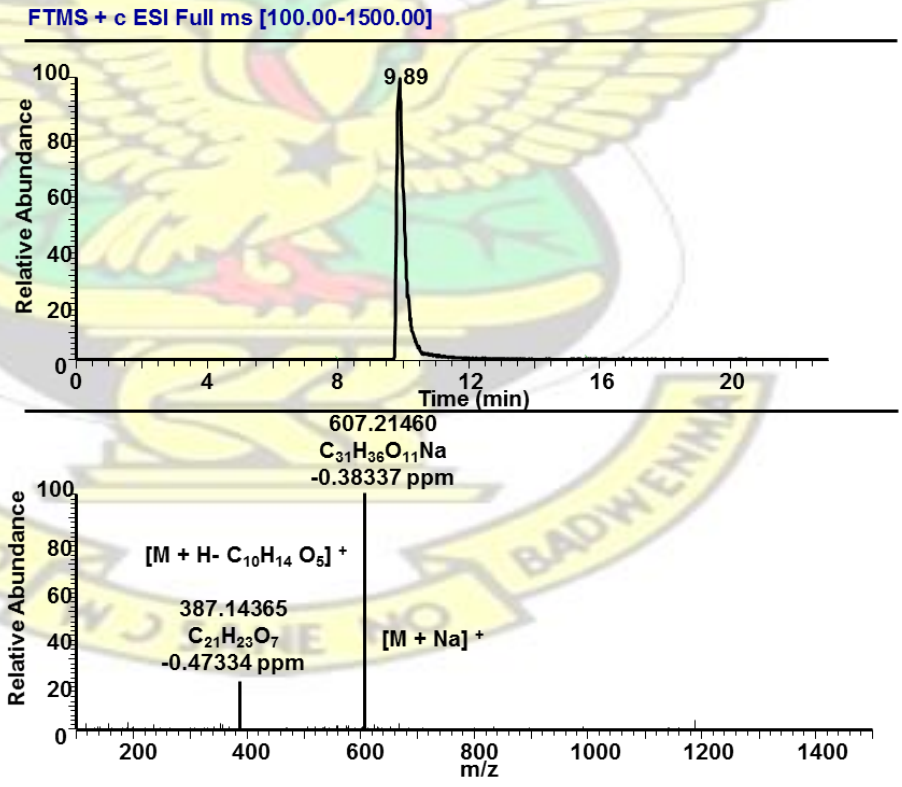

Fig. C-31 Full scan HR-MS spectrum of LH11

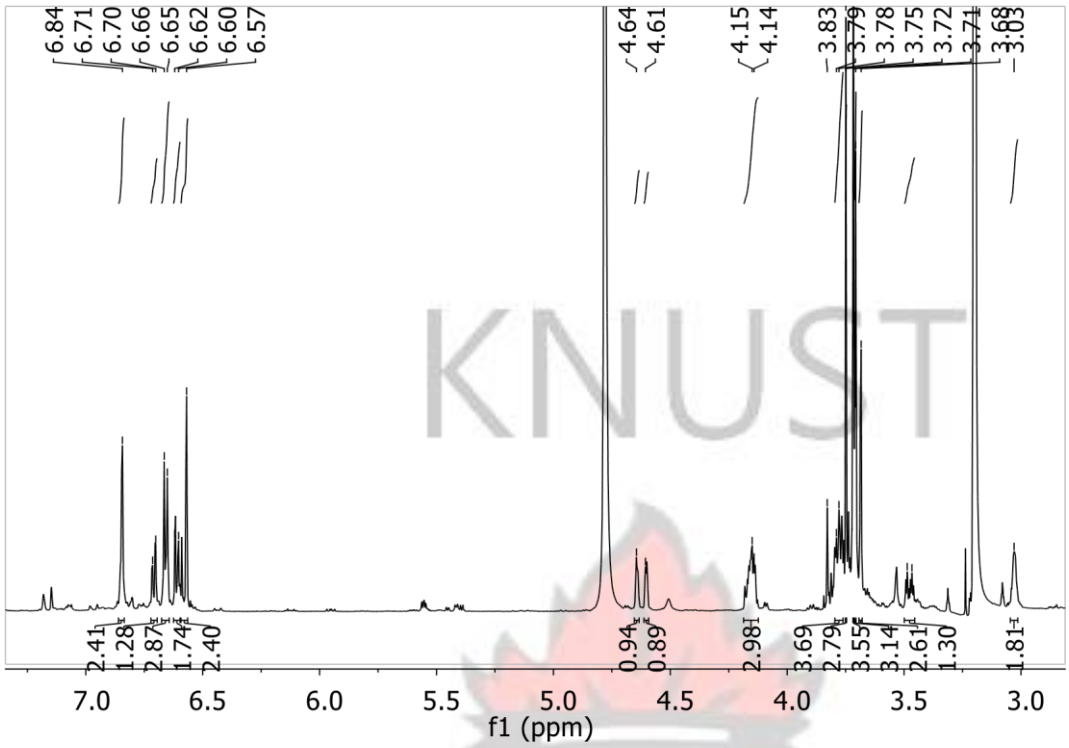

Fig. C-32 ^{1}H NMR spectrum of LH11

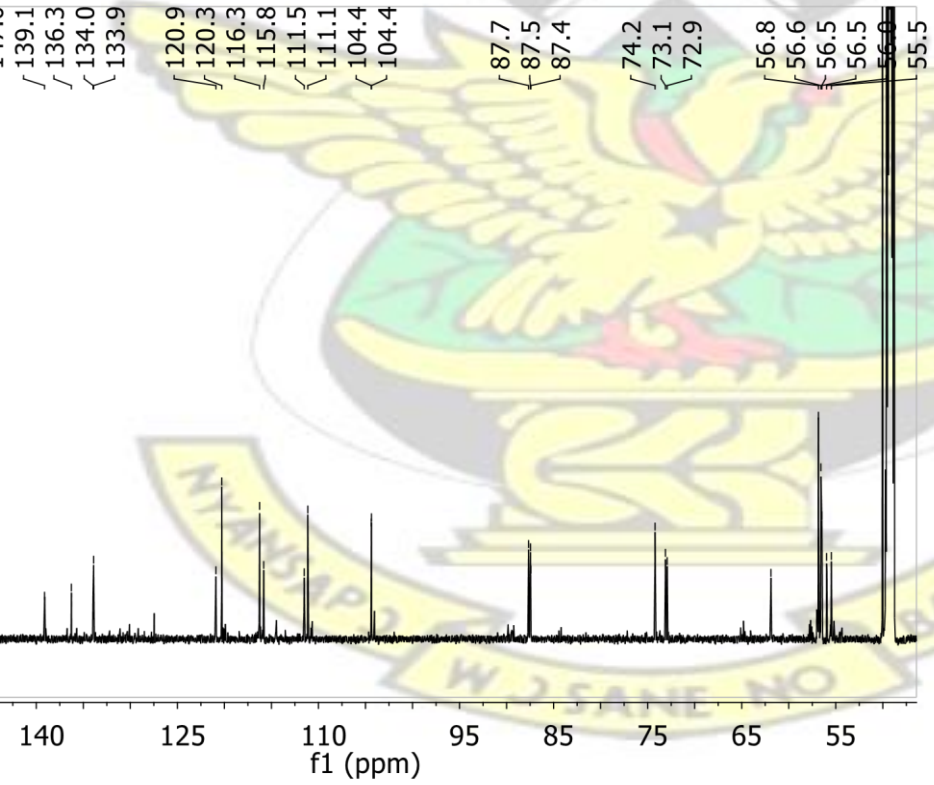

Fig. C-33 ^{13}C NMR spectrum of LH11

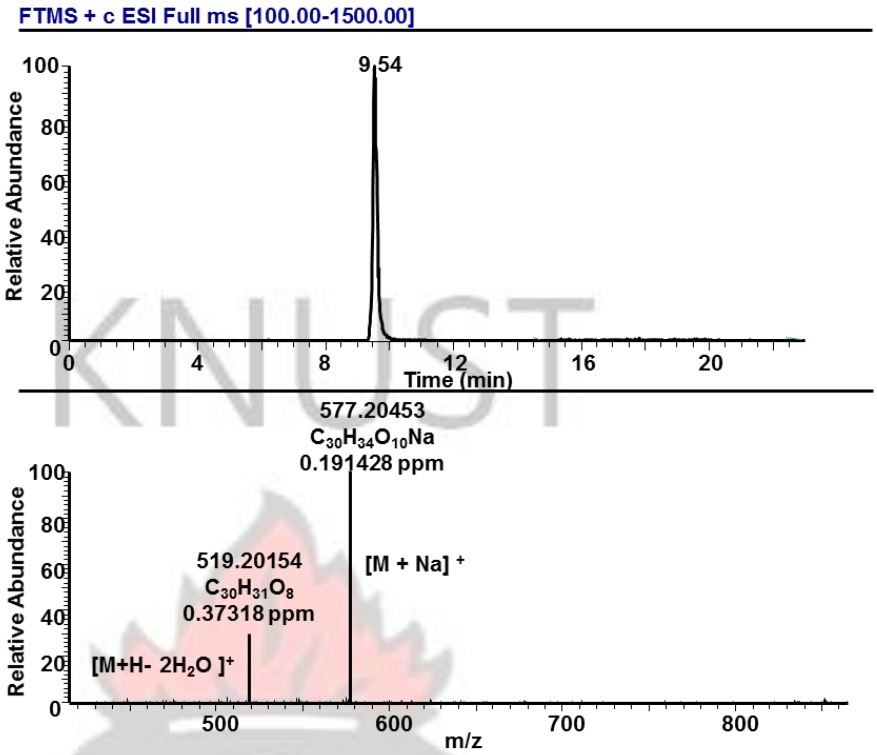

Fig. C-34 Full scan HR-MS spectrum of LH12

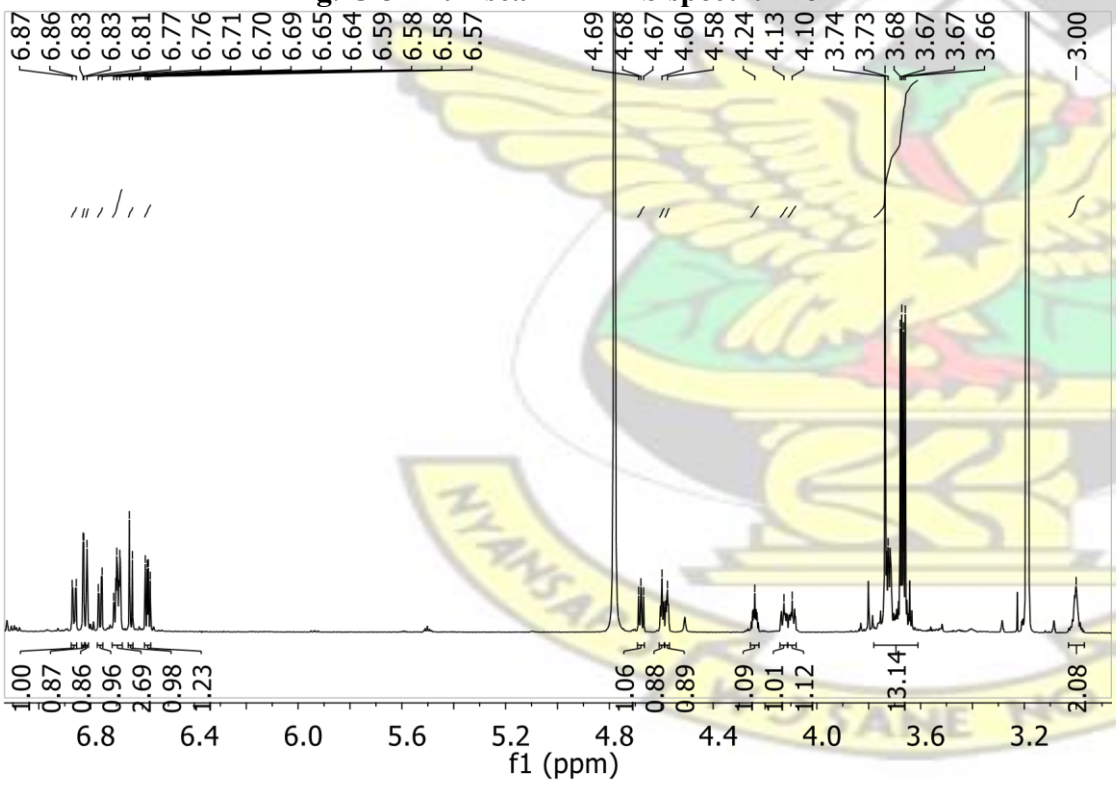

Fig. C-35 ^{1}H NMR spectrum of LH12

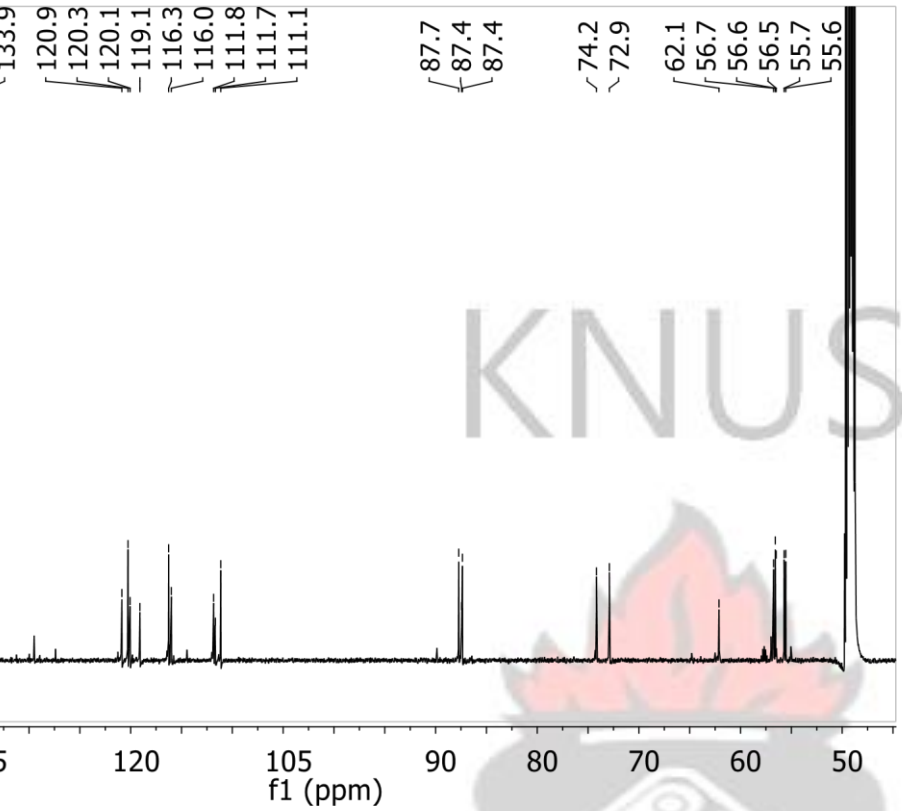

Fig. C-36 ^{13}C NMR spectrum of LH12

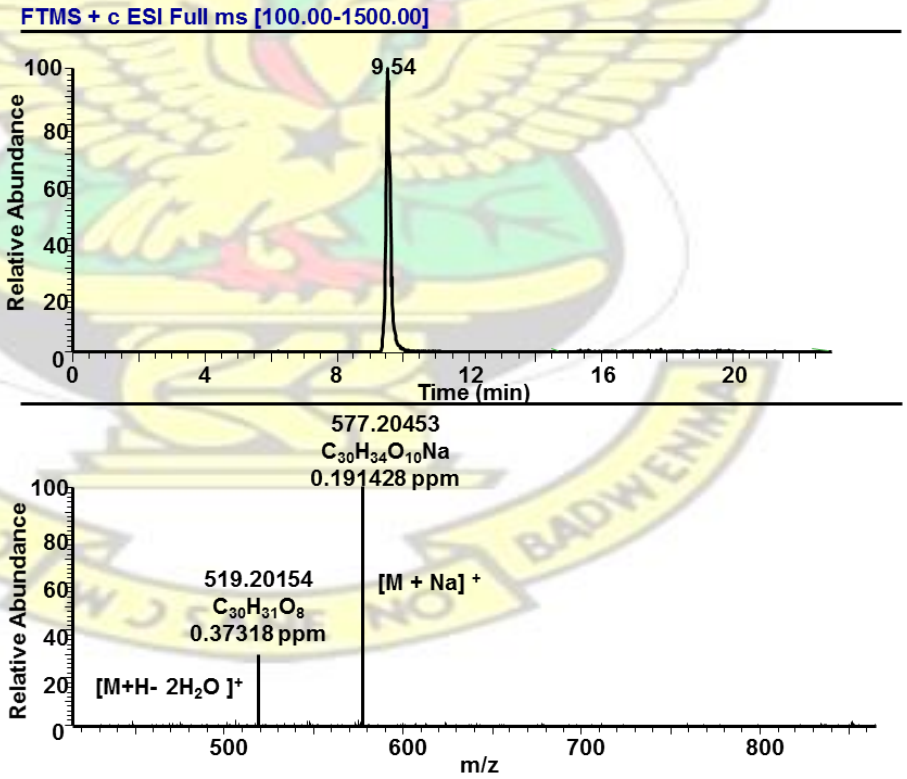

Fig. C-37 Full scan HR-MS spectrum of LH13

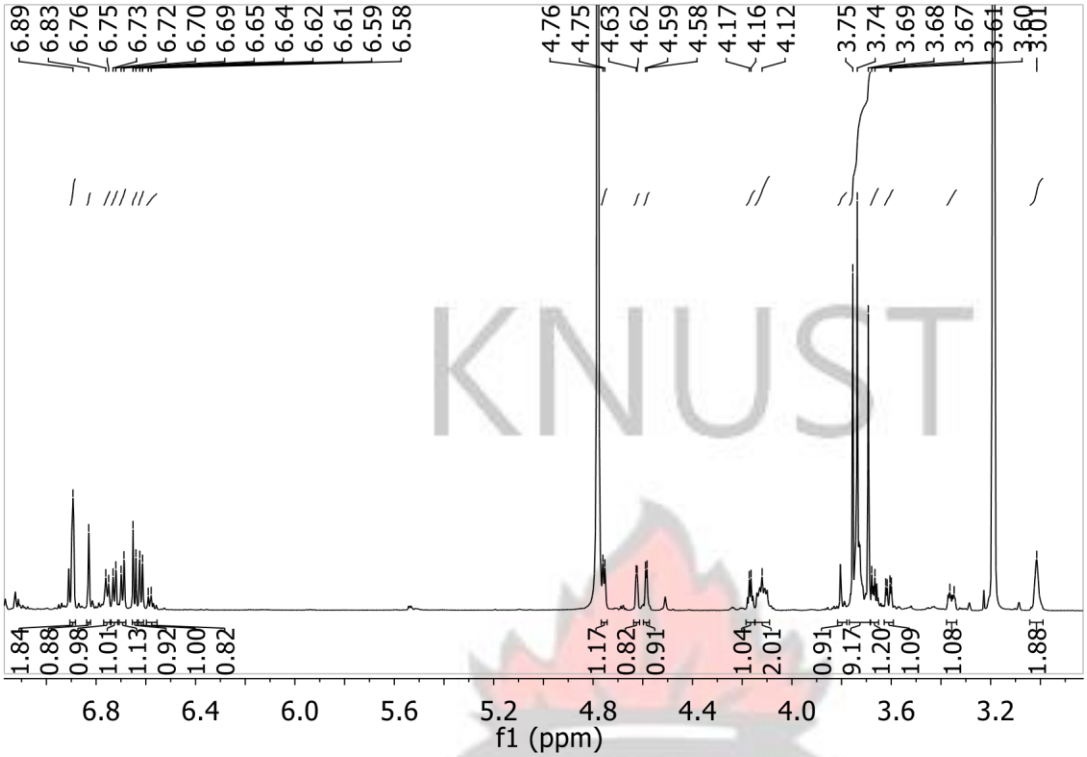

Fig. C-38 ^{1}H NMR spectrum of LH13

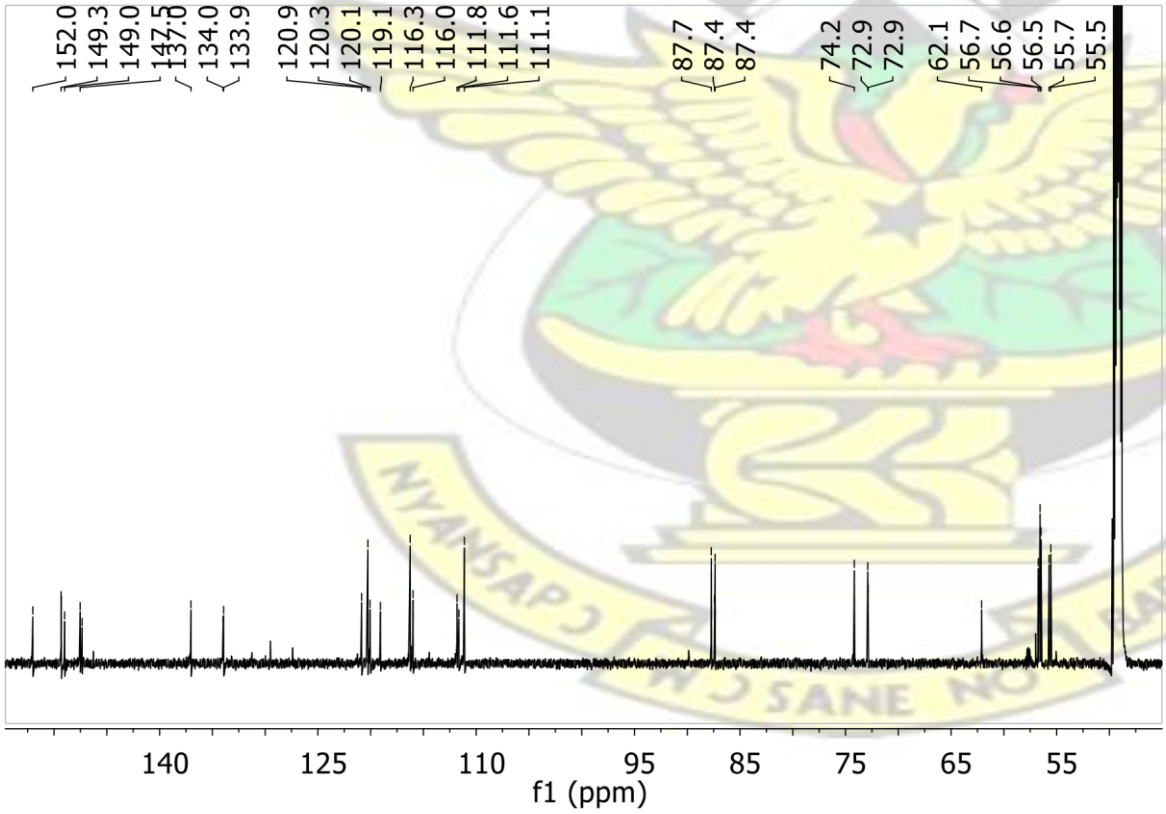

Fig. C-39 ^{13}C NMR spectrum of LH13

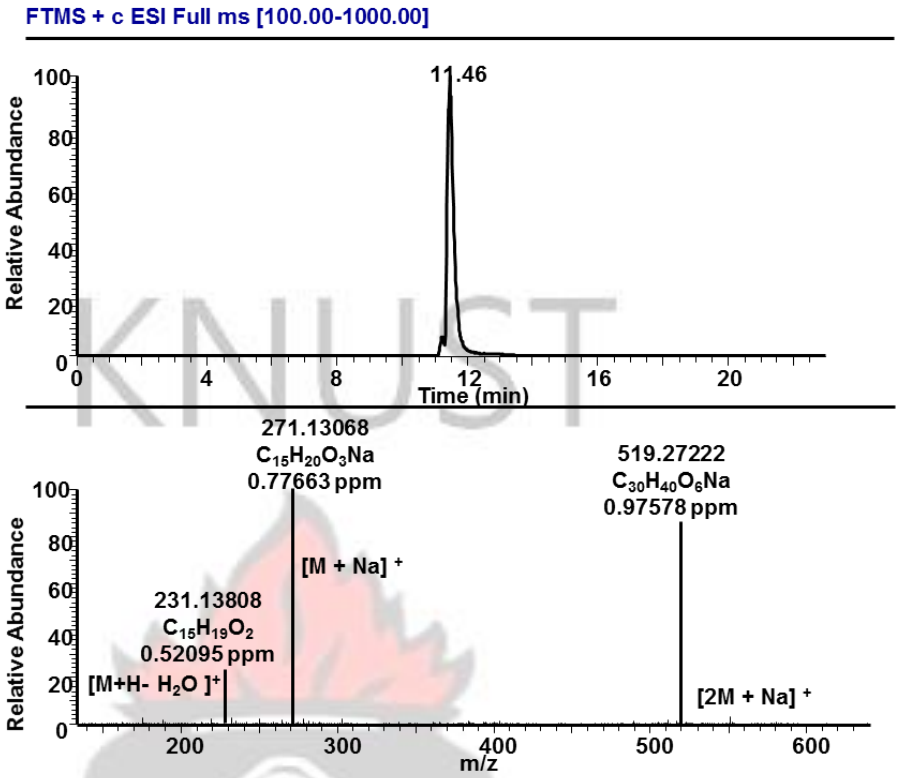

Fig. C-40 Full scan HR-MS spectrum of LH14

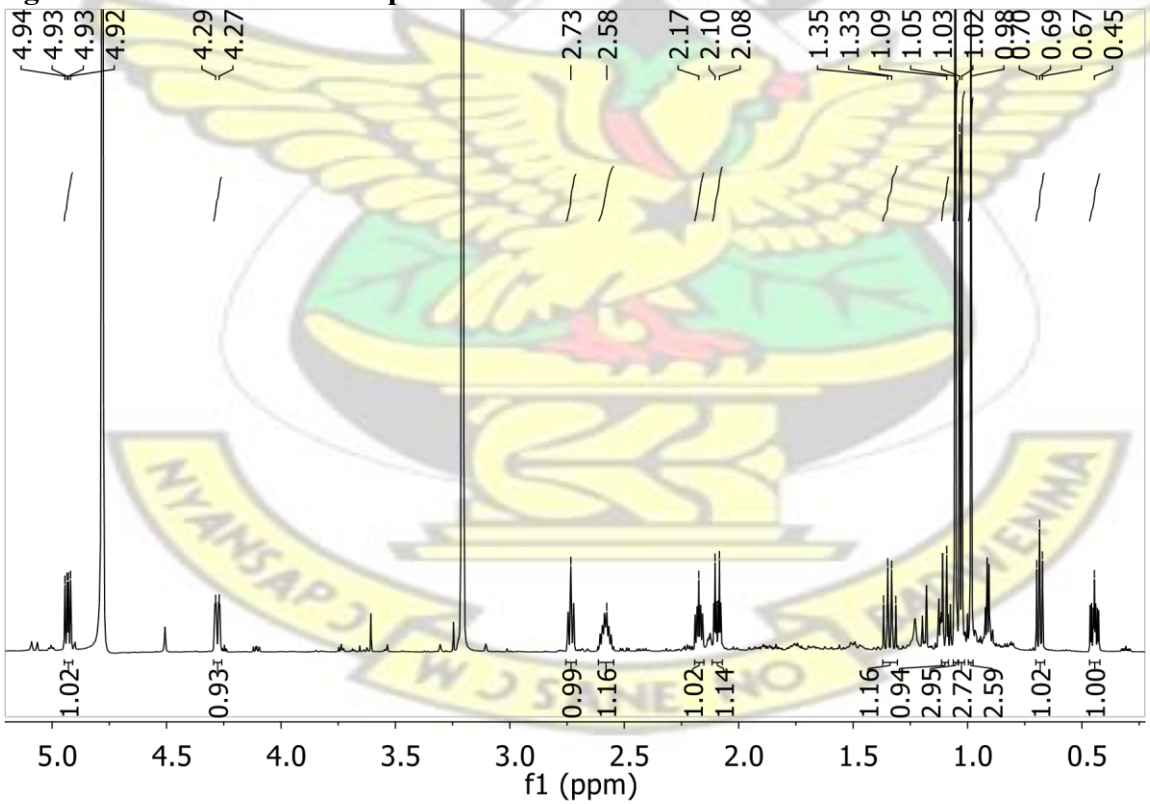

Fig. C-41 ^{1}H NMR spectrum of LH14

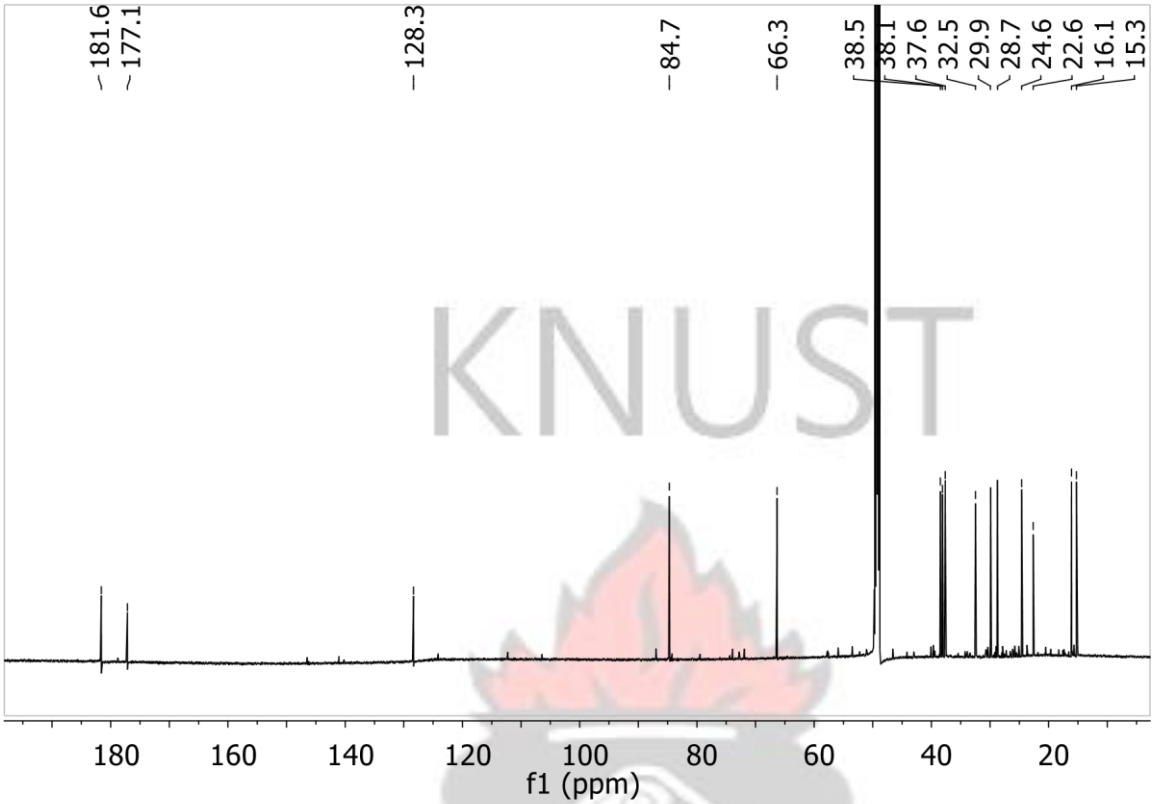

Fig. C-42 ^{13}C NMR spectrum of LH14

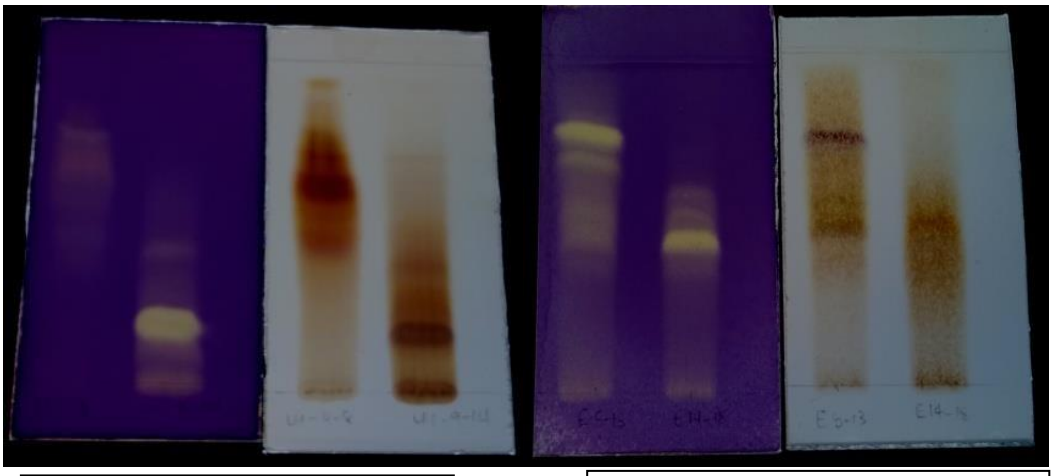

Fraction LH/D4-8, LH/D9-14

Fraction LH/E5-13, LH/E14-18

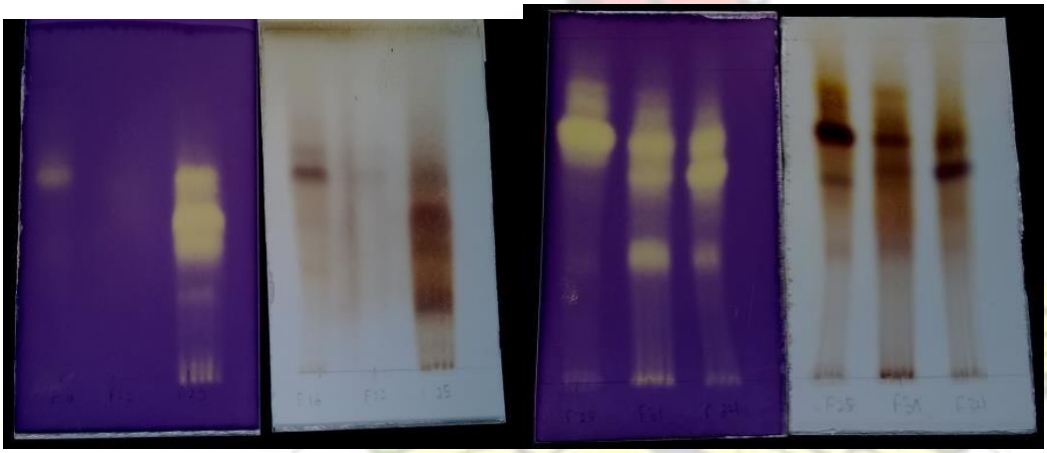

Fraction LH/F16, LH/F22, LH/F25

Fraction LH/F28, LH/F31, LH/F34

Fig. C-43: TLC DPPH Free radical scavenging activity of *L. heudelotti* fractions D-F **LIST OF ORIGINAL CONTRIBUTIONS**

Parts of the work reported in this thesis have already been published:

1. **Mireku E. A.**, Mensah M. L. K. And Mensah A. Y., Prenylated indole alkaloids from the stem bark of *Hexalobus monopetalus*. Phytochemistry Letters, 2016; 16:108-114
2. **Mireku E. A.**, Kusari S., Eckelmann D., Mensah A. Y., Talontsi F. M. and Spiteller, M., Anti-inflammatory tirucallane triterpenes from *Anopyxis klaineana* Pierre (Engl.), Rhizophoraceae). Fitoterapia, 2015; 106: 84-91
3. **Mireku E. A.**, Mensah A. Y., Mensah M. L. K., Tocher, D. A. and Habtemariam S., Anti-inflammatory properties of the stem bark of *Anopyxis klaineana* and its major constituent, methyl angolensate. Phytotherapy Research, 2014; 28: 1855-1860